1974

Performance, heat transfer and hydrodynamics of two-phase downflow thermosiphons.

Helmut. Keil
University of Windsor

PERFORMANCE, HEAT TRANSFER AND HYDRODYNAMICS OF TWO-PHASE DOWNFLOW THERMOSIPHONS

A DISSERTATION

Submitted to the Faculty of Graduate Studies through the Department of Mechanical Engineering in Partial Fulfillment of the Requirements for the Degree of Doctor of Philosophy at the University of Windsor

By

Keil, Helmut

B.A.Sc., University of Windsor, 1967
M.A.Sc., University of Windsor, 1968

Windsor, Ontario, Canada

1974

ABSTRACT

This thesis presents the results of an experimental investigation into the effect of certain geometric factors on the stable operation of a downflow heated, R-113 thermosiphon loop and an examination of the feasibility of mathematically simulating such a loop accurately. The particular model used assumed that the homogeneous flow theory was applicable in the two-phase sections and that flashing could occur at any specified liquid superheat in the riser. The study includes the effects of various riser sizes, D_R, heater length, l_H and degrees of subcooling at inlet to the heater section on the loop behaviour. The overall height H of the loops was kept constant at 13.1 feet as was the downflow annular section. The working fluid was (R - 113).

Flow visualization and instrumentation were utilized in the experimental study. The glass and copper test loop was instrumented to allow for the measurement of the mass flow rate through the loop, the fluid temperature, static pressure and void fractions around the loop, and the heater surface temperature along its length. All the loops studied used the same annular heat input downflow section with various lengths of the inside copper tube being heated electrically . The diameter of the riser was varied and several different devices were used to promote the flash initiation.

The loops would operate in the downflow heating mode only within a characteristic power input range. Gradually varying the power within this range caused the point of flash initiation in the riser to vary between approximately 2' from the top to approximately 1½' from the bottom. Outside this range, the flows became unstable resulting in a flow reversal to the more natural upflow heating mode.

For all the loops tested, the fluid remained subcooled in the downcomer heated section while bubbly type flow was present in the two-phase portion of the riser. Heat transfer mechanisms varied from single-phase forced convection to subcooled nucleate boiling as the power input was increased from the lower to the upper limit. Void fractions of up to 20% near the annulus exit were achieved in the subcooled liquid just prior to reversal. In the riser, the liquid attained superheats of up to 7°F in the initial flashing region and void fractions of up to 70% at the riser exit.

The maximum and minimum power input limits for downflow were increased by lengthening the heater and increasing the inlet subcooling. A significant improvement was found by increasing the (riser area/annular area) ratio from 1 to 2.5 but little benefit was obtained beyond 2.5 where the limits became very sensitive to the method used to initiate flashing. Increasing the inlet subcooling caused the range

of power inputs for steady operation to decrease and ultimately vanish for inlet subcooling greater than 20°F.

A satisfactory simulation of the loop for steady state downflow operation was achieved by utilizing correlations available in the literature supplemented by empirical data from this study for the local superheat required to initiate flashing in the riser. The program was then utilized to show the effect of varying the height of the loop on its maximum and minimum power inputs for stable operation.

ACKNOWLEDGEMENTS

The author is grateful to Professor W. G. Colbo[illegible], Head of the Department of Mechanical Engineering, for his continuous support and interest.

The author wishes to acknowledge the invaluable guidance and supervision of Dr. T. W. McDonald during the course of this study. In particular, the author would like to express gratitude for the enthusiastic counsel given by Professor M. B. Powley.

Thanks are also due to Messrs. R. Myers and W. Beck for their technical assistance in constructing the apparatus.

Finally, the author wants to thank B. Gaspar for initiating this project which was supported financially through National Research Council Grant No. A-0877.

TABLE OF CONTENTS

APPENDICES

LIST OF FIGURES

LIST OF TABLES

NOMENCLATURE

SYMBOL

A	effective heater surface, ft^2
A_{cs}	cross sectional flow area, ft^2
A_l	cross sectional flow area taken up by the liquid, ft^2
A_r	cross sectional flow area of the riser, ft^2
A_{ts}	cross sectional flow area of the heated section, ft^2
A_v	cross sectional flow area taken up by the vapour, ft^2
A_w	wetted surface area, ft^2
c_l	specific heat of the liquid, $Btu/lb_m-°F$
C_{sf}	coefficient in Eq. (A-13)
D	pipe diameter, ft
D_{eq}	equivalent diameter of an annulus, ft
D_b	bubble diameter
f	Blasius skin friction factor

f_a average friction factor in an annulus, Eq. (6-20)

f_{TP} two-phase friction factor in Eq. (A-32)

g_c conversion factor, 4.17×10^8 lb_m-ft/hr-lb_f

G mass velocity, $lb_m/hr\text{-}ft^2$

G_b mass velocity of the bubbles, $lb_m/hr\text{-}ft^2$

G_r mass velocity in the riser, $lb_m/hr\text{-}ft^2$

h heat transfer coefficient, $Btu/hr\text{-}ft^2\text{-}°F$

h_{fg} latent heat, Btu/lb_m

H the overall height, ft

$\bar{H}$ enthalpy, Btu/lb_m

k thermal conductivity, $Btu/hr\text{-}ft°F$

l_H heater lengths, ft

$\dot{m}$ mass flow rate, lb_m/hr

N_{Eo} Eotvos number, $(\rho_l - \rho_v) L^2 g/\sigma$

N_{Fr} Froude number, V_l^2/gD

N_{Nu} Nusselt number, hD_{eq}/K

N_{Nu}' Nusselt number defined by $\dfrac{(q/A)D_b}{(T_w - T_s)k_l}$

$N_{Nu,b}$ boiling Nusselt number defined by Eq. (A-33)

N_{Pr} Prandtl number defined by $\mu c/k$

N_{Re} Reynolds' number defined by GD_{eq}/μ_l

$N_{Re,b}$ boiling Reynolds number defined by Eq. (A-34)

N_{St} Stanton number defined by h/Gc_l

P pressure, lb_f/ft^2

P_a atmospheric pressure, lb_f/ft^2

P_{crit} critical pressure of R - 113, lb_f/ft^2

P_h heater perimeter, ft

P_w wetted perimeter, ft

Q heat flow, Btu/hr

q heat flux, Btu/hr-ft^2

r bubble radius

R_v gas constant of the vapour

S slip ratio defined by V_v/V_l

T_e fluid temperature at the exit of the heated section, °F

T_b liquid temperature at the inception of boiling, °F

T_{sat} saturation temperature, °F

T_w wall or surface temperature, °F

ΔT_{sc} liquid subcooling, $T_{sat}-T_l$, °F

ΔT_{ws} wall superheat, T_w-T_{sat}, °F

T^+ non-dimensional temperature defined in Eq. (A-18)

U slip velocity of bubbles in a constrained medium, ft/hr

$U_{s,\infty}$ slip velocity of a single bubble as given by Eq. (A-19)

V absolute velocity of the fluid, ft/hr

V_v absolute terminal velocity of the vapour bubble given by Eq. (A-21)

$\bar{v}$ specific volume in Eq. (A-32), ft^3/lb

x thermodynamic quality

x_{sub} non-equilibrium quality (ie. subcooled liquid, saturated vapour)

X vapour generation quality $\equiv [H_e - H_{sat}(P_{res})]/h_{fg}(P_{res})$

z distance from the bottom of the loop, ft

z_{bi} position at the inception of boiling, ft

z^+ non-dimensional distance in Eq. (A-18)

β coefficient of volumetric expansion, 1 /°F

μ dynamic viscosity, $lb_m/ft\text{-}hr$

ρ density, lb_m/ft^3

σ surface tension, lb_f/ft

Φ function

η non-dimensional temperature increase

α void fraction

γ specific weight, lb_f/ft^3

τ shear stress, lb_f/ft^2

SUBSCRIPTS

cs cross section

e exit of down flow section

i inlet condition to down flow section

l liquid

sat saturation condition

v vapour

w wall

CHAPTER I

INTRODUCTION

1.1 GENERAL

This thesis presents the results of a theoretical and experimental investigation carried out for the purpose of studying the overall heat transfer capabilities as well as the internal flow phenomenon within a reverse flowing thermosiphon loop; that is, one in which the working fluid flows downward over the heated section. The loop itself is a closed system, commonly called a thermosiphon, having fluid circulation due to the buoyancy forces arising as a result of the addition of external thermal energy.

Interest in this kind of thermosiphon began as a result of a study by McKay[1] in which he investigated the costs of heavy water moderated reactors. Simplification by bottom refuelling and downflow over the rod bundles was one suggestion. Subsequent work by Barns and Rogers[2] showed that downflow thermosiphoning was feasible and could be used to cool the reactor during the shut-down procedure, thus eliminating the cost of a secondary standby low capacity pump and its related equipment. He concluded, however, that further analytical and experimental data was necessary, particularly for two-phase operation.

This study outlines the behavioural characteristics of reverse flow thermosiphons and, in particular, investigates

the effect of the riser flow area to downflow area ratio, the inlet subcooling, and the heater to riser length ratio on the performance of the thermosiphon as a vapour generation system. The principles of operation of downflow thermosiphons are outlined in section 1.2 and a description of the actual tests carried out is given in section 1.3.

A simulation of the operation of such reverse flow thermosiphon loops was carried out and is discussed in chapter VI after the experimental results have been presented.

1.2 PRINCIPLES OF OPERATION OF DOWNFLOW THERMOSIPHONS

An example of the two principle modes of thermosiphon operation is shown in figure 1. In the normal flow (see figure 1a) the fluid is heated as it rises over the heated section of the tube. Vapour generation, if any, aids in the circulation as the fluid is heated.

The loops considered here are of the type shown in figure 1b. The working fluid flows from the reservoir and down a vertical tube in the direction of increasing hydrostatic pressure. The fluid's local saturation temperature increases with pressure so that even though energy is added to the fluid in the heated portion of the tube, the liquid can remain subcooled throughout. Note that any bubbles generated here will tend to rise relative to the liquid and hence oppose its downward motion.

The fluid then passes from the downward portion of

the loop, through a horizontal tube and up a second vertical tube called a riser. The pressure is now decreasing in the flow direction and a point in the riser is reached where the pressure equals the local saturation pressure. As the fluid continues to rise, flashing takes place which causes the pressure to decrease still more due to the buoyant effect of the vapour bubbles. The hydrostatic pressure difference thus developed between the heater and the riser sustains the circulation of the fluid around the loop.

The two-phase mixture jets from the riser into a heat exchanger where the vapour is condensed and then flows back into the reservoir.

During steady state operation of the loop, the circulation rate will be such that the net pressure drop around the loop will be zero. Thus the acceleration and frictional pressure losses are equal to the pressure change arising from the buoyancy of the bubbles.

The frictional pressure losses are commonly expressed as:

$$\sum \Delta P_{friction} = \sum K_i \frac{V_i^2}{2} \frac{\rho}{g_c} \qquad (1\text{-}1)$$

where the K_i's are the pressure loss coefficients around the loop for fluid friction, fittings, as well as entrance and exit losses.

The net buoyancy force developed around the loop is dominated by the two-phase flow region rather than by the natural, single-phase, density effect. Thus the hypothetical maximum buoyancy effect would be achieved with flashing starting at the base of the riser. In the actual case this limit cannot be achieved because of the formation of counter flow buoyancy effects in the heater section due to voids generated in it. In addition, the rate at which flashing can take place is controlled by other factors such as the surface tension, thermal conductivity, latent heat and specific heat of the fluid. At the lower power limit of two-phase flow operation, with flashing near the top of the riser, the system becomes very sensitive to slight changes in the position of the flash point. Thus any disturbances which can cause a change in the flash point location may cause a flow reversal when operating near one of the limits.

Non steady flow in these loops may arise from either internal or external stimulii. For example, if the power input is suddenly increased, the buoyancy in the downflow channel increases because of its increased temperature and void fraction. This initially retards the flow. When the warmer fluid reaches the riser, an increase in buoyancy occurs which substantially increases the flow. This increased flow then causes a reduction in the temperature in the heater annulus thereby enhancing the flow. However, this

cooler fluid ultimately reaches the riser thus causing a drop in the net buoyancy force which starts the next cycle. These oscillations will normally die down provided the point of flashing in the riser does not reach either the bottom or the top of the riser during an oscillation. If it does reach one of the limits, the flow will generally reverse.

Internal instabilities arise due to the intermittent nature of the bubble generation in both the boiling and the flashing mechanisms. The sensitivity of the loop to these effects may be minimized by providing good flash initiation sites in the riser. No attempt was made in this thesis to study these internal flow instabilities in detail other then through their macroscopic impact on the flow behaviour of the loop.

In summary, it is evident that the overall behaviour of downflow thermosiphon loops will be affected by the choice of fluid; the overall height H; the geometry of the conduits around the loop, particularly the heated section and the riser; the heat flux variation; flow restrictions and the temperature of the fluid at the inlet to the heated section.

1.3 THE DOWNFLOW THERMOSIPHON INVESTIGATED

One of the loops studied can be seen in figure 2. The other loops differ mainly by the types of riser sections

which resulted from geometric modifications made as the experiments were carried on.

An annulus, the geometry of which was kept fixed, was selected as the heated section of the loop. This configuration was chosen for ease of physical observation of the boiling process. An equivalent diameter of 0.25" was used as this has been found to be representative of a Canadian reactor fuel bundle.

Four different riser sizes were used and are referred to by the area ratio A_r/A_{ts} to study the effect of the velocity ratio between the two columns of fluid.

The heat flux distributions possible can be described by three parameters; namely the length of the heaters l_H, the vertical position of the bottom end of the heaters z_B and the axial heat flux distribution along the heated length. Only the effect of a uniform axial heat flux distribution using different heater lengths are reported here. Gaspar[3] studied the effect of heater position.

The overall height H, was kept fixed at 13.1', the maximum height permissible in the laboratory.

A few tests were done to study the influence of reservoir subcooling ΔT_{sc}. The non-dimensional counterpart of this variable is often expressed as $c_f \Delta T/h_{fg}$.

The test fluid chosen was refrigerant R - 113 because of its low power requirement (h_{fg} is only 65 Btu/lb$_m$), its non-toxic nature and its low boiling point (117.6°) at

atmospheric pressure. This allowed the loop to operate satisfactorily without insulation thus permitting flow visualization studies to be carried out.

The internal flow behaviour was compared to appropriate previous data. Heat transfer relations for single-phase forced convection in the range of $8000 \leq N_{Re} \leq 25{,}000$ for downflow were compared to existing correlations for internally heated annuli. Boiling data for R - 113 with heat fluxes to 25,000 Btu/hr ft^2 were compared with saturated pool boiling correlation. Frictional pressure drop data for single-phase as well as two-phase with surface boiling and slip were obtained. The data for vapour generation due to heating of a subcooled liquid was limited to flows where the fraction of the cross-sectional area taken up by the vapour (α) was less than 20%. In the riser where vapour formation occurred due to a lowering of the pressure ie. flashing, these void fractions (α) reached 75% but the percentage of mass of the vapour x remained below 5%.

The method for predicting the steady state operation of reverse flowing thermosiphons utilized homogeneous two-phase flow relations.

CHAPTER II

LITERATURE SURVEY

2.1 INTRODUCTION

A search of the literature reveals little reported work on downflow two-phase thermosiphons with which the present data could be compared. The results of some of these previous related studies are given in section 2.2. In addition, keeping in mind that the thermosiphon loops of interest function principally due to steady rather than unsteady or cyclic fluid flow, the nature of several cross-sectional phase distributions was examined and presented in section 2.3.

2.2 GENERAL BEHAVIOUR OF REVERSE FLOW LOOPS

Energy transport around a loop may be accomplished in several ways. Bonilla[4] in section 9-3 of reference [4] gives "thermalsiphon" boiling in a closed loop as one of the possibilities whose power limits for stable operation have been found as intermediate between the natural and the forced convection types. For the case of a single-phase free convection loop, Bonilla gives the following critical minimum flow rate required to maintain the downflow in the heated section:

$$\dot{m} = \left[\frac{g\beta(T_e - T_i)D_{eq}}{8f}\frac{l_h}{H}\right]^{\frac{1}{2}} \rho_l A_{ts} \qquad (2\text{-}1)$$

where $(T_e - T_i)$ is the temperature rise in the heated section

β is the coefficient of volumetric expansion

and the other variables are defined in the nomenclature. Higher flow rates are thus expected to be more steady as they can more easily overcome the opposing upward buoyancy forces in the downflowing heated section.

Chato[5] developed an analysis for natural circulation flows in vertical multi-channel systems assuming laminar flow. The experimental setup consisted of three vertical parallel glass tubes, two of which were heated, connected to common reservoirs at each end. Results showed that heating in the second channel was started after a fixed heat input in the first channel had created a downward flow in the second one, then the flow continued in the same direction until a maximum heat input was reached. At this point the flow direction in the loop was reversed. Several reversals of the flow direction were noted but no accompanying dryout condition was seen during this cyclic behaviour.

Barns[2] studied downflow thermosiphoning in a vertical reactor with a multi-channel heated section and essentially single-phase flow. To ensure single-phase downflow thermosiphoning in a system, the key factor is a sufficient loop

height to maintain an adequate flow rate. He had reservations regarding two-phase operations since undesirable pulsations may result which could lead to fluid dryout. It is evident that even for the case of steady state operation, both minimum and maximum power limits may be anticipated.

2.3 TWO-PHASE FLOW REGIMES

The common two-phase flow patterns in flow regimes for vertical flows with and without heat addition are given by Tong[6] and in a later text by Hewitt.[7] Figure 3 taken from reference 7 identifies the main patterns that may be possible in vertical flow. That is, with increasing quality, bubbly, slug, churn and annular flows may occur.

In bubbly flow, the vapour or gas phase is distributed in discrete bubbles within a continuous liquid. The void fraction is generally low.

The bubbles dispersed in a liquid will randomly lead to bubble collisions resulting in coalescence of some of them. In addition for a vertically upward flow the static pressure will fall in the flow direction thus causing the bubbles to grow to such size as to approach the diameter of the channel.

Further increases in void will lead to a break up of the slugs to form the "churn" pattern. The slugs are broken up and the vapour begins to flow up the centre of the tube forming an annular pattern containing primarily

a vapour core and a liquid film next to the tube walls.

In a study with the analysis of gas-liquid flow patterns, Quandt[8] categorized flow patterns into regimes governed by a predominate type of force. Thus two-phase regimes such as bubble and annular flows were considered pressure gradient controlled flow and to be typically well ordered and steady. Other regimes such as the slug flow he considered as gravity controlled and characteristically unsteady.

Flow regime transitions for the case of refrigerant 11 were presented by Baker.[9] Experiments were carried out using upward flowing (R - 11) in a vertical rectangular conduit. The two-phase mixture was generated by an electrically heated tube at a constant heat flux and the observed regimes were then in the unheated rectangular section above the heated one. Extension to other refrigerants and water at high pressure was made principally by the orthobaric-density (ρ_l/ρ_v) and an example of the results of the correlations is the map given in figure 4 (ρ_l/ρ_v equals 20.6). It is noted that the main regimes are the churn, annular and wispy annular. Slug flow was not observed and bubbly flow would only be present for very low qualities and be represented at the extreme left of figure 4.

As discussed by Tong[6], two-phase systems may be subject to instabilities even when operating characteristics such as the power input are kept constant. This is due

to the time variation of the two-phase regimes and their accompanying different hydrodynamic and thermo-hydrodynamic behaviour. Additional references are given in Appendix III that deal with general two-phase flow principles pertinent to the present investigation.

CHAPTER III

APPARATUS AND INSTRUMENTATION

3.1 APPARATUS

The general arrangement of a downflow thermosiphon is given in figure 2. Its principle components, which are explained below, are: the annular heated section, risers, heater cylinder assembly and condenser.

3.1.1 Annular Section (figure 5)

The annular vertical section, which had an overall length of 10.7' and an equivalent diameter of 0.0250" $\pm$ 0.008", was made from an outer tube of glass and an inner tube of copper. The ends of the annulus were sealed and the inner tube was centred using the brass plate seated with a neoprene rubber O ring shown in figure 6. Two nylon inserts (see figure 7), each containing three circumferentially spaced pins, were used to centre and secure the tube along its axial length.

The outer glass tube was made from several nominal 1" diameter QVF glass sections. Pressure and temperature probes were installed in the same types of nylon inserts at all the joints. Their exact locations are shown in figure 2.

An instrumented, seamless, drawn copper tube served as the heated surface. More details on this tube are given in section 3.1.4.

3.1.2 Risers (figures 8, 9, 10.)

The risers were made using four tube sizes, namely 5/8", 1", 1¼" and 1½" diameters. All had a common length of 13 feet but were constructed in somewhat different manners. Only the 5/8" diameter riser was fully instrumented as the others were used mainly to show the effect of diameter on loop overall performance.

The risers are identified by their diameters and the means used to initiate flashing. Risers using only the inserts are designated I-n risers where the "n" represents the actual riser diameter. Those with an orifice at the joints are designated O-n risers. Risers containing a series of equally spaced discs are designated D-n while those containing an electrically heated wire are referred to as W-n.

The I-5/8 riser (see figure 8a) consisted of nominal 5/8" diameter (0.625 $\pm$ 0.008" I.D.) QVF glass clamped together in the same manner as in the heated section. Seven pressure probes and thermocouples were located as shown. At the top the riser tube protruded into a 2 inch diameter tee such that the end of the riser was at the centreline of the 2 inch diameter reservoir shown in figure

2. The bottom of the riser was blocked and sealed with a 3/8" thick brass plate. This plate contained a hole and valve which was connected to the laboratory air supply used to initiate and maintain downflow as required to reach operating conditions.

The W-5/8 riser also seen in figure 8b was constructed from two 5' and one 3' sections of the 5/8" diameter glass. An element wire with a 0.023" diameter and an overall electrical resistance of 18 ohms was suspended in the centre of the tube.

The O-1 riser seen in figure 9a was made from identical QVF glass as the heated section. At the joints of the four locations shown in figure 9a, nylon plates 0.060" thick and orifice diameters of 0.75" were installed. Inlet and outlet connections were similar to that in the I-5/8 riser.

Two 5' and one 3' sections of nominal 1" diameter glass tubes were used to make the D-1 riser shown in figure 9b. Only the usual QVF inserts were installed at the joints but a 0.040" diameter wire containing 0.25" diameter discs spaced 4" apart were suspended along its centre.

The W-1 riser was identical to the D-1 riser except that the wire-disc arrangement was replaced by the element wire used previously in the W-5/8 riser.

Seamless copper tubing with nominal diameters of $1\frac{1}{4}$ and $1\frac{1}{2}$ inches were used to make the respective D-$1\frac{1}{4}$ and

D-1½ risers shown in figure 10a. A wire containing discs was then installed in the same way as that in the W-5/8 riser, with the disc sizes for the D-1¼ and D-1½ being 0.5" and 1.3" respectively.

The W-1¼ and W-1½ risers shown in figure 10b utilized the same copper tubes as the corresponding disc risers but contained the heating element wire used in the W-5/8 riser.

3.1.3 Working Fluid

Refrigerant 113 was used in the loop during all tests. Since the system was open to the atmosphere, some fluid always escaped during a series of tests. Thus the fluid being used had to be replenished with new liquid on a day to day basis keeping contamination to a low level.

While the complete technical data concerning the physical properties of Trichlorotrifluoroethane, R - 113, were furnished by Du Pont of Canada Ltd., both Freon 113 manufactured by Du Pont and Genetron 113 produced by Allied Chemicals of Canada Ltd. were used in the tests depending on which was available by the local suppliers. Data furnished by Allied Chemicals for their Genetron 113 was found to be identical with Du Pont's Freon 113 and hence no distinction as to whose fluid was used is made in this thesis. The relevant properties of R - 113 are listed in table 1.

3.1.4 Heater Cylinder Assembly (see figure 11)

The heated copper sheath (alloy 120) was cylindrical in shape and 12' long. Tube assembly details and dimensions are given in figure 11. Four slots 0.035" ± 0.005" deep and 0.110" ± 0.005" wide were milled along its entire axial length to serve as guides for thermocouple leads. In all there were 16 thermocouples spaced as shown in the figure. The close spacing of some of the thermocouples permitted the determination of the axial heat conduction at the ends of the heaters and the surface temperature fluctuations between the heaters.

To form a smooth surface and to contain the leads, the slots were filled with common Le Page's two component epoxy. Due to an accidental burnout condition, the slots on the bottom portion of the tube were later filled with epoxylite 813 supplied by William T. Bean Inc. Both products were good as they were not affected by the freon and retained their bond throughout the tests.

The beads of the thermocouples (0.025" diameter) were placed circumferentially away from the slot 0.050" by inserting them in holes drilled at an angle from the slot. These beads were then secured to the copper tube by peening them from the top. The thermocouples were estimated to be located 0.015" ± 0.005" from the surface of the tube.

The copper tube was heated using Chromalox cartridge heaters. One of the two 5/8" diameter heaters used was a

3' heater (35.5" heated length), the specification number CL-446R, and was rated 3500 watts at 240 volts. The other was a CL-458R, 4' heater (47.5" heated length) rated 3800 watts at 240 volts. Very early tests were done using two 10" long, 5/8" diameter CL-406R heaters. The diameter of the heaters was reduced in size to 0.618" in order to fit snugly inside the copper sheath. Male-female threaded connections were silver soldered on their ends to give a variety of heated lengths. Power leads used with these heaters were 12 gage multi-stranded asbestos covered wires with a clear plastic outer covering. These wires were used to position the heaters vertically within the copper sheath.

3.1.5 Condenser

The condenser was a shell and two tube pass unit with the cooling water in the inner copper tubes and the freon in the shell of the heat exchanger. This outer shell was made from nominal 4" diameter QVF glass and the overall length of the unit was approximately 72 inches.

There were three banks of six tubes with each tube having a 0.375" ID and a length of 10'. On inlet there were three headers, each with a control valve, while on the outlet there was one common header and valve. Each end of the U shaped condensing tubes was connected to its respective header by an accomodating length of soft, polyvinyl

tubing clamped over the copper ends. Leaking problems followed due to the freon causing the tubing to shrink, harden and eventually pull free. The problem was solved by sealing with Le Page's Plastic Rubber and keeping the tubing pressurized with a continuous flow of cooling water.

The outer shell had an opening to keep the loop at atmospheric pressure. A secondary cooling coil made from nominal 1/8" diameter tubing having a total length of 3 feet was installed at this exit to recondense some of the freon vapour that was escaping, particularly during the start up operation.

3.2 INSTRUMENTATION

The detailed specifications of the instruments used for the various measurements are listed in Appendix I. The instrumentation is as follows:

3.2.1 Thermocouple Circuitry (figure 12)

The axial fluid temperature distribution in the annular test section was obtained using eight 36 gage stainless steel sheathed iron-constantan ceramocouples all taken from the same stock. The beads, made with a spot welder, had an average diameter of 0.010". The signal obtained was then transmitted to a 24 channel thermocouple switch by means of 26 gage iron constantan leads with Thermo-Electric miniature MSP plugs and MSJ jacks used for

connections between the two wire sizes.

Temperatures in the riser, near the mass flow meter, in the copper sheath and in the bottom horizontal section were obtained using 30 gage copper-constantan thermocouples. The beads, made with a thermocouple welder, had an average diameter of 0.025" and the signal was led to a second 24 channel rotary switch by leads consisting of the same 30 gage wire.

The emf's at the two separate thermocouple switches were measured with two Honeywell potentiometers that could be read accurately to within $\pm$ 0.002 millivolts.

An ice-point unit made by Thermo-Electric (Canada) Ltd. was used as a cold reference junction for all temperature measurements. Periodic checks against an ice bath indicated that the accuracy of the unit was within the range from 0 C to 0.05 C specified by the manufacturer.

3.2.2 Static Pressure Measurements (figure 13)

Both absolute and differential pressure measurements were obtained using probes made from 0.040" ID stainless steel hypodermic tubing. These probes were installed in the nylon inserts previously mentioned (see figure 7) and functioned as wall taps. Brass fittings were silver soldered onto the ends of the probes to allow for a connection.

The leads for the differential pressure measurements consisted of nominal 1/8" diameter copper tubing. A $\frac{1}{4}$"

OD brass fitting was then soldered onto the ends of the leads. Nylon tubing $\frac{1}{4}$" in diameter joined the leads and the probes. It was found that visual inspection for air bubbles during the filling operation was made easy with this arrangement. The manometer connection had $\frac{1}{2}$" diameter neoprene rubber tubing between the glass U tubes of the manometer and a short length of nylon tubing which joined the longer copper leads. A standard hypodermic needle connected to an intravenous bottle could now be easily inserted and withdrawn for the purpose of injecting fluid to eliminate air trapped in the lines. Contact of the freon with neoprene rubber was found to result in an expansion of the rubber and eventual cracking so that the rubber connections had to be replaced approximately every three months.

The leads for the absolute pressure measurements were made entirely from the $\frac{1}{2}$" diameter nylon tubing. Connections at the ends were similar to those described previously.

The manometer for the differential pressures, including the "mass flow" meter can be seen in figure 13. The U-tubes all having diameters of 0.250" OD and 0.060" ID were inverted to allow use of the system fluid to function as the manometer fluid. The level of the manometer fluid was adjusted by means of air passed through the air valve connected to the short glass section. During fillup or after a flow reversal the air could be released, thus

purging the vapour trapped in the lines. Subsequent addition of air lowered the fluid to the desired level. Furthermore, since the manometer leads were angled down form the probe, no vapour could be found trapped during operation.

The scale on the board was such that the reading accuracy of the manometer was 0.1" of R1- 113.

The gage pressure was obtained using 0.10" ID glass U tubes, 30 inches in length, mounted vertically near the bottom of the loop. The manometer fluid was triple distilled mercury and the reading accuracy was 0.05" of H_g.

3.2.3 Density Measurement (figures 14, 15)

The mean density of the fluid in the two-phase regions of the loop was obtained with an Acou-Ray unit. The unit passes gamma rays through a slit opening of 1/8" x 1" with the one inch dimension in the vertical direction.

In the heated section, the rays emerged from the slit (see figure 14), passed along a diameter through the glass, the annular space, the copper sheath, cartridge heaters and out through the same path on the other side. The emerging rays were then picked up by the detector unit. The output from this unit is from a control console which contains a voltmeter, power supply and stabilizing circuitry. An output for a recorder is also provided for a permanent record of the events.

The operation principle of the unit is such that

the emerging gamma rays from the cross-section of the tube to the pickup unit continuously ionize a gas in a chamber. The result is a voltage signal which is affected continuously by the density of the fluid. The stabilizing circuitry of the unit merely averages this voltage signal. Further, so that the unit could be operated at its maximum sensitivity while keeping the fluctuations to less then $\pm 1\%$, the signal was averaged with an R-C network just before it reached the recorder resulting in a time constant of 5 minutes for the recorder signal.

The sensitivity of the unit and recorder were adjusted so that from an empty to full pipe there was a deflection of 90 units out of a possible 100 on the recorder giving a sensitivity of approximately 1.1 lb_m/ft^3 per division. With this value, it was not necessary to distinguish between an air filled pipe or one containing freon vapour.

The unit was checked for linearity between density and deflection by filling a glass tube with several known liquids. No deviation from linearity over the present range was noted.

The detector and source components of the unit were traversed vertically by means of a trolley. This trolley was mounted on wheels so that it could be moved from the test-section to the riser side. A winch with a self locking 20:1 gear arrangement was used to manually raise and lower the units. The slit opening was aligned with the centre-

line of the tube by means of two bars that could be locked in place by preset guides on the frame of the trolley.

3.2.4 Mass Flow Measurement (figure 16)

The mass flow rate was measured using a modified venturi meter connected to the aforementioned inverted U-tube manometer.

The venturi (see figure 16) had a throat to inlet diameter ratio of 0.527 with the straight portion of the throat 0.52" long. A total pressure probe was added and mounted in the centre such that the tip of the probe was aligned with the flow. This probe, along with a wall tap at the throat gave the maximum sensitivity.

The entire unit, flanged at the downstream end, fitted snugly into the 1" diameter glass section immediately upstream of the annulus inlet tee at the top of the annulus.

The unit was calibrated (see section 4.1) in place and the accuracy of the unit is estimated to be within 3%.

3.2.5 Power Supply Circuitry (figure 17)

Electric power was supplied to the cartridge heaters by means of two AC voltage variacs. The one was a 240 volt Variac autotransformer and was connected directly to a 220 volt AC supply. The second source was a 110 volt variac autotransformer the output of which was doubled

with a 10KVA transformer borrowed from Ontario Hydro. Total power input was measured with two 0-1000 volt voltmeters and two 0-5-20 ampere ammeters connected as shown in figure 17.

CHAPTER IV

EXPERIMENTAL PROCEDURE

4.1 GENERAL PROCEDURE

The thermosiphons were filled daily primarily to prevent accidental loss of fluid in the event of pressure connections failure. Filling was performed from the bottom of the loop where the fluid was forced into the system from a pressurized reservoir bottle. When the level of freon reached the centreline of the 2" diameter reservoir section at the top, the valve at the bottom was closed and the system was full. Air which remained trapped in the pressure leads was now purged from the lines by forcing fluid through them with a hypodermic needle connected to a pressurized supply. The level of the fluid in the sloping manometer was then adjusted to a suitable height by introducing air through the valves. In the mercury manometers the air was bled off with a hypodermic needle.

The air supply at the bottom of the riser was turned on to begin circulating the liquid. Power was supplied to the heaters causing the fluid in the system to heat up. As the fluid temperature increased, the circulation rate increased since some flashing of liquid into a two-phase mixture occured. The air was gradually turned down until eventually it was completely shut off and the loop was

operating in the desired downflow manner.

These filling and purging procedures were generally performed in approximately one hour and the loop could then be made operative in 10 to 15 minutes.

The system was permitted to reach steady state for each power setting. Steady state was clearly defined when steady readings were obtained from the manometers and potentiometers. The value of all thermocouples, power inputs, manometers, barometer, room temperature etc were measured and recorded.

The mean density measurements for a given power setting required the gamma ray unit to be moved. Initial tests were done two ways. In one test, the unit was moved to the six positions previously marked and calibrated for empty and full pipe deflections. Readings were then taken from the non-boiling to the boiling range. The second method was to leave the unit at a fixed position and vary the power input such that there was a change of density from non-boiling to boiling. In this way the density could be interpolated correctly since the sensitivity and at least one density was known from the temperature measurement. The two methods were chosen in order to check the repeatability of the void distribution and the latter method was then used in the annulus and the I-5/8 riser.

The mass flow meter required calibration since only a one point measurement of the pressure was being made. For this calibration, performed with the I-5/8 riser, the

bottom horizontal tube of the loop was removed. The bottom of the riser was then connected through a valve to a pressurized supply drum while the bottom outlet of the test-section was connected by a valve to a drum on a Toledo scale. Fluid circulated at various rates, depending on the constant head and valve setting, through the loop and into the second drum. When the manometer reading was steady and the rate of weight increase on the scale appeared constant, initial and final weights, time interval and the manometer reading were recorded. The same rates were repeated several times and the entire operation was performed over a range of mass flows. The results are given in figure 18.

The power limits of the thermosiphons were obtained by increasing the inputs in small increments and allowing the system to reach steady state. The power variation near the limits was 5% and the limits quoted are those within 5% of the reversal.

The loop was open to the atmosphere at the top and it was considered that there was no change in pressure there due to vapour formation in the loop. Tests showed that a small change in liquid level had a negligible effect on the performance.

Still and high speed motion pictures were taken during the course of several test runs.

4.2 MODIFICATIONS AT VARIOUS STAGES OF DEVELOPMENT

The loop underwent a series of geometric changes as the experiments proceeded. It was found that the single most significant factor governing the stable operation of two-phase downflow thermosiphons was the requirement of suitable nucleating devices in the risers to initiate the flashing. A chronological sequence of the consequences of various changes that were made follows.

The initial test run with a 5/8" diameter riser consisting of three long sections of glass and standard QVF connections resulted in the loop not functioning. An orifice was then inserted in the riser 5' from the top with the result that flashing began downstream of this orifice making the loop operative. However, the stable operation was such that the maximum length of the flashing mixture was only approximately 5' out of a total possible length of 13'.

It was felt that perhaps the size and position of the orifice was significant. Thus a 5/8" diameter riser was made similar to that shown in figure 8a but with a 5' section rather than the 2' and 3' pieces at the top. It was found that orifices were not required anywhere along the length since flashing occurred at these inserts. Furthermore, tests using smaller orifices showed the performance actually decreased. In the meantime the two 10" heaters originally used were replaced by the 3' and 4' heaters

previously described. This was done to allow a higher input at a lower heat flux in an effort to lower the position of flashing in the riser. The final I-5/8 riser described was such that flashing could occur further up the riser and hence lower the minimum operating point.

The requirement of nucleating devices was most clearly demonstrated when the 1" diameter risers were installed. The first riser was identical to the O-1 riser but without the 0.752" diameter orifices. The loop would not function without them nor would it operate with orifices having diameters of 0.88". The final orifice diameter of 0.75" was required.

Since an improvement in performance was noted as the riser size increased, it was decided to increase the riser diameters further. However, larger glass sizes were not readily available and were very heavy. Furthermore, only overall performance data was sought and thus the entire riser was made out of copper as one unit with no instrumentation. Since it was apparent from the O-1 loop that a continuous distribution of nucleating devices was desirable, a wire disc arrangement was suspended in the centre resulting in the D-1¼ and D-1½ risers. A dependence of disc size on riser diameter was later found for stable downflow operation.

The requirement of 1¼" diameter discs in a 1½" diameter tube for proper initiation of flashing was felt to significantly reduce the maximum circulation rate and the corresponding power dissipation. Thus risers consisting of the four

previous tubes were so constructed that they contained a heated wire capable of generating bubbles that could act as nucleation sites. These were the W-n risers.

4.3 DESCRIPTION OF SPECIFIC SERIES OF TESTS

The specific series of tests done to establish the overall behaviour of downflow thermosiphons are described in detail in Appendix II. The purpose of each can be categorized into three main areas which are listed and discussed below:

The first series of tests was done to show the effect on the power limits of riser size and heated lengths in the presence of minimum flow restrictions, reservoir temperature near its saturation temperature (ie. $\Delta T_{s,i} = 0$.) and bottom end of the heated length at the exit of the annulus. For these tests, the W-n risers are used.

The second group of tests shows the effect of different nucleating devices on the overall behaviour. All previously described risers are used. The heated section was kept constant at 7' and the reservoir subcooling and heater position were the same as in the first tests.

The third group of tests was meant to give indications of a number of variables which were either difficult to study with the present apparatus or were of an exploratory nature. The variables considered are inlet subcooling, flow resistance by means of a valve at the bottom cross-

over section of the loop and transient heater temperature during a reversal.

The tests for which internal flow data were obtained are also shown in Appendix II. Performance data showed that the maximum circulation rates were not significantly increased with the risers larger than those with a 1" diameter. Thus the heat transfer, void fraction and pressure loss data all taken for a given run were limited to the 5/8" and 1" risers shown in the Appendix. The flashing data was taken on the I-5/8 riser.

CHAPTER V

EXPERIMENTAL RESULTS

5.1 EXPERIMENTAL PERFORMANCE OF DOWNFLOW THERMOSIPHONS

5.1.1 Power Dissipation and Circulation Rates

The overall performance or ability of downflow thermosiphons to dissipate energy is shown in figures 19 to 21. These results were obtained under the conditions which were found to be best; that is, the heater length was the longest (7'), at the bottom ($z_B = 0$, see figure 2) and flow restrictions were at a minimum (ie. W-n risers). The reservoir temperature was kept at approximately 116°F.

The power dissipation limits using different riser sizes are given in figure 19. Observations in the two glass risers, W-5/8 and W-1, revealed that single-phase heat transfer was present in the heated section at the lower power level and flashing occurred in the riser at approximately 1½ feet from the top. At a power input of approximately 60% of the maximum, subcooled boiling began in the heated section. This boiling became more vigorous and the void generation rates increased with further gradual increases in power. At the upper limit, heater section void fractions as high as 25% were measured. Some of these vapour bubbles were carried over into the risers where flashing then began within 2 feet from the bottom. Figure 19 also reveals that

the limits are independent of area ratios greater than approximately 3 but are appreciably affected for lower values. However, further discussions on riser behaviour (see section 5.1.2) will show that operative or design requirements become more severe as the riser size increases.

The circulation rates in these loops are shown in figure 20 as a function of input power Q. It can be seen that the flow rate increases linearly with power and the slope $d\dot{m}/dQ$ is a maximum for the A_r/A_{ts} equal to 2.3, which gives the largest range of operation. It is also to be noted that the maximum flow rates achievable (H and the heated section are constant) seem to be approaching a limit as the area ratio increases.

The exit fluid temperatures using the W-n risers and previous operating conditions are given in a non-dimensional form in figure 21. The efficiencies η_1 and η_2 shown in the figure are defined as the actual fluid temperature increase realized over the maximum possible, ie. where the fluid exits from the heated channel at the saturation temperature. For the evaluation of η_1, the saturation temperature used is that corresponding to the hydrostatic pressure (ie. $P_a + \gamma_1 H$). Thus efficiency represents the variation of ΔT_1 with riser size. Since the inlet temperature was kept fixed at 116°F, it follows that T_e decreases at the upper limit and remains constant at the lower limit as the area ratio increases. The saturation temperature at the actual experimentally measured pressure at the base of the loop was used in the

evaluation of η_2 as shown in the figure. At the upper power limit, this efficiency initially increases and reaches a constant of 0.81 as the area ratio increases. What this indicates is that the fluid always remains subcooled in the heated section of the loop and that the decrease in T_e with area ratio is due to a lowering of the pressure as a result of increased frictional losses with the higher flow rates. A similar η_2 variation is seen at the lower power limit. A subsequent model for predicting stable regions of operation uses η_1 to generate an initial mean power input for a given loop.

The above observed trends of the power dissipation limits, circulation rates, and decreasing maximum fluid temperatures as the area ratio increases are due to a number of interrelated parameters. Consider, for example, what happens to the pressure in the two vertical columns such as those previously shown in figure 2. In order for the fluid to flow in the direction indicated, the piezometric pressure must decrease in the flow direction. In fact, the larger this pressure gradient, the higher will be the circulation rate and thus factors that raise the pressure at the bottom of the riser and/or decrease it at the outlet of the heated section will be favourable. As the area ratio increases and becomes >1, there will be a pressure recovery of the velocity head in the riser side. This has the same effect as a lower fluid temperature at the inlet to the riser in so far as it delays the flashing until further up the tube, a condition known to reduce the circulation rate. More significantly,

however, is the fact that with an increasing area ratio lower frictional losses will occur in the riser and since the pressure is fixed at atmospheric at the top, it means a lowering of the pressure and corresponding saturation temperature at the bottom. At the same time as there is a tendency for lower fluid velocities in the riser, there is an increase in $\dot{m}$ (see figure 20) so that the velocity in the heated section increases as the area ratio increases. This higher velocity increases the frictional losses and hence lowers the pressure and corresponding saturation temperature. Since there is a limit to the void fractions that can be tolerated in the heated section and since the void present is a function of the subcooling, lower maximum fluid temperatures must result as observed.

The effect of using different heater lengths on the power limits of the previous loops is shown in figures 22 and 23. It is evident in figure 22 that the effect of different heater lengths becomes more pronounced as the area ratio increases; for example, the area ratio of 0.9 shows only a 10% rise in the maximum energy dissipation for a variation of the heated length (l_H/H) from 0.2 to 0.5 while at an area ratio of 5.1 this increase is approximately 30%. On the other hand, while increasing the heated lengths for downflow thermosiphons is possible, the improvement in performance seems minor for l_H/H greater than 0.5 for the two glass risers used since the flashing occurred virtually

over the entire length. While the actual lower limits were not obtained for these loops using the instrumented heater sheath, some early tests with an I-5/8 riser and short heaters indicated no operation for l_H/H less than 0.07.

The circulation rates and fluid temperature increase ratios η_1 and η_2 for the shorter three and four foot heaters were found to be similar to those shown in figures 20 and 21 for the seven foot heater. This would imply that, within the limits tested, the heat flux distribution is not one of the dominating factors controlling the mass circulation rate.

This area of the study was limited in the number of heated lengths that could be investigated because of the presence of the 3' heater below the 4' one. The space between the bottom of the loop and the floor was 1.5' so that the 4' heater could only be lowered to a minimum value of z_B equal to 1.5'. Thus the power limit shown for the 4' heater was that actually obtained at z_B equal to 1.5 and its value increased by a constant value of 20%. This correction was found by R. Gaspar[3] using this heater and the first 5/8" diameter riser described in section 4.2.

Comparison of the heat transferring capability of the downflow thermosiphon with the normal flow is shown in figure 24. The minimum operating limits of the two modes of operation are similar. Below this limit the downflow loop will reverse itself while the normal flow loop will pulsate. It was observed that in the normal flow at

these low powers, the fluid spontaneously flashed at various positions above the heated section. These transient conditions caused erratic heater temperature and fluid pressure fluctuations. Since the flashing occurred in a similar fashion to that in the riser for downflow operation, it may have been possible to lower this minimum limit somewhat by artificial nucleation sites. While this was not done, since these tests were merely to show comparison of the two modes of operation, it may be an interesting possibility for future problems of this nature. At the upper limit, it is evident that the normal flow loop operates to much higher power limits than the downflow type. The maximum shown for the normal operation was that obtainable with the present equipment and it is expected that the limit is somewhat beyond that shown here.

5.1.2 Riser Behaviour

A significant characteristic of the downflow thermosiphons studied is that single-phase subcooled liquid entered the bottom of the risers and vapour generation occurred due to flashing. For these loops to operate, the flashing had to be initiated by artificial nucleation sites so that the vapour formation could take place within approximately 2.0 feet of where the fluid temperature equalled its local saturation temperature. The effects of the various devices used (see section 3.1.2) on the power limits are shown in figures 25 and 26. The size and power requirements for the

discs and heater wires respectively are given in figures 27 and 28.

As seen in figure 25, the effect of discs and inserts are minimal initially but gradually decrease the performance. The corresponding mass velocities G_{riser} shown in figure 26 are somewhat similarly affected; that is, there is no significant difference in fluid velocity between risers of the same size except for the one giving an area ratio of 5.1. This peculiar behaviour is a result of the disc and power requirements shown in figures 27 and 28. The required orifice area ratio, defined as the total crossectional riser area minus the disc area divided by the riser area, is seen to become smaller (requiring larger discs) as the riser size increases. The result is that the circulation rate will be reduced due to increased frictional resistance of the proportionately larger discs. The power limits using the W-n risers are also shown. Power requirements for sufficient bubble production to properly initiate flashing are given in figure 28. It was found that for smaller area ratios the power required for the wire compared to the maximum that could be dissipated in the heated section is less than 10%. At the area ratio of 5.1 this requirement has risen to approximately 20%.

It is evident from this data that the effect of the size of the riser in addition to the relative dimensions previously used must be considered. The size of the bubbles

generated have not been seen to be significantly affected by an increase in riser area since they are governed by the surface tension, thermal properties etc. Hence, for a physically larger riser more sites are required so that together, they can provide a sufficient initial void fraction (approximately 5% in our loops) to cause flashing within the required riser length. It may, therefore, also have been more correct to use A_r rather than the area ratio in the above two figures. The latter was used, however, for convenience of identification between the previous performance data and the appropriate requirements set out here. Further study may need to be made on the effect of pipe size on flashing for a given fluid before scaling up of the loops will be successful.

Another interesting feature can be seen in figure 26 by examining, for example, the 1" diameter risers. The D-1 and W-1 both show a linear variation between the mass velocity G and the power input Q. The slight difference may be due to the frictional effect of the discs in the D-1 riser. A deviation from linearity is observed in the O-1 risers due to the lack of distributed nucleating devices. It was observed that when the power input was increased but insufficient to initiate flashing at a next device further down the riser, the mass flow rate was approximately the same. With additional power a sudden jump in the flashing position occurred and the flow rate increased. Inspection of the O-1 riser geometry in figure 9a shows no orifice

within the bottom three feet of the riser and hence the mass flow rate could not increase with power input near the maximum operating limit as seen in figure 26. A similar event occurred with the I-5/8 riser.

5.1.3 Other Effects

The results of other observations made during the development and testing of the loops are shown in figures 29 to 31.

The effect of a change in inlet subcooling (ie. changing the reservoir temperature) is given in figure 29. Increasing the reservoir subcooling allowed an increase of maximum heat dissipation of approximately 30% over that at the saturated condition. The minimum power limit, however, was increased even more resulting in a range of operation which would appear to vanish for higher inlet subcooling. This was verified indirectly by our inability to achieve operation of the loop during start up until the reservoir temperature exceeded 100°F. Exit temperatures were the same as those previously found for the saturated reservoir conditions.

The effect of a valve located at the outlet of the heated section can be seen in figure 30. A reduction of the power limit was noted when the valve was approximately three-quarters closed. It was felt originally that the valve would lower the pressure on the riser side and hence lower the point of flashing thus increasing the flow rate. In actual fact, the circulation rates were reduced and this in turn gave the power limits shown.

Some transient heater temperatures for the W-5/8 risers during flow reversals below the minimum operating limit are shown in figure 31a. The maximum temperature rise was 7.5% over the downflow value and no burnout condition was noted. Complete reversal from downflow to normal upflow took place within 40 seconds. The corresponding results for reversal occurring when the power input is above the maximum operating limit is given in figure 31b. At the bottom of the heater, the temperature actually decreased during a reversal. The heat transfer mechanism occurring in this region was subcooled nucleate boiling which is dependent on the fluid saturation temperature. Thus when the flow rate decreased, there was an increase in void volume which lowered the pressure and hence heater temperature. At the top of the heated section, on the other Hand, forced convection heat transfer took place and this caused the fluctuating heater temperatures shown. The oscillating nature of this curve is due to the fact that the fluid oscillated two or three times before the final upflow condition was reached.

These tests were repeated several times to check the heater temperatures at locations between the end positions discussed above. No temperature excursions in excess to those above were noted. Consideration may also need to be given to the fact that the reversal, being a transient phenomenon, would be affected by the inertia of the fluid. Thus while some observations made using larger risers showed

no significant deviations from the above results, there was, however, the somewhat offsetting effect that the loop containing a higher mass had a lower initial riser velocity before reversal took place.

5.2 HEAT TRANSFER RESULTS AND CORRELATIONS

5.2.1 Surface and Fluid Temperature Distributions

Some typical surface and fluid temperature distributions in the axial flow direction are shown in figures 32 to 36. This data was subsequently used to evaluate the heat transfer coefficients and wall superheats occurring in the operation of these loops. The two risers used, that is, the I-5/8 and O-1, represented the data for the complete range of Reynolds' numbers possible.

From an examination of the wall temperatures given in these figures, it is evident that the nominal 3', 4' and 7' heaters had actual heated lengths of only 2.65', 3.75' and 6.4' respectively. During the grinding operation to reduce the overall diameter, the ends of the heaters were made approximately 0.003" smaller than the central portion of the tubes. The brass joint had an even smaller diameter. Thus at these positions on the heater there was no contact with the copper sheath resulting in the observed lengths. The surface areas used for the calculation of the heat fluxes were all based on these experimentally determined

lengths.

The data for the 7' heater is shown in figures 32 and 34. Note the severe effect of the joint. Virtually no heat is transferred across the joint by the copper sheath as is evidenced by the fact that the spot on the sheath where no heat generation occurred radially remained only 5° above the fluid temperature. A similar trend was seen at the ends, where using the temperature gradients indicated, the amount of heat conducted out axially was less than 1% and has been neglected. The beginning of the heated section was constructed using the heater length indicated in figure 33 and the slopes on the top heater were obtained by moving the heaters vertically and locating the temperature shown starred the same distance from the inlet. Another interesting result is shown in figure 34. For the maximum power setting indicated, the fluid separated around three centering pins located 2' from the bottom and formed three columns. Each of these wakes or cavities was approximately $\frac{1}{4}$" wide giving a total flow area reduction of 40%. Examination of the heated surface further revealed that no new bubbles were forming in this portion of the tube. Thus it was evident that the reduction in flow area increased the velocity such that boiling was suppressed and forced convection took over. A calculation of the heat transfer coefficient from a forced convection correlation at this velocity was in agreement with that obtained by these wall temperature measurements.

Figure 35 shows the 4' heater. It was from this

figure that the actual heated length for the nominal 4' heater was obtained. Some boiling occurred at all but the lowest power setting and the slopes indicated over the inlet portion were the same as those of the fluid temperature distribution. Since all subsequent heat transfer coefficients were based on actual readings, these constructions of the distributions were only made for visual purposes and, thus, no additional error to heat transfer correlations was introduced here.

The wall temperatures at the maximum heat fluxes attainable with these loops ie. those using the 3' heater, are given in figures 33 and 36. Some boiling occurred at all the power inputs indicated. In figure 33, the actual heated length and the temperature gradients at both inlet and outlet are illustrated. Both figures show that the effect of increased heat and accompanying increase in void fraction is to actually suppress the wall temperatures. As previously discussed, in the nucleate boiling process, the heat transfer potential is the wall superheat ($T_w - T_{sat}$). The generation of vapour has been found to lower the pressure and hence saturation temperature. Thus, depending on the degree of boiling and/or void present, increasing the heat flux will either only moderately change or maintain the wall temperatures as observed.

The accompanying liquid axial temperature distributions shown in these figures were all reasonably linear. While a deviation from linearity, even with a constant heat flux,

may be expected due to the energy required by the boiling process for the generation of vapour, a calculation of the quality (assuming slip S equals 1), for a α_{max} of 20% results in only a 0.35°F drop in temperature. This, in light of the fact that the accuracy of the measurement was only $\pm$ 2°F can account for suppression of non-linearity shown.

An estimate of the convective heat transfer coefficients at the outer glass tube was made using the heat losses calculated from the energy equation and all liquid flow in the tube. In addition, temperatures were obtained of the outer glass and of the room. These resulting coefficients were then used to estimate heat losses during boiling in the tube and losses thus found were generally <5% of the power input. Thus fluid temperature measurements were considered adequate for the evaluation of fluid properties and temperature potentials ($T_w - T_l$), but not accurate enough to establish a subcooled axial liquid temperature distribution for future use in the evaluation of void fractions.

5.2.2 Heat Transfer Coefficients Realized

The axial distributions of the heat transfer coefficients obtained from the previous data is shown in figures 37 to 39. These coefficients are defined in the usual single-phase way ie.

$$h = \frac{Q}{A}/(T_w - T_l) \qquad (5\text{-}1)$$

The variation of h over the heated length of the

nominal 7' heater is shown in figure 37. Note the gradual increase in these coefficients as the heat flux and hence boiling intensity increases. In the case of the 3' heaters shown in figure 39, the heat transfer coefficients increased by as much as 30% over the non-boiling case.

The corresponding Reynolds' and Nusselt numbers for these coefficients resulted in the map given in figure 40. All fluid properties used were evaluated from the experimentally obtained fluid temperatures. During the non-boiling runs, the values of h and hence Nusselt numbers N_{Nu} were relatively constant over the heated length. Increasing the power input to the heated surface initiated and/or further increased the boiling causing larger increases in Nusselt numbers in the flow direction.

The non-boiling data was correlated using Reynolds' number and Nusselt number as independent and dependent variables respectively. The results obtained were:

$$N_{Nu} = 0.070\ N_{Re}^{0.78} \qquad (5\text{-}2)$$

When this is reduced to Wiegand's[A-3] geometry factors and Prandtl number dependence, it becomes

$$N_{Nu} = 0.029\ N_{Re}^{0.78}\ N_{Pr}^{0.4}\ (D_o/D_i)^{0.45} \qquad (5\text{-}3)$$

The data used to obtain equation (5-3) was for Reynolds' numbers greater than 10,000. The estimate of the Grashof number for limited data at a Reynolds'

number equal to 8000 showed the buoyancy effect to be negligible while the experimental results give Nusselt numbers to be 15% lower than that indicated by equation (5-3). Since the functional dependence of the Nusselt number on the Reynolds' number to the 0.8 power is well established (see table II) and inclusion of this data results in a variation of the Reynolds' number to the 0.87 power, it was not included in the correlation.

Comparison of the present correlation with that of other investigators given in table II showed no significant difference. Similar conclusions were reached by Stenning[12] in comparing upflow and downflow heat transfer in vertical pipes.

5.2.3 Subcooled Nucleate Boiling

The heat flux given in figure 41 as a function of the wall superheats are for all the readings obtained under boiling conditions. This data exhibits considerable scatter from the inlet to the outlet (that is from left to right on a constant heat flux line) of the boiling tube, since the two regimes of nucleate boiling are present (Appendix III-1.2). Due to the heating, the fluid's temperature and hence wall temperature will increase in the flow direction in the regime of partial nucleate boiling. The increase in wall temperature, however, will increase the boiling intensity for the same heat flux and thus generating more bubbles that can act as heat pumps

to cool the tube. A limit to the increase in heat transfer coefficient for a given heat flux is known to exist and this limit forms the fully developed nucleate boiling curve. For this reason, the data chosen for a boiling correlation was that where the wall superheats were approximately constant for a given heat flux. This produced the line shown in figure 41. The line obtained by Tang[17] for saturated pool boiling is also shown for comparison. The wall superheat required to initiate boiling was found to be approximately 14°F, a figure used for the simulation.

The Rohsenow correlation for the present (R-113-copper surface) as well as that of previous investigators, is shown in figure 42. The values obtained for the coefficients C_{sf} and r equal 0.0043 and 0.29 respectively. As discussed by Tang, there is a definite dependency of r on surface preparation technique while the coefficient C_{sf} is somewhat dependent on the geometric arrangement and the unpredictable nucleating characteristics of the heating surface. In light of the fact that the boiling wall superheats and boiling Reynolds numbers $N_{Re,b}$ have possible maximum errors of $\pm$ 2% and $\pm$ 8% respectively, the differences between saturated pool boiling and the present nucleate downflow boiling are not considered to be significant.

5.3 VOID FRACTIONS

5.3.1 Subcooled Nucleate Boiling

The axial density and void fraction distributions pertaining to the tests for which the temperatures were previously reported are given in figures 43 to 47. No density measurements could be made below one foot from the bottom due to the shape of the unit and the presence of the horizontal portion of the loop. There were further limitations to physical axial locations because of the presence of the glass joints.

As seen in the figures, the maximum void fraction for which steady state data was taken is approximately 20%, but in the majority of the loop's operating range α is below 10%. It can be seen that considerably higher void fractions and heat fluxes can be tolerated using the larger diameter riser.

In figures 45 and 46 are shown more complete distributions of the density variation. The rate of change is approximately linear right up to the end of the heated section of the tube. The measurements at the end show that the bubbles collapsed fairly rapidly. Considering the velocity of the bubbles and the liquid to be equal (to be discussed further) to 3.4 ft/sec at the highest power input, the collapse rate of freon 113 $d\alpha/dt$ has been calculated

as 27% per second when the liquid is subcooled by 10°F. Similar results were obtained at the other flow rates.

The void fractions in the presence of cavitation which occurred at the maximum power input are those shown in figure 45. In this run, the fluid separated at the bottom centering pins and flowed in three columns of fluid. The void columns were observed to be each approximately $\frac{1}{4}$" wide at the pins and gradually decreased in size until they disappeared near the exit.

In order to obtain the slip between the phases in the above flows, the relative velocity of the bubbles was calculated from Stokes' law. Since the maximum rise velocity, and hence slip, would occur with the largest bubbles, it was only necessary to establish an upper limit to the diameters of the bubbles present. This was done by a physical comparison between the bubbles and known dimensions of some isolated scratches on the surface of the heated wall. The maximum diameter of the bubbles was thus estimated to be 0.02". Then assuming, as did Nicklin,[18] that the bubbles are travelling in the central portion of the annulus so that V_{max} - Slip Velocity $\doteq V_{mean}$. A similar conclusion was reached by examining some high speed films of the two-phase mixture which showed that the bubbles were of similar size, very spherical and did not appear to be displaced relative to one another. The entire mixture was seen to move in unison in the downward direction.

of the tube, the fluid temperature drops approximately 0.2° per foot giving an average heat loss of 80 Btu/hr per foot. When the flashing begins, the liquid temperature decreases further due to vapour formation. It is noted that the measured temperature distributions in the flashing portions of the tube are also fairly linear. The distribution with the highest inlet temperature and hence highest flow rate was that obtained using the non-instrumented heated section, which had allowed a somewhat higher upper limit.

The corresponding pressure distribution is shown in figure 50. In the single-phase region, the distribution is seen to be linear. The flashing region shows a lower pressure mainly due to the lowering of the gravitational pressure component caused by the drag on the liquid by the vapour bubbles. A nearly linear pressure distribution is noted in this portion of the riser as well.

The void distributions in the riser are shown in figure 51. These values were obtained from the density measurements and using fluid properties evaluated at the temperature obtained in figure 49. It can be seen that the distributions are reasonably parallel to each other and that the void fraction increases most rapidly immediately after flashing is initiated. The highest void fractions had vapour carryover of approximately 2% from the heated section. Note that in the presence of these initial voids, the explosive nature of initial flashing has been considerably

reduced.

Using the results of these three figures, the slip S and the liquid superheats $T_l - T_{sat}$ were evaluated. Assuming thermal equilibrium between the two phases and that flashing occurred at the position in the riser where the fluid temperature equalled the saturation temperature, the quality x was calculated using equation (6-12). This value was substituted into equation (6-7) along with the appropriate void fraction given in figure 51 to obtain S. These results are represented by the upper distribution in figure 52a. The procedure was repeated by substituting the values of the measured temperatures in equation (6-12). The results of this calculation are intermediate between the equilibrium method described above and the Bankoff slip model also shown. It can be seen that all three evaluations have become approximately equal when α is 75%. The value of S at this void fraction was thus taken to be that shown. At low voids, large differences occurred due to the extremely low quality, ($\leq$0.1%), involved in the evaluation of S. In order to obtain S in this low void fraction range, physical observations were made of the bubble velocity and the slip S was found to be approximately equal to 1.5. Bankoff's model was seen to be adequate for the present case. Note also that since the slip obtained using the measured temperatures

was between the completely equilibrium model and the one deemed to be correct, the liquid temperature measurements in flashing flows will tend to give some average value between the superheated liquid and cooler vapour.

The liquid superheats, as a function of the void present, are given in figure 52b. Comparison of the two distributions leads one to believe initially, in the case of low voids, the error in measurement due to the presence of vapour is small. Accuracy requirements for the liquid temperatures become impractically high, however, due to the low quality. As the vapour content increases, the error in assuming that the temperature obtained equals the liquid temperatures becomes greater until α is approximately 50%. Beyond that point, the difference in the two models decreases due to the fact that the phases are approaching equilibrium saturation conditions.

Another interesting aspect to be noted in figure 52b is the apparent increase in superheat after some vapour bubbles have been produced. Recall in section IV-2.2.2 that the growth of the bubbles is a function of the thermal properties. A bubble generated at a given position z in the riser will travel at a rate approximately 1.5 times the liquid velocity up the riser. However, the liquid is flowing in the direction of pressure and hence saturation temperature decrease and the bubble is generated in a region where the liquid superheat is 5°F. Thus by the

the time the bubble has grown such that the growth accelerates the flashing by lowering the local pressure and hence saturation temperature, the bubbles' position is further up the tube where the superheat is higher. A liquid superheat curve for water flashing in a adiabatic vertical tube given by Delhaye[11] is seen to behave similar to that obtained by the present results.

5.4 PRESSURE LOSSES

5.4.1 Subcooled Nucleate Boiling

The pressure gradients existing in the annular section of the loop using the three heaters and the I-5/8 and O-1 risers are given in figures 53 to 57. Examination of these figures will show an inlet effect resulting in a lower pressure gradient and an exit effect giving higher ones than those in the central portion of the flow passage.

It is known that in the developing region of an annulus, the friction factors are higher than in the subsequent fully developed flow. Wiegand's[(A-3)] study gave a fully developed length in the Reynolds' number range indicated for his heat transfer correlation of 20 D_{eq}. In the present case this would be a length of 0.42 feet which is within the region of the inlet pressure drop reading. Other studies by Farman and Beckman[(A-2)] on the effect of a 90° entrance on the developing length gave similar results.

At the exit, the fluid streamlines curve in order to exit from the T section. An examination of the location

of the pressure probe in this area shows that the probe's opening is in the area of the curved streamlines, thus giving higher pressure gradients. Subsequent values of the friction factor neglected the first and last measurements shown on these graphs.

The gravitational and momentum components of the pressure gradient were evaluated using equation (A-31) and (6-16) respectively. The resulting mean friction factors in equation (6-20) were then calculated from the remaining friotional component of the total pressure gradient and plotted as a function of the local liquid Reynolds' number, only; ie.

$$N'_{Re} = \frac{G}{(1-\alpha)\mu_l} D_{eq} \qquad (5\text{-}4)$$

The two symbols used in figure 58 are to differentiate the results obtained with and without boiling occurring at the inside surface. It is evident from the scatter that no significant difference between the two cases could be made. This may be partly due to the fact that for a given inlet Reynolds' number, the presence of voids caused an increase in the local liquid Reynolds' number. Thus, since the data is in the vicinity of the smooth wall value, the friction factor would decrease. In addition, an analysis of the possible errors in the friction factors ($\pm$ 16% for non-boiling and $\pm$ 24% for the boiling data),

shows that unless the differences were substantially larger than these limits, no significant difference could be established. Thus it seems reasonable to use non-boiling friction factors in the low void range studied here.

5.4.2 Vertical Flashing Flow

The experimentally determined pressure gradient variation in vertical flashing flow is shown in figure 59 for the four power inputs for which the void and temperature measurements have previously been discussed (see section 5.3.2). Also given in this figure for the sake of comparison are the gradients obtained using the modified homogeneous flow theory and the measured void fraction data (equation A-32 in section III-3.2).

It can be seen that the gradient in the single-phase region is approximately constant since a higher frictional component was accompanied by lower gravitational components. In the flashing region, the gradient decreases in this region of the riser. However, as the distance from the initial point of flashing increases, the rate at which the pressure gradient decreases becomes less severe.

The pressure gradients in the limited flashing region studied here were also obtained using the homogeneous flow theory and are seen to be generally lower than the experimental values by 8% at the exit. The friction factor used in these calculations was 0.008 which was the average value

obtained from data in the single-phase region. While this value is higher than the smooth wall value of 0.006 in the Reynold's number range considered here ie. $24,500 \leq N_{Re} \leq 38,000$, the effect of the joints and nylon inserts present in the I-5/8 riser can create disturbance and frictional drag not otherwise expected in a smooth glass tube.

The friction factors obtained by assuming the density to be that given by equation (A-32) and measured pressure gradient are seen in figure 60b to be more than twice as high as the single-phase value. This is thought to be due to the flashing causing a developing flow in the tube. It is known that in the entrance regions of pipes and annuli, the friction factors for the same Reynolds' number are higher than in the subsequent fully developed region. As in single-phase flow, theoretical prediction of these factors would require consideration of the velocity and void profiles in the radial and axial directions over a wide range of Reynolds' numbers, inlet conditions and viscosities.

CHAPTER VI

ANALYTIC MODEL

6.1 INTRODUCTION

The method used to simulate the steady state operation of reverse flow thermodiphons is an iterative procedure in which a mass flow is assumed, the steady-state one-dimensional equations applied around the loop for both single and two-phase flow, and flow rates adjusted to ultimately give a zero pressure change around the loop. The calculations proceed for different power inputs from minimum (where no flashing occurs in the riser) to a maximum (where $d\dot{m}/dQ$ becomes negative).

The equations are stated and the various relations used in the model are given in section 6.2. The basic assumptions and solution procedures are given in section 6.3.

6.2 CONSERVATION EQUATIONS

The steady state, one-dimensional conservation equations used in the present model are given below. These equations do not consider the effects of mass addition or chemical reactions. The equations are:

$$\text{Continuity: } \frac{d\dot{m}}{dz} = 0 \qquad (6\text{-}1)$$

Energy: $\frac{d}{dz}(\dot{m}_l \bar{H}_l) + \frac{d}{dz}(\dot{m}_v \bar{H}_v) = q_{\text{net in}} P_h$ (6-2)

Momentum: $\frac{dP}{dz} = -\frac{\tau^P_w}{A_{cs}} - \bar{\rho}\frac{g}{g_c} - \left(\frac{dP}{dz}\right)_{\text{acceleration}}$ (6-3)

i) Continuity Equation

In the presence of two-phases, equation (6-1) becomes

$$\frac{d\dot{m}}{dz} = \frac{d}{dz}(\dot{m}_v + \dot{m}_l) = 0 \qquad (6\text{-}4)$$

Equation (6-4) can be integrated and rearranged by introducing the quality x and the void fraction α. That is

$$x = \dot{m}_v/\dot{m}$$

and $$\alpha = A_v/A_{cs}$$

Therefore, from equation (6-4)

$$\dot{m} = (\dot{m}_v + \dot{m}_l) = \text{Constant} \qquad (6\text{-}5)$$

or $$\frac{x}{1-x} = \frac{\dot{m}_v}{\dot{m}_l} = \frac{\rho_v A_v V_v}{\rho_l A_l V_l} \qquad (6\text{-}6)$$

Therefore,

$$S \equiv \frac{V_v}{V_l} = \frac{x}{1-x}\,\frac{1-\alpha}{\alpha}\,\frac{\rho_l}{\rho_v} \qquad (6\text{-}7)$$

ii) Energy Equation

The energy equation (6-2) can be integrated considering that there is zero quality on inlet to the heated section.

$$\int_{(\dot{m}_l\bar{H}_l)_i}^{\dot{m}_l\bar{H}_l} d(\dot{m}_l\bar{H}_l) + \int_0^{\dot{m}_v\bar{H}_v} d(\dot{m}_v\bar{H}_v) = \int_0^{l_H} q_{\substack{net \\ in}} P_h \, dz \qquad (6\text{-}8)$$

$$\text{or} \quad \dot{m}_l\bar{H}_l - (\dot{m}_l\bar{H}_l)_i + \dot{m}_v\bar{H}_v = q_{\substack{net \\ in}} P_h (l_H - z) \qquad (6\text{-}9)$$

where the net energy added is expressed as

$$q_{\substack{net \\ in}} P_h = \frac{\text{Power Input}}{\text{foot}} - \frac{\text{Heat Loss}}{\text{foot}} \qquad (6\text{-}10)$$

Introducing the quality into equation (6-9) and rearranging gives:

$$x_{sub} = \frac{q_{net_{in}} P_h (l_H - z)/\dot{m} - (\bar{H}_l - \bar{H}_{l,i})}{\bar{H}_v - \bar{H}_l} \qquad (6\text{-}11)$$

Considering that vapour formation can take place under non-equilibrium conditions, equation (6-11) is expanded to:

$$x_{sub} = \frac{q_{\substack{net \\ in}} P_h (l_H - z)/\dot{m} - c_l(T_{sat} - T_l(z=l_H))}{h_{fg} + c_l(T_{sat} - T_l)} \qquad (6\text{-}12)$$

iii) Momentum Equation

Assuming that the vapour and liquid components can each be represented by a mean velocity, the acceleration component of the pressure gradient is written as

$$\left(\frac{dP}{dz}\right)_{acceleration} = \frac{1}{A_{cs} g_c} \frac{d}{dz} \left(\dot{m}_v V_v + \dot{m}_l V_l\right) \quad (6\text{-}13)$$

Introducing the quality, void fraction and mass flow per unit area G, equation (6-13) becomes

$$\left(\frac{dP}{dz}\right)_{acceleration} = \frac{G^2}{g_c} \frac{d}{dz}\left[\frac{x^2}{\alpha \rho_v} + \frac{(1-x)^2}{(1-\alpha)\rho_l}\right] \quad (6\text{-}14)$$

For the low qualities achieved in bubbly flows, the vapour acceleration term is negligible compared to the liquid acceleration term. In addition, the dx/dz term is negligible compared to the dα/dz term. Thus:

$$\left(\frac{dP}{dz}\right)_{acceleration} = \frac{G^2}{g_c} \frac{(1-x)^2}{\rho_l} \frac{d}{dz}\left[\frac{1}{1-\alpha}\right] \quad (6\text{-}15)$$

or

$$\left(\frac{dP}{dz}\right)_{acceleration} = \frac{G^2}{g_c \rho_l}\left[\frac{(1-x)}{(1-\alpha)}\right]^2 \frac{d\alpha}{dz} \quad (6\text{-}16)$$

The pressure gradient due to the shear forces on the boundaries of an annulus can be written as

$$\frac{\tau P_w}{A_{cs}} = \pi\left[(\tau D)_{outer} - (\tau D)_{inner}\right]/A_{cs} \quad (6\text{-}17)$$

where each τ is related to its friction factor f by

$$\tau = f \rho_l \, V_l^2/2 \, g_c \qquad (6\text{-}18)$$

If separate friction factors are available then

$$\frac{\tau P_w}{A_{cs}} = \frac{2 G^2}{g_c \rho_l} \left[\frac{1-x}{1-\alpha}\right]^2 \frac{f_o D_o + f_i D_i}{D_o^2 - D_i^2} \qquad (6\text{-}19)$$

In terms of an overall annulus friction factor

$$\frac{\tau P_w}{A_{cs}} = \frac{f_a}{D_{eq}} \frac{G^2}{g_c} \left[\frac{1-x}{1-\alpha}\right]^2 \frac{1}{\rho_l} \qquad (6\text{-}20)$$

If the two-phase mixture can be considered as a single homogeneous fluid having a mean density $\bar{\rho}$ and velocity $\bar{V}$,

$$\tau_{w,n} = f \bar{\rho} \frac{\bar{V}^2}{2 g_c} \qquad (6\text{-}21)$$

Then $$\frac{\tau P_w}{A_{cs}} = \frac{f}{D_p} \frac{2}{g_c} \frac{G^2}{(1-\alpha)\rho_l + \alpha \rho_v} \qquad (6\text{-}22)$$

Equation (6-20) was used in the annular section ($\alpha < 20\%$) while equation (6-22) was used in the riser.

The mean density used to evaluate the gravitation component of the pressure gradient was obtained using equation (A-31).

6.3 MODEL

6.3.1 Assumptions

In using the relations given in section 6.2 for calculating the various pressure changes around the loop, the following assumptions are made.

1. No slip between phases in the subcooled boiling region (section 5.3.1).

2. Transition from single-phase heat transfer to subcooled boiling occurred when the wall superheat, as calculated for single-phase forced convection, reached a value where the heat flux calculated by the boiling mechanism exceeded that for the forced convection mechanism.

3. In the subcooled boiling region, the liquid temperature distribution varies as that in the relation

$$\frac{T_l - T_b}{T_{sat} - T_b} = \text{Tanh} \frac{(z_{bi} - z)\, q\, P_h}{\dot{m}\, c_l (T_{sat} - T_b)} \qquad (6\text{-}23)$$

where T_{sat} is the saturation temperature based on the local static pressure.

4. Frictional pressure gradients in the subcooled boiling region were calculated sequentially for increments along the annulus using single-phase relationships but allowing for the increase in liquid velocity due to the presence of voids. The momentum component was evaluated using equation (6-16).

5. No vapour carryover from the heated section to the riser is considered to take place.

6. The liquid remains in a single-phase state until its temperature reaches a superheat condition of 3°F above

the local saturation temperature. Beyond this point the fluid flashes at such a rate that the liquid temperature decays linearly along the balance of the riser equalling the condenser saturation temperature at its exit.

7. For the flashing region it was assumed that the fluid could be treated as a homogeneous one having an apparent velocity and density calculated using the continuity equation (6-7) with values of slip S obtained from Bankoffs' model. In addition, a friction factor equal to that used in the single-phase portion of the riser was utilized in the remaining, two-phase portion. The acceleration component was evaluated using equation (6-16).

6.3.2 Model Critique

A discussion of the previous assumptions is given in the following section. Additional references are given in Appendix III and are designated as An.

Assumption 1 was found valid for R - 113 under the present flow conditions. This assumption can easily be modified for other fluids with larger bubbles and lower slip ratios. The points of initiation of boiling have been found by Rohsenow[A6] and Gause[A7] for water and R - 113 respectively. Thus for other surfaces and fluids, these relations can be used to replace the constant value used in the present model. Assumption 3 concerning the liquid temperature distribution has been found valid for both water

and other refrigerants.

In the riser, vapour carryover from the annulus into the riser occurred only for power inputs within 10% of the maximum. Thus the inherent loop operation is not dependent on vapour carryover. Assumption 6 is perhaps the most serious limitation. At present no general method exists for predicting the initial flashing superheat. From the present experiments, the flashing was initiated from bubble sites generated by cavitation devices or a boiling surface such as a wire thus giving two different mechanisms for flashing inception. The present model predicts the ideal, or limiting, power rates possible - ie. when the flashing initiates at or near saturation conditions. While assumption 7 was found valid for the low quality flows found here, any of the standard methods such as Lockhardt-Martinelli could be used for higher qualities expected for loops with larger heights H.

6.3.3 Solution Technique

A flow chart of the computer program is outlined in Appendix VI. A brief description of the method follows.

The program generates an initial estimate of the mean power input for a given loop from the following equation.

$$Q_{in} = \dot{m} c_l (T_e - T_i) \qquad (6\text{-}24)$$

The mass flow rate was calculated by considering that one column is liquid while the other has vapour formation initiating at one half the height of the column. Thus the initial mass flow rate of the liquid is estimated by

$$\dot{m} \doteq \rho_l A_r \sqrt{\frac{\rho_l - \bar{\rho}}{\rho_l} 2 \left[\frac{H}{2}\right] g}$$

or $$\dot{m} = \rho_l A_r \sqrt{\alpha H g} \qquad (6\text{-}25)$$

In addition, the temperature rise for any height H can be estimated with the help of figure 21. For example

$$(T_e - T_i) = .45(T_{sat,h} - T_{sat,i}) \qquad (6\text{-}26)$$

where $T_{sat,h}$ is the temperature corresponding to the hydrostatic pressure at the exit of the heated section.

For the power input and mass flow rate, the heater wall temperature in the downflow column is calculated using a single-phase heat transfer coefficient. If the wall superheat $(T_w - T_{sat})$ is found above that required for inception of boiling (14°F in present case), a two-phase calculation of pressure drop, quality etc. is made. For lower wall superheats, single-phase pressure changes are calculated.

In the upflow column, where the pressure decreases in the flow direction, the location where the local saturation temperature equals the local liquid temperature (or some-

what below the liquid temperature to allow for liquid superheating) is determined using the energy equation. The pressure and quality are now evaluated up the riser to the exit.

The pressure at the exit is compared with the known reservoir pressure. For a calculated exit pressure higher than that of the reservoir, the mass flow is increased. For a lower exit pressure, the mass flow rate is decreased.

The resulting mean power inputs and mass flow rates are then varied incrementally, first progressively increasing until the maximum power limit is reached ($\dot{m}/dQ = 0$) and then decreasing from the mean values to the minimum. Since there is a good degree of linearity between the power input and mass flow rate over the steady state operating range, the entire range was evaluated with a minimum of computing effort.

The basic procedure is expected to be valid but the two-phase model will need to be changed if a flow regime map such as that given in figure 4 indicates a regime for which the homogeneous flow theory is not valid. To make this check, the initializing procedure for mass flow rates and temperature rise given here may provide useful information such as mass flow rates, temperature rises, etc., that is, flow parameters required to estimate the flow regime.

CHAPTER VII

COMPARISON OF COMPUTED AND EXPERIMENTAL LOOP BEHAVIOUR

7.1 Flow Patterns

As was the case of the higher pressure test for freons and water reported by Baker[9] (see section 2.3), no slug flow was noted in the present tests. As indicated in the literature survey, however, expansion processes may be erratic if the intermediate phases between bubbly and annular flow are present. For that case, steady thermosiphon operation may be limited. Also the Baker maps for steam-water and freons at higher pressure are useful although limited to specific geometries.

In the present downflow heated section, the bubbles generated during boiling were found to be generally less than 0.020" in diameter. The Froude number was always greater than 0.31 and the vapour was removed as predicted by the map based on air-water studies given in reference 16. Also being of such relatively small size, the bubbles contributed no significant fluctions to the loop operation. Upward buoyancy forces in the heated section during steady downflow were calculated to be negligible.

The procedure described in section 6.3 was tested using primarily the homogeneous flow model. For other applications when dealing with different fluids and geometries,

an investigation into the general flashing and boiling behaviour may be necessary in order to make appropriate changes in the model. The method of solution is expected to be similar.

7.2 Comparison of Computed and Experimental Results

Computed flow rates and power inputs for the four riser sizes previously discussed are shown in figure 61. The maximum power limits are taken to be where $\dot{m}/dQ = 0$ since a negative value of $\dot{m}/dQ$ represents an unstable condition which would result in reversal for a real system. For this region an increase in Q reduces the flow rate, thereby increasing the void fraction in the heated section which in turn results in a further decrease in mass flow rate until dryout and flow reversal occur. The minimum power limits predicted are those when flashing has ceased in the riser.

The computed results incorporating the power inputs shown in figure 28 are also given. In the W-5/8 and W-1 risers, no significant difference could be distinguished as the powers were relatively low. In the W-1½ and W-1½ risers, the computed distributions agree with the experimental results at the upper limits. The computed lower limits are higher than observed. The heated wire caused boiling and hence early flashing thus resulting in decreased lower limits. On some experimental tests with the W-1 riser

it was noted that the flashing position in the riser could be lowered by as much as 1.0 foot when the power in the heated wire was increased.

In order to generalize the data as much as possible the loop flow circulation rate was nondimensionlized using the Reynolds number for single phase flow at the inlet to the annular heating section. The power input rate was non-dimensionalized through the product of this Reynolds number and a vapour production quality term

$$X = \{\text{Net heat input} - \dot{m} C_\ell [T_{sat,i} - T_i]\} \dot{m} h_{fg,i}$$

Figure 62 shows the composite predicted results for the test loop configuration using R-113. The dotted lines represent the locus of the predicted limits of operation. The minimum power input limits are little affected while the maximum power limits increase as l_H/H increases.

Figures 63 and 64 show comparisons of the predicted and experimental results as functions of flow area ratio and heater length ratio respectively. The computer solution indicates no operation possible above area ratios of 11.5. Furthermore, the range of operation decreases and the maximum Reynolds numbers and power input remain relatively constant for area ratios greater than approximately 4. Agreement is good for the higher heater length ratios but differences of up to 20% occur for the shorter heaters. This difference is possibly due to the empirical void fraction predictions in subcooled nucleate flow boiling.

Figure 65 shows the effect of reservoir subcooling

on the system performance. No operation is found to be possible for reservoir subcooling above 21°F. Extrapolation of a least squares-fit of the experimental data predicted a limit of approximately 22°F. The power limits agree within 10% while the predicted Reynolds' numbers are approximately 15% lower than the experimental values. It is noted that the differences of the computations and experiments are no more than the observed scatter of the subcooled data.

Figures 66 and 67 give computed characteristics when the working fluid is water and the liquid superheat required to initiate the flashing remains at 3°F. The characteristics in figure 66 look very similar in shape to those obtained with R - 113 in figure 62. The same data presented as a function of area ratio in figure 67 show quite different behaviour. The Reynolds' number continues to increase with an increase in area ratio. Larger operating ranges over a wider range of area ratios are indicated than with R - 113. The limiting values of area ratios at the minimum and maximum are 0.4 and 14 respectively. Agreement with the water data at the one available point is good.

The solution for loops at various heights using R - 113 and l_H/H equal to 0.5 is shown in figure 68. With an increase in height the maximum power input increases, while the flow rate or Reynolds' number begins to approach a constant. It should be noted that the resulting increase

in the fluid temperature rise along the heater is due to an increase in the saturation temperatures at the base of the loop. On the other hand the frictional pressure drop increases thereby reducing the potential increase in flow rate with increasing overall height.

In conclusion, it is evident that from the experimental observations on the fluid flow, heat transfer and overall loop behaviour it is possible to predict operating characteristics under a variety of area ratios, heater lengths, inlet subcooling etc. However, while the general computing procedure can produce these operating characteristics, proper initiation of flashing must be provided in order to obtain these performances in practice.

CHAPTER VIII

CONCLUSIONS AND RECOMMENDATIONS

The results of the experimental and theoretical study lead to the following conclusions.

1. It has been found that it is feasible to predict the operating characteristics of downflow two-phase thermosiphons provided suitable assumptions concerning the initiation and behaviour of flashing are made. The predictions can then include the effects of heater length ratios, area ratios, inlet subcooling, riser diameter and height on the vapour generation rates possible.

2. The correlation for single-phase forced convection found in this investigation was identical to Farman and Beckman's. Model predictions were better when the present correlation was used rather than the more well known Wiegand relation.

3. Sufficient means to initiate flashing in the riser must be provided for stable downflow operation. This was accomplished in tests using cavitation devices or a heated wire such that boiling occurs on its surface.

4. The slip during flashing flows studied here (void fractions up to 75%) was indicated to be that given by the Bankoff model. Several degrees of liquid superheated c in the flashing portion of the riser were noted and incorporated in the model.

5. The fluid temperature at the exit of the heated section always remained below the local saturation temperature thus only subcooled boiling occurred in the heated section.

6. The saturated pool boiling correlations appear applicable to the present subcooled nucleate flow boiling data. Values of C_{sf} and r in the Rohsenow equation for boiling were found to be 0.0043 and 0.29 respectively for this copper surface - R - 113 combination. The data falls between the Tang correlation and that of Lieppert and Dougall.

7. The slip between the liquid and vapour phases was seen to be negligible for the subcooled downflow nucleate boiling considered here ($D_b \leq 0.02$").

8. The non-dimensional liquid temperature rise along the heater section during downflow subcooled boiling

was found to vary as the hyperbolic tangent of the non-dimensionalized distance down the annulus rather the more common exponential relationship.

9. Friction factors in the annular heated section were found to be essentially the same for both the boiling and non-boiling cases.

10. From both experimental observations and predictions, it was found that the largest range of operation occurred at an area ratio of 2 to 3 where the upper limit was also within 8% of the maximum limits attained with the larger area ratios.

11. Comparison between downflow and normal flow operation shows that the lower power input limits for stable operation are similar but the downflow loop reverses and the normal flow loop oscillates.

12. An increase in inlet subcooling increases both the upper and lower power input limits. The minimum limit, however, showed a higher power increase with the result that the range of operation became progressively smaller. No operation with a 1" diameter riser was possible

at an inlet reservoir subcooling greater than approximately 22°F. Predictions indicate a value of 21°F.

13. Experimental measurements indicated that no excessive heater temperature transients were noted during reversals.

14. Studies using water as the working fluid showed reasonable agreement between the predicted power limits and those attainable with the single geometry tested.

It is recommended that for application of the present data and method to other fluids and geometries, studies be made on the initiation and subsequent flashing behaviour of the chosen fluid. Otherwise deviations of actual performance from the model predictions may be significant.

REFERENCES

1. McKay, I. N. — April, 1967. Design simplification in the HWR. CANADIAN NUCLEAR TECHNOLOGY. 16: 25-27.

2. Barns, G. M. and Rogers, J. T. — 1969. Downflow thermosiphoning in a nuclear reactor. SECOND CANADIAN CONF. OF APPLIED MECHANICS. 241-242.

3. Gaspar, R. — M.A.Sc. Thesis. Oct. 1973. University of Windsor.

4. Bonilla, C. E. — 1958. NUCLEAR ENGINEERING HANDBOOK. New York: McGraw-Hill.

5. Chato, J. C. — November, 1963. Natural convection flows in parallel channel systems. TRANS. ASME. 85 (series C): 339-345.

6. Tong, L. S. — 1965. BOILING HEAT TRANSFER AND TWO-PHASE FLOW. New York: John Wiley.

7. Hewitt, G. F. and Hall-Taylor, N. S. — 1970. ANNULAR TWO-PHASE FLOW. New York: Pergamon Press.

8. Quandt, E. — 1965. Analysis of gas-liquid flow patterns. CHEMICAL ENGINEERING PROGRESS SYMPOSIUM SERIES. No. 57, 61: 128-135. Boston.

9. Baker, Jill — 1965. Flow regime transitions at elevated pressures in vertical two-phase flow. ANL - 7093.

10. Simpson, L. L. — June 17, 1968. Sizing piping for process plants; Section 1: Process piping systems. CHEMICAL ENGINEERING. 75: 192-214.

11. Delhaye, J. H. — 1969. General equations of

two-phase systems and their applications to air-water bubble flow and to steam-water flashing flow. ASME Paper No. 69-HT-63.

12. Pujol, L. and Stenning, A. H. 1969. Effect of flow direction on the boiling heat transfer coefficients in vertical tubes. SYMPOSIUM SERIES OF THE CANADIAN SOCIETY FOR CHEMICAL ENGINEERING. pp. 401-453. New York: Plenum Press.

13. Dean, R. C. J. 1953. AERODYNAMIC MEASUREMENTS. Cambridge, MIT Press.

14. Schrock, V. E. 1969. Radiation attenuation technique in two-phase flow measurements. Two-phase Flow Instrumentation. ASME PUBLICATION. pp. 24-35.

15. Petrick, M. and Swanson, B. S. 1958. Radiation attenuation method of measuring density of a two-phase fluid. REV. SCI. INSTR. 29, No. 12: 1079-1085.

16. Simpson, L. L. 1968. Sizing piping for process plants. CHEMICAL ENGINEERING. 192-256.

17. Tang, T. S. 1970. A study of nucleate boiling heat transfer over a horizontal rotating cylinder. Ph.D. Thesis, University of Windsor.

18. Nicklin, D. J. 1962. Two-phase bubble flow. CHEMICAL ENGINEERING SCIENCE. 17: 693.

19. Petrick, M. July, 1962. A study of vapour carryunder and associated problems. ANL 6581.

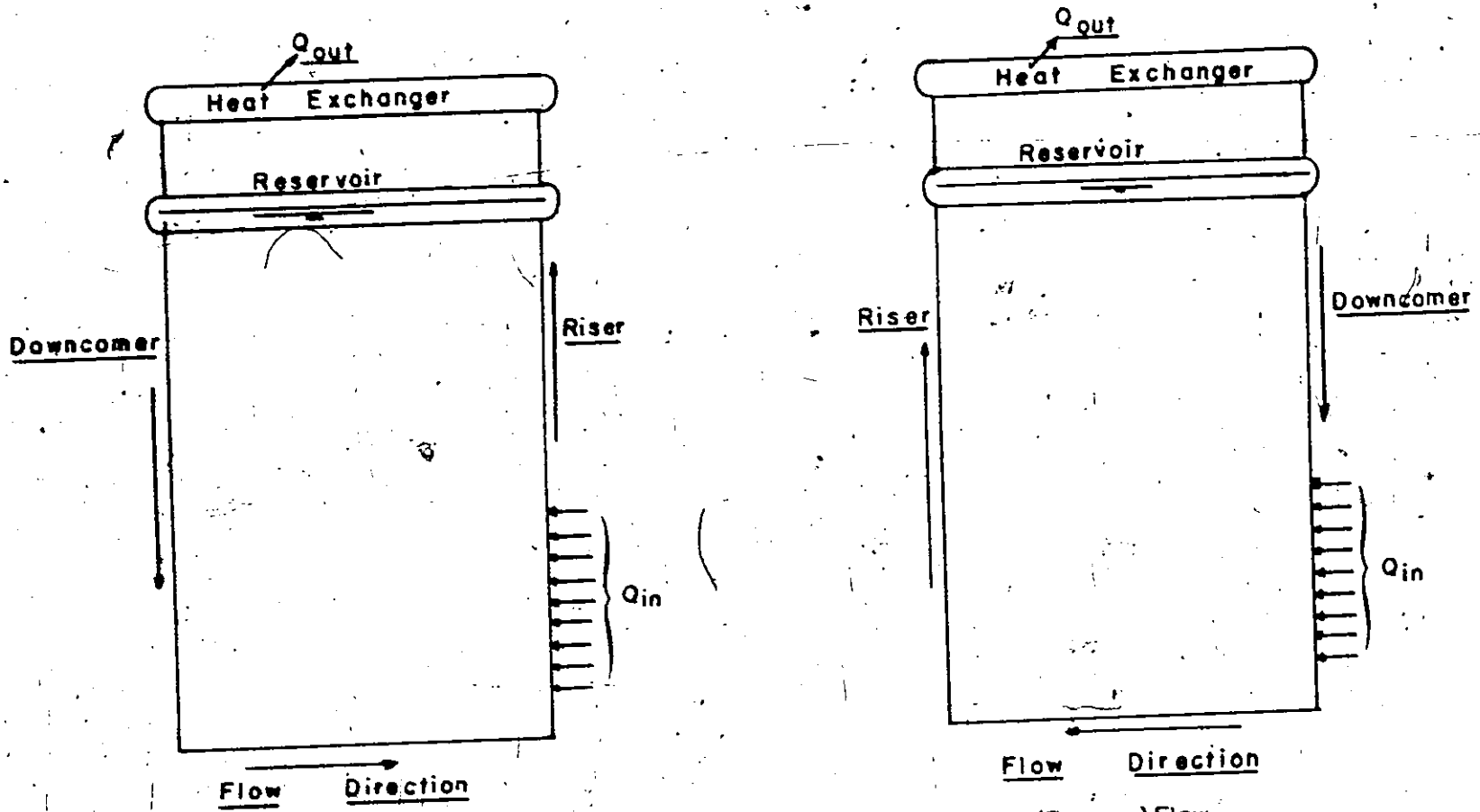

Fig 1 Principle Modes of Thermosiphon Operation

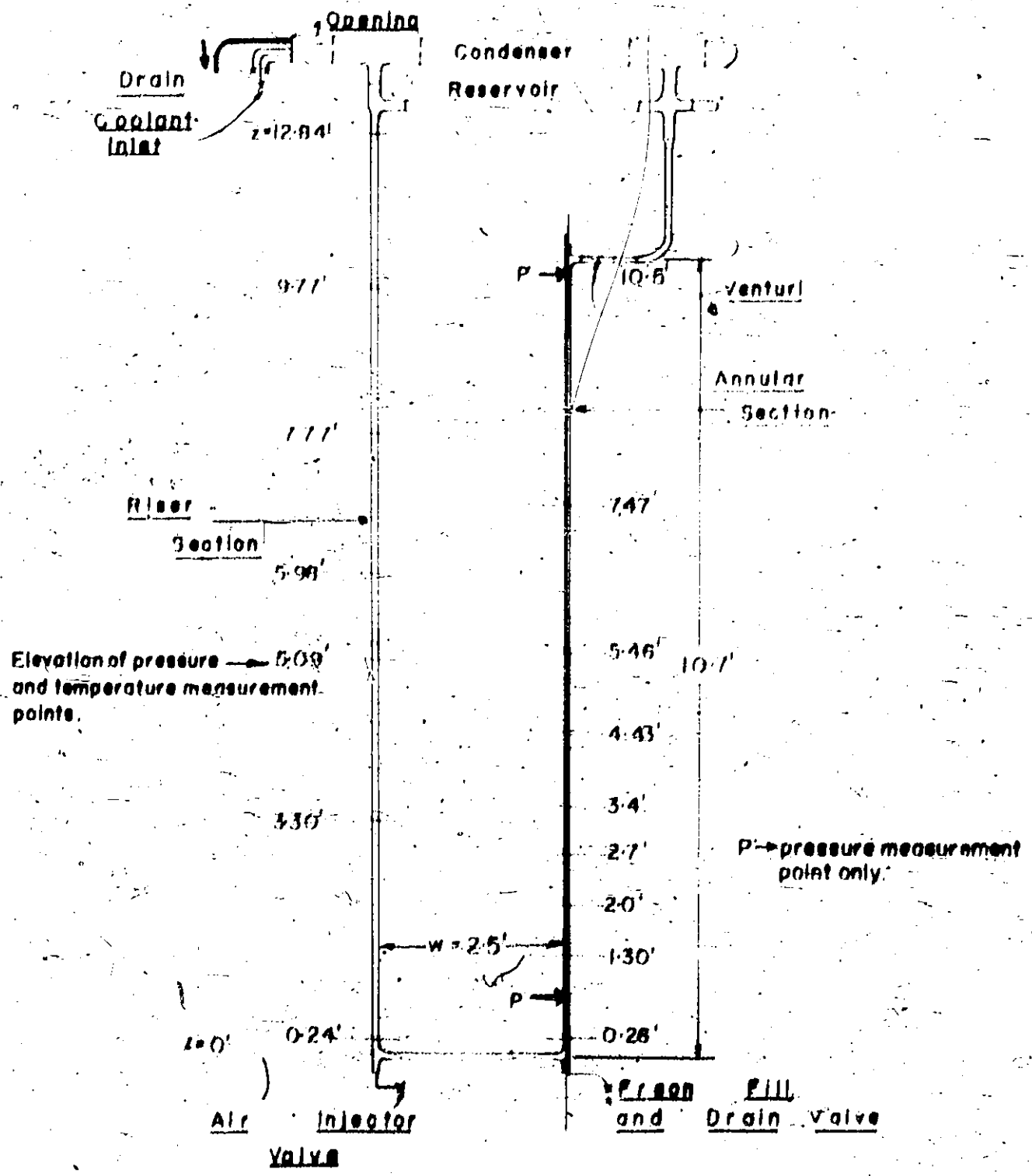

Fig 2 Downflow Thermosiphon Apparatus

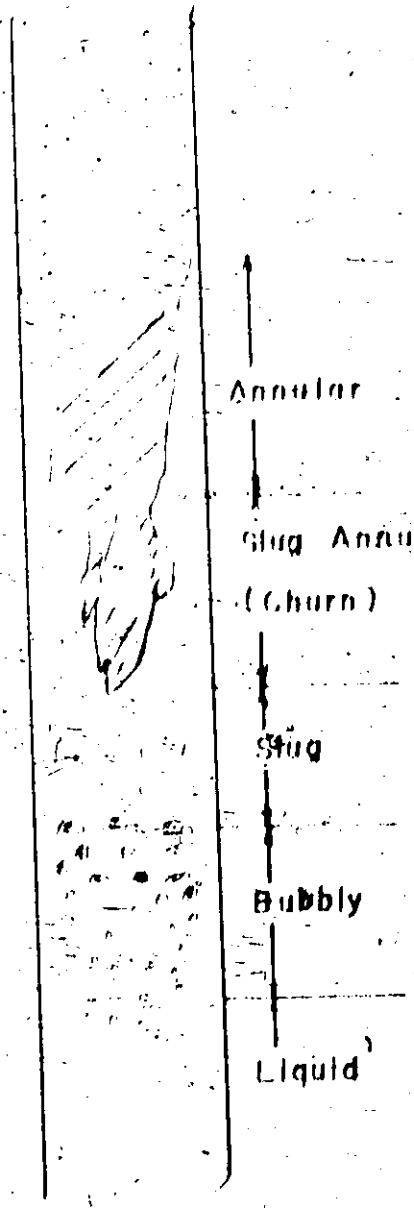

Fig 3 Flow Patterns In Vertical Flow

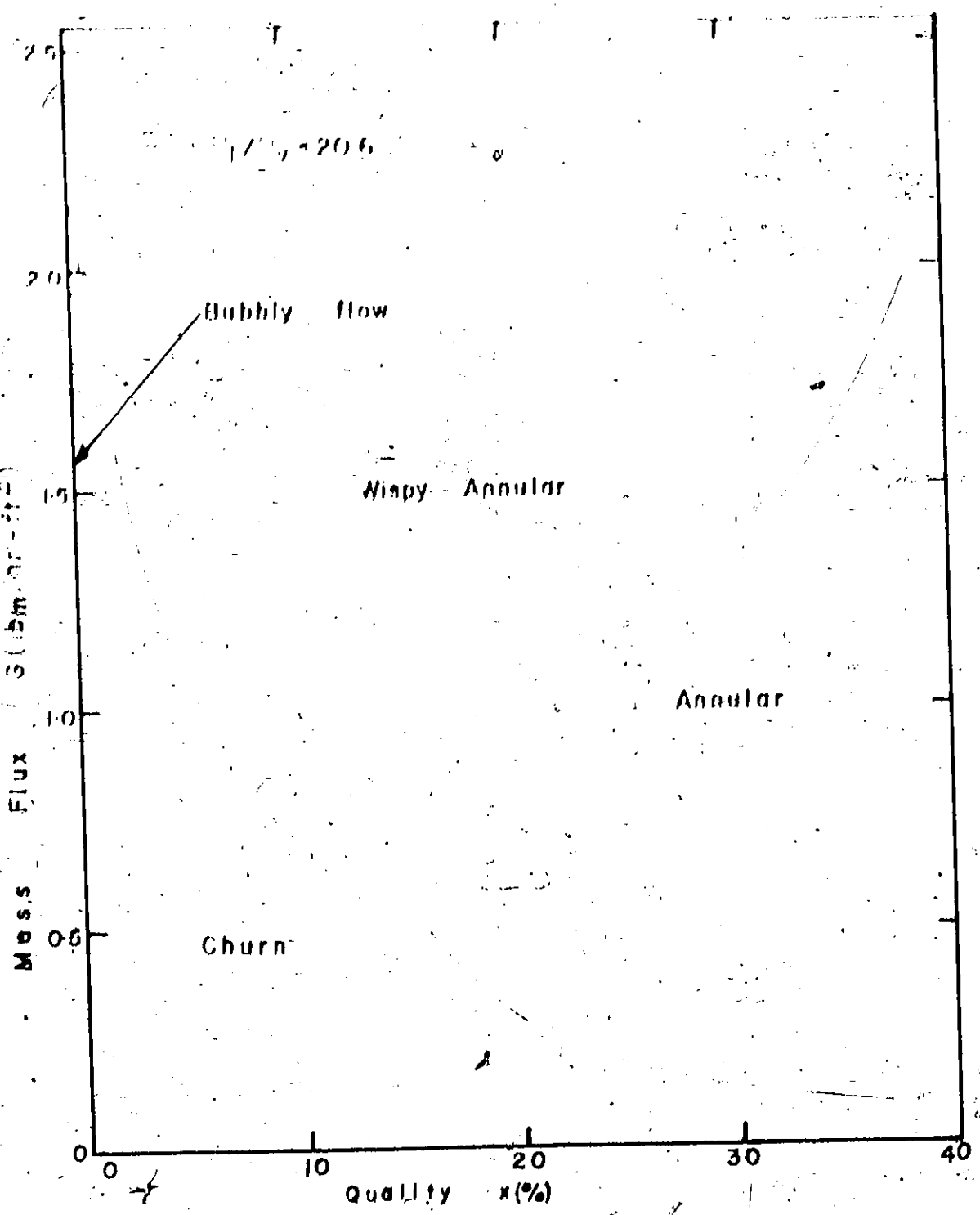

Fig 4 Flow Regimes (G vs x)

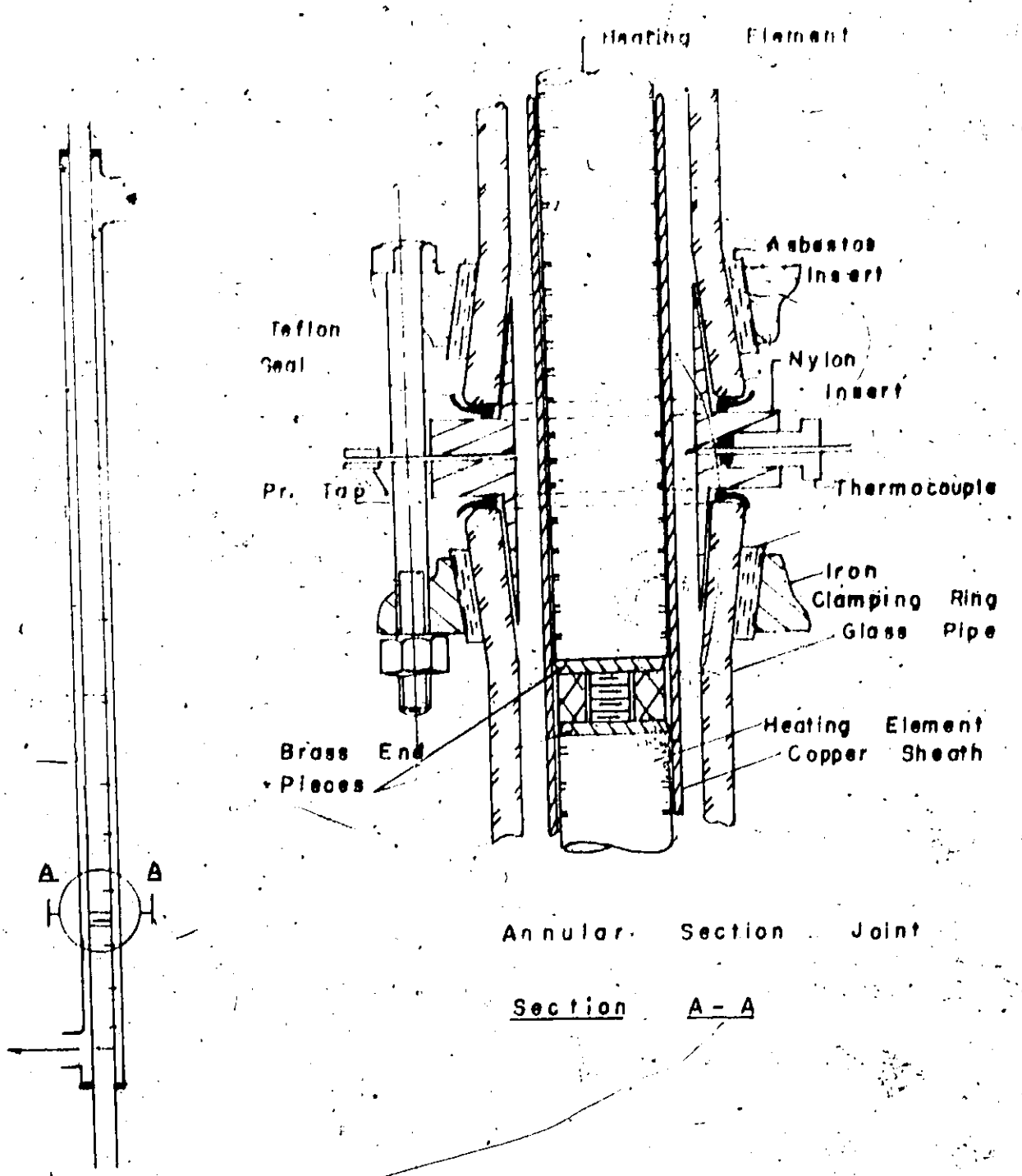

Fig 5 Annular Heated Section

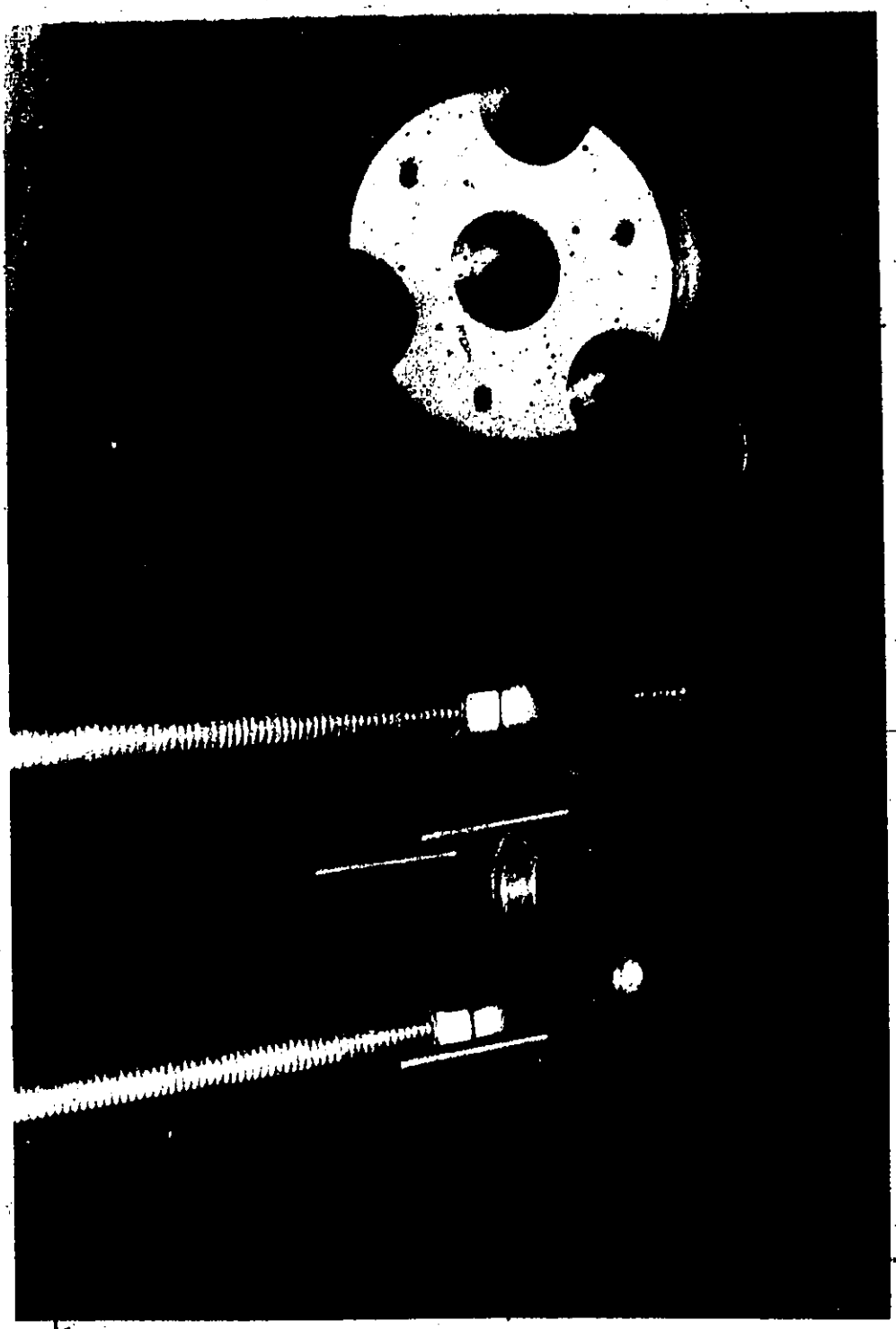

Fig 6 Brass End Plates

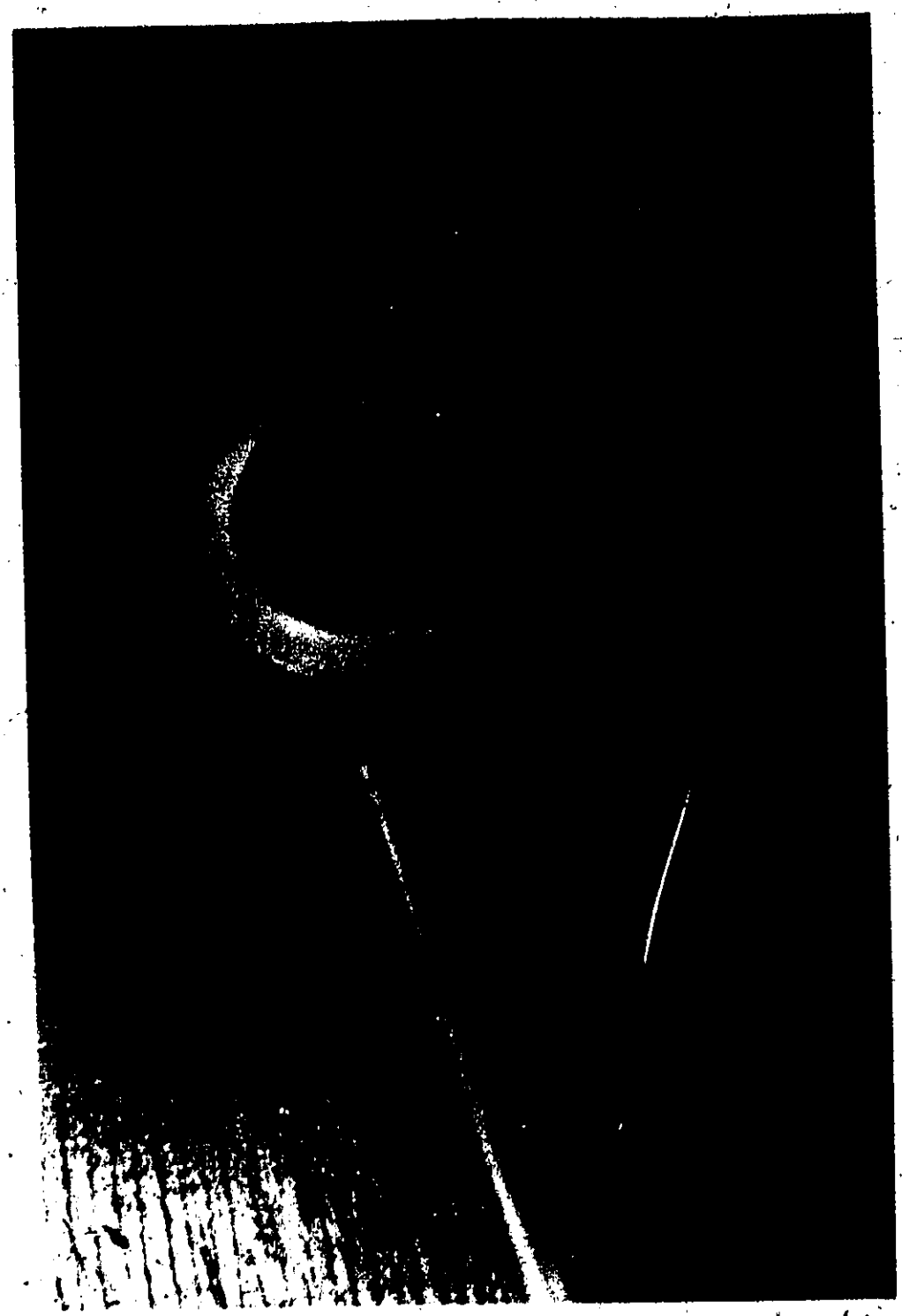

Fig 7 Nylon Inserts

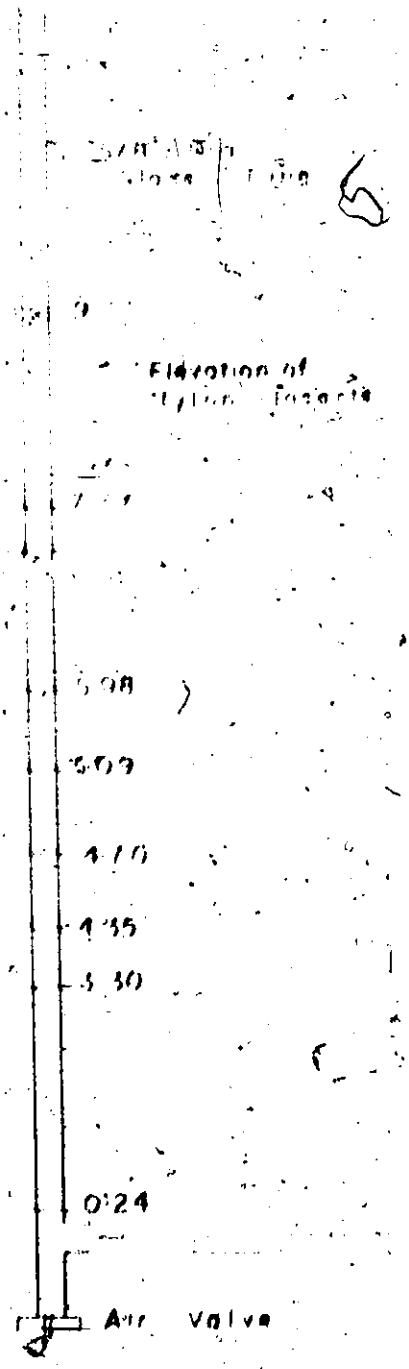

Fig 6a 1-5/8 Riser

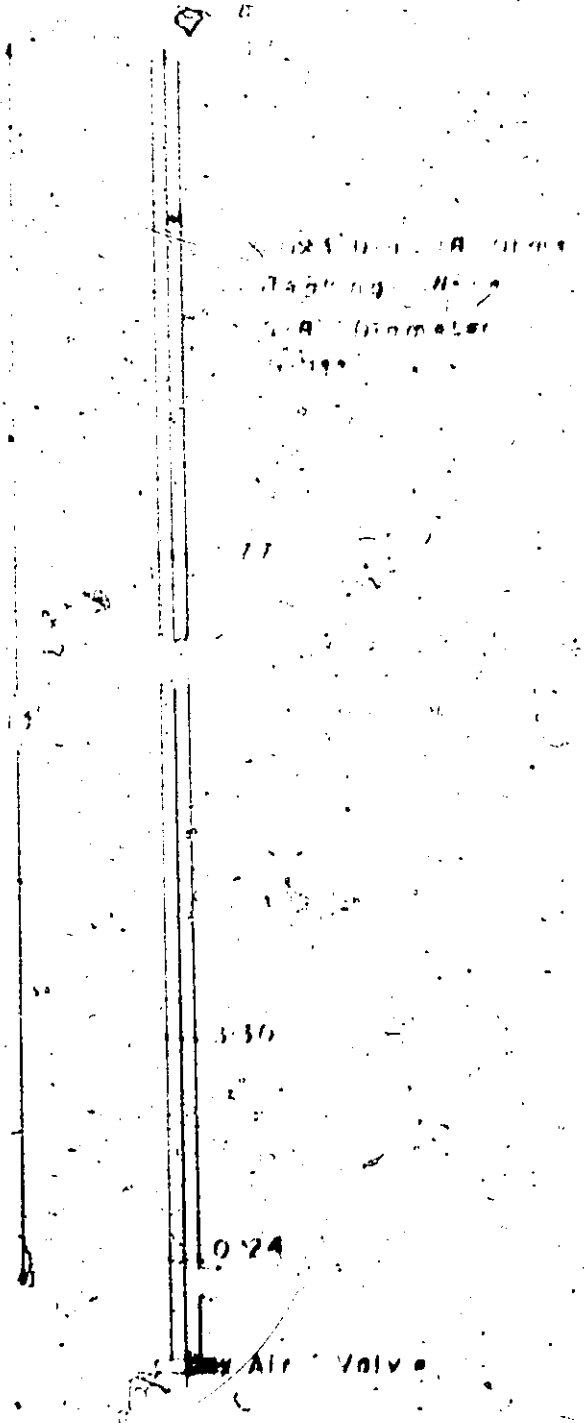

Fig 6b W-5/8 Riser

The Nominal 5/8" Dia. Risers

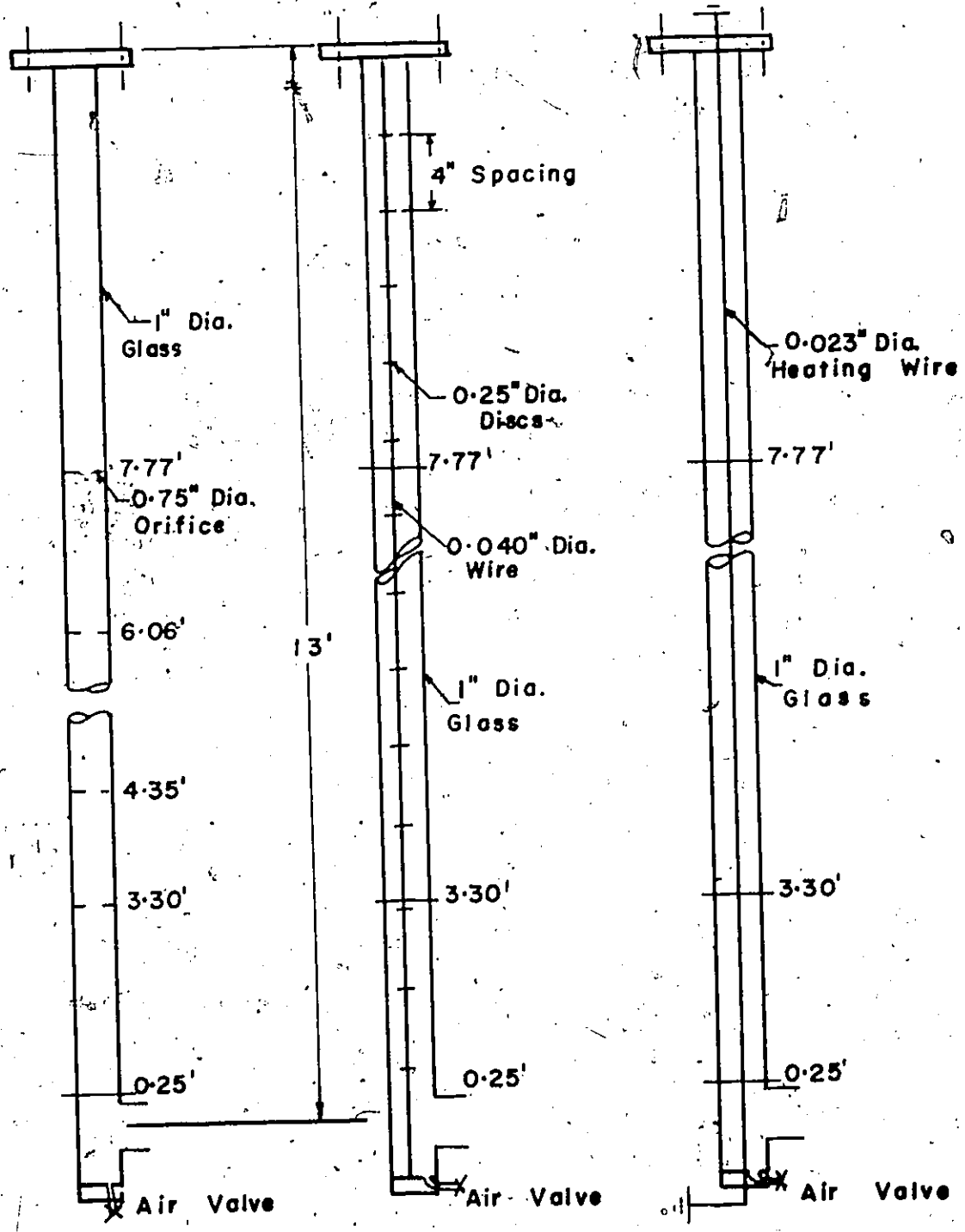

Fig 9a O-1 Riser Fig 9b D-1 Riser Fig 9c W-1 Riser

The Nominal 1" Dia. Risers

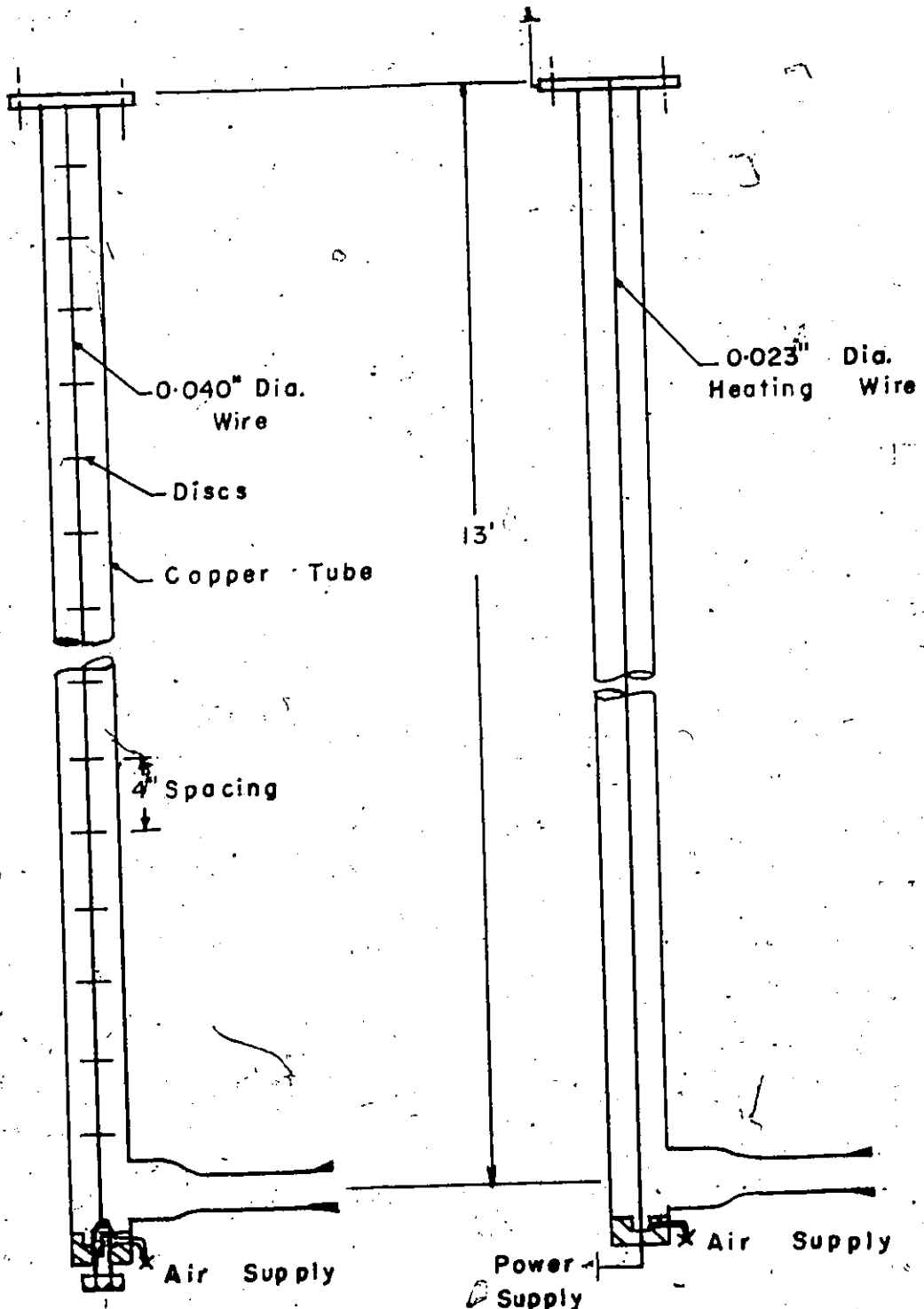

Fig 10a. D-$1\frac{1}{2}$ & D-$1\frac{1}{4}$

Fig 10b W-$1\frac{1}{2}$ & W-$1\frac{1}{4}$

The Nominal $1\frac{1}{2}$" & $1\frac{1}{4}$" Diameter Risers

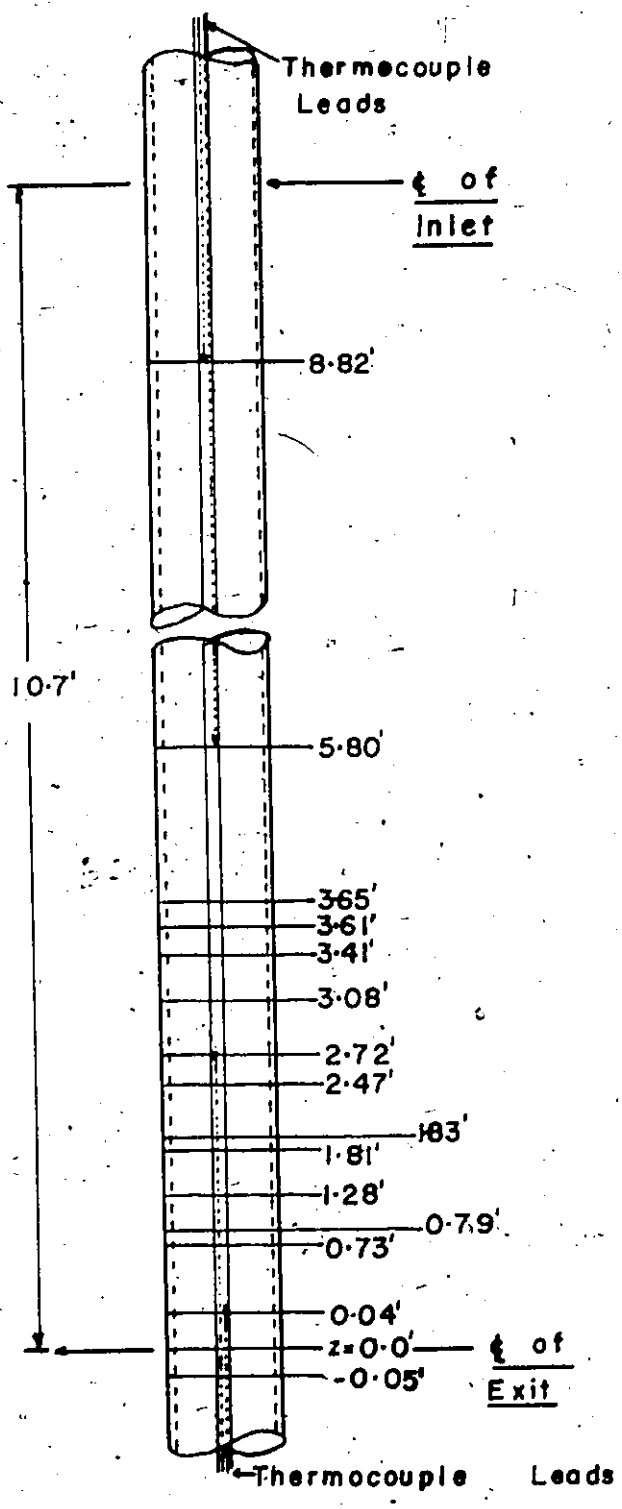

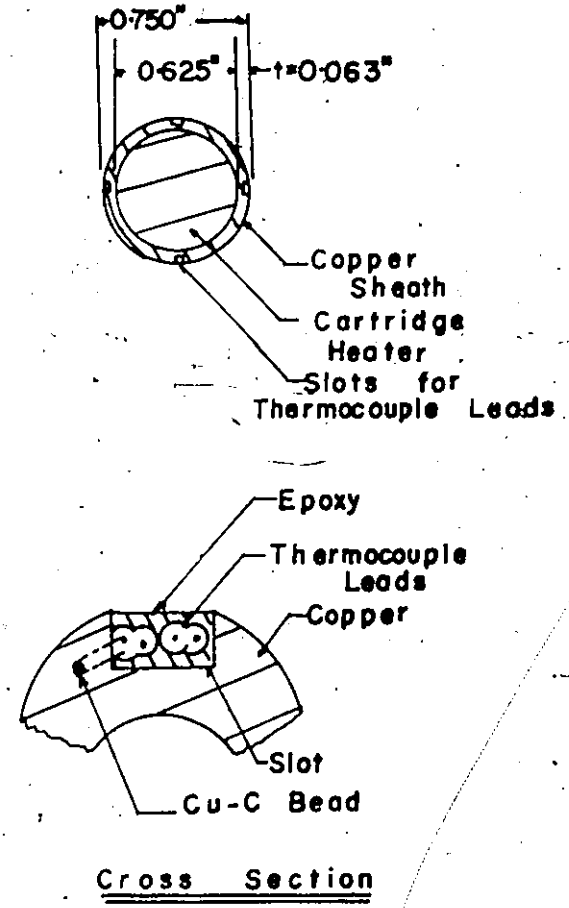

Fig II Instrumented Heater Cylinder Assembly

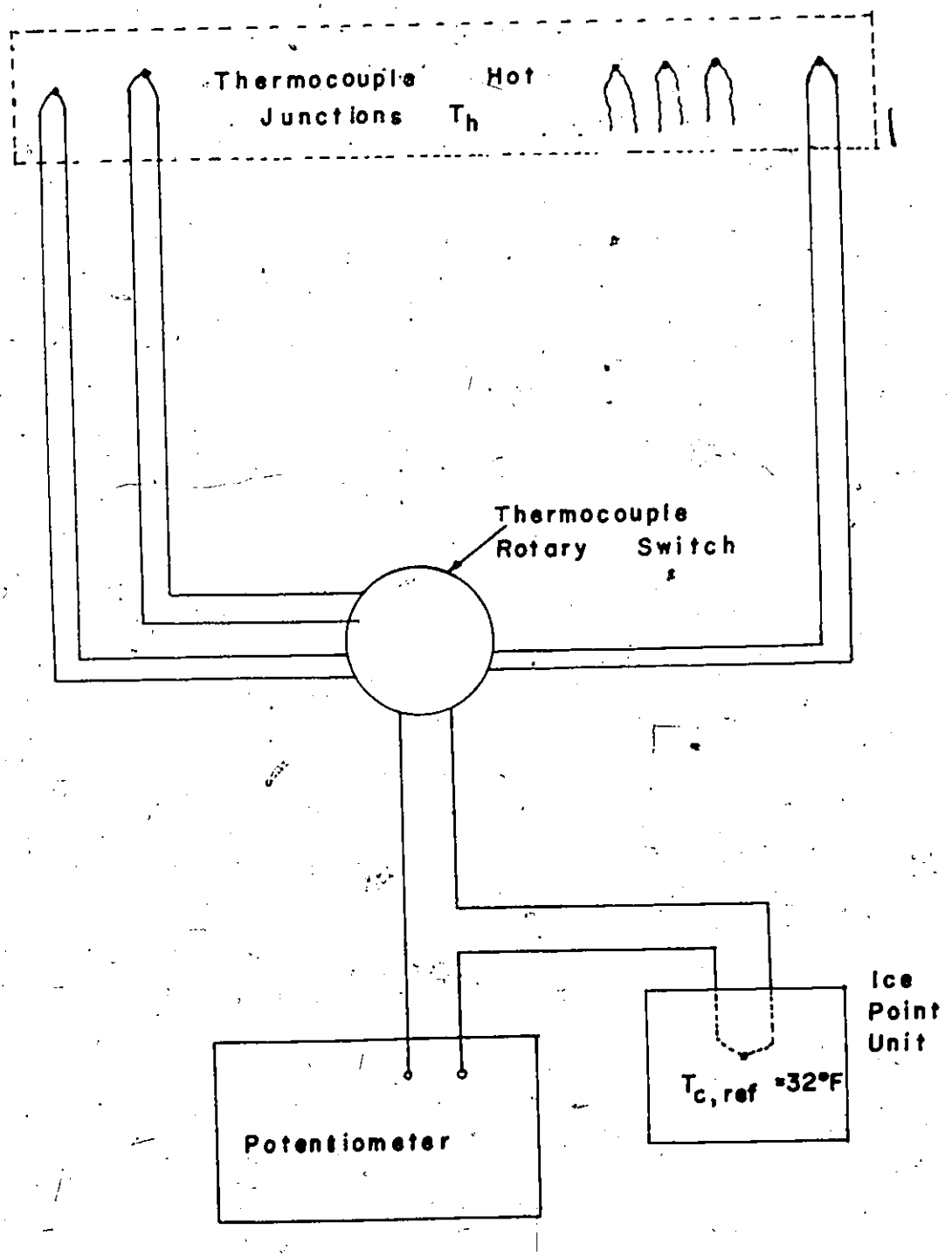

Fig 12 - Thermocouple Circuitry

Fig 13 Inverted U-Tube Manometer

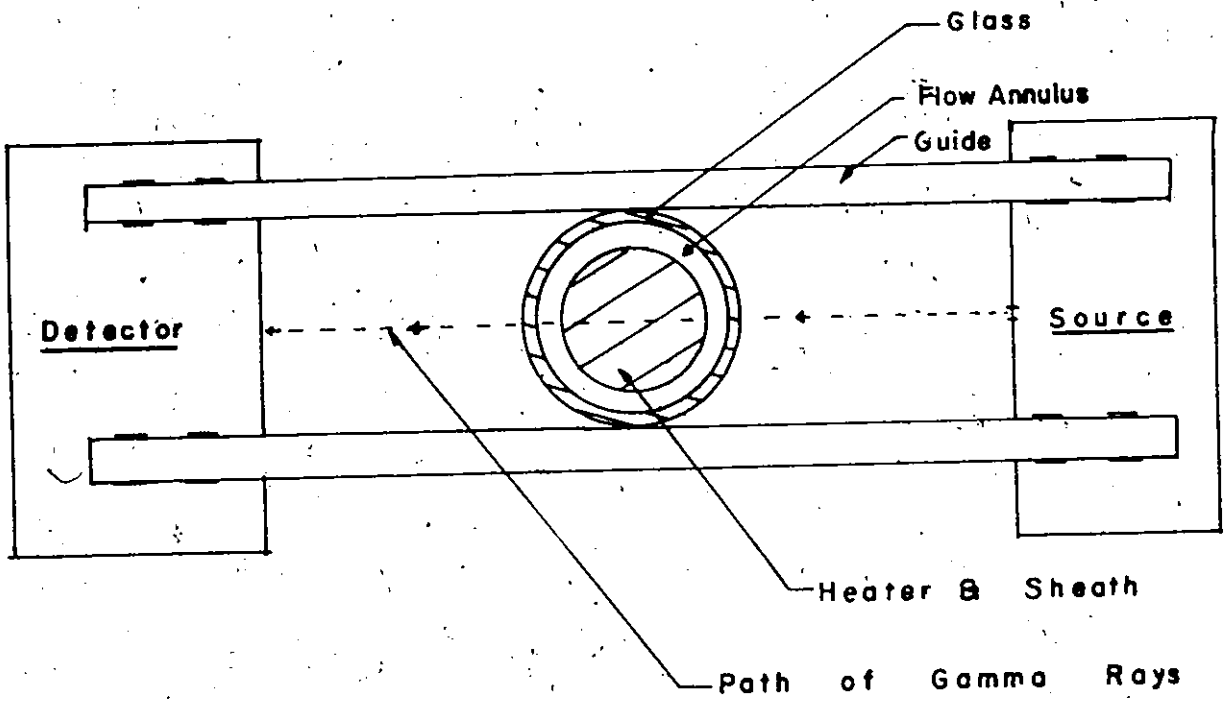

Fig 14 Path of Gamma Rays

Fig 15 Gamma Ray Unit

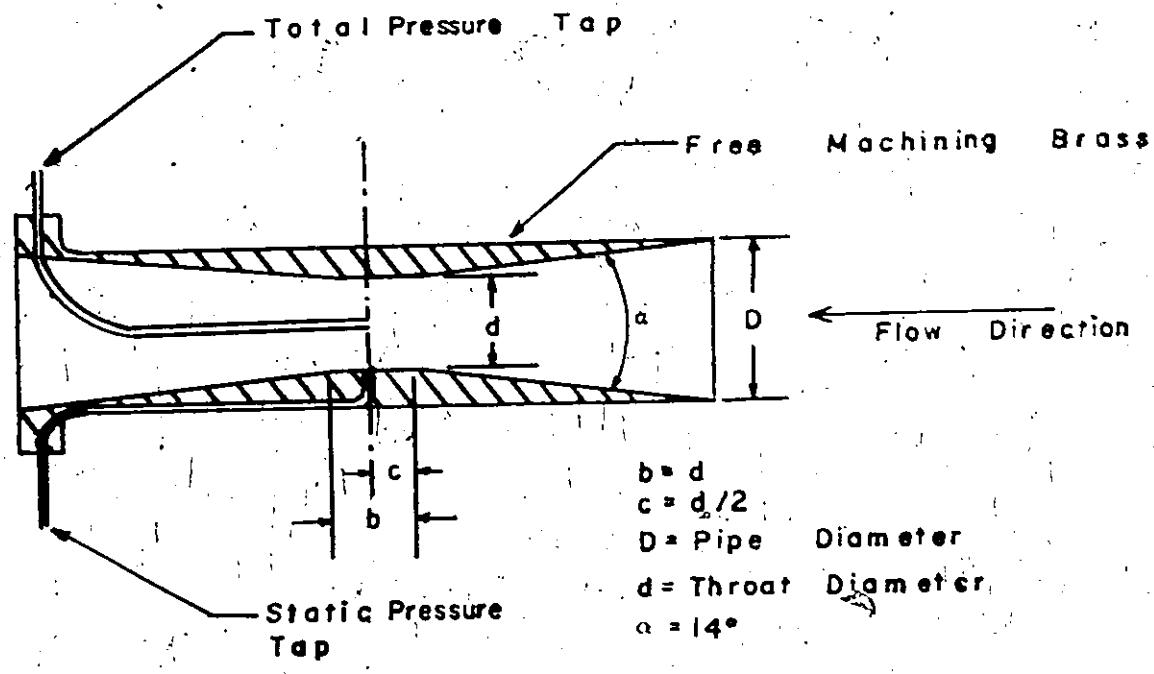

Fig 16 Venturi Mass Flow Meter

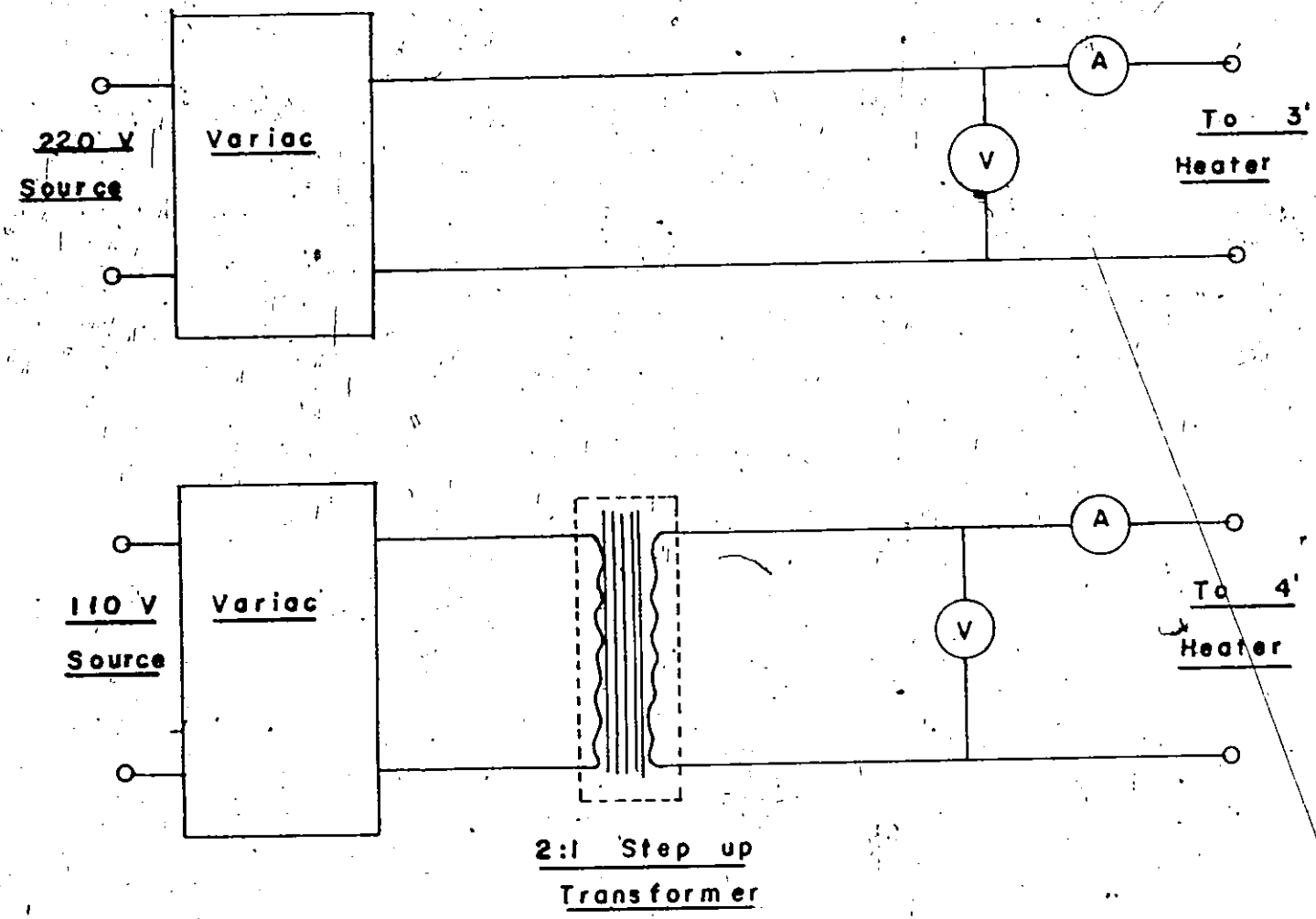

Fig 17 Power Supply Circuitry

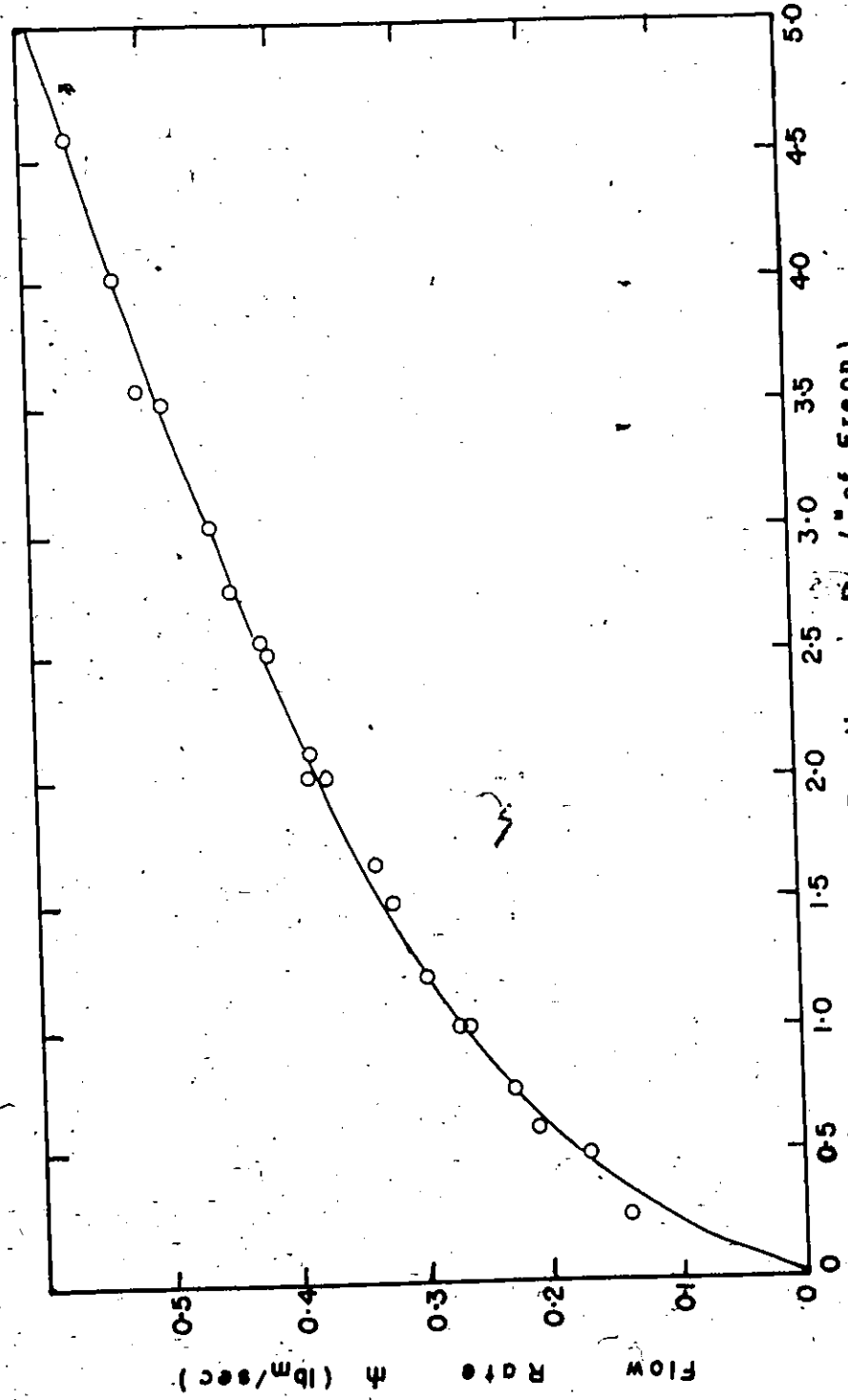

Fig 18 Calibration of Mass Flow Meter

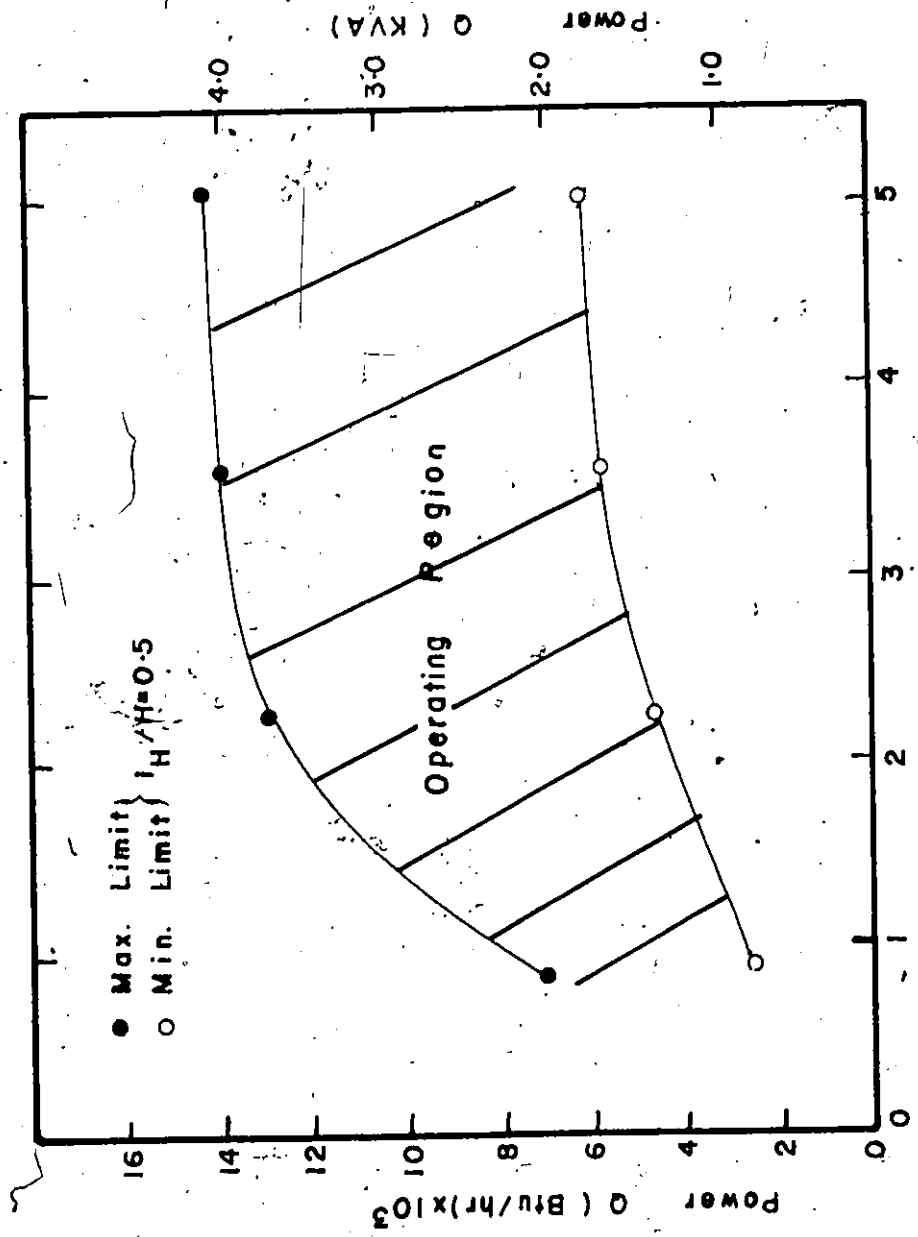

Fig 19 Stability Limits of Downflow Thermosiphons (W-5/8, W-1, W-1$\frac{1}{4}$, W-1$\frac{1}{2}$)

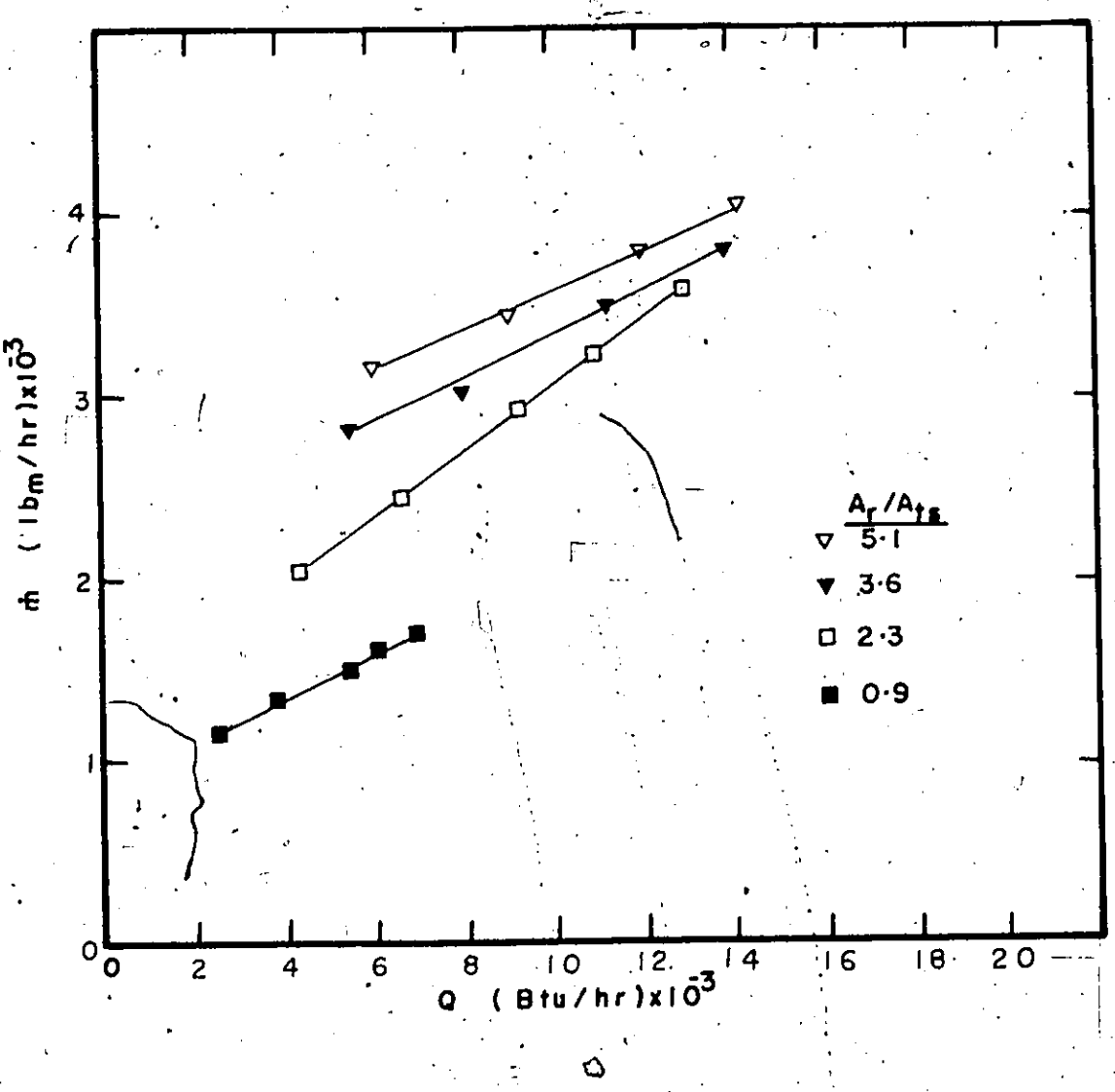

Fig 20 Circulation Rates

(W-5/8, W-1, W-1¼, W-1½)

$l_H/H = 0.5$

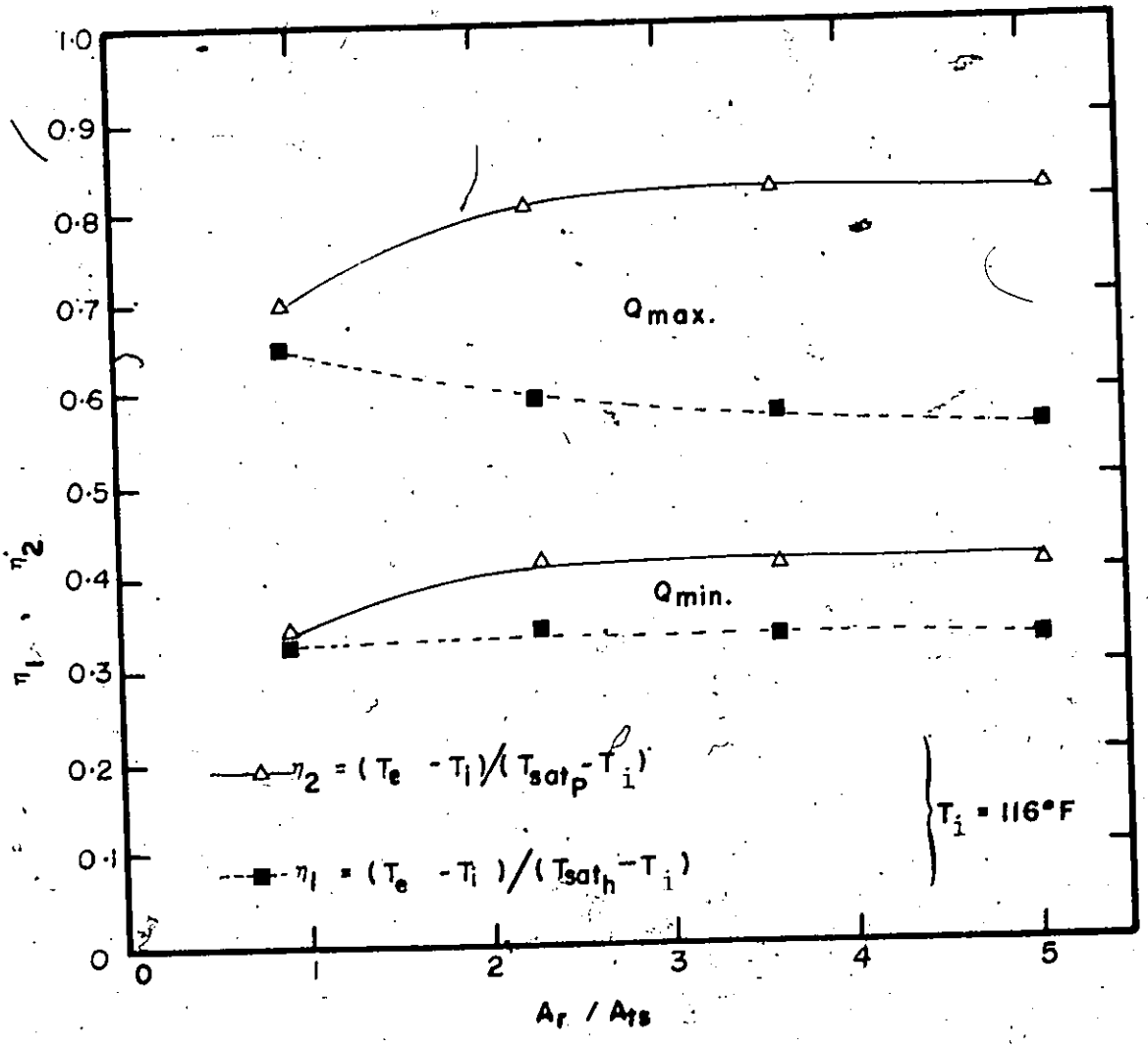

Fig 21 Non-Dimensional Outlet Fluid Temperatures

(W-5/8, W-1, W-1¼, W-1½)

$l_H/H = 0.5$

T_{sat_P} = T_{sat} for operating pressure at Z=0

T_{sat_h} = T_{sat} for p=$p_{atmos.} + \gamma H$

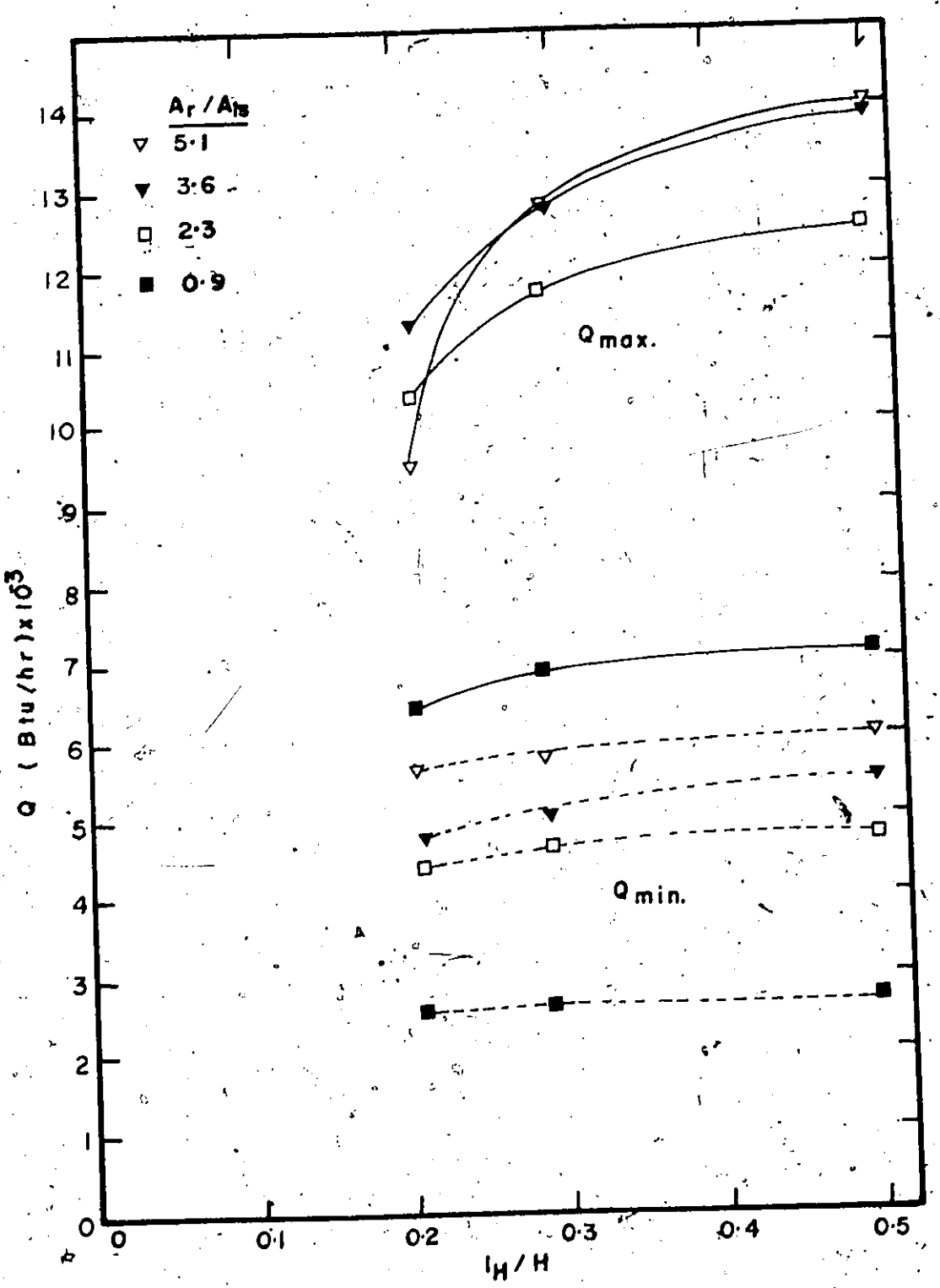

Fig 22 Effect of Heater Length On Power Dissipation Limits (W-5/8, W-1, W-1$\frac{1}{4}$, W-1$\frac{1}{2}$)

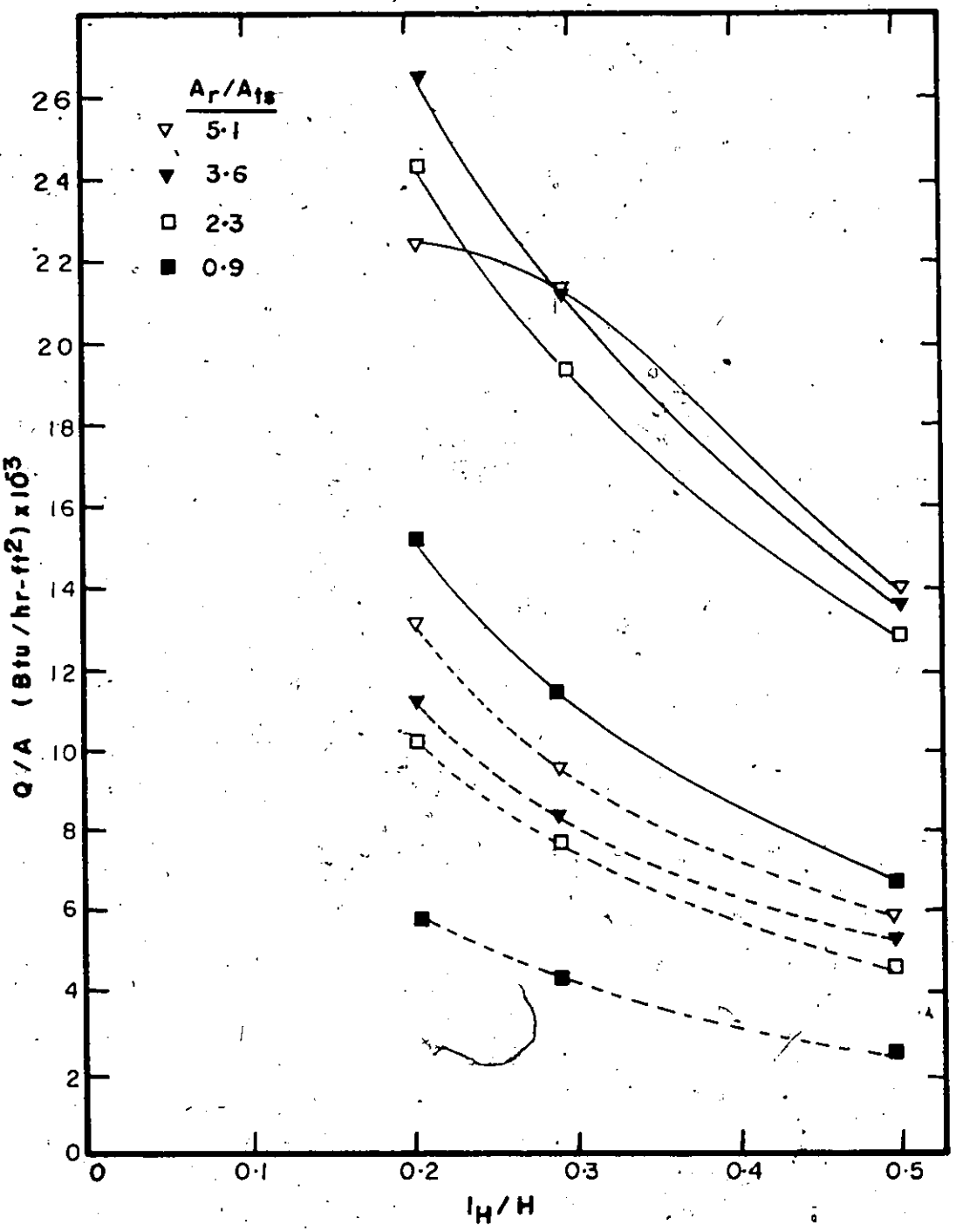

Fig23 Heat Flux Limitations of Downflow Thermosiphons (W-5/8, W-1, W-1¼, W-1½)

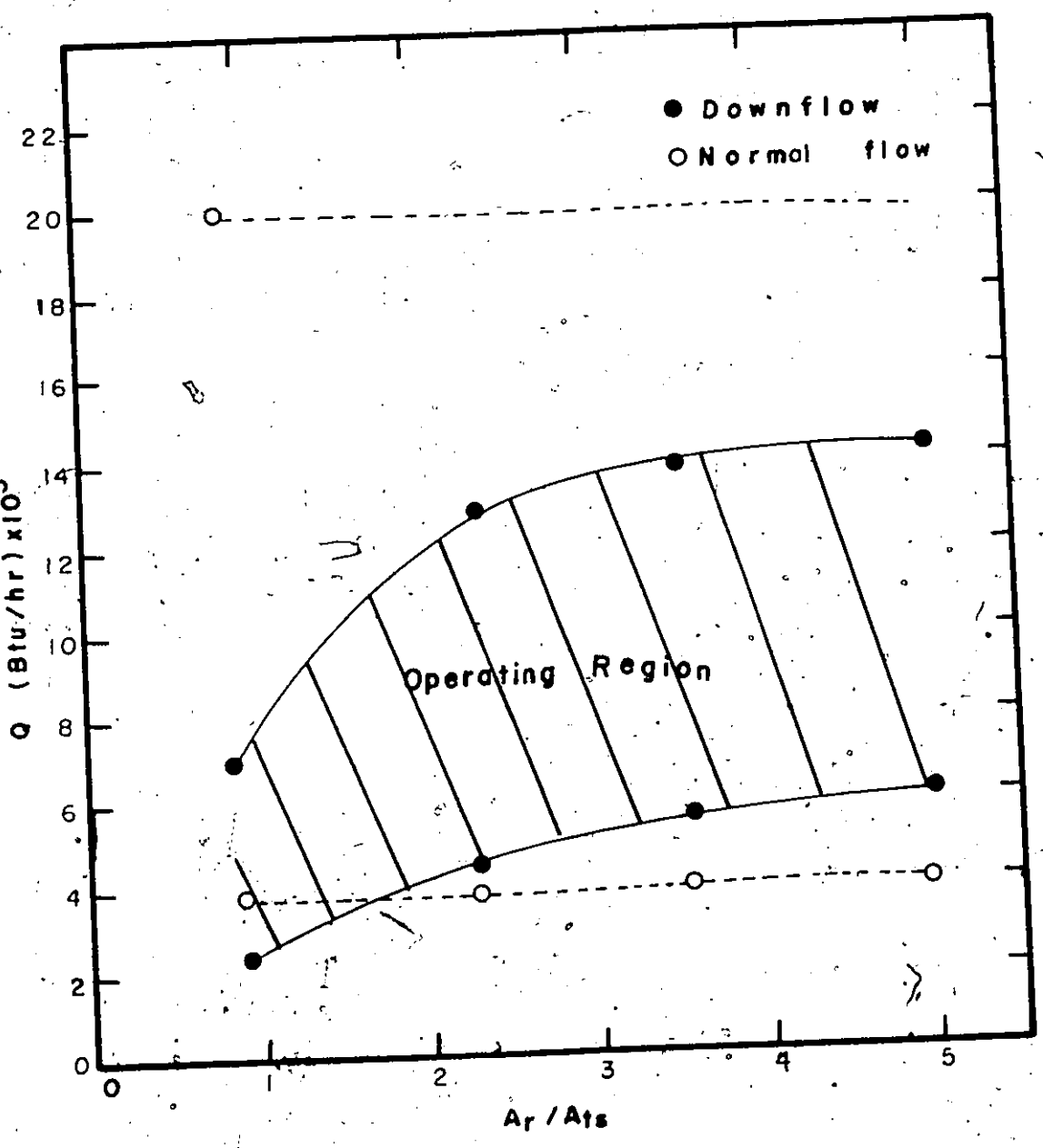

Fig 24 Comparison of Power Dissipation of Normal flow and Downflow Thermosiphons.

$l_H/H=0.5$

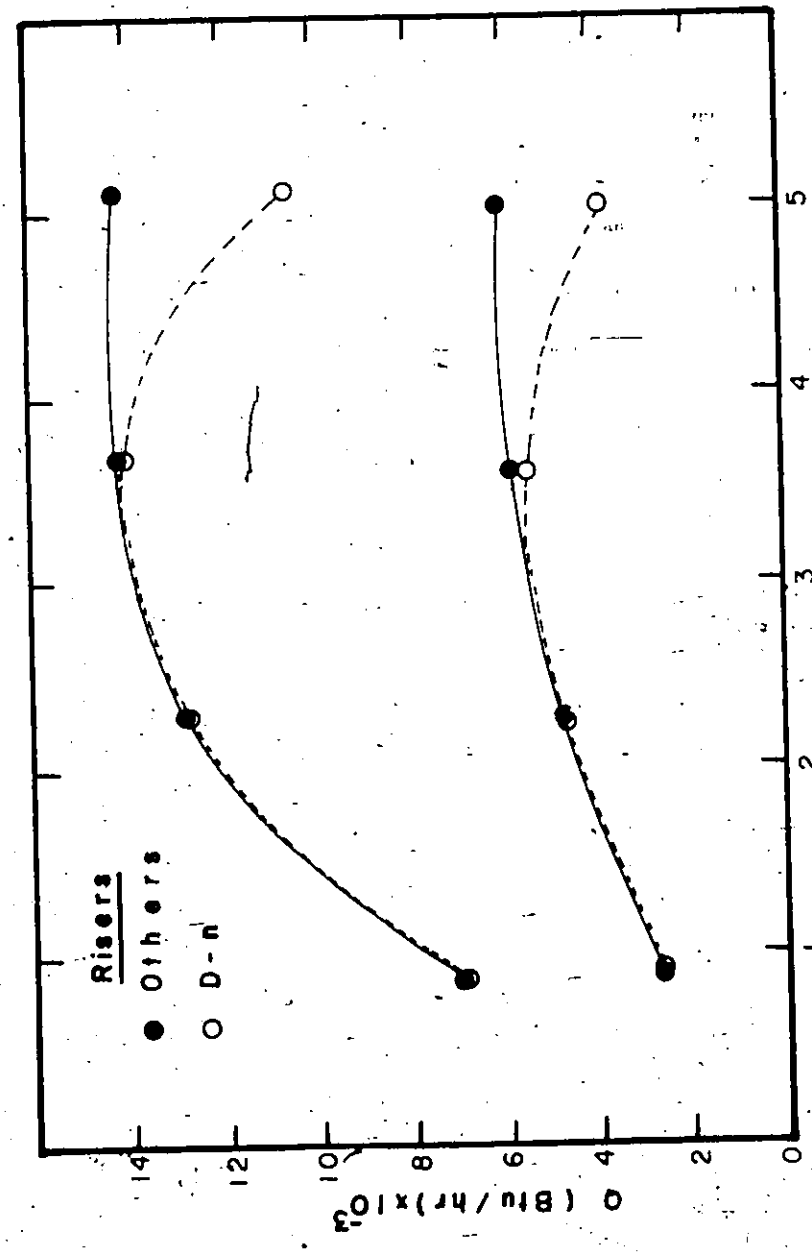

Fig 25 Stability Limits using Risers with Various Nucleating Devices

(I-5/8, W-5/8, D-1, W-1, O-1, D-1¼, W-1¼, D-1½, W-1½)

$l_H/H=0.5$

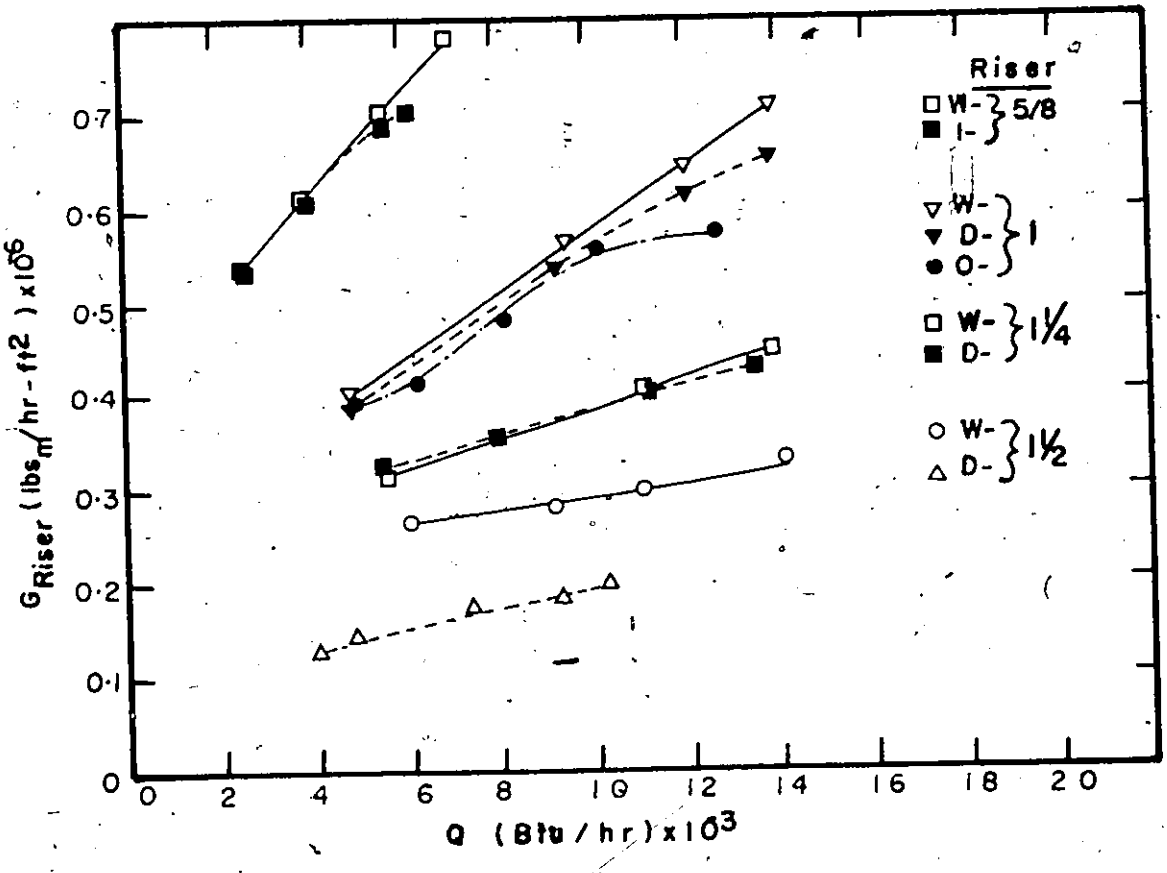

Fig 26 Mass Fluxes in the Risers
$l_H/H=0.5$

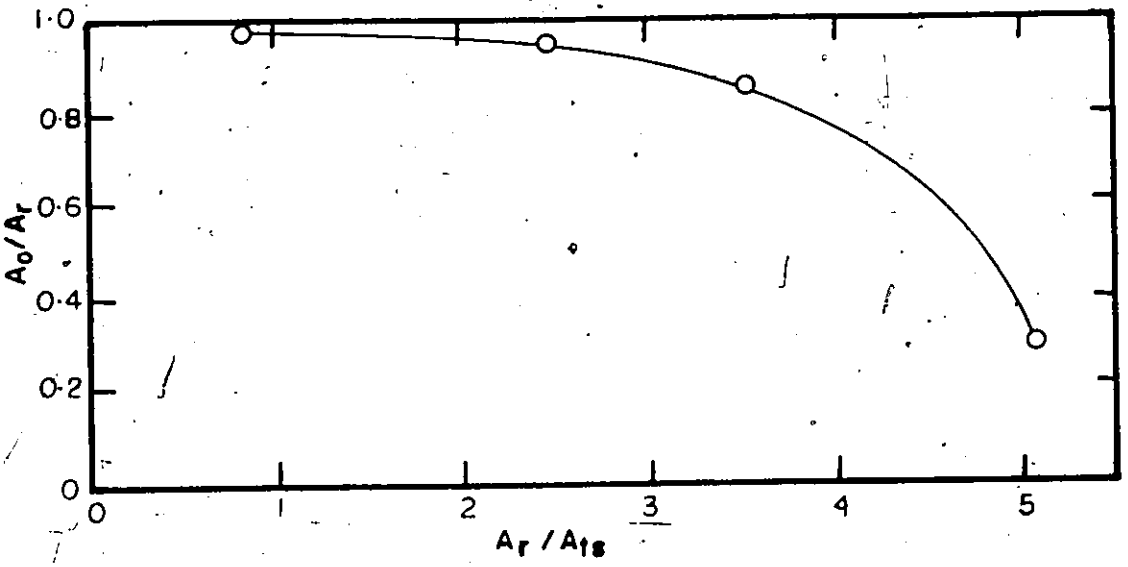

Fig 27 Orifice Size Req'd to Initiate FLashing (D-n Risers)

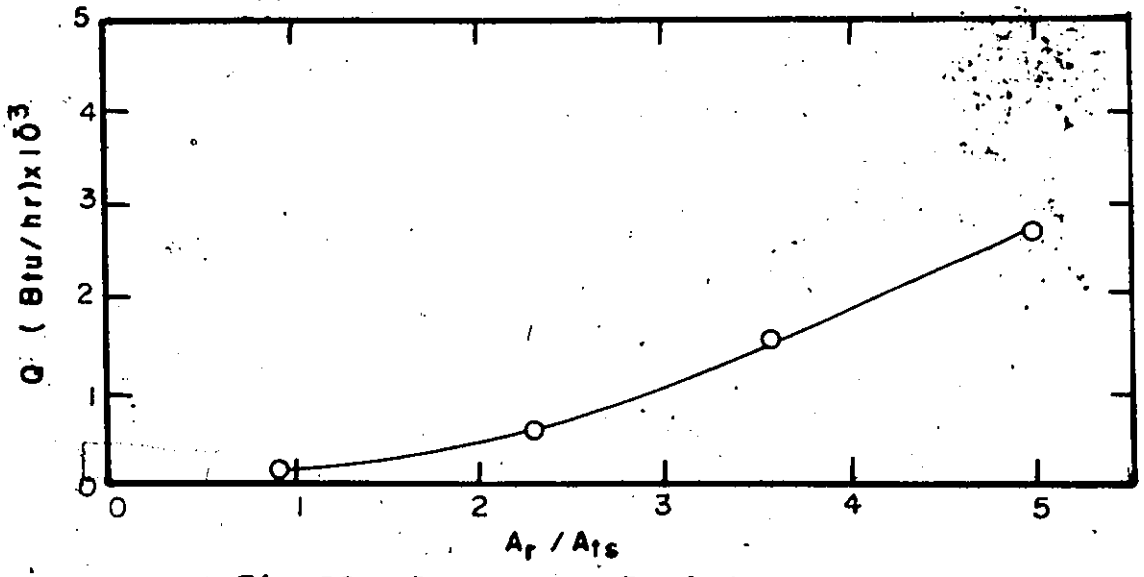

Fig 28 Power Required to Initiate Flashing (W-n Risers)

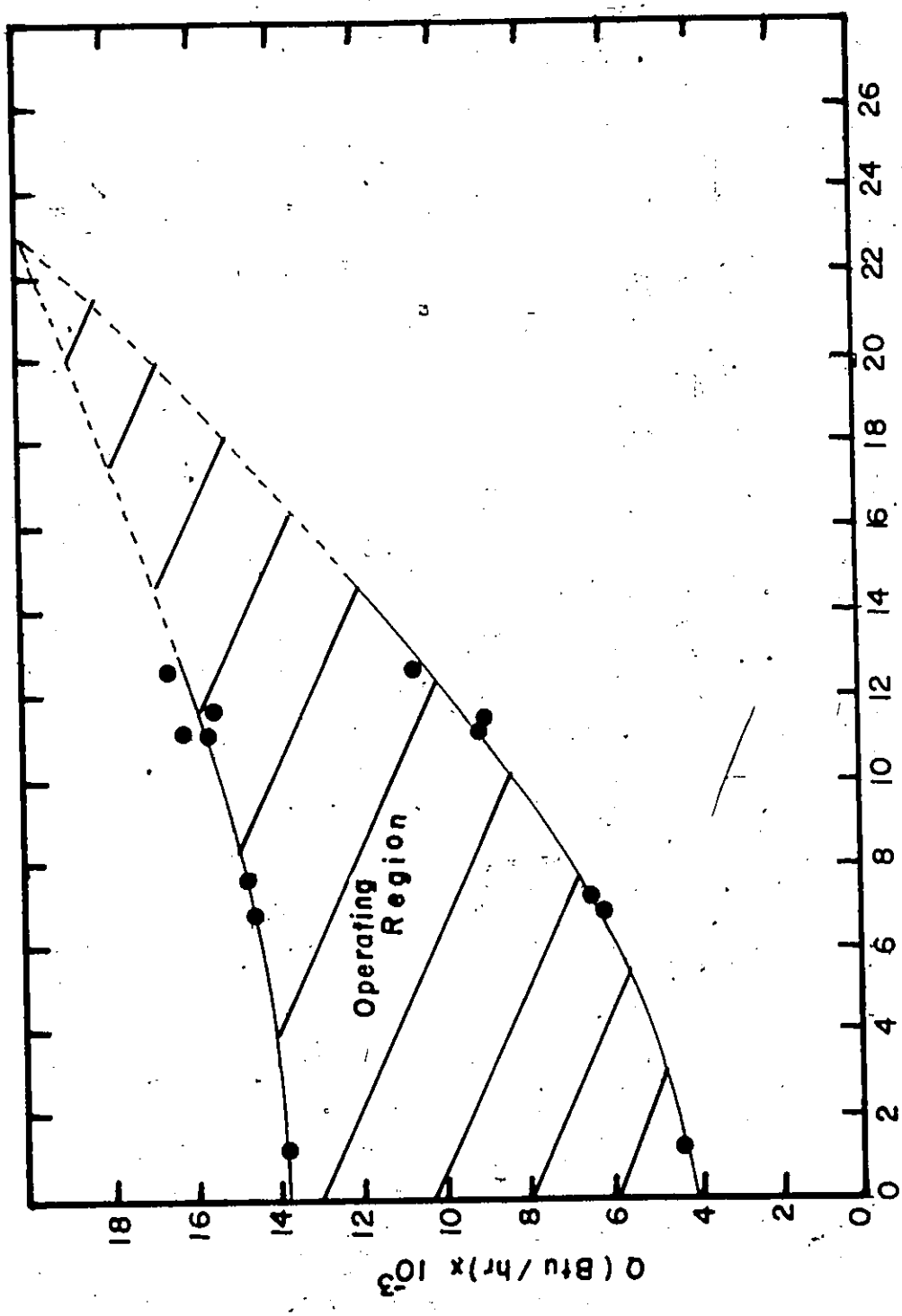

Fig 29 Effect of Inlet Subcooling on Stability Limits (D-1 Riser)
$l_H/H=0.5$

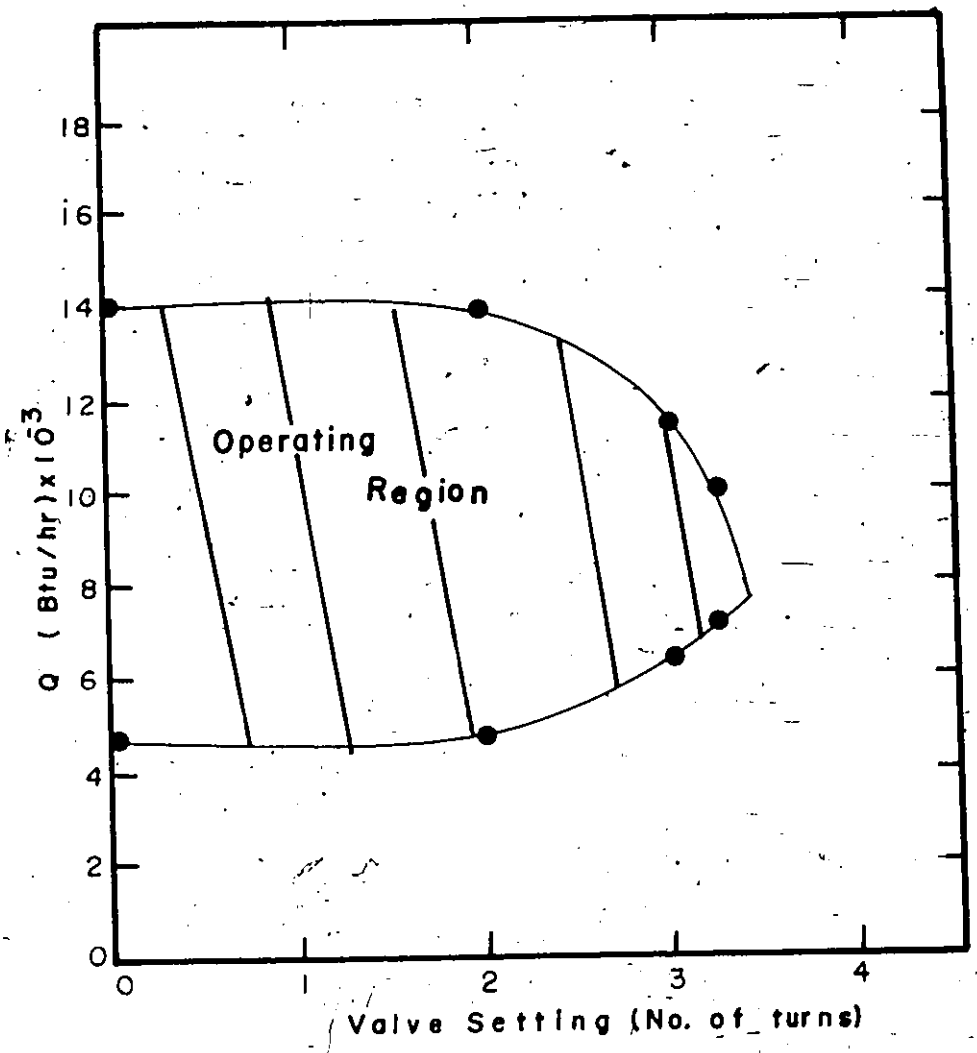

Fig 30 Effect of a Flow Restriction on Power Limits (D-1 Riser) $l_H/H=0.3$

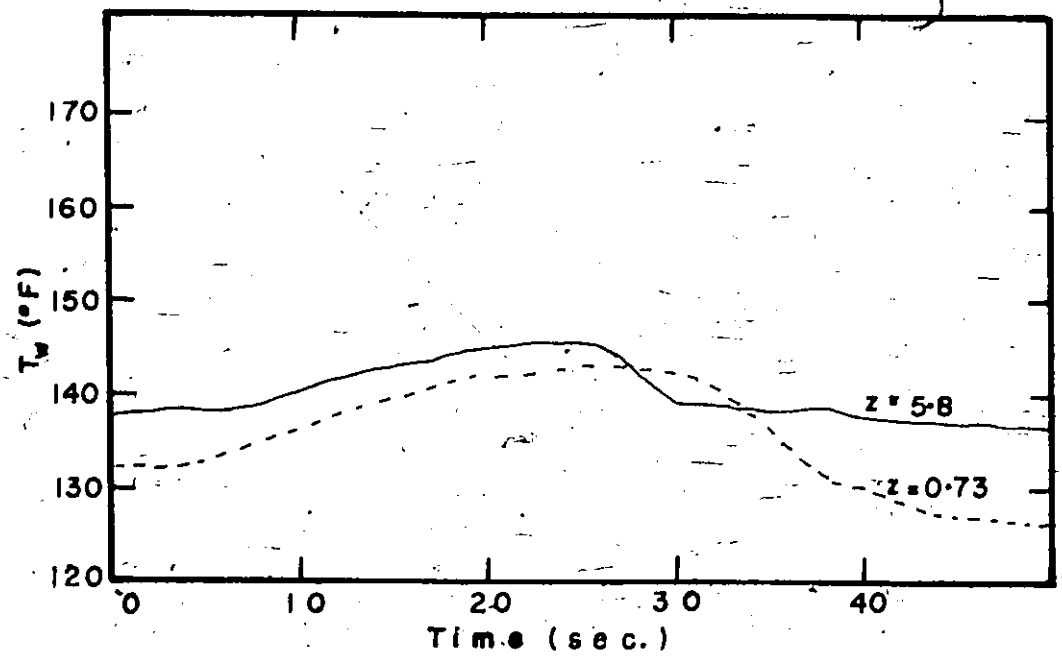

— Minimum Power Reversal

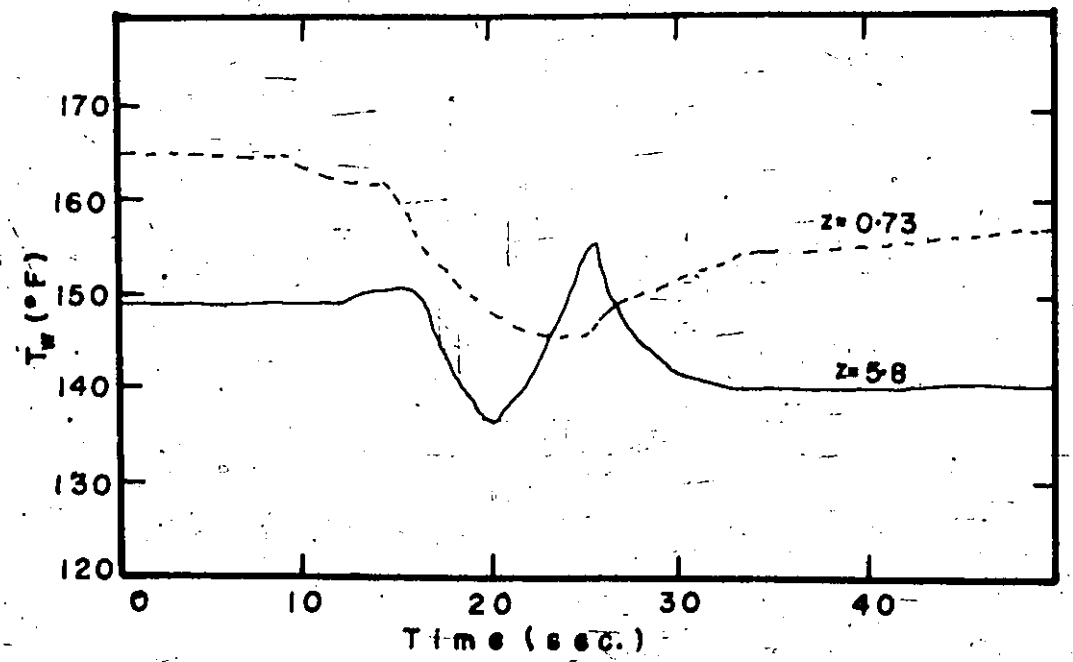

Fig. 31 Maximum Power Reversal

Heater Surface Temperature During Flow Reversal.

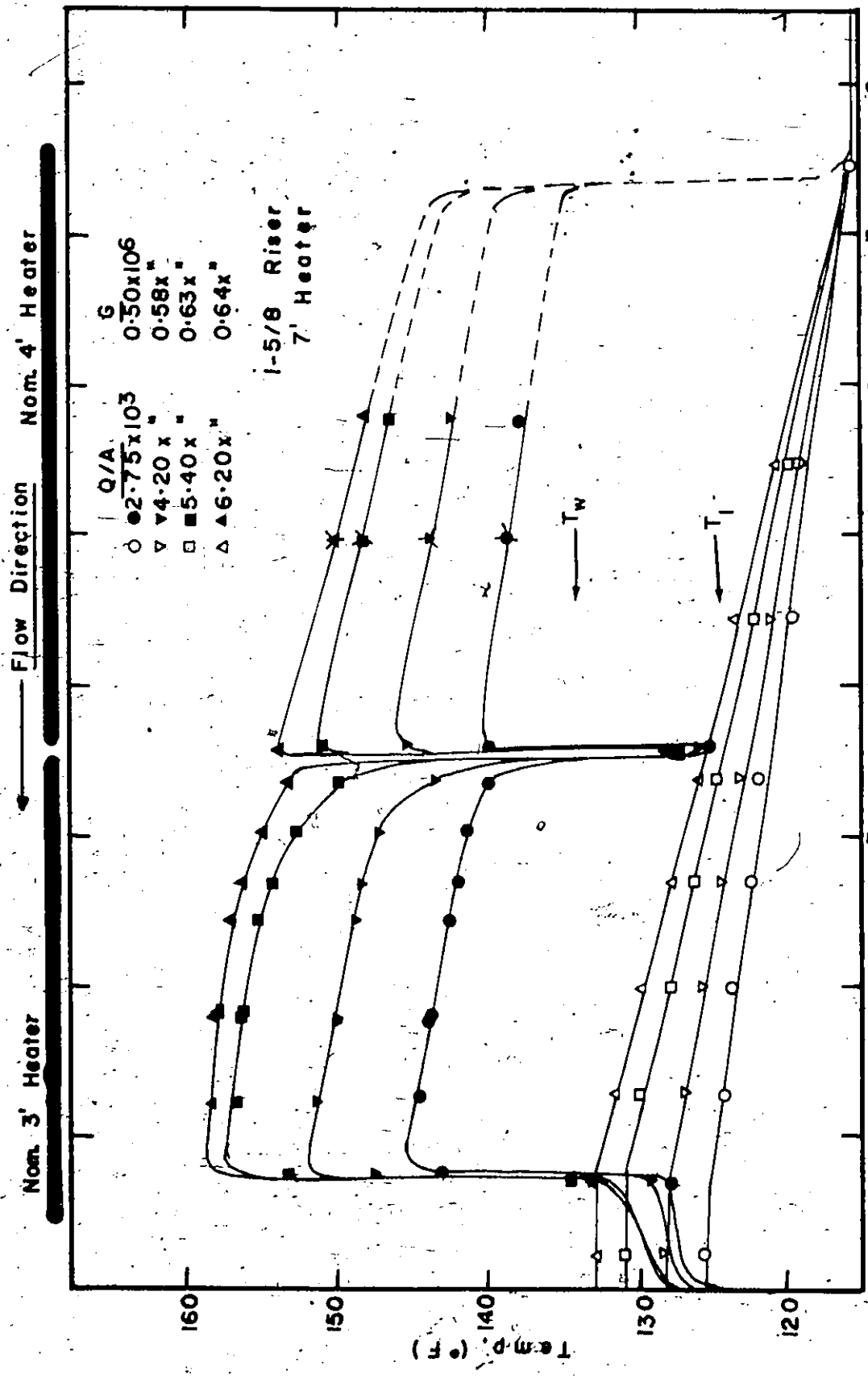

Fig 32 Axial Fluid and Wall Temp. Distributions

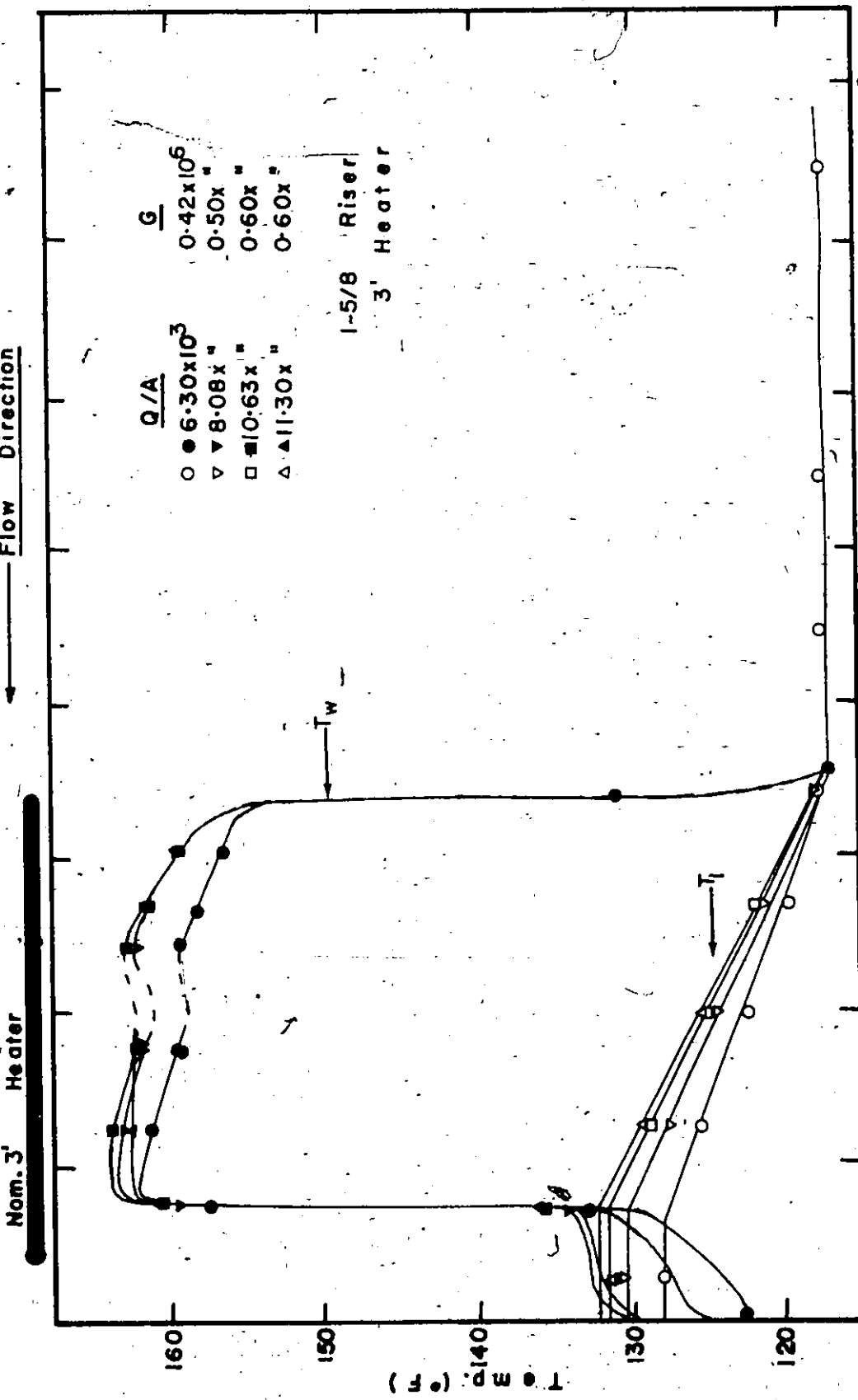

Fig 33 Axial Fluid and Wall Temp. Distributions

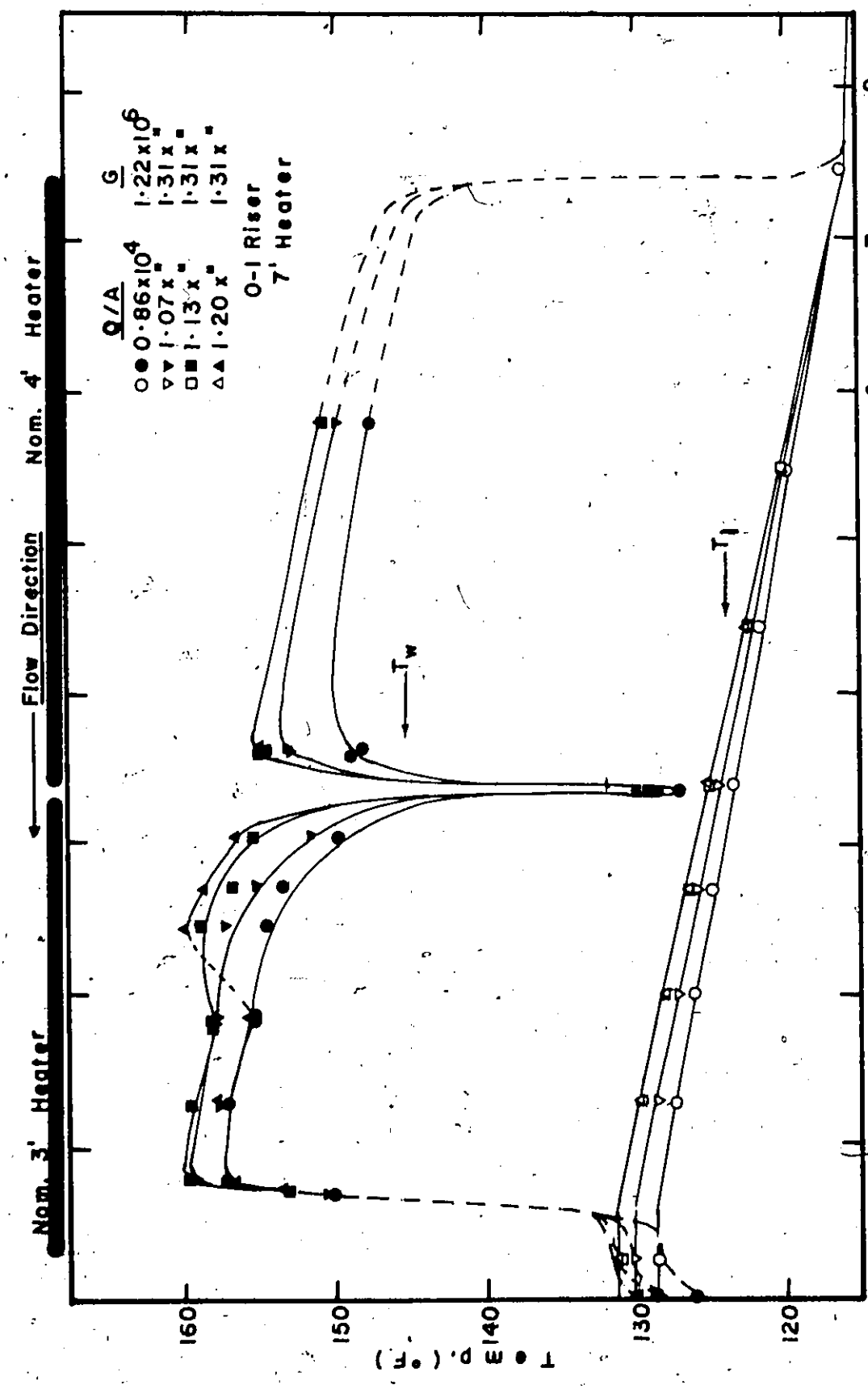

Fig 34 Axial Fluid and Wall Temp. Distributions

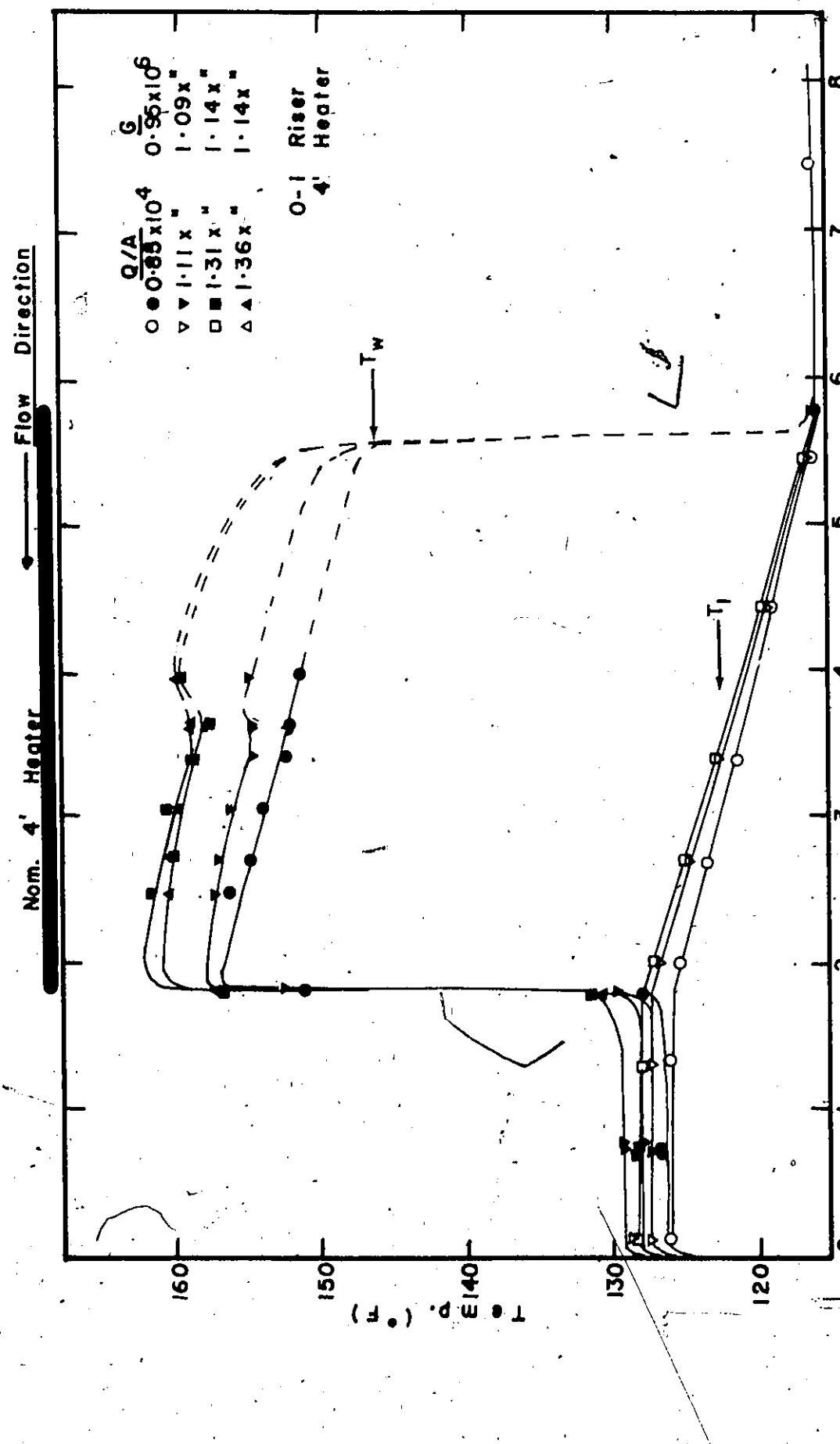

Fig 35 Axial Fluid and Wall Temp. Distributions

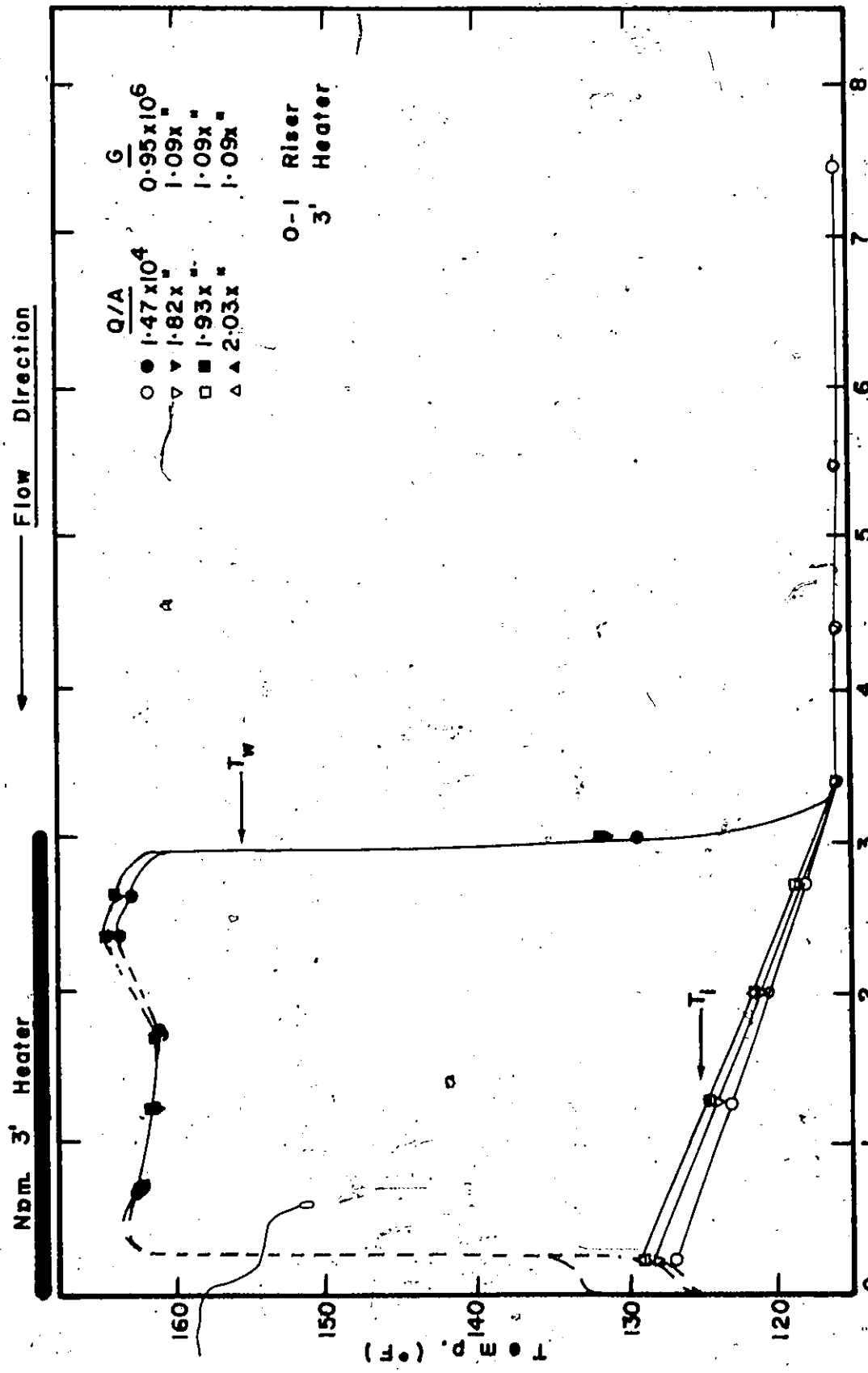

Fig 36 Axial Fluid and Wall Temp. Distributions

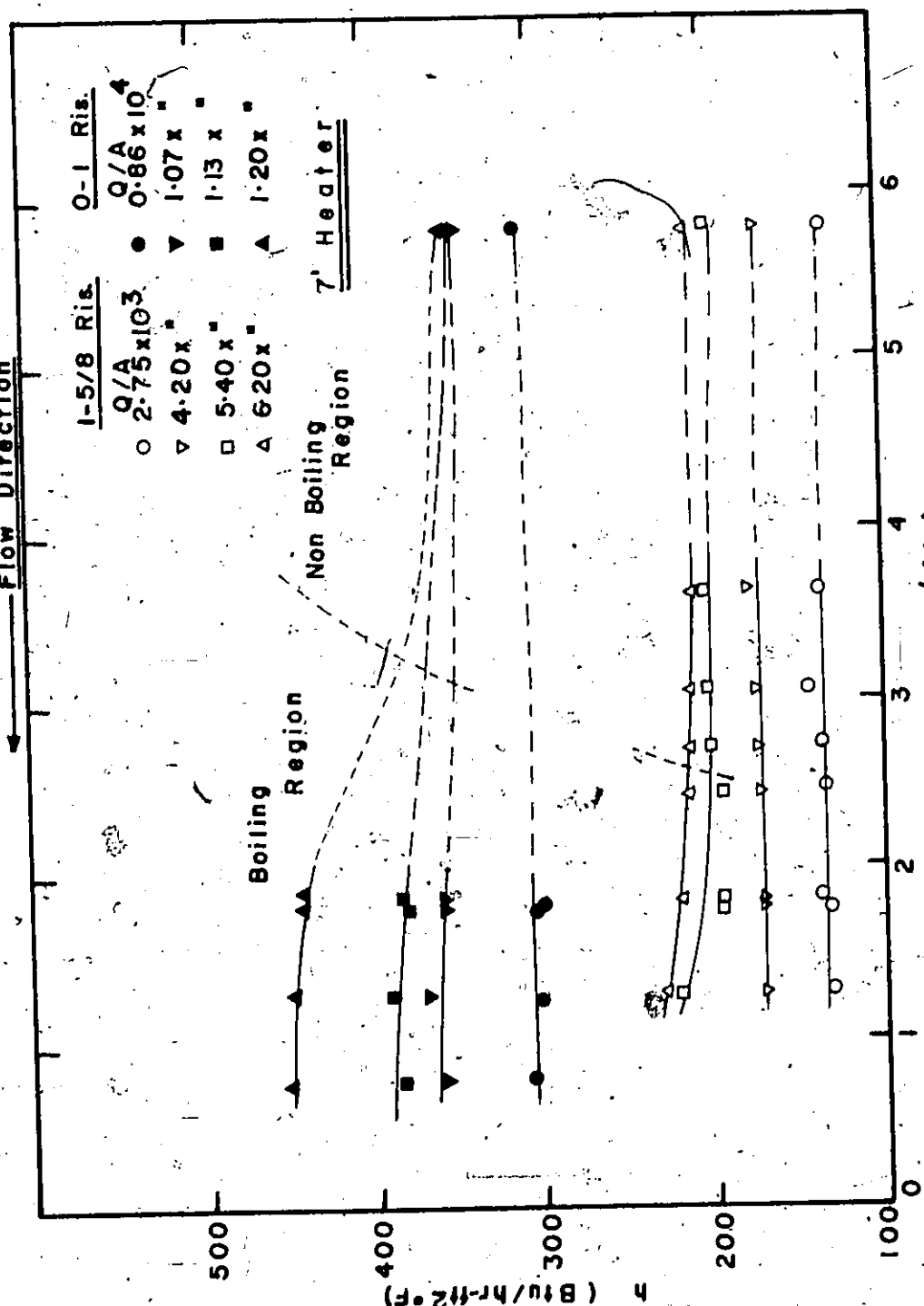

Fig 37 Axial Heat Transfer Coeff. Distributions

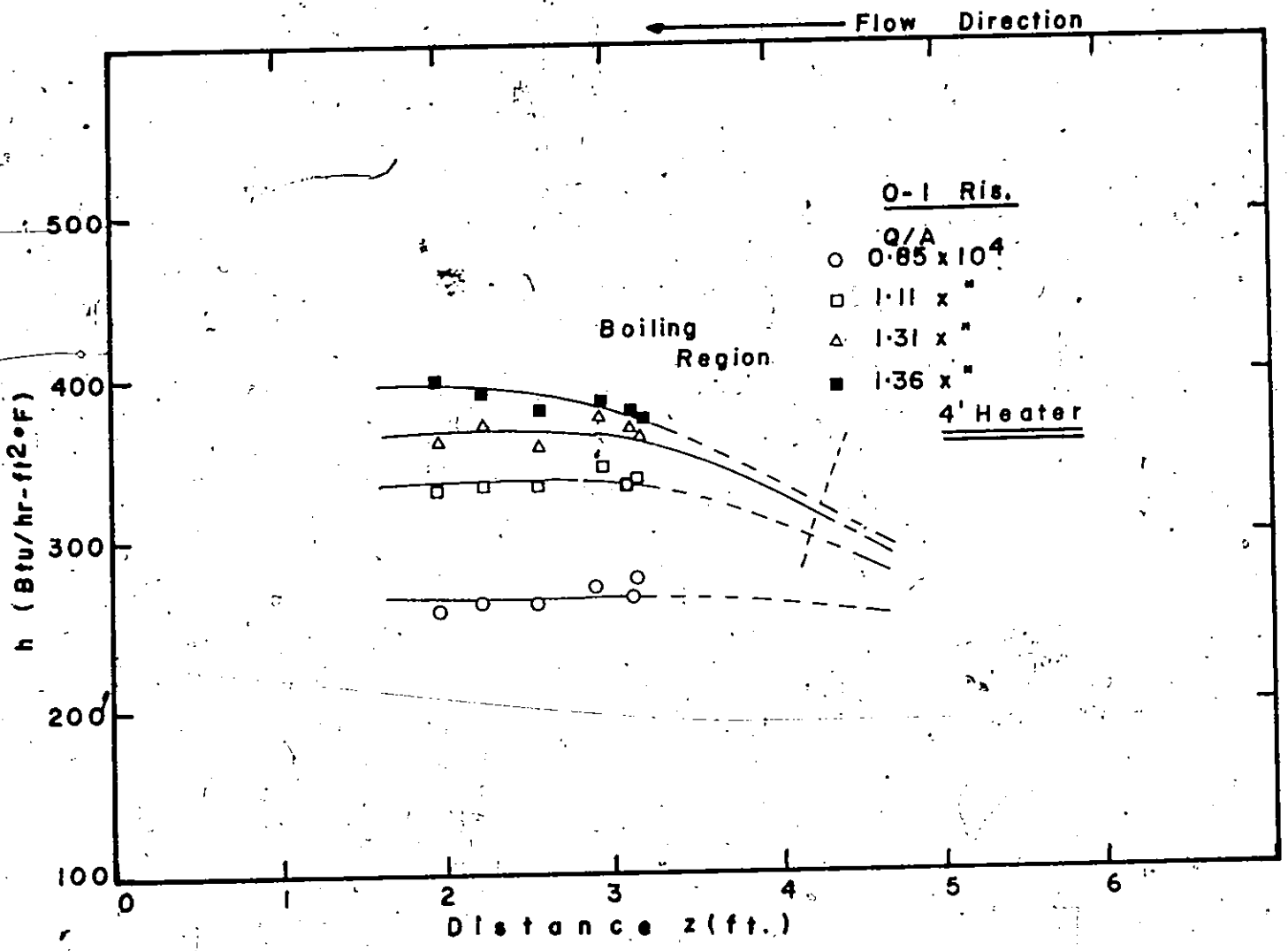

Fig 38 Axial Heat Tranfer Coeff. Distributions

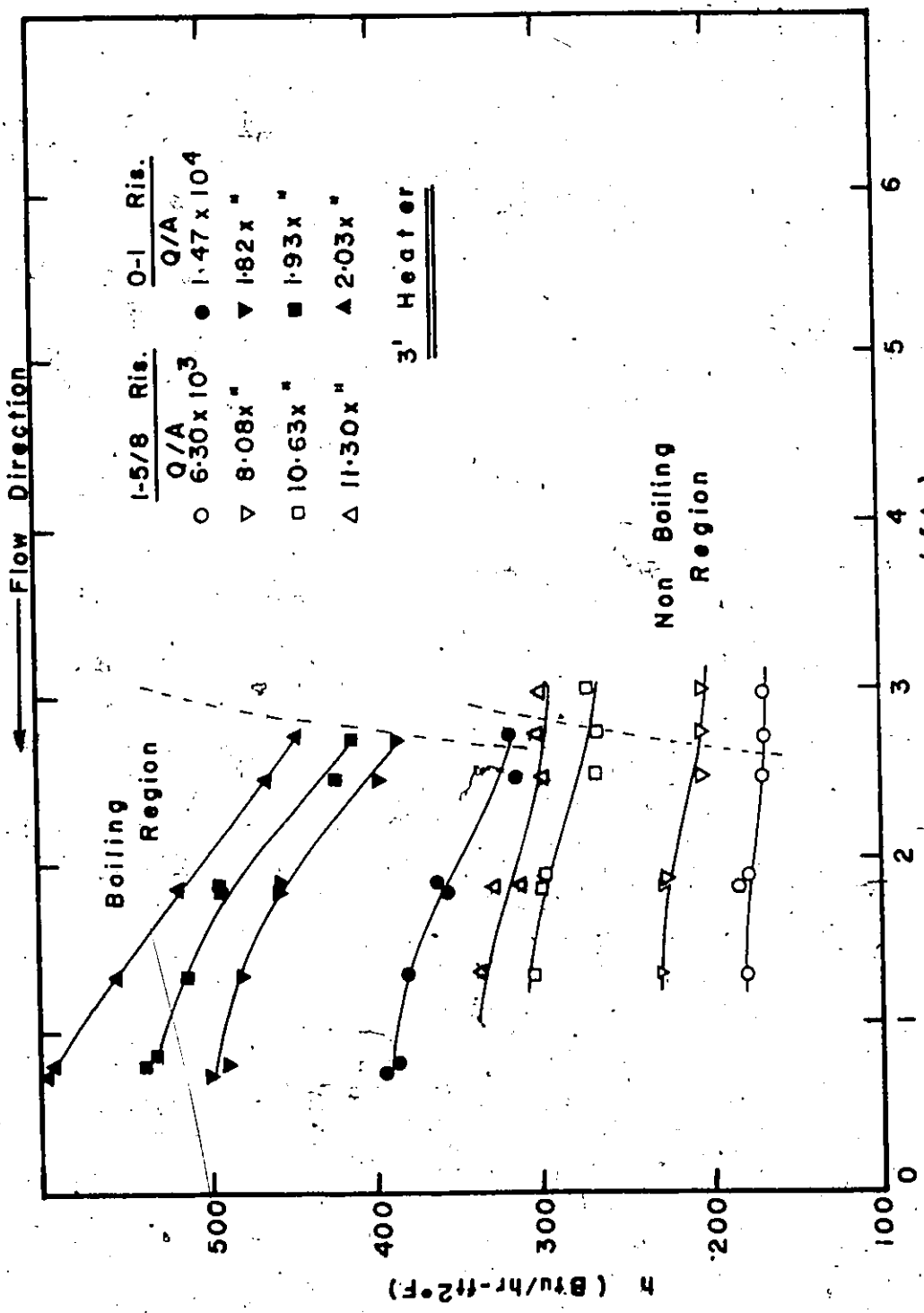

Fig 39 Axial Heat Transfer Coeff. Distributions

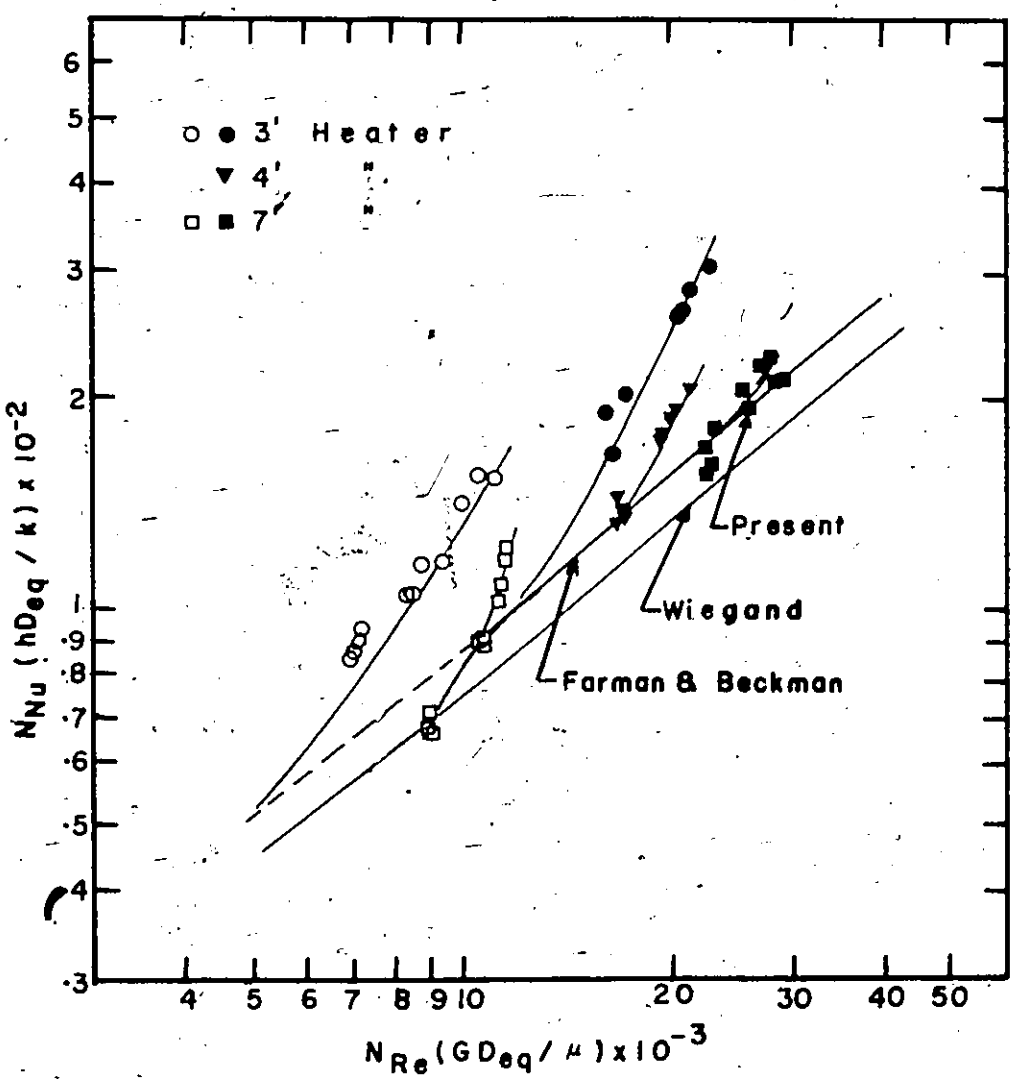

Fig 40 Nusselt Numbers Realized

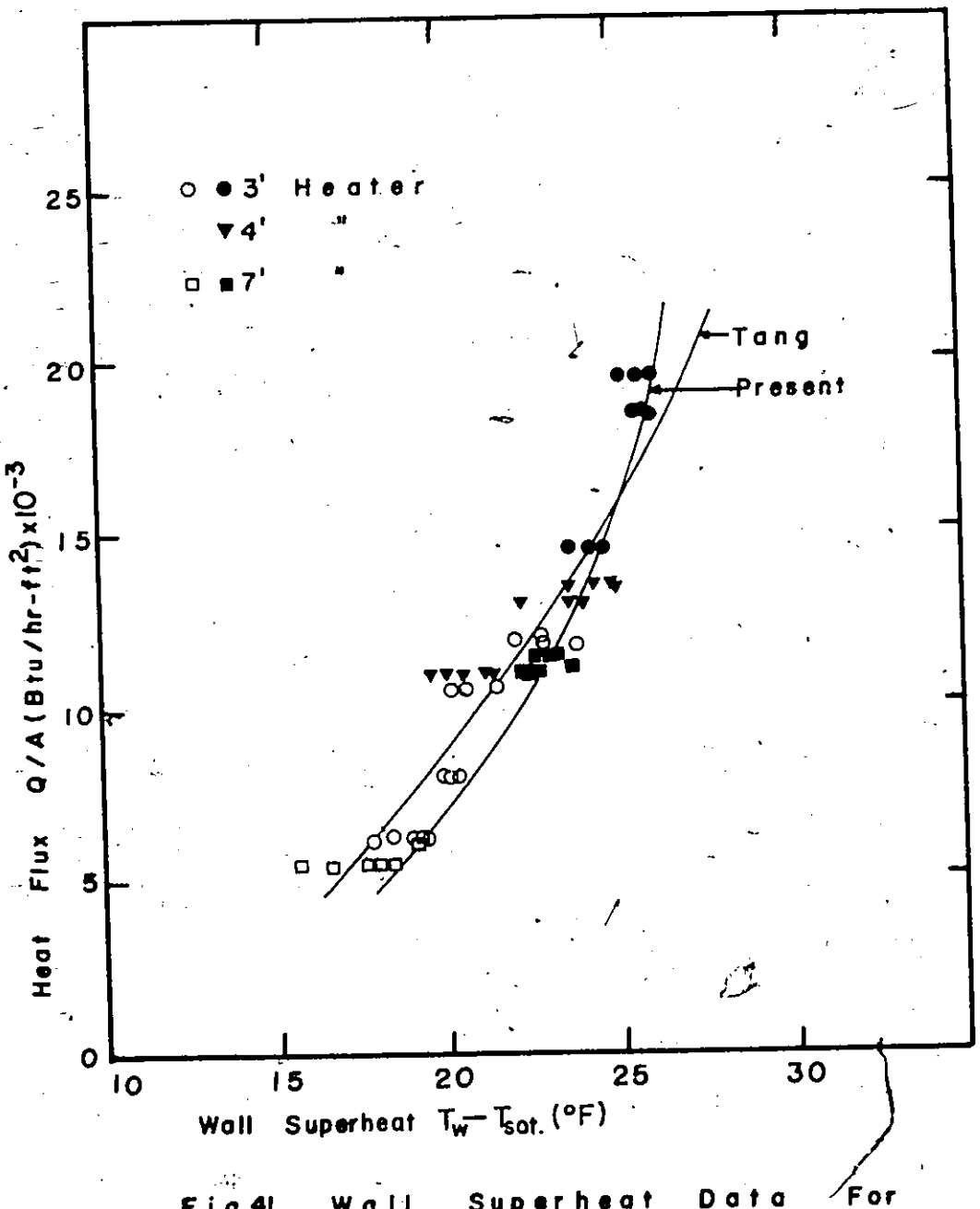

Fig 41 Wall Superheat Data For Subcooled Nucleate Flow Boiling

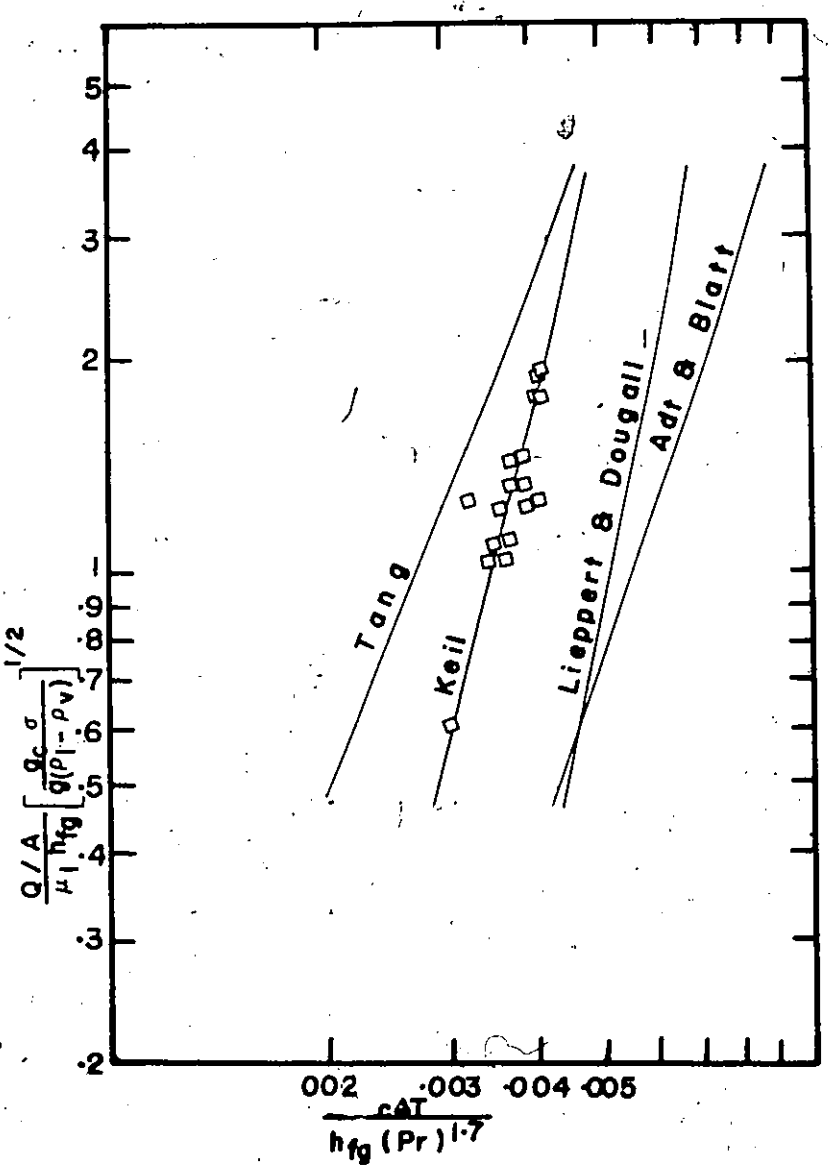

Fig 42 Rohsenow Corrolation for Boiling

(Copper- R-113 Combination)

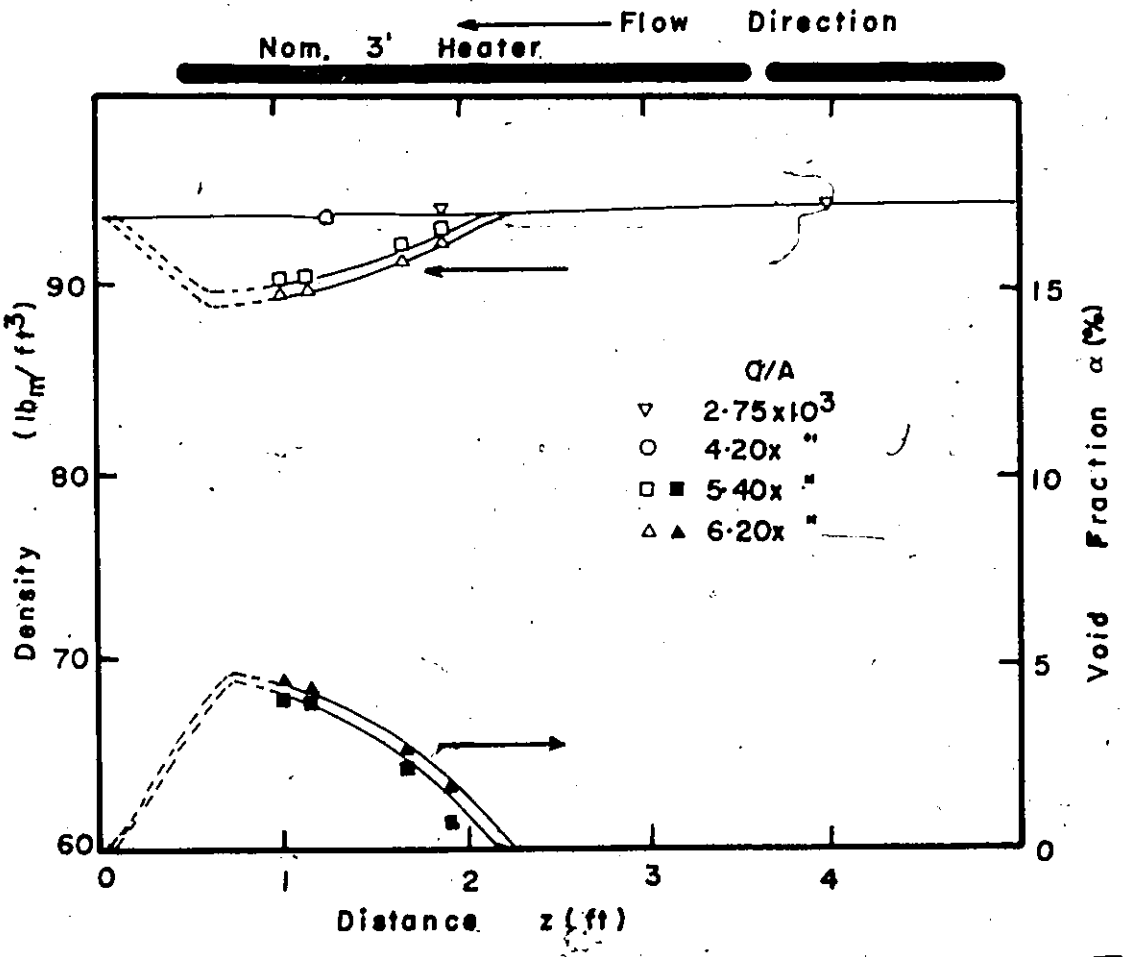

Fig 43 Axial Density and Void Distribution In Subcooled Nucleate Boiling (7' Heater & 1-5/8 Riser)

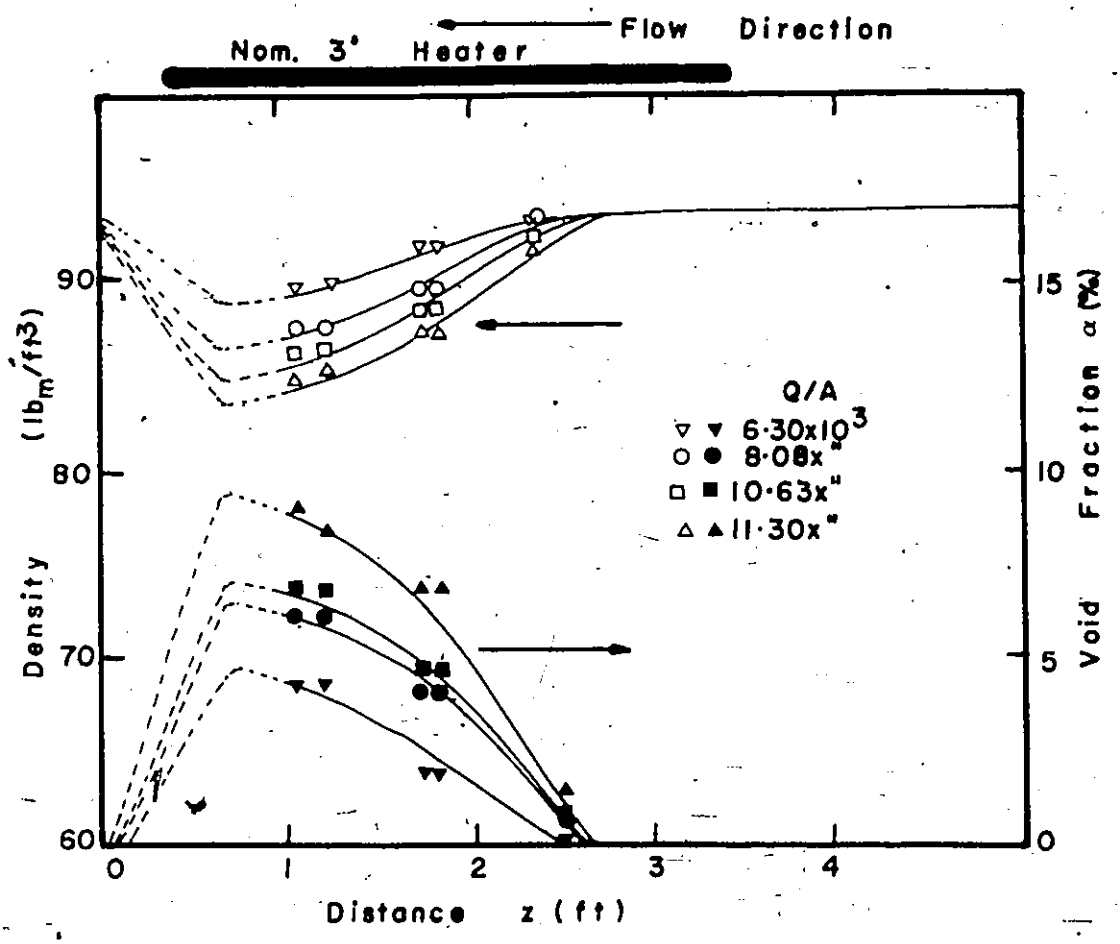

Fig 44 Axial Density & Void Distribution In Subcooled Nucleate Boiling (3' Heater & 1-5/8 Riser)

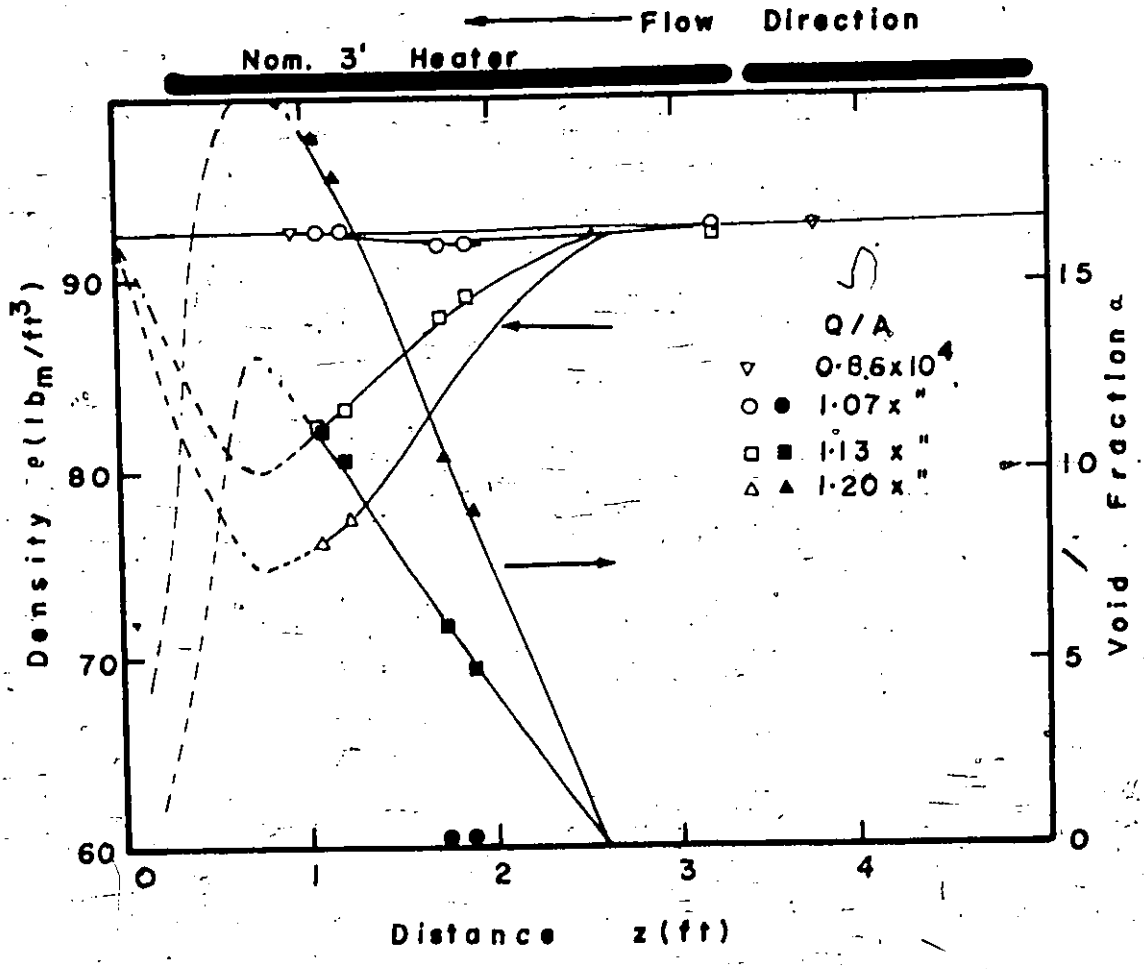

Fig 45 Axial Density and Void Distribution in Subcooled Nucleate Boiling (7' Heater & 0-1 Riser)

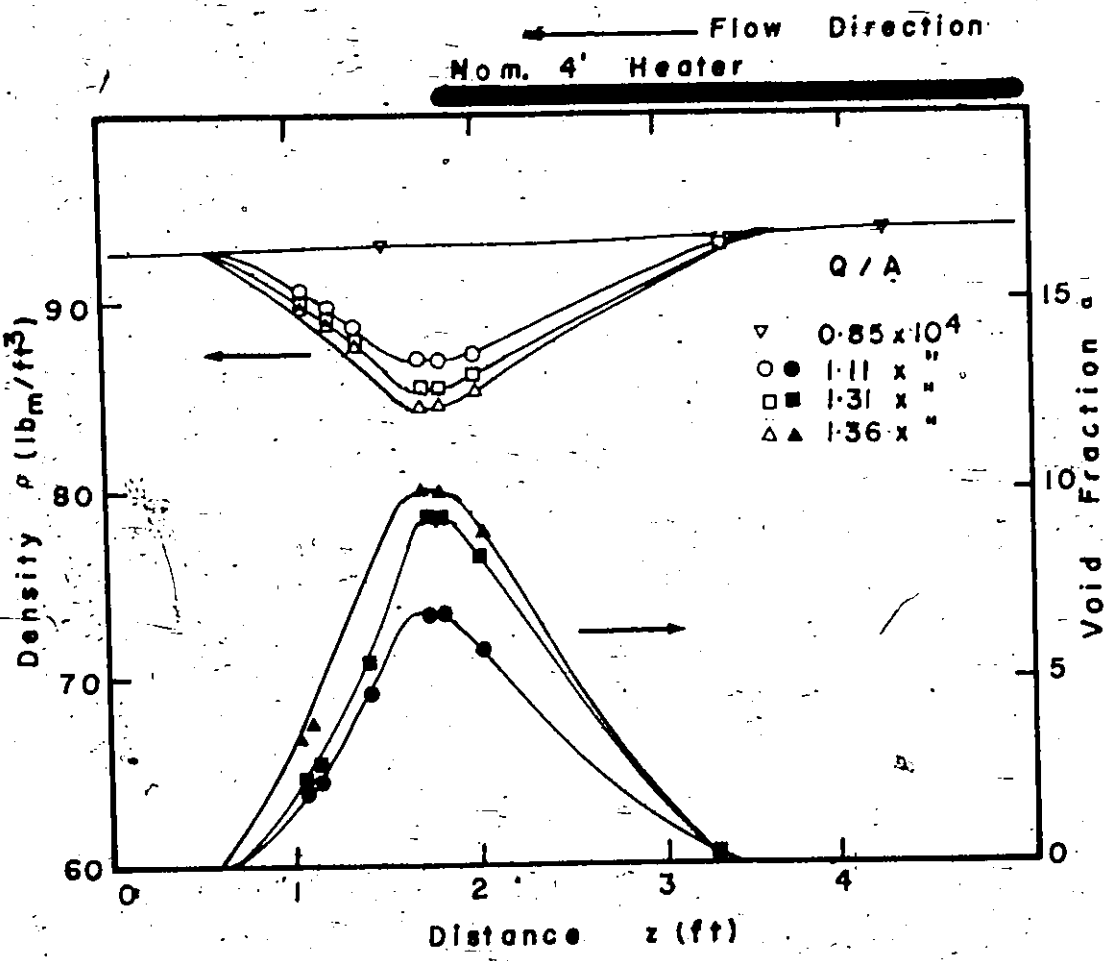

Fig 46 Axial Density and Void Distribution in Subcooled Nucleate Boiling (4' Heater & 0-1 Riser)

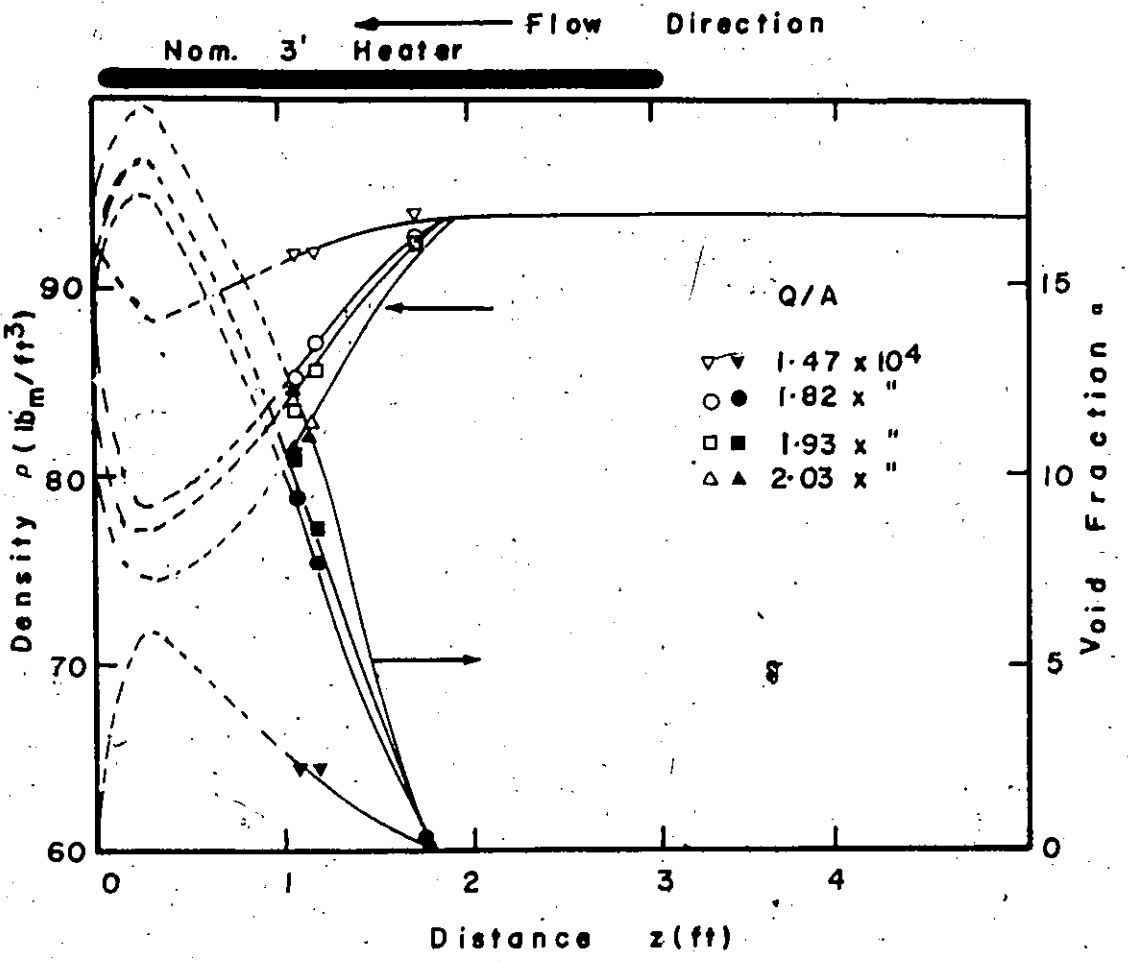

Fig 47 Axial Density and Void Distribution In Subcooled Nucleate Boiling (3' Heater & O-I Riser)

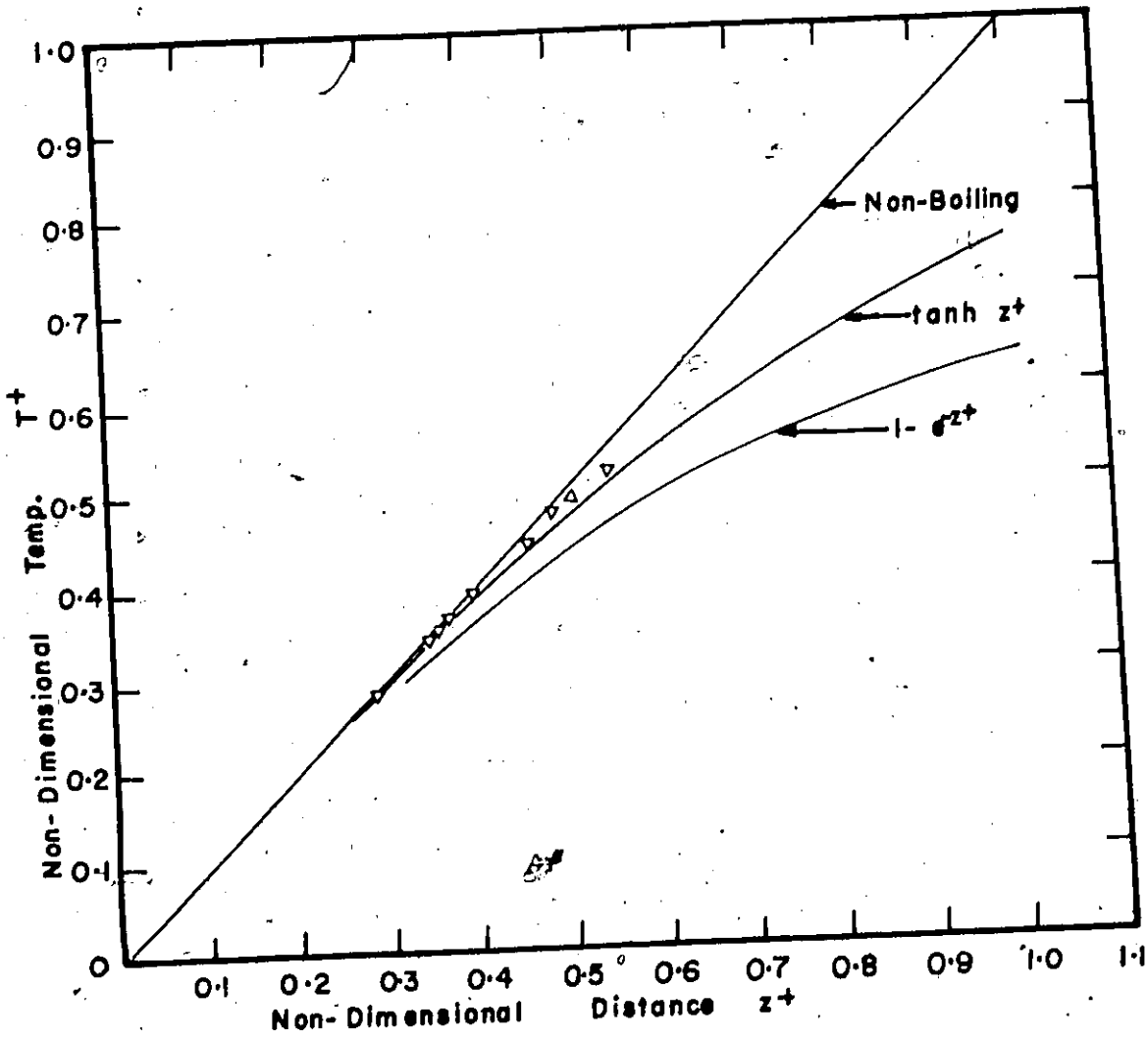

Fig 48 Non-Dimensional Liquid Temperature Distribution in Nucleate Subcooled Boiling.

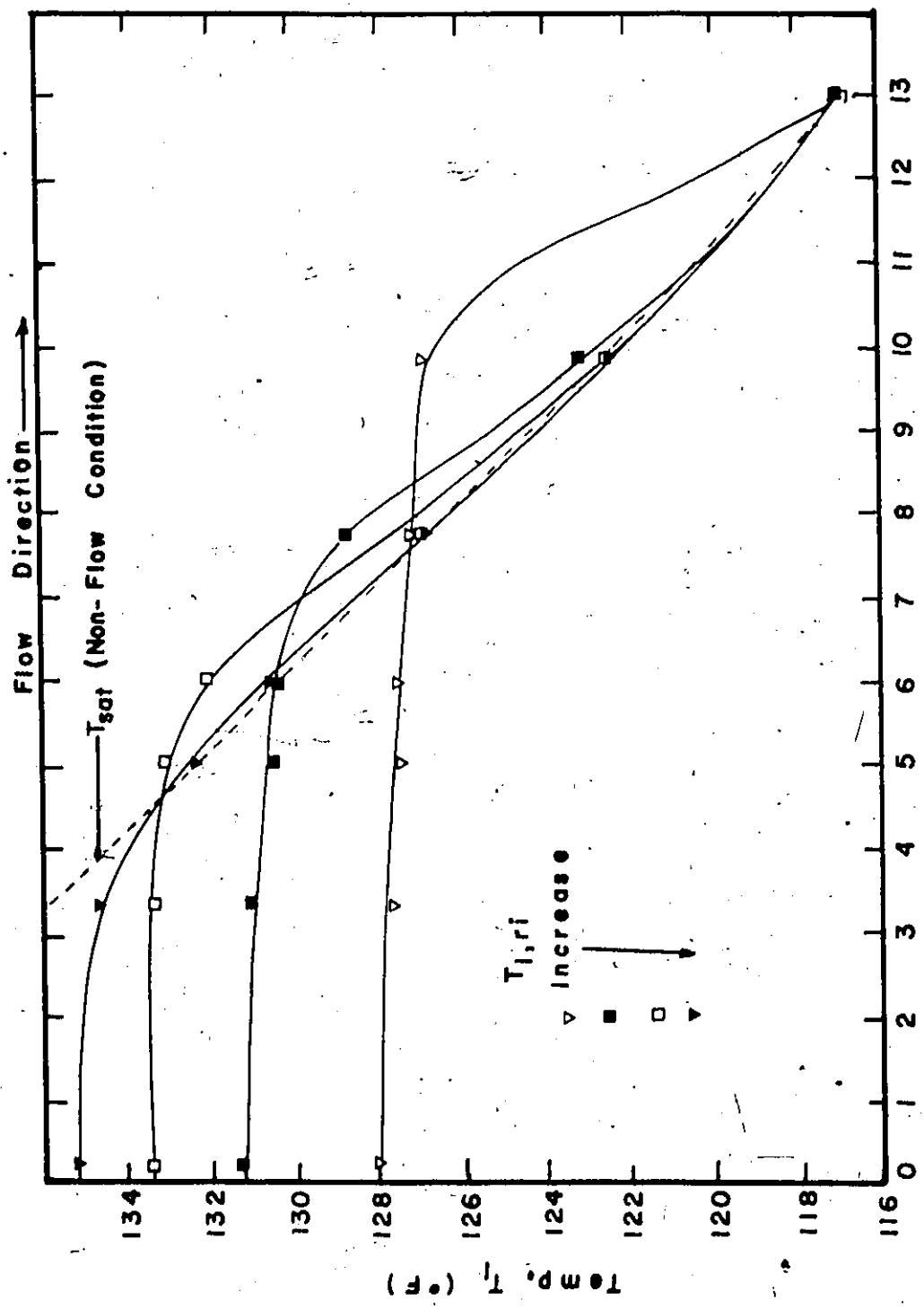

Fig 49 Measured Axial Temp. Distr. in Vertical Flashing Flow. (1-5/8 Riser)

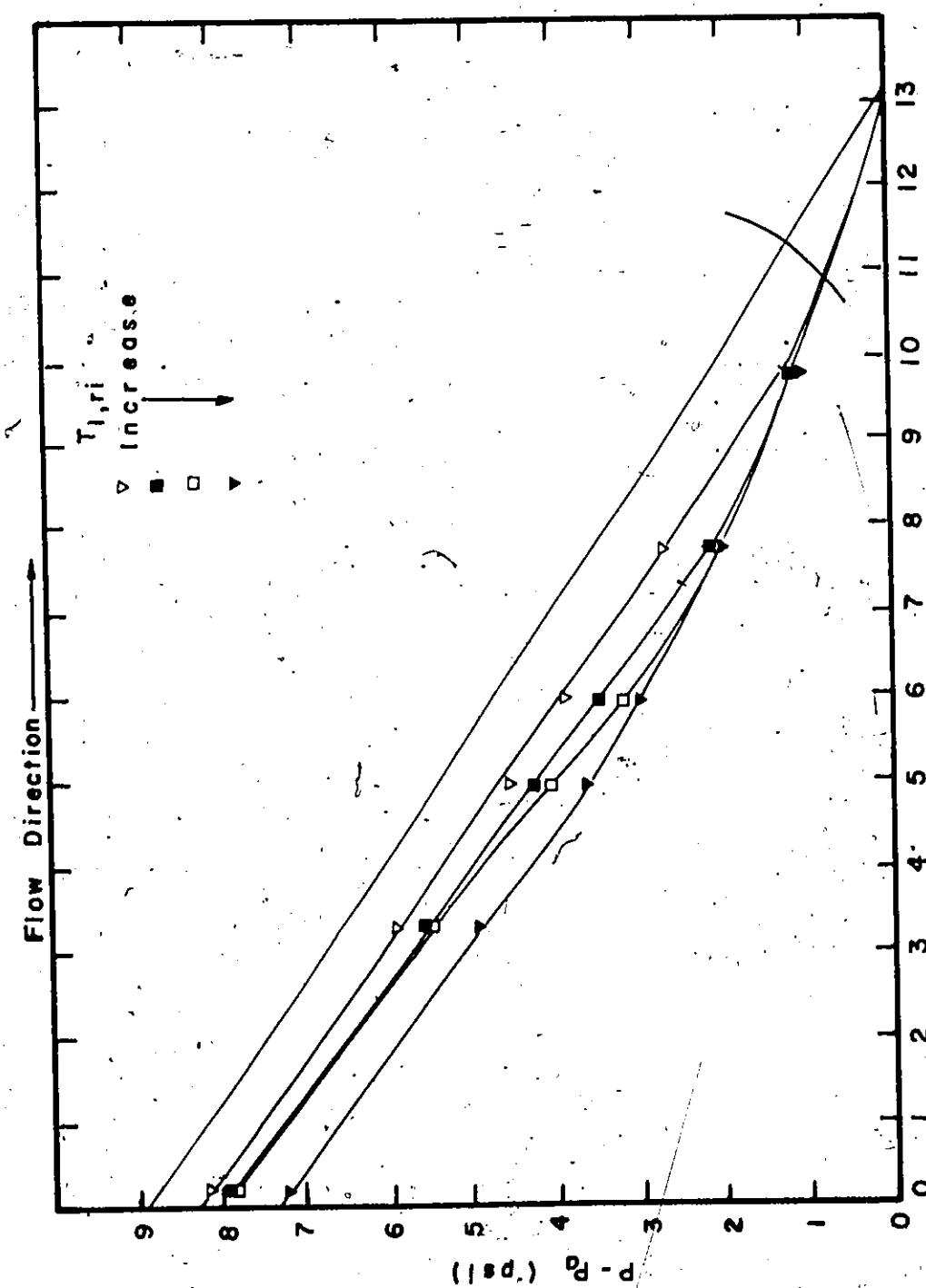

Fig 50 Measured Axial Pressure Distr. In Vertical Flashing Flow. ($1-\frac{5}{8}$ Riser)

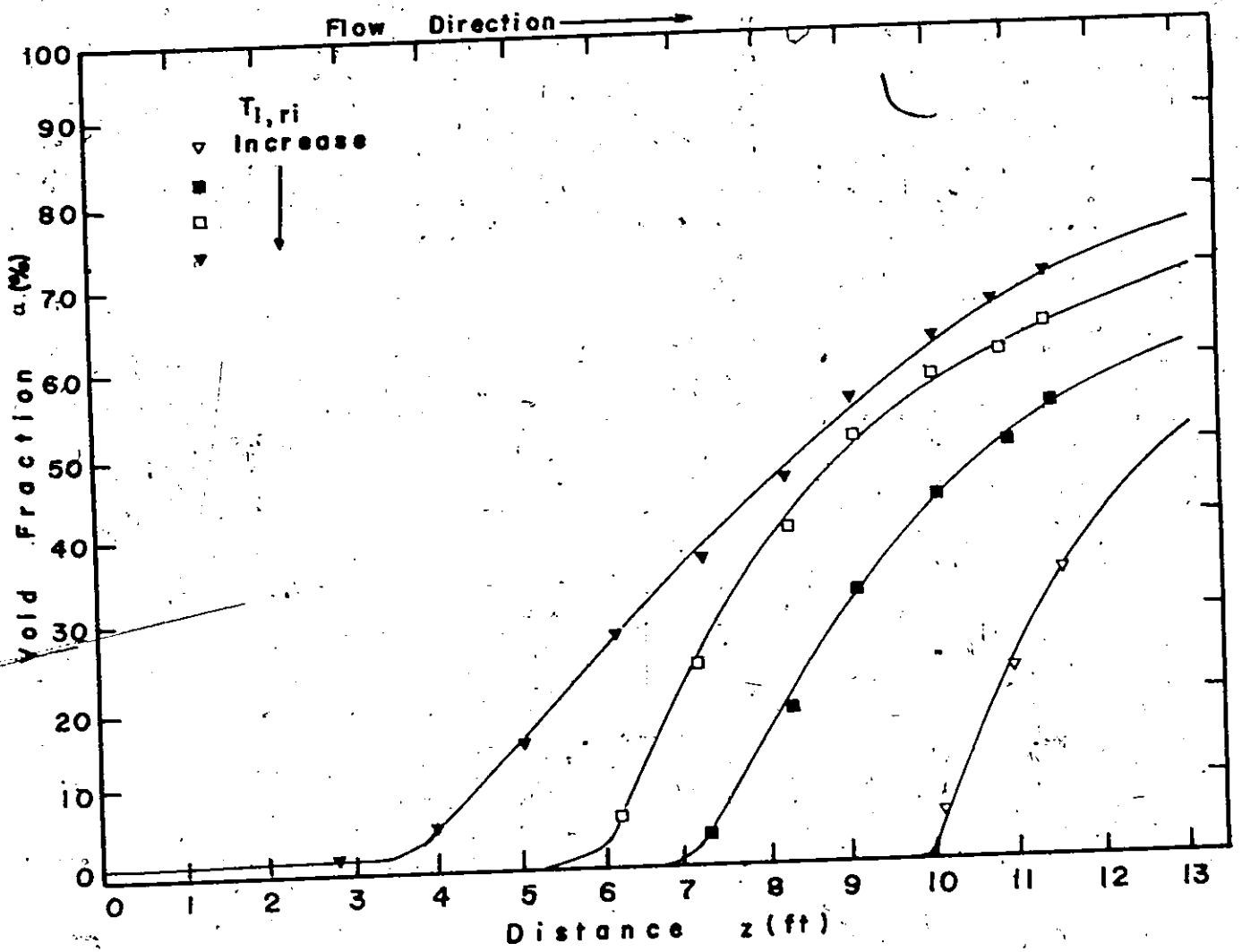

Fig. 51 Measured Axial Void Fraction Distr. In Vertical Flashing Flow. (1-5/8 Riser)

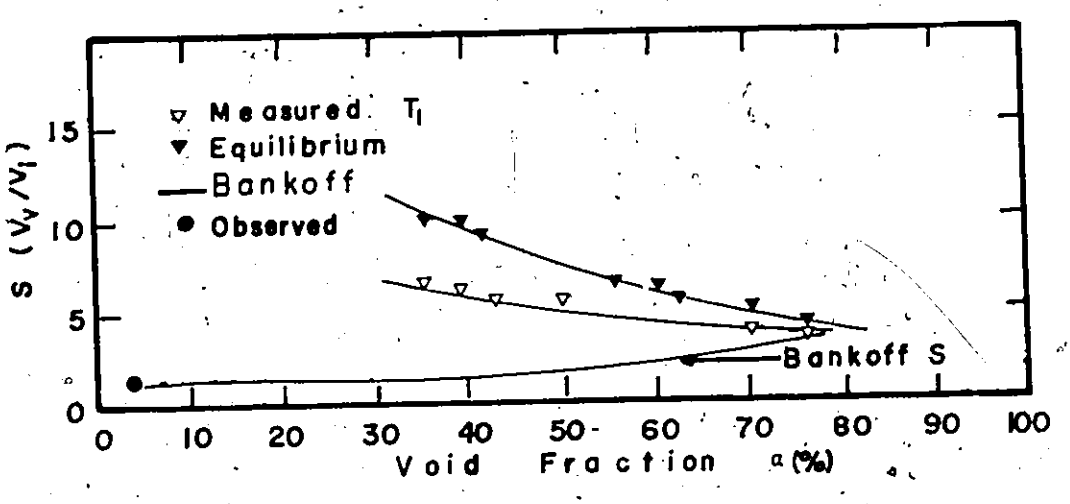

Fig 52a Slip In Vertical Flashing Flow

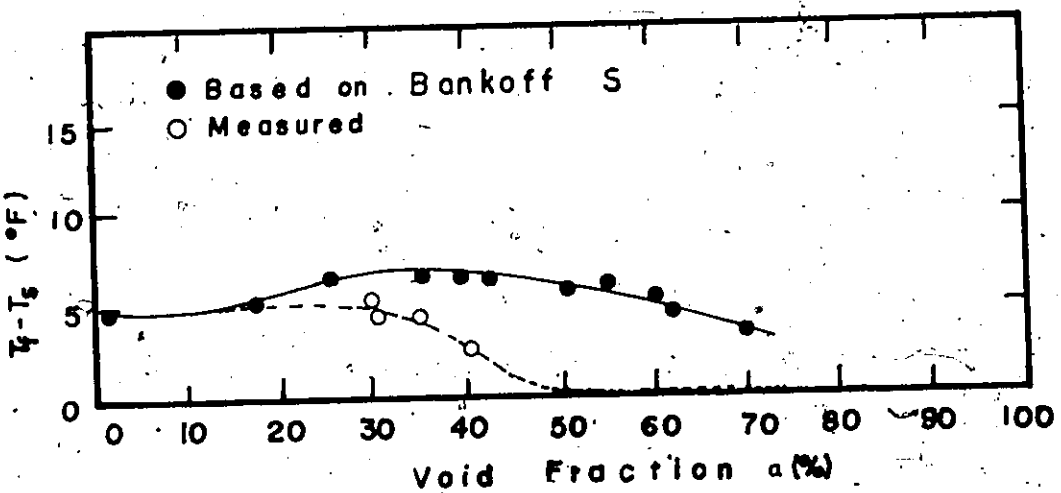

Fig 52b Liquid Superheats In Vertical Flashing Flow.

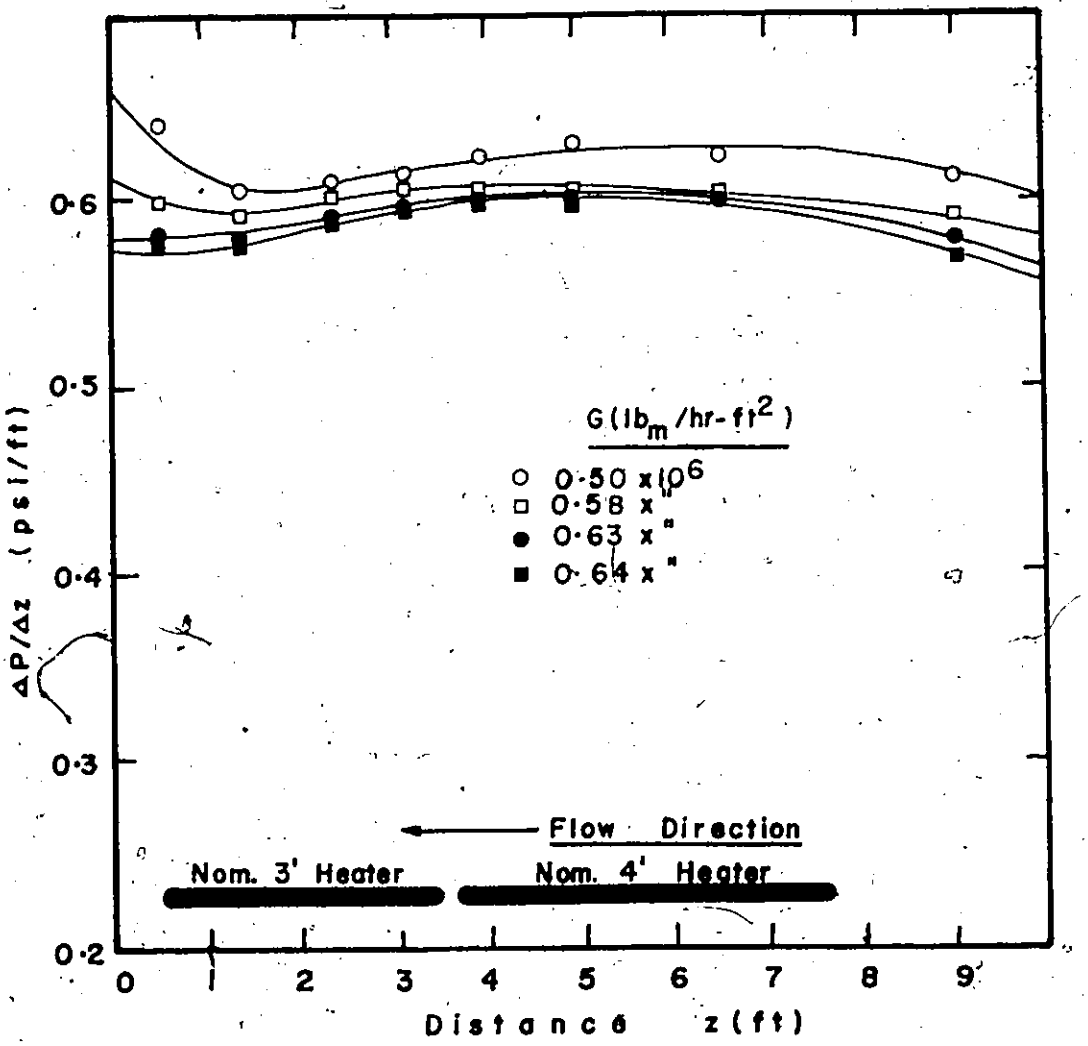

Fig 53 Pressure Gradient In Subcooled Nucleate Boiling (7' Heater & 1-5/8 Riser)

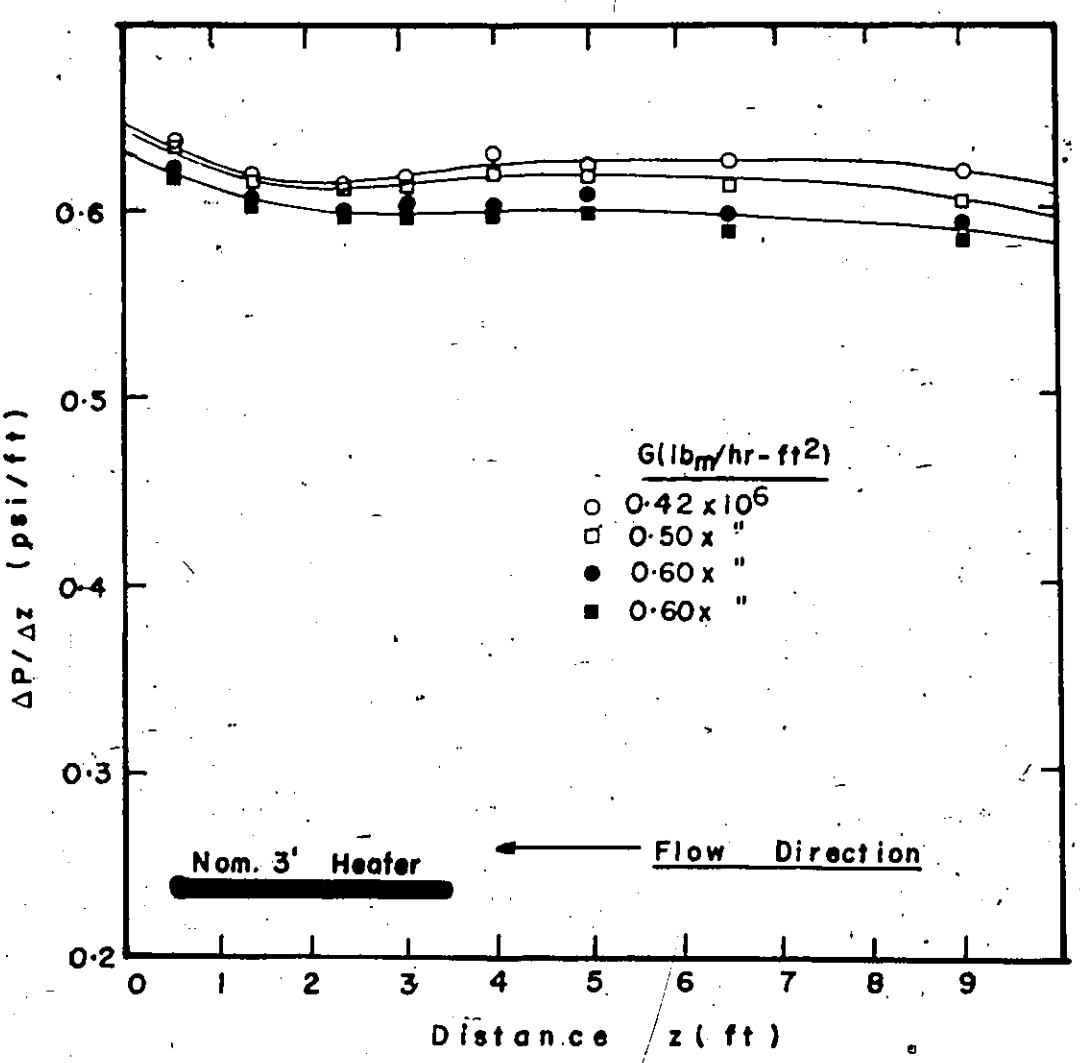

Fig 54 Pressure Gradient In Subcooled Nucleate Boiling (3' Heater & 1-5/8 Riser)

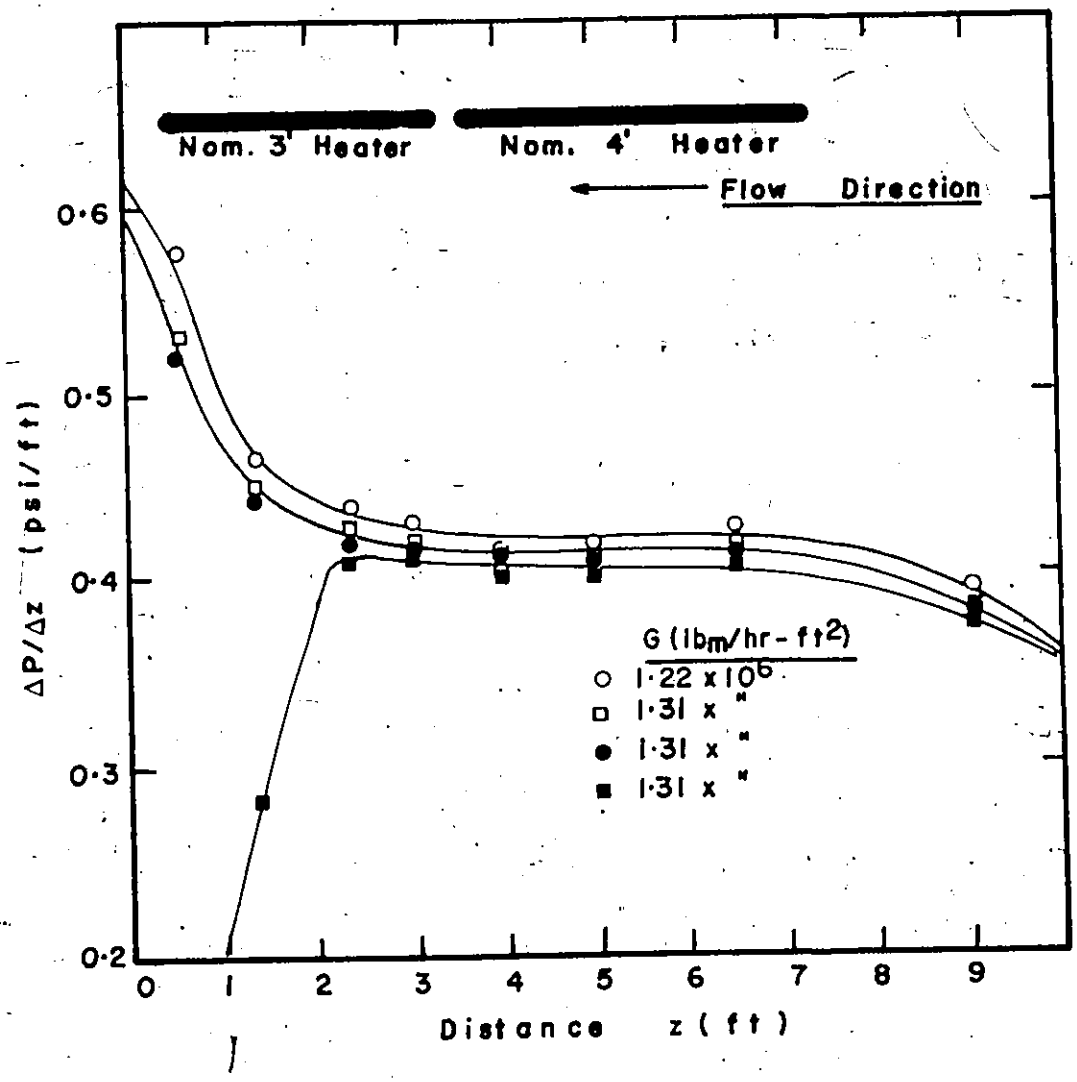

Fig 55 Pressure Gradient In Subcooled Nucleate Boiling (7' Heater & O-I Riser)

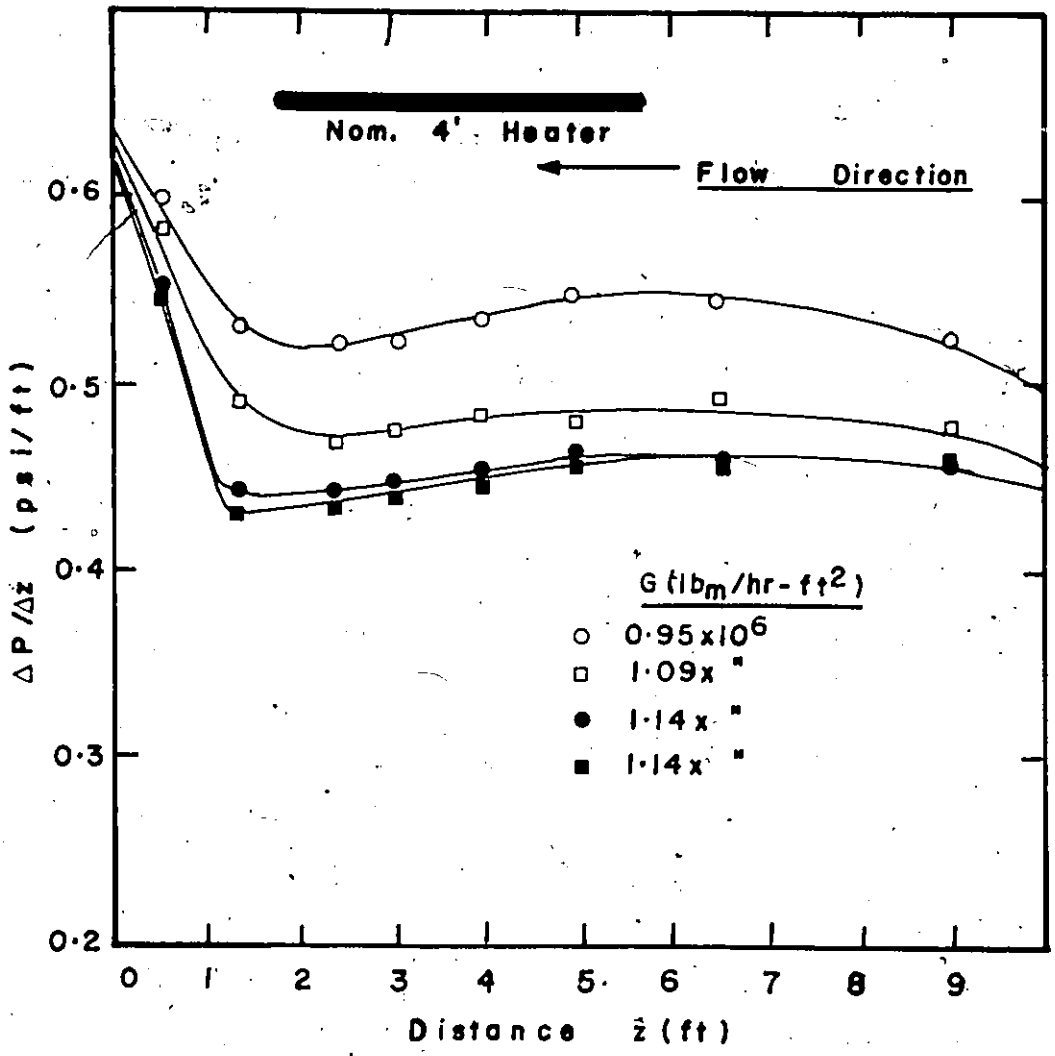

Fig 56 Pressure Gradient In Subcooled Nucleate Boiling (4' Heater & 0-1 Riser)

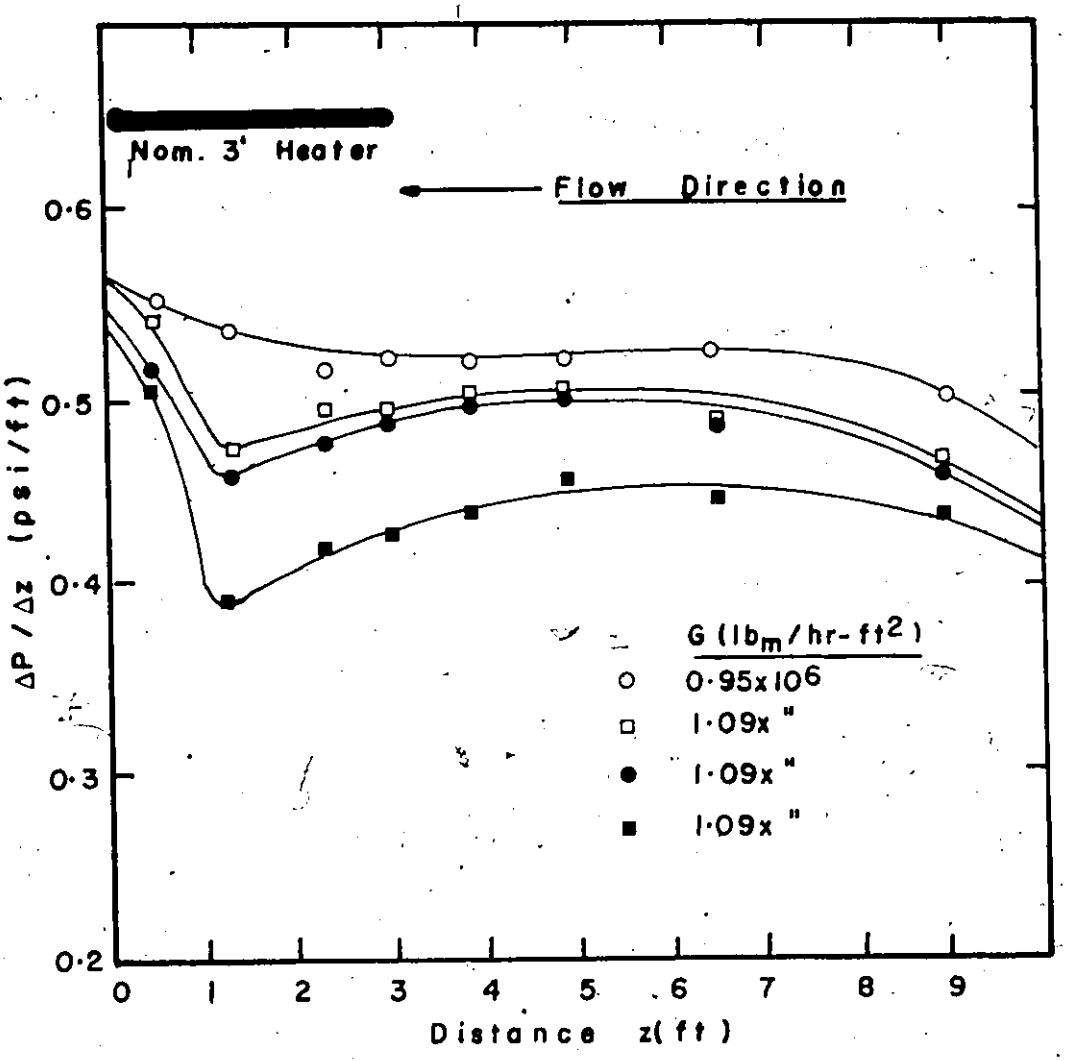

Fig 57 Pressure Gradient In Subcoole Nucleate Boiling (3' Heater & 0-1 Riser)

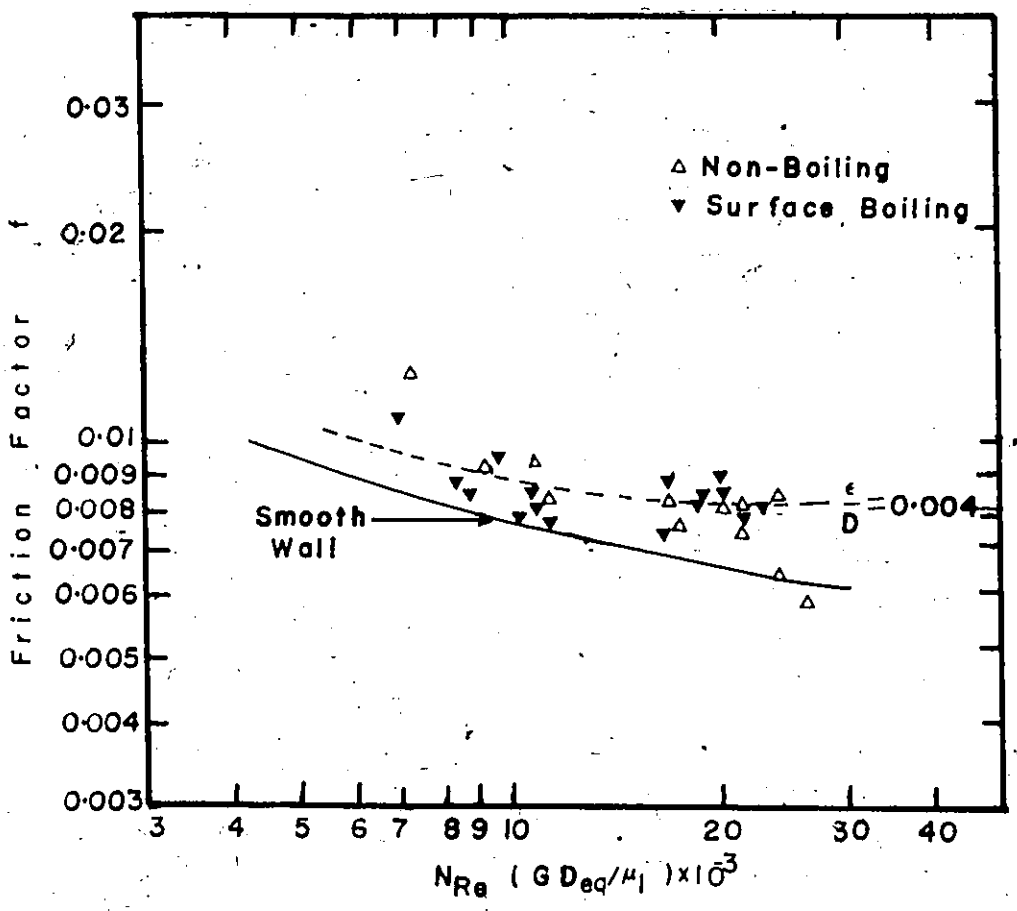

Fig 58 Friction Factors In An Annulus (D_o / D_i = 1·33)

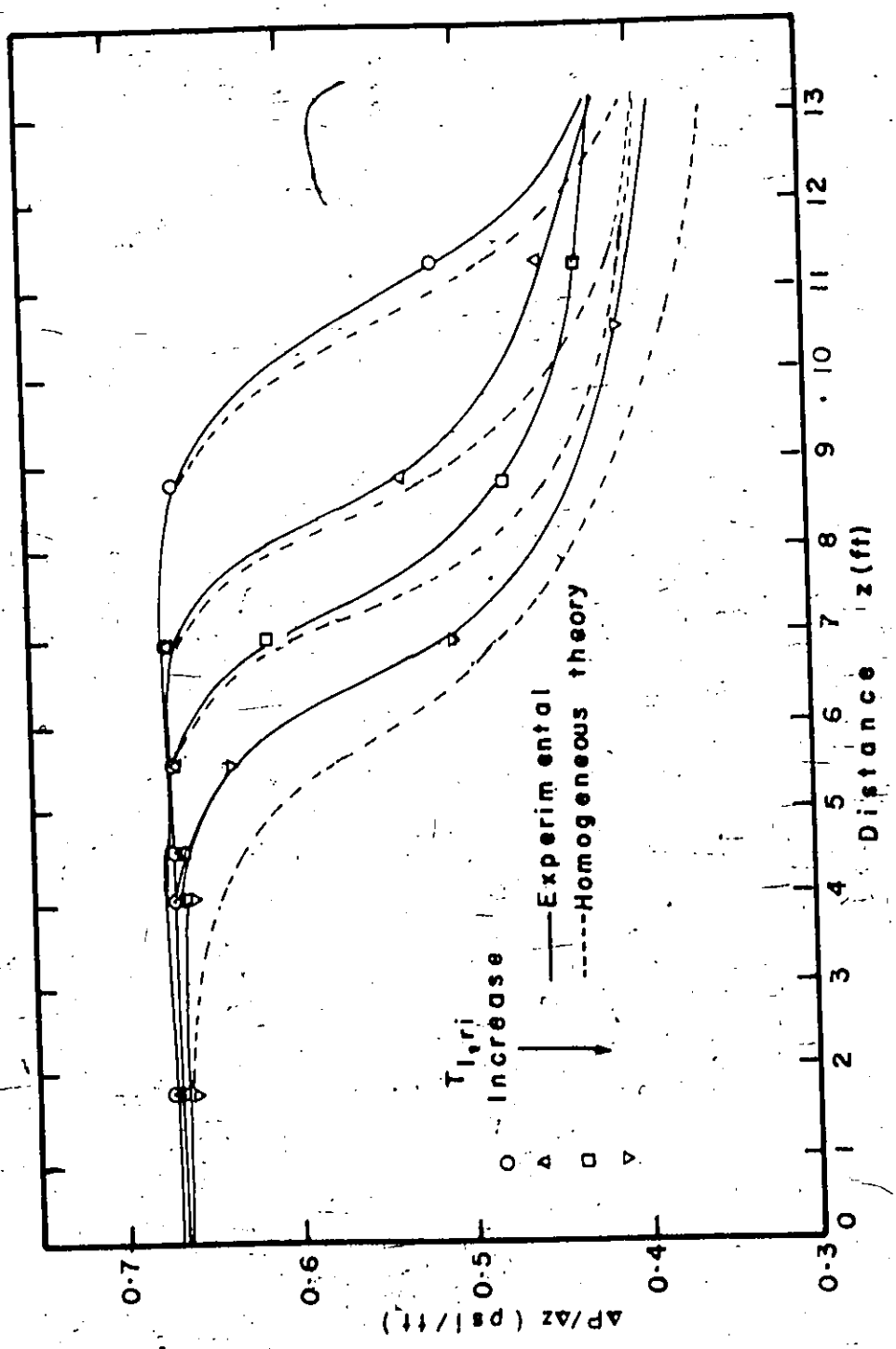

Fig. 59 Pressure Gradient In Vertical Flashing Flow

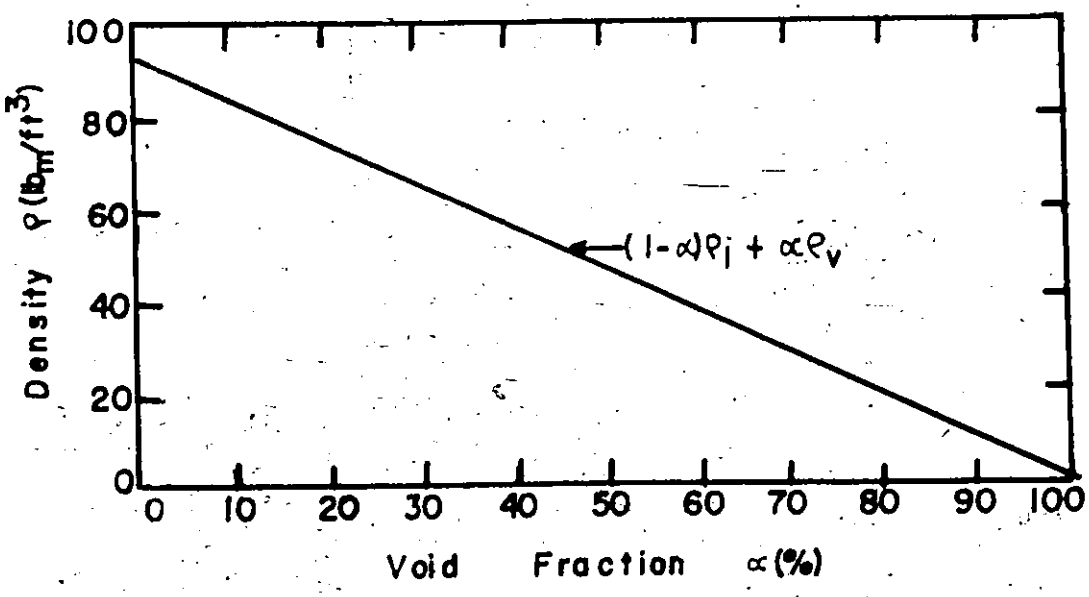

Fig. 60a Density In Vertical Flashing Flow

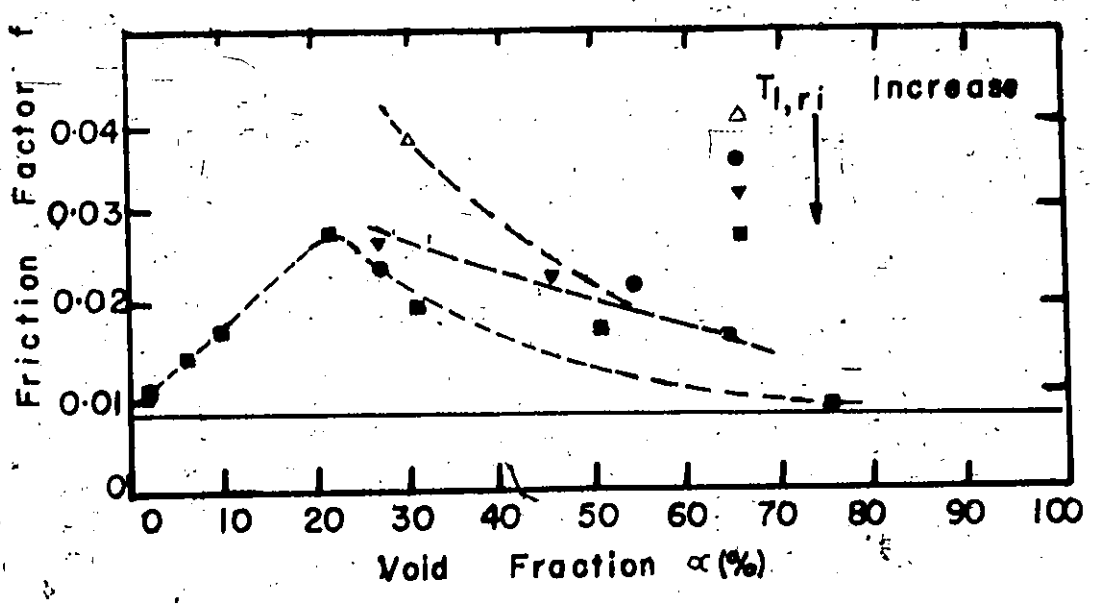

Fig 60 b Friction Factors In Vertical Flashing Flow.

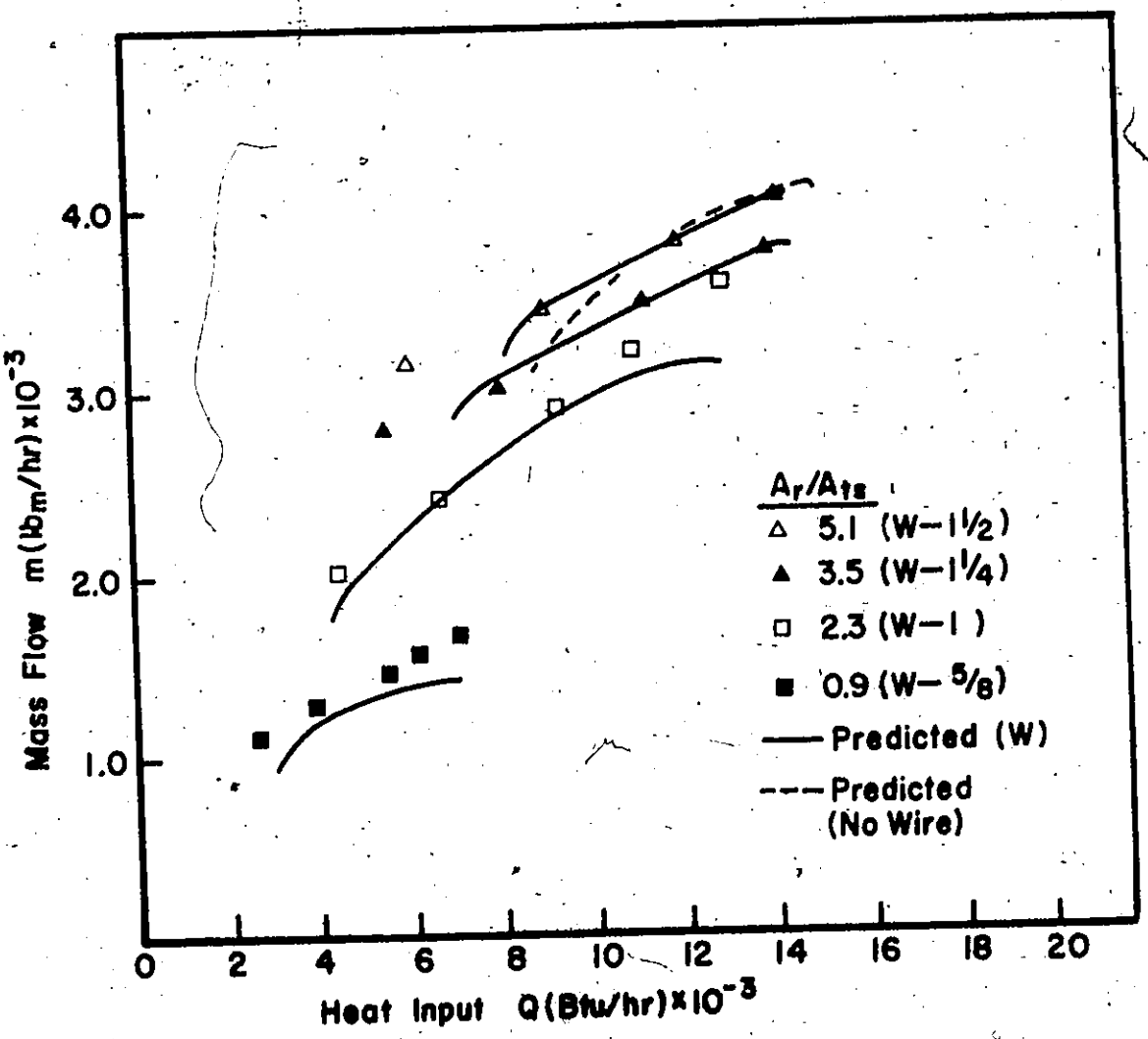

Fig.61 Computed and Experimental Flow Rates Vs. Heat Inputs.

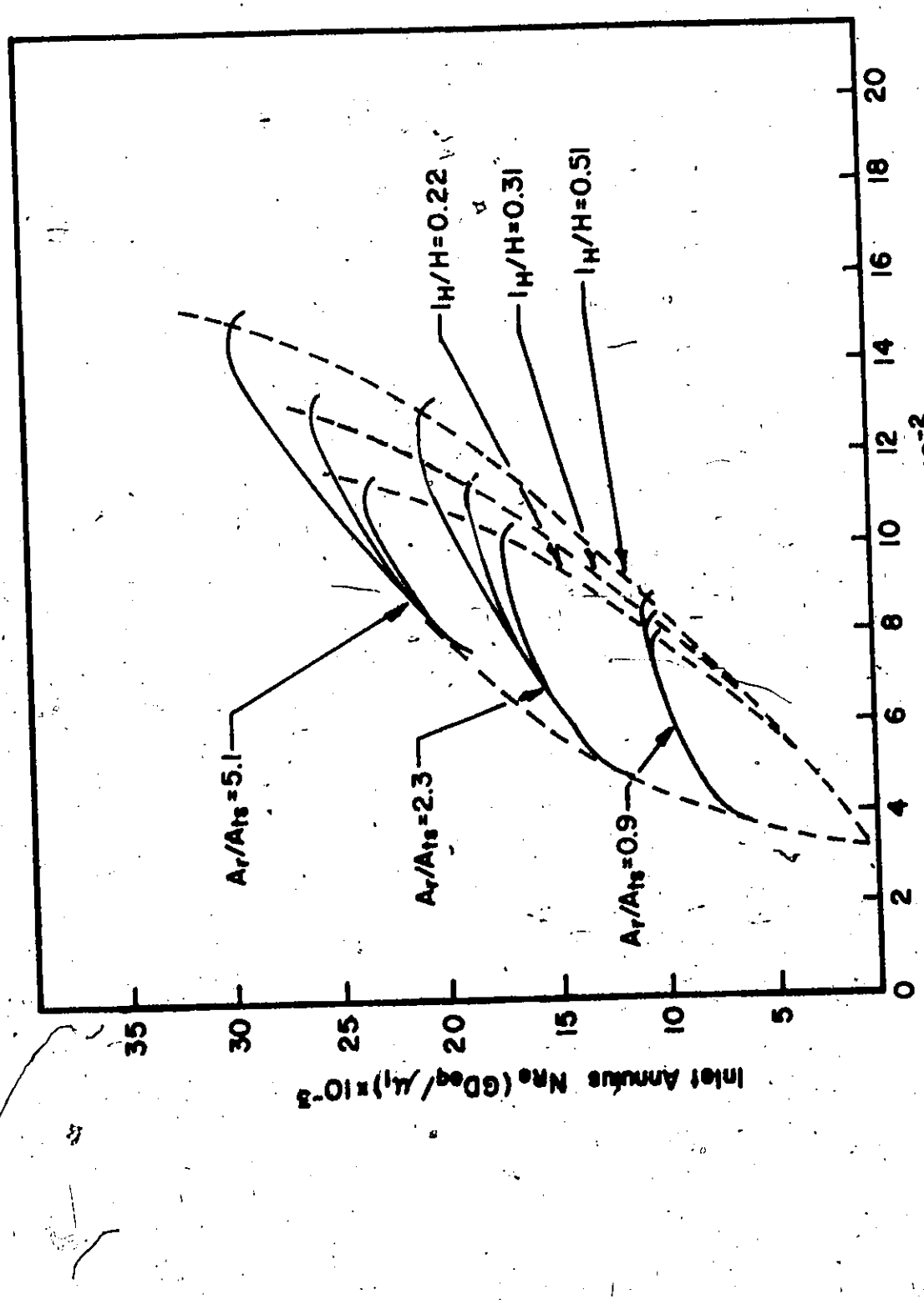

Fig.62 Predicted Characteristics For Different A_r/A_{ts} And l_H/H Ratios (R-113).

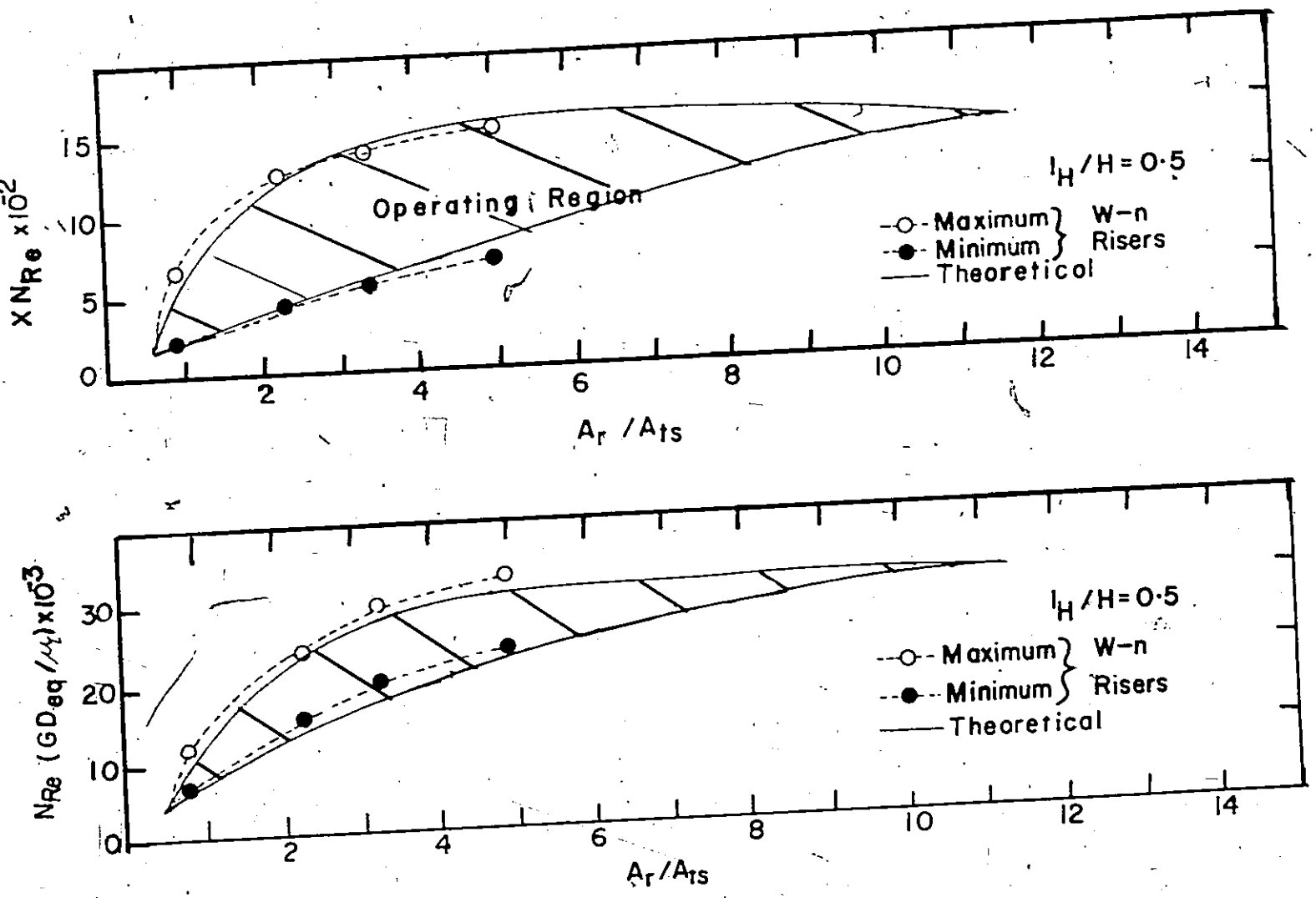

Fig 63 Effect of Area Ratio on XN_{Re} and N_{Re}

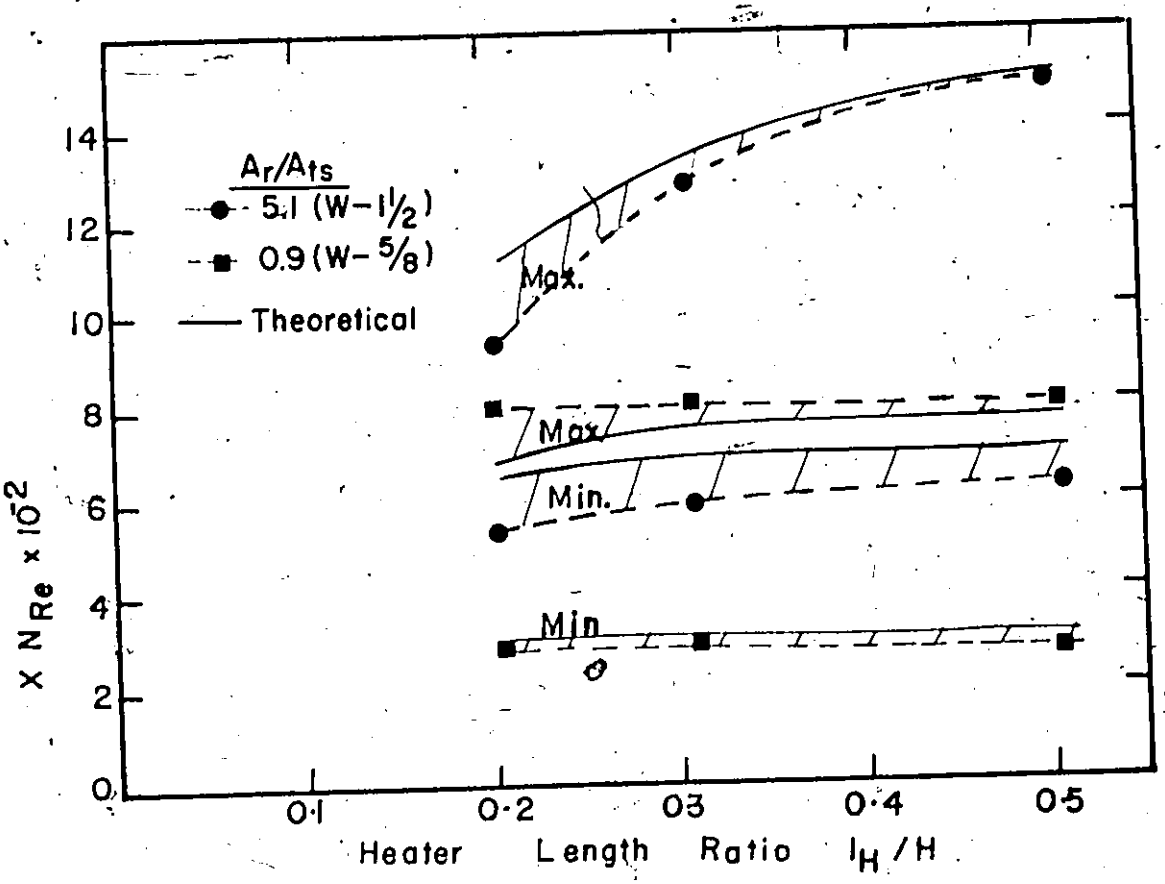

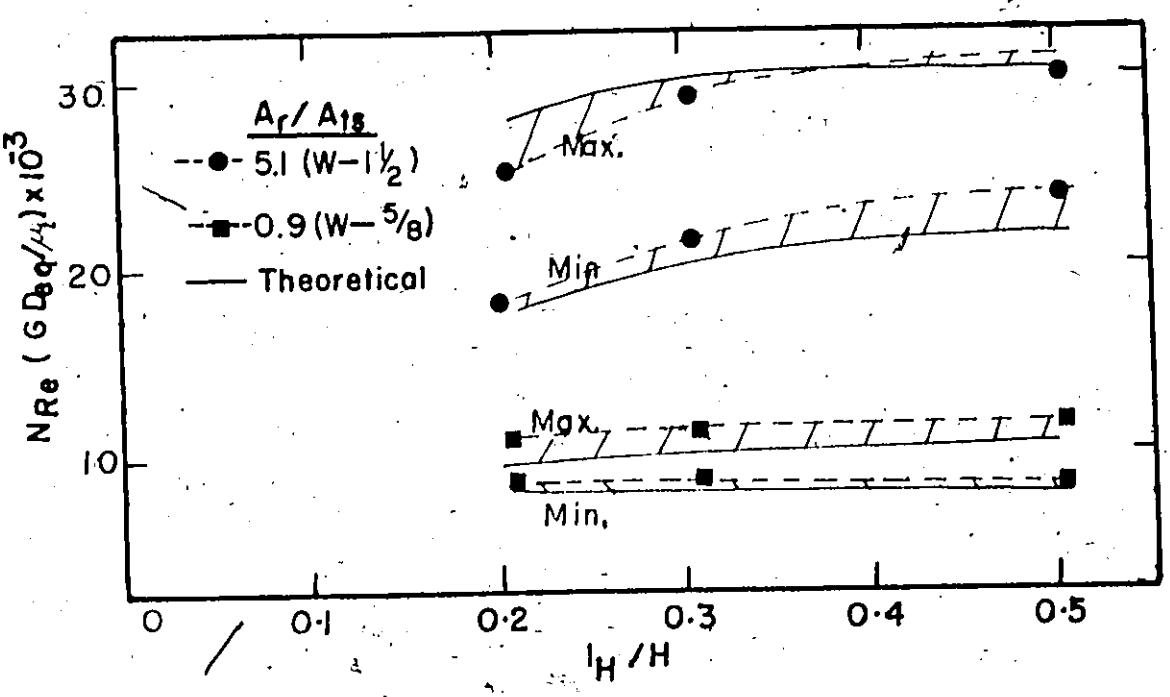

Fig 64 Effect of Heater Length on N_{Re} and X N_{Re}

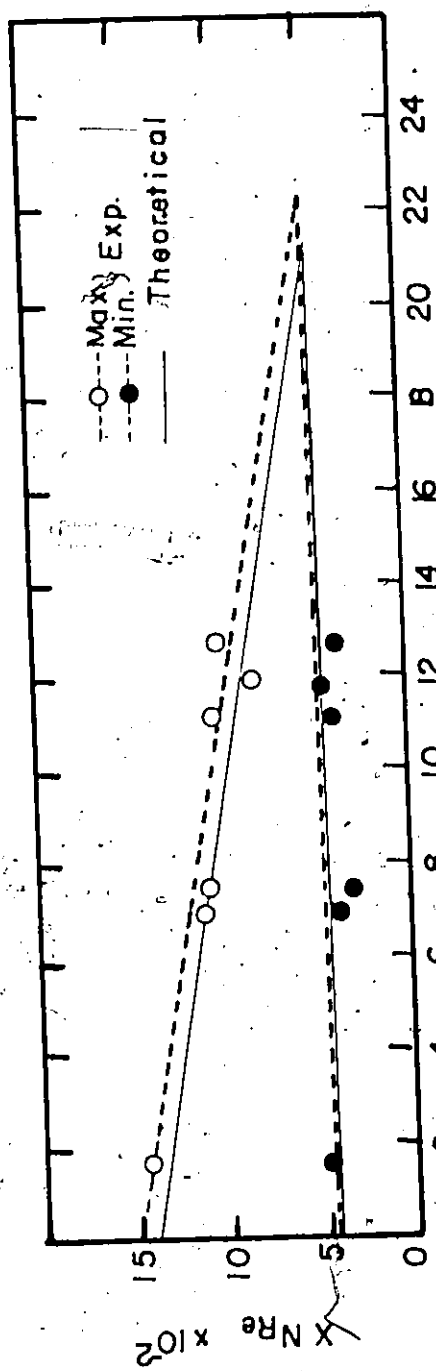

Fig 65 Effect of Reservoir Subcooling on N_{Re} and X N_{Re}

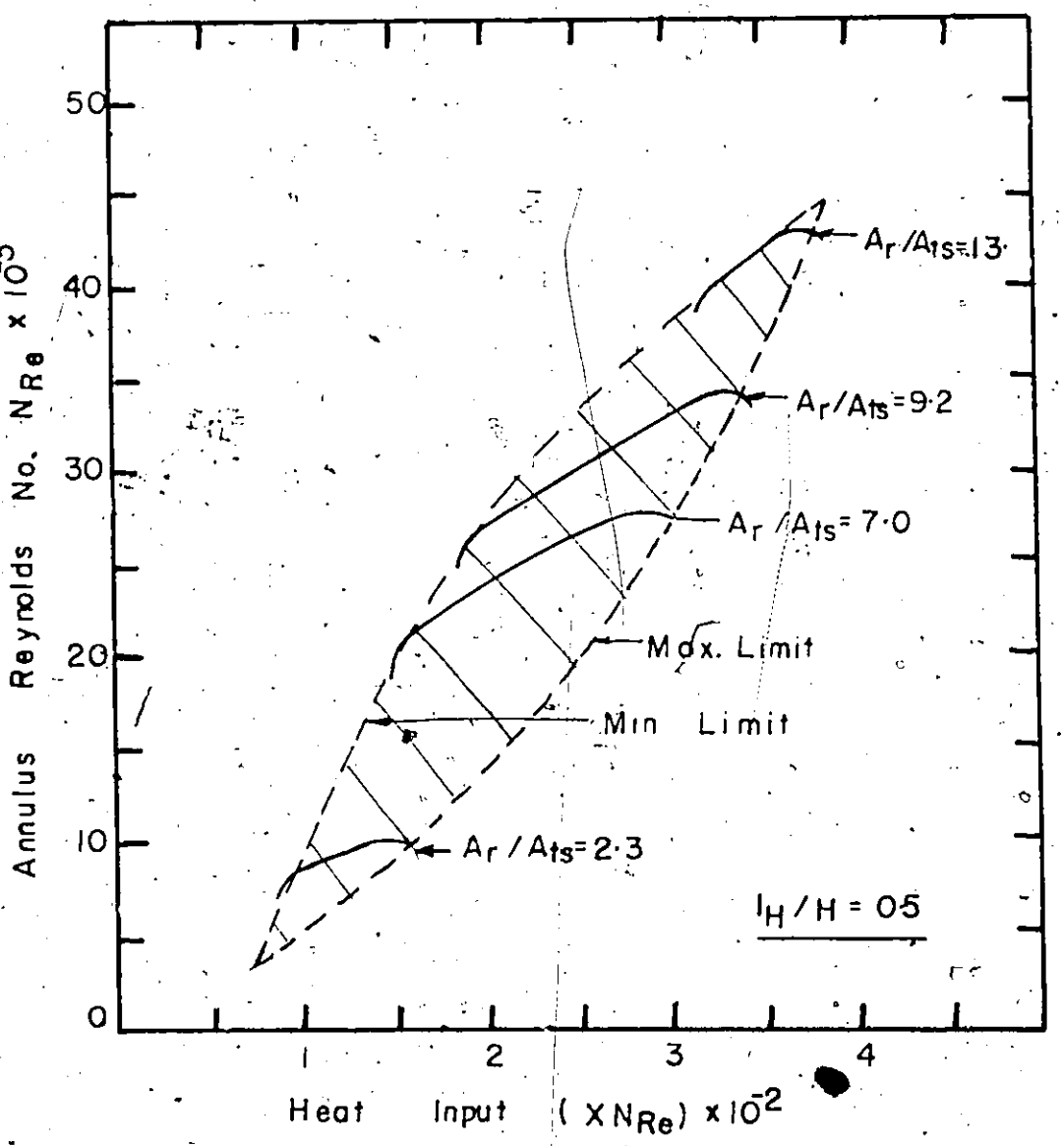

Fig 66 Predicted Characteristics For Different A_r/A_{ts} Ratios (H_2O)

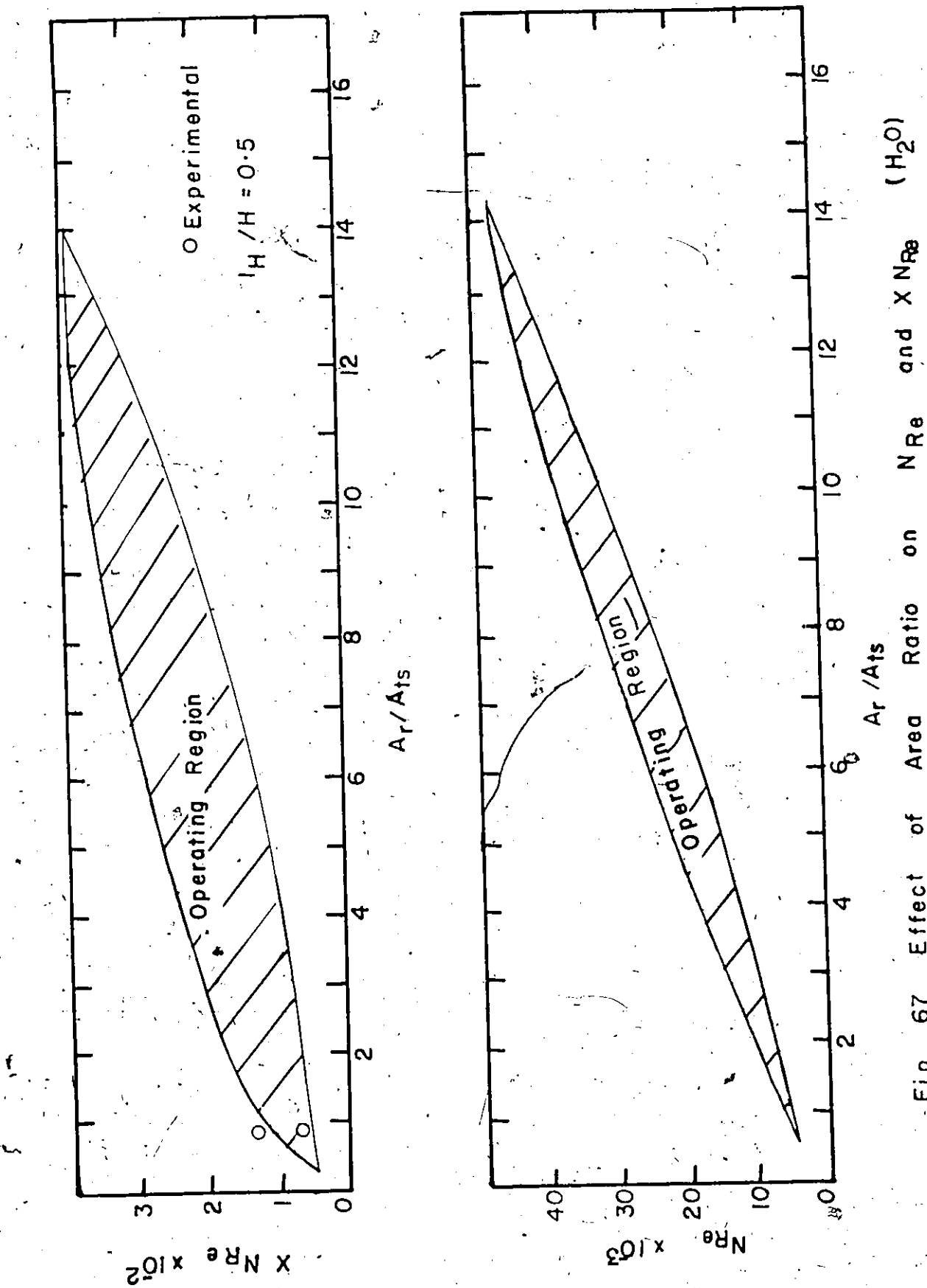

Fig 67 Effect of Area Ratio on N_{Re} and $X N_{Re}$ (H_2O)

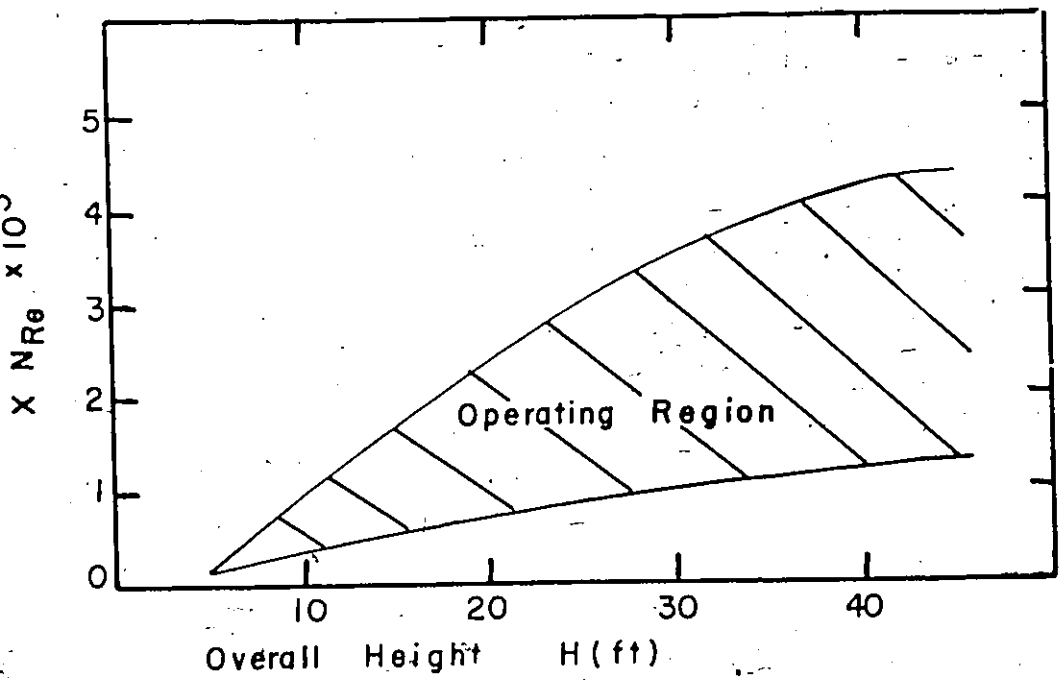

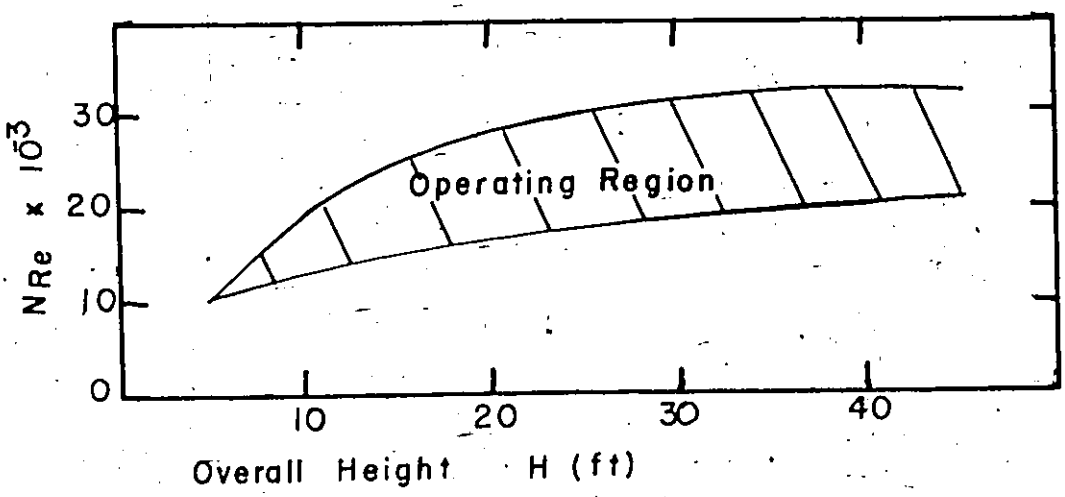

Fig 68 Effect of Height on N_{Re} and X N_{Re} (Predicted)
R-113, l_H/H=0.5

TABLE I PHYSICAL PROPERTIES OF R-113*

Boiling point at 1 atm. (°F)	117.63
Density, liquid at B. P. (lb_m/ft^3)	94.25
Density, saturated vapour at B. P. (lb_m/ft^3)	0.461
Specific heat, liquid at B. P. (B. t. u./lb_m-F)	0.225
Heat of vaporization at B. P. (B. t. u./lb_m)	63.12
Thermal conductivity at B. P. (B. t. u./hr-ft- F)	0.04
Viscosity, liquid at B. P. (lb_m/ft-hr)	1.2
Surface tension at B. P. (lb_f/ft)	0.00109

*Information furnished by Du Pont of Canada (Tech. Bulletin B-2)

TABLE II Single-phase Forced Convection Correlations

$$N_{Nu} = a \cdot N_{Re}^{b} \cdot N_{Pr}^{n} \cdot \Phi(D_o/D_i)$$

Investigators	"a"	"b"	"n"	"Φ"	Remarks
Monrad & Pelton A1	0.020	0.8	1/3	$(D_o/D_i)^{0.53}$	$N_{Re} > 10,000$
[illegible] A3	0.023	0.8	0.4	$(D_o/D_i)^{0.45}$	$N_{Re} > 10,000$
Dittus & [illegible] A2	0.023	0.8	0.4	$(D_o/D_i)^{0.45}$	$N_{Re} > 10,000$
[illegible] A5	0.020	0.8	0.4	(D_o/D_i)	$7000 \geq N_{Re} \leq 10,000$
[illegible] Deinforello A4	0.023	0.8	1/3	1	$5000 \geq N_{Re} \leq 20,000$
Heil	0.023	0.78	0.4	$(D_o/D_i)^{0.45}$	$N_{Re} > 10,000$

TABLE III Values of "C_{sf}", "s", "r" and correlation coefficient of Rohsenow correlation (Eq. 2-15) Copper surface - R - 113 combination

Investigators	"s"	"r"	"C_{sf}"	Coeff. of Correlation
Lippert & Dougall[A12]	1.7	0.20	0.0059	-
Bl[illegible]tt & Mit[A11]	1.7	0.33	0.007	-
Tang[17]	1.7	0.38	0.0137	0.993
Keil	1.7	0.29	0.0043	0.787

APPENDIX I

LIST OF EQUIPMENT AND INSTRUMENTATION

1. Accu-Ray Density Measuring Systems, Series 300, Model DH 5, Industrial Nucleonics Corporation, Columbus, Ohio, U. S. A.
2. Ammeters, Weston Model 82, Rectifier Type 0-1000V., Multi-range, Weston Instruments, Mississauga, Ontario.
3. Automated Ice Point Reference Unit, Model 80020-6, 110-115VAC, 0.00 C to 0.05 C Accuracy, Thermo-Electric (Canada) Ltd., Brampton, Ontario.
4. Automated Line Voltage Regulator, Type 1570-AS8, 115V., 50A., Regulator Unit and Control Unit, Serial No. 363, General Radio Company, Concord, Mass., U. S. A.
5. Autotransformer, VARIAC, Type WSMT3, 0-140V. Range 5A, 120V., General Radio Company, Concord, Mass., U. S. A.
6. Autotransformer, VARIAC, Type W5MT, 0-240 V. Range, 25A., General Radio Company, Cambridge, Mass., U. S. A.
7. Cartridge Heaters, Chromalox,
   240 V., 2600 W., 5/8" diameter, 36" L., C1-446R;
   240 V., 3800 W., 5/8" diameter, 48" L., C1-458R;
   120 V., 1700 W., 5/8" diameter, 103/4" L., C1-406R.
   Edwin L Wiegand Company, Pittsburgh, Pa., U. S. A.
8. Constant Temperature Bath, 115V., 900W., 0.1 C Divisions, Lab-Line Instruments Inc., Chicago, Illinois, U. S. A.

9. High-Speed Camera, Model K2001R, HYCAM, with RLLE-4 Lens, Red Lake Laboratories, Inc., Santa Clara, Clara., U. S. A.
10. Potentiometers, Model No. 2745, Rubicon Instruments, Minneapolis-Honeywell Regulator Company, Philadelphia, Pa., U. S. A.
11. Thermocouple Rotary Switches, Type UFMF 24/2, 24 Circuits, Thermo-Electric (Canada) Ltd., Brampton, Ontario.
12. Thermocouple Welder, KUP-L-WELD, Cat. No. 73-075, 115 V., Burrell Corp., Pittsburgh, Pa., U. S. A.
13. Thermometers, 66°-80°F (0.2°F Division), 80°-120°F (0.2°F Division), CENCO, U. S. A.
14. Transformer, 20:1, Step-down Transformer, 10KVA Rating, Ontario Hydro Comm., Windsor, Ontario.
15. Two-Channel Recorder, Model 7100B, Strip Chart Recorder, Hewlett Packard (Canada) Ltd., Point Clair, Quebec.
16. Volt Meters, Weston Model 82, Rectifier Type 0-1000V., Multi-range, Weston Instruments, Mississauga, Ontario.
17. Weldmatic Spot Welder, Model No. 1048B, Unitek, 0-100 Watts/sec., Dual Range, United Corporation, Montrovia, California, U. S. A.

APPENDIX II

SPECIFIC SERIES OF TEST RUNS FOR EACH RISER AND HEATER LENGTH

A Performance

a) Four Different Riser Sizes and Three Heater Lengths

Riser	W = 5/8"	W = 1"	W = 1½"	W = 2"
Heater				
-	X	X	X	X
-	X	X	X	X
-	X	X	X	X

Note: 1) Inlet subcooling: $T_{l,reservoir} = T_{sat,\ reservoir}$

2) Heater at the bottom of the annular section ($z_B = 0$)

b) Effect of Different Nucleating Devices

Riser Size	5/8	1	1¼	1½
Nucleation Devices				
Inserts Only	X			
Orifice Rings		X		
Suspended Discs		X	X	X
Electrically Heated Wire	X	X	X	X

Note: 1) Tests with 7' heater

2) Inlet subcooling: $T_{l,reservoir} = T_{sat,reservoir}$

3) Heater at the bottom of the annular section ($z_B = 0$)

c) Other Effects

Riser	I - 5/8	" - 1	" - 1½	W-1½
Effect				
Subcooling		X		
Valve			X	
Transient temperatures during a reversal	X			

Note: 1) Tests with 7' Heater

2) Heater at the bottom of the annular section ($z_B = 0$)

B Internal Flow Studies

a) Annular Section

Riser

I - 5/8

O - 1

Heater

X

X

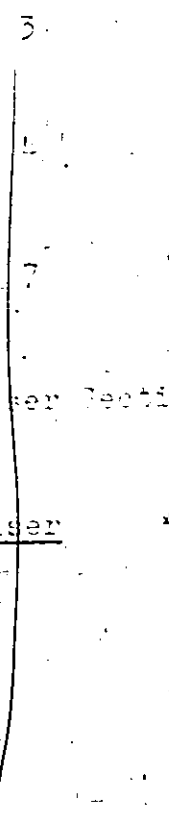

b) Riser Section

Riser

I - 5/8

X

APPENDIX III

SURVEY OF RELEVANT HEAT TRANSFER AND TWO-PHASE FLOW LITERATURE

III-1.1 SINGLE-PHASE FORCED CONVECTION

An early correlation for the heat transfer coefficient at the inner surface of an internally heated annulus was obtained by Monrad and Pelton.[A1] The correlation was for turbulent flow in smooth, long tubes such that the velocity and temperature profiles were fully developed. The relation is:

$$N_{Nu} = 0.020\ (N_{Re})^{.8}\ (N_{Pr})^{.33}\ (D_o/D_i)^{.53} \qquad (A\text{-}1)$$

The properties were evaluated at the mean bulk temperature and $N_{Re} > 10{,}000$.

Farman and Beckman[A2] show essentially the same functional dependence on the Reynolds' and Prandtl numbers, but a different function of D_o/D_i.

$$N_{Nu} = a\ (N_{Re})^{.8}\ (N_{Pr})^{.4}\ (D_o/D_i) \qquad (A\text{-}2)$$

Variation has been noted among investigators' results, however, in the value of the constant multiplier a and the form of the annular geometry correction factor $\phi(D_o/D_i)$. Wiegand[A3] examined a number of correlations and obtained the following relation:

$$N_{Nu} = 0.023\ (N_{Re})^{.8}\ (N_{Pr})^{.4}\ (D_o/D_i)^{.45} \qquad \text{(A-3)}$$

The correlation is recommended over the range of D_o/D_i from 10 to 1, viscosity not greater then twice that of water and $N_{Re} > 5000$. Properties are to be evaluated at the bulk mean temperature.

Later experiments by Miller, Byrnes and Benforado[A4] using water in the range of Reynolds' numbers from 5000 to 22,000 were substantially in agreement with Wiegand. Other studies by Foust and Christian[A5] and Farman and Beckman[A2] showed the multiplying coefficient did not precisely agree. They had values of .01034 and 0.029 respectively.

Deviations from above correlations may be the result of such factors as various as inlet conditions, eccentricities and perhaps tube roughnesses.

III-1.2 SUBCOOLED NUCLEATE BOILING

III-1.2.1 Transition Regime

In order to predict the onset of surface boiling, Rohsenow[A6] made the commonly accepted assumption that bubbles originate from small cavities at the heating surface. Vapour trapped in these cavities expands as it is heated and overcomes the surface tension of the fluid. At equilibrium, the excess pressure between the vapour and the liquid is given by

$$(P_v - P_l) = \frac{2\sigma}{r} \qquad \text{(A-4)}$$

for a spherical interface. The Clausius - Clapyron equation using the perfect gas approximation becomes:

$$\frac{dP_v}{dT_v} = \frac{\rho_v h_{fg}}{T_v} = \frac{h_{fg} P_v}{R_v T_v^2} \qquad (A-5)$$

Equation (A-5) on integration and combination with equation (A-4) becomes:

$$T_v - T_{sat} = \frac{R_v T_{sat} T_v}{h_{fg}} \ln\left[1 + \frac{2\sigma}{P_l r}\right] \qquad (A-6)$$

Rohsenow then assumed a linear liquid temperature distribution near the surface, that is:

$$T_l = T_w - (Q/A)\,(y/k_l) \qquad (A-7)$$

He postulated further that the nucleus of a hemispherical shape with radius "r" will grow if the liquid temperature at a distance y=r from the wall is greater than the vapour temperature given in equation A-6. Thus by plotting equation A-6 and by drawing equation A-7 tangent to it for a given heat flux, the wall temperature was found for incipient boiling. Repeating the procedure for R - 113 over a pressure range of 15 to 20 psi, Gause[A7] obtained the following:

$$(Q/A)_i = 9.14\, p^{1.028}\, (T_w - T_{sat})^{2.17} \qquad (A-8)$$

where p is in psi and $(T_w - T_{sat})$ in ^oF.

Gause's data shows that this relation can be used only

for commercial surfaces that have roughnesses greater than 40 micro-inches. For a R-113-glass combination he obtained a constant superheat of approximately 15°F for heat fluxes up to and greater than 100,000 Btu/hr ft^2.

The evaluation of the heat transfer coefficient in this regime presents a difficulty due to the presence of two mechanisms, forced convection and nucleate boiling, both of which are governed by different transport properties. The common solution has been to extrapolate the correlations of the neighbouring regimes.

McAdams[A8] considered the two curves to simply intersect. Rohsenow[A9] suggested the superposition principle:

$$Q/A = Q/A_{For\ Conv} + Q/A_{Boiling} \qquad (A-9)$$

where $Q/A_{For\ Conv}$ { is obtained from a forced convection correlation

and $Q/A_{Boiling}$ { is evaluated from a pool boiling correlation (to be discussed). (A-10)

In the later study reported in reference A6, Rohsenow suggested that the boiling components of the total heat flux should be based on actual flow boiling data in this regime rather than a saturated fully developed nucleate pool boiling correlation.

III-1.2.2 Fully Developed Nucleate Boiling

The heat transfer mechanism in fully developed nucleate boiling is characterized by its relative insensitivity to subcooling or flow velocity as discussed by Forster and Greif.[A10] Thus they propose the use of saturated pool boiling correlations for flow boiling at low heat fluxes.

The most common pool boiling correlation derived for a variety of fluids and heat transfer surfaces is that of Rohsenow. His correlation, discussed in reference A9, is based on the principle that the heat transfer is due to bubble convection and thus analogous to single-phase flow, so that:

$$N_{Nu} = f(N_{Re}, N_{Pr,l}) \qquad \text{(A-11)}$$

He then found empirically:

$$\frac{N_{Re}, N_{Pr,l}}{N_{Nu}} = C\, N_{Re}^{\ r}\, N_{Pr,l}^{\ s} \qquad \text{(A-12)}$$

$$\frac{c_l\,(T_w - T_{sat})}{h_{fg}} = C_{sf}\left[\frac{q/A}{\mu_l h_{fg}}\sqrt{\frac{g_c\sigma}{g(\rho_l - \rho_v)}}\right]^r N_{Pr,l}^{\ s} \qquad \text{(A-13)}$$

where C_{sf} is a constant depending on the surface - fluid combination

s is generally taken as 1.7

r is experimentally found to be 0.33

The pool boiling data of Tang[17] for a copper - R - 113 combination showed C_{sf} and r equal to 0.0037 and 0.38 respectively. Results of other investigators A11, A12 for this fluid surface combination is given in table III.

III-2 VOID FRACTIONS

III-2.1 Axial Void Fraction Distribution in Subcooled Nucleate Boiling

Typical axial void fraction and liquid temperature distribution along a tube are given by Bowring[A13] who considers axial void fraction distributions in terms of three regions. In region 1, also called the wall voidage region, the subcooling is high and no vapour is flowing. Void fractions are usually negligible. Region II begins where the bubbles leave the surface and is considered to be the beginning of significant vapour generation. The liquid remains subcooled. The bulk boiling or region III exists from the point of liquid saturation.

The one-dimensional continuity and energy equations for the evaluation of average void fractions in the subcooled boiling regimes have commonly been used.[A14] [A15] From the continuity equation one obtains (see section 6.2).

$$\alpha = \frac{1}{1 + S(\rho_v/\rho_l)\ (1 - x)/x} \qquad (A-14)$$

where S equals V_v/V_l and is known as the slip.

To evaluate the quality x, use is made of the one dimensional energy equation which becomes, assuming negligible kinetic and potential energy changes and no effects of surface tension or chemical reaction (see section 6.2):

$$x_{sub} = \frac{q\,(z_{bi} - z)\,P_h/\dot{m} - c_l(T_l - T_b)}{h_{fg} + c_l(T_{sat} - T_b)} \qquad (A\text{-}15)$$

This relation, however, introduces another unknown, namely the liquid bulk temperature, T_l. As discussed by Zuber, Staub and Bijaard[Al4], theoretical evaluation of the liquid temperature T_l poses a number of difficulties and they propose instead two empirical non-dimensional axial temperature distributions from which the bulk liquid temperature can be evaluated. These relations are:

$$T^+ = 1 - e^{z^+} \qquad (A\text{-}16)$$

and

$$T^+ = \tanh z^+ \qquad (A\text{-}17)$$

where

$$T^+ = \frac{T_l - T_b}{T_{sat} - T_b}$$

$$z^+ = \frac{z - z_{bi}}{z_{sat} - z_{bi}} \qquad (A\text{-}18)$$

and

$$z_{sat} - z_{bi} = \frac{\dot{m}\, c_l (T_{sat} - T_b)}{q\, P_h}$$

Most of their data as well as that of Staub and Neimi[A16] supported the first relation but no comparison with downflow data was made.

The slip "S", may be obtained from a study of bubble dynamics. Petrick[19], in discussing the motion of single bubbles, recommended using Stokes' law for $N_{Re} \leq 2$ (the Reynold's number is based on bubble diameter) to determine the terminal velocity.

$$U_{s,\infty} = \frac{D_b^2 \, g \, (\rho_l - \rho_v)}{18 \mu_f} \qquad \text{(A-19)}$$

Peebles and Garber[A17], in their series of experiments on spheres of various sizes, found Stokes' law valid for $N_{Re} \leq 2$.

The fact that the bubbles are contained in a pipe or annulus may require a correction to be applied to the terminal velocity $U_{s,\infty}$. Harmathy[A18] showed that the ratio of the terminal velocity of a bubble in a constrained medium to one in an infinite medium is given as

$$\frac{U}{U_{s,\infty}} = f\left[N_{Eo}, \frac{D_b}{D}\right] \qquad \text{(A-20)}$$

From the solution presented in a graphical form, a negligible effect on the bubble terminal velocity for the case of falling spheres ($D_b/D < .1$) was found.

To evaluate the absolute velocity of the vapour bubble, Nicklin[18] pointed out that the bubbles will be

travelling in the central portion of the tube so that:

$$V_v = V_l [C_o + (S - 1)] \qquad \text{(A-21)}$$

where C_o equals 1.2 for turbulent flow and also for low void fraction flows,

and S is greater than 1 for upflow, less than 1 for downflow and $V_l \doteq \dot{m}/(1 - \alpha)\rho_l A_{cs}$ since the quality is low.

An empirical correlation for S recommended for steam-water in downflow was also obtained by Petrick:

$$S = .63\ (N_{Fr})^{.4} \left[\frac{x}{1 - x}\left(\frac{\rho_l}{\rho_v}\right)\right]^{.2} \qquad \text{(A-22)}$$

where N_{Fr} equals V_l^2/gD. The equation was based on data with pressures between 14.7 and 1500 psi; velocities from 1 to 7 fps, qualities from 0.0005 to 0.1 and bubble diameters between 0.1 and 0.5 inches.

III-2.2 FLASHING VERTICAL FLOW

III-2.2.1 General Discussion

The process occurring when a saturated liquid flows into a region of lower pressure thereby resulting in vapour formation is called flashing. The amount of this vapour generated and the extent to which the two phases are in equilibrium can vary considerably depending on a number of factors. These were discussed by Fauske[A19] and include geometric inlet conditions, nucleating surface properties

flow lengths and fluid properties.

Fauske performed experiments on the maximum rate of discharge of saturated water through tubes with length to diameter ratios (L/D) from 0 to 40. For an orifice or L/D equal to 0, large liquid superheats were indicated since only single-phase metastable liquid was observed passing through. This result was observed previously by a number of other investigators. [A20, A21] It is felt that the contact time of the fluid as it passed through the orifice was too short for bubble nucleation and growth to take place.

For L/D between 0 and 12, he observed partially metastable two-phase flow, while for L/D greater than 12, the phases seem to be in thermal equilibrium. He also found that, as in single-phase flow, there is a critical pressure ratio which gives the maximum rate of discharge. For water using a 0.25" diameter tube this pressure ratio has been given as 0.55. It is possible that overall height limitations may result when the flow rates through the risers are at their maximum.

III-2.2.2 Initiation of Flashing

As in nucleate boiling, the flashing process requires a superheated liquid and initial nucleii of finite size (see equation (A-4) and (A-6) in section III-1.2.1). However, for these flows, the tube walls are essentially adiabatic so that there is no superheating due to heat transfer.

Hence the nucleation sites must be provided by other means such as bubble injection, boiling on electrically heated wires which act as bubble producers or making use of the hydrodynamic phenomenon of cavitation. A monograph on cavitation by Knapp, Daily and Hammot[A22] summarizes various aspects of the subject. Of particular interest is the observation that bubbles or cavities can form in wakes at the centres of finite vortices such as occur behind discs since these are centres of minimum pressures in the flow field. No cavitation data had been reported regarding the inception of cavitation for R - 113.

In the presence of some finite bubbles of vapour in a superheated liquid, the bubble interspersed liquid "explodes" into a two-phase mixture, as observed by Brown and York.[A23] In their studies with jets, they also noted that the heat conduction was dominant over most of the growing period of the bubbles. They used Forster and Zuber's solution for bubble growth to assess the rate of bubble volume increase. The solution for the bubble radius is:

$$r = r_o + Kt^{\frac{1}{2}} \qquad \text{(A-23)}$$

$$\text{where} \quad K = \frac{c_l \Delta T_{l,sat}}{h_{fg}} \left(\frac{\rho_l}{\rho_v}\right)\left(\frac{\pi k}{\rho c}\right)_l^{\frac{1}{2}} \qquad \text{(A-24)}$$

and t is the lapsed time for the bubble to grow from its initial radius r_o.

To calculate the void fraction in a tube from the above bubble growth solution is not possible since some other factors such as the number of initial sites and the superheats $\Delta T_{l,sat}$ as the bubbles grow must be known. As in subcooled nucleate boiling, empirical liquid superheat temperature distributions are required.

III-2.2.3 Flashing Flows in Long Tubes

Benjamin and Miller[A24], in presenting a design method for horizontal piping carrying a flashing mixture of steam and water, assumed equilibrium between the two phases and neglected slip. The properties of the two-phase mixture were evaluated by considering the expansion process to be isentropic. Subsequent measurement of the axial pressure distribution showed it to be approximately linear. Studies by Fauske[A26] on critical two-phase flow revealed that differences in fluid properties using either constant entropy or constant enthalpy were minor.

The slip S, may be calculated using the Bankoff[A27] model for vertical two-phase flow. He considered a model in which the mixture flows as a homogeneous suspension of bubbles in the liquid. Thus while there is no relative motion at a given radial position in the pipe, the vapour will still travel faster due to the larger amount of vapour in the centre of the pipe where the velocity is greater. The correlation derived from steam-water data is:

$$S = \frac{1 - \alpha}{k - \alpha} \qquad \text{(A-26)}$$

where $k = k_o + (1 - \alpha)\alpha^r$

and $r = 3.33 + .58\ (P/P_{crit}) + 4.74\ (P/P_{crit})^2$

and $k_o = .71 + .001\ P$

III-3 PRESSURE LOSSES

III-3.1 Pressure Losses in Subcooled Nucleate Boiling

Several empirical correlations for the pressure drops in horizontal tubes with negligible momentum changes were developed for steam-water flows; see, for example, Reynolds[A28], Owens and Schrock[A29], Tarasova[A30] and Bergles and Dormer[A31]. The authors, in references A30 and A31 obtained a correlation using the following variables:

$$\frac{(\Delta P/\Delta l)_{TP}}{(\Delta P/\Delta l)_{SP,l}} = \Phi\left[\frac{l}{L}\ ,\ q\ ,\ P,\ G\right] \qquad \text{(A-27)}$$

where $(\Delta P/\Delta l)_{TP}$ is the pressure gradient in the boiling section

$(\Delta P/\Delta l)_{SP,l}$ is the pressure gradient in the non-boiling section

(l/L) is the ratio of length from the inception of the subcooled boiling to total length required to saturate the liquid

and the other variables are as defined in the nomenclature.

In vertical tubes, the total pressure gradient is commonly considered to consist of three components:[6]

$$\frac{dP}{dz} = \left(\frac{dP}{dz}\right)_{\substack{\text{wall}\\ \text{friction}}} + \left(\frac{dP}{dz}\right)_{\text{mom.}} + \left(\frac{dP}{dz}\right)_{\text{elevation}} \qquad \text{(A-28)}$$

The total pressure gradient for steam water flows could be evaluated by making use of an emperical correlation of the form of equation (A-27) and adding the elevation component to it. The frictional component in equation (A-28) has also been evaluated using friction factors suitable for two-phase flow.

Sabersky and Mulligan[A32] considered that the effect of the bubbles was to cause increased friction losses due to the bubbles acting as surface roughness. They found for their water data that Reynolds' analogy ie. $N_{St} = f/2$ was applicable in nucleate boiling. The friction coefficient f was obtained from:

$$\left(\frac{dP}{dz}\right)_{\substack{\text{wall}\\ \text{friction}}} = \frac{2 f \rho V^2}{D g_c} \qquad \text{(A-29)}$$

where V was the adjusted velocity of the liquid $V_i/(1-\alpha)$ and V_i equalled the inlet fluid velocity.

A similar study was made by Jordan and Leppert[A33] using an annular geometry. Their data had a scatter of +39% and -20% about the mean line $N_{St} = f/2$. They also indicated that Reynolds' analogy was not valid in rough

tubes.

Staub[A16] successfully used the bubble diameter as the roughness parameter to calculate the frictional shear forces holding bubbles on the surface.

The momentum pressure gradient can be expressed as:

$$\frac{dP}{dz} = \frac{G^2}{g_c} \frac{d}{dz}\left[\frac{x^2}{\alpha \rho_v} + \frac{(1-x)^2}{(1-\alpha)\rho_l}\right] \qquad \text{(A-30)}$$

The elevation component of the total pressure gradient for vertical flows is evaluated using the mean density.

$$\left(\frac{dP}{dz}\right)_{\text{elevation}} = \left[(1-\alpha)\rho_l + \alpha \rho_v\right] \frac{g}{g_c} \qquad \text{(A-31)}$$

III-3.2 Pressure Losses in Vertical Flashing Flow

The two-phase regime noted in the present vertical flashing flows is bubbly flow. Thus methods of calculating pressure gradients suitable for this flow pattern are reviewed below. For higher voids and qualities, annular flow may exist for which a correlation such as that of Lockhart-Martinelli[A34] may be suitable.

Wallis[A35] concludes that the homogeneous flow theory is a good approximation in most cases of bubbly flow. This theory, previously proposed by Owens[A36], assumes that the two-phase mixture can be replaced by an equivalent single fluid and the relative motion between the phases neglected. The total pressure gradient is considered to consist of the three

components defined as follows:

$$\left(\frac{dP}{dz}\right)_{friction} = \frac{f_{TP}\, G^2\, \bar{v}}{2\, D\, g_c}$$

$$\left(\frac{dP}{dz}\right)_{mom.} = \frac{G^2}{g_c}\frac{d\bar{v}}{dz} \qquad \text{(A-32)}$$

$$\left(\frac{dP}{dz}\right)_{elevation} = \frac{1}{\bar{v}}\frac{g}{g_c}$$

where $\bar{v} = \frac{1}{\bar{\rho}} = v_l\left[1 + \frac{x}{v_l}(v_v - v_l)\right]$

which reduces to

$$\bar{v} = \frac{1}{(1-\alpha)\rho_l + \alpha\rho_v}$$

for the case of no slip. Wallis found that the use of a value of 0.005 for the two-phase friction factor for Reynolds numbers up to 10^5 resulted in a maximum deviation of $\pm$ 25%.

REFERENCES: APPENDIX III

A1. Monrad, C. C. and Pelton, J. F. 1942. Heat transfer by convection in annular spaces. TRANS. 38: 593-608.

A2. Lorenz, R. A. and Mesmith, R. H. 1967. Entrance region heat transfer in an annulus. CHEMICAL ENGINEERING PROGRESS SYMPOSIUM. No. 79, 63: 57-65.

A3. Hoegand, J. 1945. Annular heat transfer coefficients for turbulent flow. A.I.Ch.E. TRANS. 41: 147-152.

A4. Miller, P. J.; Agnew, J. J.; and Benfordado, H. M. 1955. Heat transfer to water in an annulus. A.I.Ch.E. JOURNAL. 1, No. 4: 502-504.

A5. Fount, A. S. and Christian, G. A. 1940. Non-boiling heat transfer coefficients in annuli. A.I.Ch.E. TRANS. 36: 541.

A6. Bergles, A. E. and Rohsenow, W. M. 1964. The determination of forced convection surface boiling heat transfer. TRANS. ASME. 86: 365-372.

A7. Gnaus, S. W., Jr. and Coumou, K. G. 1965. Heat transfer and fluid flow inside a horizontal tube evaporator: Phase I. ASHRAE.

A8. McAdams, W. H. 1954. HEAT TRANSMISSION. pp. 268-378. New York: McGraw-Hill.

A9. Rohsenow, W. M. 1962. HEAT TRANSFER, A SYMPOSIUM. University of Michigan.

A10. Forster, K. E. and Greif, R. February, 1959. Heat transfer to a boiling liquid - mechanisms and correlations. TRANS. ASME. 81 (Series C): 43.

A11. Blatt, T. A. and Adt, R. R., Jr. 1964. An experimental investigation of boiling heat transfer and pressure drop characteristics of Freon 11 and 113. A.I.Ch.E. JOURNAL. 10, No. 3: 369.

A12. Lippert, T. E. and Dougall, R. S. 1968. A study of the temperature profiles measured in the thermal sublayer of water, freon 113, and methyl alcohol during pool boiling. ASME PAPER NO. 69-HT-7.

A13. Bowring, R. W. 1962. Physical model based on bubble detachment and circulation of steam voidage in the subcooled region of a heated-channel. INSTITUTT FOR ATOMENERGI REPORT HPR-10.

A14. Zuber, N.; Staub, F. W.; and Bijwaard, G. 1966. Vapour void fraction in subcooled boiling and in saturated boiling systems. PROCEEDINGS OF THIRD INTERNATIONAL H.T. CONF. 5: 24.

A15. Ahmad, S. Y. November, 1970. Axial distribution of bulk temperature and void fraction in a heated channel with sublet subcooling. TRANS. ASME. 92(Series C): 595.

A16. Staub, F. W. and Neimi, R. O. May, 1969. Heat transfer and hydraulics, the effect of subcooled voids. FINAL REPORT NYO-3679-8.

A17. Peebles, F. N. and Garber, H. J. February, 1953. Studies in the motion of gas bubbles in liquids. CHEM. ENG. PROGRESS. 49: 88.

A18. Harmathy, T. Z. June, 1968. Velocity of large drops and bubbles in media of infinite or restricted extent. A.I.Ch.E. JOURNAL. 6, No. 2: 281-288.

A19. Fauske, H. E. 1965. The discharge of saturated water through tubes. CHEMICAL ENGINEERING PROGRESS SYMPOSIUM.

SERIES - HEAT TRANSFER. Cleveland. No. 59, 61: 210-216.

A20. Burnell, J. G. 1947. Flow of boiling water through nozzles, orifices and pipes. ENGINEERING. 164: 572-576.

A21. Bailey, J. F. 1951. Metastable flow of saturated water. TRANS. ASME. 73: 1109-1116.

A22. Knapp, R. T.; Daily, J. W.; and Hammit, F. G. 1970. Cavitation. ENGINEERING SOCIETY MONOGRAPHS. New York: McGraw-Hill.

A23. Brown, R. and York, J. L. 1962. Sprays formed by flashing liquid jets. A.I.Ch.E. JOURNAL. 8, No. 2: 149-153.

A24. Benjamin, H. N. and Miller, J. G. 1942. The flow of a flashing mixture of water and steam through pipes. ASME. 64: 657.

A25. Dickson, A. N. and Markham, V. E. Sept., 1969. Adiabatic flashing flow of water in tubes. SYMPOSIUM OF FLUID MECHANICS AND MEASUREMENTS IN TWO-PHASE FLOW SYSTEMS.

A26. Fauske, H. 1961. Critical two-phase steam-water flows. PROCEEDINGS OF THE 1961 HEAT TRANSFER AND FLUID MECHANICS INSTITUTE. 79-83.

A27. Bankoff, S. G. 1960. A variable density single-fluid model for two-phase flow with particular reference to steam-water. TRANS. ASME. 82(Series C): 265.

A28. Reynolds, J. B. 1954. Local boiling pressure drop. USAEC REPORT ANL-5178.

A29. Owens, W. L., and Schrock, V. E. 1960. Local pressure gradient for subcooled boiling of water in vertical tubes. ASME PAPER No. 60-WA-249.

A30. Tarasova, V. V.; Leontien, A. I.; and Oriov, V. M. 1966. Pressure drop of boiling subcooled water and steam-water mixture flowing in heated channels. INT. H.T. CONF. 4: 178.

A31. Bergles, A. E. and Dormer, T., Jr. 1969. Subcooled boiling pressure drop with water at low pressure. INT. J. HEAT MASS TRANSFER. 12: 459-470.

A32. Sabersky, R. M. and Mulligan, H. E. 1955. On the relationship between fluid, friction and heat transfer in nucleate boiling. JET PROPULSION. 25, No. 1:: 9-12.

A33. Jordan, D. P. and Leppert, T. G. 1962. Pressure drops and vapour volume with subcooled nucleate boiling. INT. J. HEAT MASS TRANSFER. 5: 751-761.

A34. Lockhart, R. W. and Martinelli, R. C. January, 1949. Proposed correlation of data for isothermal two-phase, two-component flow in pipes.

A35. Wallis, G. B. 1969. ONE DIMENSIONAL, TWO-PHASE FLOW. New York: McGraw-Hill.

A36. Owens, W. L. 1961-62. Two-phase pressure gradient. INTERNATIONAL DEVELOPMENTS IN HEAT TRANSFER: PART II. p. 363.

APPENDIX IV

ERROR ANALYSIS

This appendix contains a discussion of the maximum errors that may have arisen using the instrumentation discussed in Chapter III. The primary purpose was to study the overall loop behaviour. The maximum and minimum power limits reported were obtained and repeated almost daily over a six month test period. Most of the internal flow data was repeated approximately two to four times and this was felt sufficient to check on the suitability of existing correlations for heat transfer and friction factors. Deviations of repeated measurements were generally of the same magnitude as the maximum errors discussed below.

1) Errors in Thermocouple Readings

For a stable input to the precision potentiometer, the dial could be read accurately to a reproducible value of ± 0.002 millivolt which thus introduced a reading error of approximately $\pm 0.1^{\circ}F$ in each temperature measurement. This is probably the maximum reading error in all the temperature measurements. The corresponding temperature from the emf's of the thermocouples (and appropriate standard conversion tables) were compared to calibrated CENCO thermometers having a $0.2^{\circ}F$ divisions, comparison

was made using a constant temperature bath, and no correction was found to be necessary. Errors due to fluctuations were found to be negligible.

In addition to the above mentioned reading error, a possible installation error of $\pm 0.1^{\circ}F$ arises in the copper wall temperature measurements due to the uncertainty of the exact location of the thermocouple bead in the cross section of the tube. The conduction losses of all these thermocouples were considered negligible. Overall wall temperatures were thus measured within $\pm 0.2^{\circ}F$.

The fluid temperature measurements were estimated to be within $\pm 0.2^{\circ}F$. In the heated section and other single-phase portions of the loop this could be interpreted as the liquid temperature. Due to the low voids generated ($\leq 20\%$) in the heated section, the bubbles were seen to be isolated and swept past the bead. In the flashing portion of the loop, the error between the measured and the true liquid temperature was found to depend on the degree of subcooling and void fraction present. In the present case the maximum error was $3^{\circ}F$ when $\alpha \approx 50\%$.

ii) Errors in Pressure Readings

A report by Dean[13] dealing with air and water flows shows no significant errors in pressure measurements caused by slight irregularities in the wall taps. Therefore, the error due to the construction of the present taps

was considered negligible since all holes were reamed before installation.

The sloping manometer had a reading accuracy of $\pm$0.1" of freon-113. While within 5% of the power limits the pressure fluctuations were as high as $\pm$1" of freon - 113, the heat transfer, void and pressure loss data was taken in the stable operating region where the fluctuations were less than $\pm$0.1" of freon - 113.

Other errors that were considered but found negligible were the angular position of the manometer board and the response time. The probable maximum error for the differential measurements can be considered to be $\pm$0.15psi.

The mercury manometers had a reading accuracy of $\pm$0.10" of H_g. The pressure fluctuations were negligible in the stable operating region.

111) Errors in Density Measurement

The reading accuracy of the recorder which was connected to the Accu Ray Unit was $\pm$0.10". There was a fluctuation due to the randomness of the source decay. This randomness was present even under isothermal conditions when the density was known to be constant. The mean of the signal was used as the reading. The overall accuracy of the density measurement is $\pm$ 1.1 lb/ft^3.

Calculations were also made as to the change in the path length when the cross section was heated. A negligible error was found due to this thermal expansion.

iv) Power Measurements

Possible reading and instrument errors were:

		Parallax	Instrument
A. C. Voltmeter	0-250V	±0.25V	±0.5% Full Scale
	0-500V	±0.5V	±0.5% Full Scale
A. C. Ammeter	0-20A	±0.025A	±1.0% Full Scale

The circuit error was found to be -0.2% and -0.4% for the lowest and highest fluxes respectively. Therefore the maximum possible errors in measured power inputs are:

Highest heat flux (235V, 11A) ±1.6%

Lowest heat flux (71V, 4.25) ±2.4%

v) Mass Flow Measurements

The major uncertainty is due to the in place calibration of the mass flow unit. The mass balance had a reading accuracy of 0.1 lb giving a possible error in the weighed quanity of 0.2%. The response time of the operator in the starting and stopping procedure was estimated at 1 second thus giving an error of ±2%. A further possible reading error of ±1% gives a total overall accuracy of ±3.2%. Calculations showed that the temperature changes were negligible. A correction was made to account for the effect of the different fluid density during

loop operation than that at which the calibration took place.

vii) Heat Transfer Data

The estimates given here are based on the maximum errors previously estimated for the primary data such as temperature, pressure, power and flowrate variations. The probable errors are then expected to be significantly less than these maximum values given here. The possible effect of temperature and pressure errors in the evaluation of the fluid properties was found negligible and is not included nor is the possible error in properties of the R-113 quoted by the manufacturers.

a) Non Boiling Data

If we consider the maximum error in power measurement at 3.8%, the error in ΔT at 5.4°F or 2% and an error in surface area of 4%, the heat transfer coefficient could have a maximum error of ±9.8%.

The local Nusselt number was evaluated using a constant value of equivalent diameter of 0.25". However the actual dimensions have a 3% variation resulting in a Nusselt number accuracy of ±12.8%.

The Reynolds number was calculated to have a maximum possible error of 6.2%.

b) Boiling Data

The boiling Nusselt number, defined as

$$N_{Nu,b} = \frac{q_t \Delta T}{N_{Pr}^{1.7}\, h_{fg}} \qquad (A-33)$$

has a maximum possible error of 2% for a minimum wall superheat of 15°F and possible error in temperature measurement of ±0.3°F. The boiling Reynolds' number defined as-

$$N_{Re,b} = \frac{q}{A \mu_l h_{fg}} \frac{\ell}{g_c} \left[\frac{\sigma}{(\rho_l - \rho_v)}\right]^{\frac{1}{2}} \qquad (A-34)$$

was found to have a maximum possible error of ±8%.

vii) Void Fraction Calculation

The void fraction was evaluated from the measured density by the following relation.

$$\alpha = \frac{\rho_l - \rho}{\rho_l - \rho_v}$$

In both the annulus and the riser, the bubbles and liquid are seen to be well interspersed resulting in a bubbly flow. Also the collimating beam of 0.13" width is only 20% of the total width of the tube (Schrock had an error of 7.3% for a beam 50% of the channel width). Furthermore, these large errors are reported to be due

to "photon streaming" which occurs when the void tend to be in laminae parallel to beam path. While this bias was not seen here, the unit's voltage/variation from an empty to a full pipe remains linear so that the results obtained would be almost identical even if either pattern were present. It is estimated then that the void fractions were measured with an accuracy of $\pm 5.0\%$. This is also the accuracy quoted by the manufacturer.

viii) Friction Factors

The friction factors evaluated are subject to errors in equivalent diameter D_{eq}, void fraction, mass flow G, pressure drop P, possible slip S. In examining the experimental arrangement, it is evident that the pressure measurement drop for such small lengths (see figure 2) could be as much as 10% in error. The overall maximum error in friction factors is $\pm 24\%$.

APPENDIX V

COMPUTER PROGRAMMES

FOR DATA REDUCTION

```
$PRINTOFF
C DATA REDUCTION  HELMUT KEIL
      DIMENSION ALA(16)
      DIMENSION TPLUS(6),ZPLUS(6)
      DIMENSION HRN(16)
      DIMENSION REB(16),RPN(16)
      DIMENSION RE(16)
      DIMENSION PA(8)
      DIMENSION PR(8)
      DIMENSION DE(6),ZDE(6)
      DIMENSION VT(8),ZVT(8)
      DIMENSION VTW(16),ZTW(16)
      DIMENSION PRC(8),ZP(8),DZP(8),R(8),PH(8)
      DIMENSION T(8),TW(16)
      DIMENSION ALPA(6),X(6)
      DIMENSION HSP(16),HTP(16),TED(16),TSD(16)
      DIMENSION DRO(8),RO(8)
      DIMENSION PGA(8),PPRG(8),FF(8)
      DIMENSION HMU(16)
   11 FORMAT (8F8.3)
   12 FORMAT (6F8.3)
   13 FORMAT (F8.3)
   14 FORMAT (2F8.3)
   15 FORMAT (F8.3,I3)
   16 FORMAT (I2)
      READ 12,ZDE(1),ZDE(2),ZDE(3),ZDE(4),ZDE(5),ZDE(6)
      READ 11,ZVT(1),ZVT(2),ZVT(3),ZVT(4),ZVT(5),ZVT(6),ZVT(7),ZVT(8)
      READ 11,ZP(1),ZP(2),ZP(3),ZP(4),ZP(5),ZP(6),ZP(7),ZP(8)
      READ 11,DZP(1),DZP(2),DZP(3),DZP(4),DZP(5),DZP(6),DZP(7),DZP(8)
      READ 11, PH(1),PH(2),PH(3),PH(4),PH(5),PH(6),PH(7),PH(8)
      DO 1 I=1,16
    1 READ 13, ZTW(I)
    3 CONTINUE
      READ 12,DE(1),DE(2),DE(3),DE(4),DE(5),DE(6)
      READ 11, VT(1),VT(2),VT(3),VT(4),VT(5),VT(6),VT(7),VT(8)
      DO 2 I=1,16
    2 READ 13, VTW(I)
      READ 11, PR(1),PR(2),PR(3),PR(4),PR(5),PR(6),PR(7),PR(8)
      READ 11, ALA(1),ALA(2),ALA(3),ALA(4),ALA(5),ALA(6),ALA(7),ALA(8)
      READ 13,Q
      READ 14,Q1,Q2
      READ 13,RMF
      READ 15, AL,NT
      READ 14,AL1,AL2
```

```
      READ 14,PB,DP
      READ 11, DRO(1),DRO(2),DRO(3),DRO(4),DRO(5),DRO(6),DRO(7),DRO(8)
      READ 17,RO(1),RO(2),RO(3),RO(4),RO(5),RO(6),RO(7),RO(8)
      READ 13,ZB
      READ 16,J
      HI=33.
      TI=117.
      HV=93.
      HLI=33.
      DIO =1./12.
      HFG=61.3
      DI= .75/12.
      ACS=(3.1416/4.)*(DIO*DIO-DI*DI)
      Z=13.12
      DEQ=.25/12.
      PH=PB+BP
C EVALUATION OF TEMP.
      DO 40 I=1,8
   40 T(I)=34.364*(VT(I)-1.36)+80.
      DO 41 I=1,16
   41 TW(I)=42.964*(VTW(I)-1.058)+80.
C EVALUATIN OF PRESSURES
      DO 42 I=1,8
      P(I)=.0282*PH(I)
      PRG=P(I)/DZP(I)
      PGA(I)=.685-PRG
      PA(I)=PB+P(I)-PH(I)
      PB=PA(I)
   42 CONTINUE
C EVALUATION MASS FLO RATE
      AM=SQRT(RMF/13.8744)
      AS=(3.1416*DI-.44/12.)*AL
      G=AM/ACS
      QPR=(Q/AS)*3600.
C EVALUATION OF VOID FRACTION
      DO 43 I=1,5
      S=1.
      DEV=.403+(T(4)-110.)/117.5
      DEL=103.555-.0712*T(4)-.000003*(T(4)*T(4))
      ALPA(I)=(DEL-DE(I))/(DEL-DEV)
      X(I)=1./(1.+((1.-ALPA(I))/ALPA(I))**(DEL/DEV*S))
      ZVO1=AL+ZB-ZDE(J)
      HL=(((QPR/3600.)*(AG/AL)*ZVO1)/AM+HLI-X(I)*HV)/(1.-X(I))
      PG=PA(1)-P(1)+PH(1)
      PS=PG-(PG-PA(8))*ZDE(I)/10.305
      TSAT=117.4625+3.6801*PS-.079*PS*PS
      TPLUS(I)=(HL-HI)/((TSAT-TI)*.29)
```

```
      HSAT=27.+.229*(TSAT-91.)
      DZRL=AM*(HSAT-HL(I))/((QPR/3600.)*(AS/AL))
      ZPLUS(I)=(AL+ZB-ZDE(I))/DZPL
   43 CONTINUE
C EVALUATION OF HT COEFF.
      DO 44 N=1,16
      TE=T(1)-(T(1)-T(8))*(ZTW(N)-ZB)/AL
      TED(N)=TW(N)-TE
      IF (TED(N)) 71,71,72
   71 HSP(N)=0.
      GO TO 73
   72 CONTINUE
      IF(ZTW(I)-(ZB+AL1)) 101,101,102
  101 CONTINUE
      AS1=(3.1416*DI-.44/12.)*AL1
      QPR=(Q1/AS1)*3600.
      GO TO 103
  102 CONTINUE
      AS2=(3.1416*DI-.44/12.)*AL2
      QPR=(Q2/AS2)*3600.
  103 CONTINUE
      HSP(N)=(QPR/TED(N))
   73 CONTINUE
      PG=PA(1)-P(1)+PH(1)
      PS=PG-(PG-PA(8))*ZTW(N)/10.305
      TSAT=117.4625+3.6801*PS-.079*PS*PS
      TSD(N)=TW(N)-TSAT
      CL=.2205+(.0285/100.*(TSAT-100.))
      HFG=63.25-((63.25-63.09)/2.*(TSAT-116.))
      VISC=(.497-(TSAT-120.)*(.564-.497)/20.))/100.*.0673
      TK=.041-(.041-.035)*(TSAT-100.)/80.



      SUT=.00129*((417.4-TSAT)/349.4)**1.2
      REB(N)=(QPR*.286*SQRT(SUT))/(VISC*HFG*10.**4)
      PRN(N)=((VISC*CL)/TK)*3600.
      RPN(N)=CL*TSD(N)/(HFG*PRN(N)**1.7)
      TK=.041-(.041-.035)*(TE-100.)/80.
      HNU(N)=(.25/12.)*(HSP(N)/TK)
   44 CONTINUE
C EVALUATION OF FRICTION FACTORS
      DO 48 I=1,8
      IF (DRO(I)) 81,80,81
   80 CONTINUE
      PRM=0.
      GO TO 82
   81 CONTINUE
      PRM=((G*G)/(32.2*RO(I)))*(DRO(I)/(RO(I)*DZP(I)))
   82 CONTINUE
```

```
      FPRG(I)=(RO(I)-PRM-PGA(I)*144.)/144.
      FF(I)=(16.1*RO(I)*DEQ*((1.-ALA(I))**2.)*FPRG(I)*144.)/(G*G)
      VISC=(.497-((T(I)-120.)*(.564-.497)/20.1)/100.)*.0673
      RE(I)=(G*DEQ)/(VISC*(1.-ALA(I)))
   48 CONTINUE
C OUTPUT
      PRINT 61
   61 FORMAT (8H   ZP(I) ,8H   T(I)   ,8H PAG(I) ,8H FPRG(I),8H   FF(I))
      DO 49 I=1,8
   49 PRINT 21,ZP(I),T(I),PGA(I),FPRG(I),FF(I),RE(I)
   21 FORMAT (6(F12.5))
      PRINT 62
   62 FORMAT (8H ZVTC(I),8H   TW(I))
      DO 50 I=1,16
   50 PRINT 22,ZTW(I),TW(I)
   22 FORMAT (2F8.3)
      PRINT 63
   63 FORMAT (8H ZDE(I) ,8H ALPA(I),8H   X(I))
      DO 51 I=1,6
   51 PRINT 23,ZDE(I),ALPA(I),X(I)
   23 FORMAT (3F8.3)
      PRINT 64
   64 FORMAT (10H   ZVTC   ,10H   TED(I)   ,10H   HSP(I)   ,10H   TSD(I))
      DO 52 I=1,16
   52 PRINT 25,ZTW(I),TED(I),HSP(I),TSD(I)
   25 FORMAT (4F8.3)
      PRINT 24
   24 FORMAT (10H   ZP(I)   ,10H   RE(I)   ,10H   PRN(I))
      PRINT 27,QPR
   27 FORMAT (F10.3)
      DO 53 I=1,16
   53 PRINT 26,ZTW(I),PRN(I),HNU(I)
   26 FORMAT (3(F12.4,5X))
      PRINT 88
   88 FORMAT (12H   ZP(I)   ,12H   RE(I)   ,12H   PRN(I))
      DO 54 I=1,16
   54 PRINT 26,ZTW(I),REB(I),RPN(I)
      DO 89 I=1,6
      PRINT 90, ZPLUS(I),TPLUS(I)
   90 FORMAT (2F20.5)
   89 CONTINUE
      IF (J) 3,3,66
   66 CONTINUE
      CALL EXIT
      END
```

```
$JOB   WATFIV  S7030300082,KP=26   KEIL
C  HEAT TRANSFER CORROLATIONS        KEIL
      DIMENSION ANU(100),RE(100)
      DIMENSION X(100),Y(100)
   11 FORMAT (F15.6)
      READ 16, N,A0,B0
   16 FORMAT (I3,2F8.3)
      UN=N
      DO 1 I=1,N
      READ 11,ANU(I)
      Y(I)=ALOG10(ANU(I))
    1 CONTINUE
      DO 2 I=1,N
      READ 11, RE(I)
      X(I)=ALOG10(RE(I))
    2 CONTINUE
   23 CONTINUE
      SUMYS=0.
      SUMXS=0.
      SUMX=0.
      SUMY=0.
      SUMXY=0.
      DO 3 I=1,N
      YS=Y(I)*Y(I)
      XS=X(I)*X(I)
      XY=X(I)*Y(I)
      SUMXY=SUMXY+XY
      SUMXS=SUMXS+XS
      SUMY=SUMY+Y(I)
      SUMYS=SUMYS+YS
      SUMX=SUMX+X(I)
    3 CONTINUE
      SM=(UN*SUMXY-SUMX*SUMY)/(UN*SUMXS-SUMX*SUMX)
      B=(SUMXS*SUMY-SUMX*SUMXY)/(UN*SUMXS-SUMX*SUMX)
      B=10.**B
      RB=SQRT((UN*SUMXS-SUMX*SUMX)*(UN*SUMYS-SUMY*SUMY))
      R=(UN*SUMXY-SUMX*SUMY)/RB
      PRINT 13,SM,B,R
   13 FORMAT (3(F15.5,3X))
      XM=SUMX/UN
      XMS=XM*XM
      XDSS=0.
      ESS=0.
      DO 14 I=1,N
      E=Y(I)-(B+SM*X(I))
      ES=E*E
      ESS=ESS+ES
      XDS=(X(I)-XM)*(X(I)-XM)
      XDSS=XDSS+XDS
```

```
14 CONTINUE
   SYS=ESS/(UN-2.)
   SB=SQRT(SYS/XDSS)
   SA=SQRT(SYS*(1./UN+XM6/XDSS))
   B=SM
   A=B
   TB=ABS(B-BO)/SB
   TA=ABS(A-AO)/SA
   PRINT 15,TB,TA
15 FORMAT (2F10.3)
   CALL EXIT
   END
```

```
$JOB   WATFIV  S703000082,KF=26   KEIL
C  FLASHING  FLOW
      DIMENSION  DENM(10)
      DIMENSION  FRTH(10),FD(10)
      DIMENSION  RMO(10),FMPR(10),FMF(10)
      DIMENSION  FP(10),RO1(10)
      DIMENSION  ROA(10)
      DIMENSION ROC(10),REO(10)
      DIMENSION ZP(10),DZP(10),ZDE(10),P(10),D(10),ALP(10)
      DIMENSION T(10),DALP(10),FPR(10),FF(10),RE(10),PHI(10)
      DIMENSION  XTT(10),PR(10)
      IN=1
      READ 12,ZP(1),ZP(2),ZP(3),ZP(4),ZP(5),ZP(6),ZP(7)
      READ 12,DZP(1),DZP(2),DZP(3),DZP(4),DZP(5),DZP(6),DZP(7)
   36 CONTINUE
      READ 12, P(1),P(2),P(3),P(4),P(5),P(6),P(7)
      READ 12,D(1),D(2),D(3),D(4),D(5),D(6),D(7)
      READ 12,ALP(1),ALP(2),ALP(3),ALP(4),ALP(5),ALP(6),ALP(7)
      READ 12, T(1),T(2),T(3),T(4),T(5),T(6),T(7)
      READ 12,DALP(1),DALP(2),DALP(3),DALP(4),DALP(5),DALP(6),DALP(7)
      READ 11,RMF
   11 FORMAT (F8.3)
   12 FORMAT (7F8.3)
      DB=.08/12.
      DR=.625
      N=7
      ACS=(3.1416/4.)*(DR/12.)*(DR/12.)
C     MASS  FLOW  RATE
      AM=SQRT(RMF/13.8744)
      G=AM/ACS
C     EVALUATION  OF  FRICTION  FACTORS
      DO 3 I=1,N
      VISC=(.497-((T(I)-120.)*(.564-.497)/20.))/100.+.067*3600.
      ALGR=DALP(I)/DZP(I)
      BK=.71+(1.-ALP(I))*ALP(I)**3.361
      S=(1.-ALP(I))/(BK-ALP(I))
      ROL=103.555-(0.07126*T(I))-(.000636*T(I)*T(I))
      ROV=.4489+((.4649-.4489)/2.*(T(I)-116.))
      ROA(I)=(1.-ALP(I))*ROL+ALP(I)*ROV
      DRAT=ROL/ROV
      IF (ALP(I)) 37,37,38
   37 CONTINUE
      X=0.
      REO(I)=0.
      ROC(I)=ROL
      FD(I)=0.
      GO TO 39
   38 CONTINUE
C     DRAG  THEORY
      X=1./(1.+((1.-ALP(I))/ALP(I))*DRAT/S)
      REO(I)=((G/(1.-ALP(I)))*(S-1.)*DB/VISC)*3600.
      DPD=ROL-ROA(I)
```

```
      ROC(I)=ROL-DPD
      FD(I)=DPD*64.4*ROL/((G*(S-1.)/(1.-ALP(I)))**2.)
   39 CONTINUE
      RE(I)=(G*3600.)*DR/(V1SC*12.)
      PRM=(G*G)*(((1.-X)/(1.-ALP(1)))**2.)*ALGR/(32.2*ROL)
      PR(I)=(1.-P(I)/(DZP(I)*24.))*97.9/144.
      FPR(I)=(PR(I)*144.-ROC(I)-PRM)/144.
      FF(I)=16.1*ROA(I)*DR*FPR(I)*144./(G*G*12.)
      PHI(I)=FPR(I)/FPR(1)



      XTT(I)=((X/(1.-X))**.9)*(DRAT**.5)*(2.**.1)
C     HOMOGENEOUS THEORY
      F=.008
      FP(I)=F*G*G*12./(16.1*ROA(I)*DR)
      ROM(I)=(PR(I)*144.-FP(I)-PRM)
      FRTH(I)=FP(I)+ROA(I)+PRM
C     MODIFIED HOMOGENEOUS THEORY
      DENM(I)=ROL/(1.+X*ROL*(1./ROV-1./ROL))
      FMPR(I)=(PR(I)*144.-DENM(I)-PRM)/144.
      FMF(I)=16.1*DENM(I)*DR*FMPR(I)*144./(G*G*12.)
      FRTH(I)=FRTH(I)/144.
      FP(I)=FP(I)/144.
    3 CONTINUE
C   OUTPUT
      DO 33 I=1,N
      PRINT 32,ZP(I),PR(I),FPR(I),FF(I),RE(I),PHI(I),XTT(I),ROC(I)
   32 FORMAT (8F10.3)
      PRINT  40,FP(I),ROM(I),ROA(I),F,PR(I),FRTH(I)
   40 FORMAT (10X,6F10.3)
      PRINT  41,FPR(I),FMF(I),FD(I),REO(I),DENM(I),FMPR(I)
   41 FORMAT  (10X,6F10.3)
   33 CONTINUE
      IN=IN+1
      IF (IN-4) 34,34,35
   34 CONTINUE
      GO TO 36.
   35 CONTINUE
      CALL EXIT
      END
```

APPENDIX VI

FLOW CHART AND COMMENT STATEMENTS

FOR LOOP SIMULATION

INPUT DATA I

Geometry of Loop (N, NL, NO, NI, NR, M, V, VT)

Heater Inlet Temperature (TLI)

Fluid properties (VISC, G, TCAT, SF, DENS, TT)

EVALUATION OF COEFFICIENTS II

Areas (downcomer AD, horizontal section AH, riser AR)

Pressures (inlet PROS, horizontal section PHS)

Heater surface area AS

TOC = 0

INITIAL ITERATION III

Assuming all liquid at TLI, flashing when $x = H/2$ with a mean void fraction $\alpha_m = 40\%$ and no friction, the mass flow rate $AM = AR\rho_l (\alpha_m H/2)$

The pressure at the bottom is $PB = \rho_l H g/g_c$

Evaluate the mean power input
MEAN = AM x 3(TSATS - TLI) x 0.45

The exit fluid temperature TLS = TLI + MEAN/(AM x 3)

CALCULATE STATIC PRESSURE AT THE EXIT OF THE DOWNCOMER

(See SUBROUTINE at the end) IV

CALCULATE PRESSURE DROP THROUGH HORIZONTAL A.I. SECTION V
SINGLE-PHASE REGION

Calculate the pressure gradient in the bottom single-phase region of the riser $\left(\frac{dP}{dz}\right)_1 V_1/2g$ and find the pressure at the bottom of the riser becomes

$$PBR = PB' - \Delta P_f - \Delta P_{elbows}$$

Evaluate pulsation pressure PRS for TIASTR = (TLOS - 3)
where TLOS = TLS - HC x AIPS x DZRR (TLS - TROOM)/(AI x 4)
and DZRR = H/2 on first iteration
= previous ZRR on subsequent iterations

Find ZRR = (PBR - PRS)/(dP/dz)

AXIAL PRESSURE VARIATION ALONG THE TWO-PHASE REGION VI
OF THE RISER

Divide the two-phase region into M increments of length (H - ZRRA)/(M)

At each increment x = C(TJEC - TR)/HFG

and TR = TSATR - (TSATR - TROOM)ZRR/(H - ZRRA)

Calculate $dP/dz = \bar{\rho} DZR\ G/g_c - f/D(G^2/\bar{\rho}_E) - \Delta P_{MOM}$

and $\bar{\rho} = (1 - ALF)\rho_1 + ALF\rho_v$

$$\Delta P_{MOM} = \frac{GR^2}{\rho_1 g}\left[\frac{1 - x}{1 - \alpha}\right]^2 \frac{d\alpha}{dz}$$

Evaluate P locally

Go to next increment

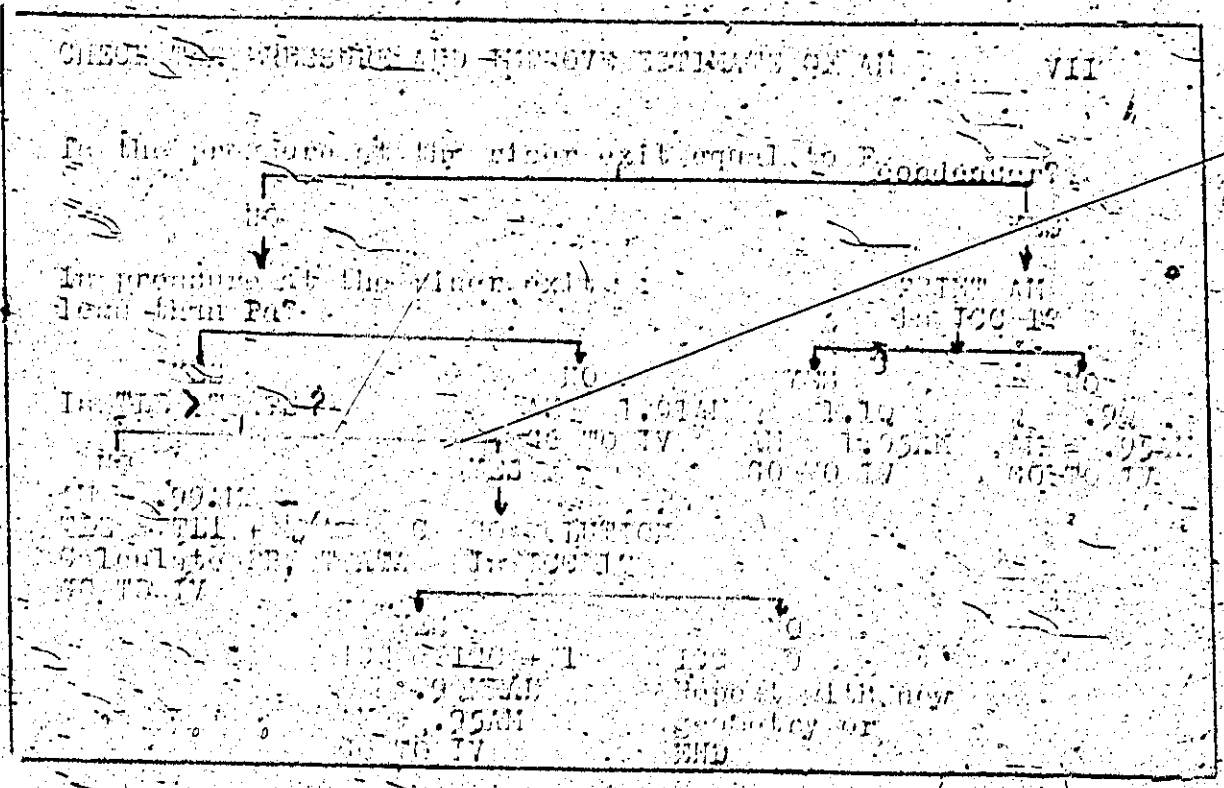

Calculate

$$P = P_1 g\Delta z/g_c - [(\Delta p/\Delta z)_f (\rho_1 v^2/2g)]$$

Calculate TSAT from local pressure

If (TI - TSAT) $\geq$ 1.0°F

Assume boiling starts at bottom of increment

TBI = Z at bottom of increment
TLBI = TL at bottom of increment

For the next increment calculate the following quantities at the bottom of the increment

Calculate TL - TLBI using Eq. (A-24)

The quality at the bottom

$$x = \frac{q'' P_h (ZBI - Z)/\Delta W - C_{pl}(TL - TLBI)}{H_{fg} + C_{pl}(TSAT - TL)}$$

The void fraction at the bottom

$$AVP = 1/\left(1 + \frac{1 - x}{x}\left(\frac{\rho_1}{\rho_v}\right)^n\right) \text{ where } n = 1$$

$$P = \rho_1 g\Delta z/g_c + (f\,\Delta z/D_H)(G/1 - AVP)^2/\rho_1 g_c + \Delta P_{mom}$$

TSAT (at the end of the increment as a function of local P)

If Z $\neq$ 0, GO TO statement 7
= 0, return to main program

```
      SUBROUTINE
C     [illegible]
      DIMENSION [illegible]
      DIMENSION [illegible]
      DIMENSION ALP(100)
      READ [illegible]
      READ [illegible]
      READ [illegible]
   30 FORMAT (5E10.4)
   31 FORMAT (2E10.3)
   32 FORMAT (4I3)
   33 FORMAT (2E10.4)
      I=1
      ICC=0
      ZH=0.
      ZSUM=H=2.
      PI2D=4.1176
      ATOD=3.1416/180.
      HC=1.0/760.
      PI4D=3.1416/4.
      PI8D=3.1416/8.
      ALT=1.1416*((ZSUM+H)**2-(ZSUM+H-1.)**2)/4.
      A=1.1416*D**2/4.
      AI=1.1416*DI**2/4.
      ICC=ICC+1
      AT=1.1416*D*ZH
      V1RC=7.477-(3.1-1.)*(.004-.477/20.)*1./100.*.0673
      DELTA=A.A-((A.A-AL*2.)/2.*(TL1-116.))
      U=SQRT(GAMMA*R*T)
      TSATA=(1.+(GAMMA-1.)/2.*XMO**2)/(144.-.07)*P*P/(144.*144.)
      TSATA=TSATA
      XMO=XMO*.6
      ACC=ACC*SQRT(TAL/ATA)
      ACC=ACC*(1.-(XMO*(C-(C-1.)*XK)*H/XDENG*2.))
      QMAX=AAA.A*.5*RHO*(TSATA-TL)
      Q(1)=QMAX
      QCONV=HC*ATS*(TL-TW)
      Q(1)=Q(1)-QCONV
      TLT=TL+Q(1)/(AAA*.2)
      IF(ICC-1)
      CON=AM/AW
      G=AM/AC
      GO=AM/AO
      RL=TL+40(1)/(AM*.2)
      QI=Q(1)
      CALL DRETON (AM,ZT,U,TL,QI,QT,TLT,TSATA,PI)
```

```
      [illegible]
      [illegible]
      [illegible]
      [illegible]
C     [illegible]
 70   CONTINUE
      [illegible]
      IF [illegible] 511,[illegible]
 511  CONTINUE
      [illegible]
      GO TO 513
 512  CONTINUE
      [illegible]
 513  CONTINUE

      [illegible]
      [illegible]
      [illegible]
      [illegible]
      [illegible]
      [illegible]
      [illegible]
      [illegible]
      [illegible]
      [illegible]
      [illegible]
      [illegible]
C     TWO-PHASE [illegible]
      [illegible]
      [illegible]
      [illegible]
      [illegible]
      [illegible]
      [illegible]
      [illegible]
      [illegible]
      [illegible]
      [illegible]
      [illegible]
      [illegible]
      [illegible]
      [illegible]
      [illegible]
      IF [illegible] 201,201,202
 201  CONTINUE
      X=0.
```

```
      GO TO 203
202   CONTINUE
      X=DELTC-(IC-1)*HET
203   CONTINUE
      DENSL=DA*(1.-(1.-DA/DO)*X/2.*(TR(I)-110.))
      DENSV=.00031*((.00301-.00030)*X/2.*(TR(I)-110.))
      IC=1.0
      ALP(1)=AK*(1.+AK)
      DELTA(1)=(1.+ALP(1))*(1.-ALP(1))*DENSV
      IF(N-1) 36,30,36
36    CONTINUE
      DF=DENSL
      GO TO 37
37    CONTINUE
      DF=(DENSL(N)+DENSL(N-1))/2.
38    CONTINUE
      DFA=DF
      RHOBF=DFA*32.*(DIA/12.)*32.*DIA
      ALP(N+1)=.7*2.*2.
      GO TO 27
27    CONTINUE
      IPASS=2.
      GO TO 28
28    CONTINUE
      RHOBA=(RHOBF/(1.-ALP(N+1))*32.*2.)*((1.-Z)/(1.-ALP(N+1)))**2.)
      DELTA=RHOBA*(ALP(N+1)-ALP(N+1-1))/DZRA
      GO TO 40
29    CONTINUE
      IF(N-1) 40,40,41
40    CONTINUE
      DZ(N)=DZR
      GO TO 42
41    CONTINUE
      DZ(N)=DZ(N-1)-(DELTA*(DZ(N-1)-DZR)/(DELTA-DL*DZR
42    CONTINUE
      Z(N+1)=Z(N)+DZ(N)
      DZRT=Z(N+1)-Z(N)
      TD(N+1)=TD(1)-(TD(1)-111.6)*DZRT/(1.-Z(N+1))
10    CONTINUE
      N=N+1
      IF(Z(N)-DD-H)-DZ(1)-2y.) 50,50,60
60    CONTINUE
      IF(DZ(N)-DZ(1)) 50,50,52
50    CONTINUE
      IF(IT-ICATC) 111,111,112
112   CONTINUE
      PRINT 70
```

```
      FORMAT (1H0,10X,'SPECIFIED
     IF (ICC-1) 400,400,401
400  CONTINUE
     ICC=ICC+1
     GO TO 222
405  CONTINUE
     ICC=0
     GO TO 406
111  CONTINUE
     AM=AM*.005
     GO TO 51
52   CONTINUE
     AM=AM*1.005
53   CONTINUE
     C=AM/ATC
     TLC=TL*100./(AM*2500)
     QT=Q(1)
     CALL PSETEV (A,QT,U,TL,ID,D,TLE,TSATA,PIS)
     PIS=PIS-C*C/(2.*AM*AM)
     TSATA=117.*ALOG(1.+QT*TSATA/117.)
     GO TO 70
54   CONTINUE
     XU=.2*Q(1)/(3.*TU*AM)/HFG
     QT=QT*(1.-XU)
     XMDOT=XMDOT*N
     AM=AM*3600.
     Q(1)=Q(1)*3600.
     QDOT=Q(1)/AG
     PIS=PIS/144.
     PD(1)=PD(1)/144.
     PWISE=PD/144.
     GD=GD*3600.
     TLC=TLC
     PRINT 30, Q(1),AM,XMDOT,HFG
     PRINT 31, DU,DT,TDAYWHL,HSW
     PRINT 32, PA,TLT,AT,TDO
     PRINT 34, A,D,TLC
     PRINT 35, AM,GD,Q(1),QDOT
     PRINT 36,PWISE,PD(1),TLE,TSATA
36   FORMAT (1H0,10(1X,E11.3))
     AM=AM/3600.
     Q(1)=Q(1)/3600.
     IF (ICC-1) 401,401,402
401  CONTINUE
     Q(1)=Q(1)*1.1
```

```
     AM=AM*1.20
```

```
      GO TO 73
  402 CONTINUE
      IF (TLI-(TLI(10.)) 407,407,408
  407 CONTINUE
      GO TO 406
  408 CONTINUE
      Q(I)=Z(I)*.5
      AM=.25*AM
      GO TO 73
  403 CONTINUE
      Q(I)=QMEAN*.9
      AM=AM*.95
      GO TO 73
  406 CONTINUE
      IF (JJJ) 21,21,20
   21 CONTINUE
      GO TO 22
   20 CONTINUE
      CALL EXIT
      END
      SUBROUTINE PROP(AM,GT,HL,DO,DI,TLE,TSAT,PU)
      DIMENSION Z(100),ALP(100)
      G=.222
      AS=3.1416*(DO**2-DI**2)/4.
      AT=3.1416*(DO*DO-DI*DI)/4.
      N=10
      DEL=DO-DI
      TLI=116.
      AML=10.7
      VIS=(.497-((TLI-120.)*(.364-.497)/20.))/100.**.0673
      G=AM/ATS
      T=.041-(.041-.031)*(TLE-100.)/80.
      TK=T*9./5.+32.
      REN=G*DEL/VIS
      PRN=VIS*.720/T
      UNN=.023*(REN**.8)*(PRN**.4)*(.62/DI)**.45)
      DENSL=24.43-(0.*.13-71.6)/2.*(TLE-116.)
      DENSV=.401/((.0821*T+.497)/2.*(TLE-116.))
      HH=UNN*TK/DEL
      TW=TLE-QT/(.5*HH)
      IF (TRIN-60.)504,504,504
  503 CONTINUE
      DENS=24.43-((24.43-71.6)/2.*(TLE-116.))
      UNGR=(HL**3.)*(DENS**2)*(DENSL-DENSV)/(VIS**2.)
      UNGR=.62*(UNGR**(1/4))*3.25
      UNN=UNN+UNGR
      HH=UNN*TK/DEL
      TW=TLE-QT/(.5*HH)
  504 CONTINUE
      TWTS=TW-TSAT
      VISC=(.497-((TLI-120.)*(.364-.497)/20.))/100.**.0673
```

```
      DENS=94.41-(TW-116.)*.0362
      RE=G*DENS*VH*D/VI
      IF (RE.GT.2000.) GO TO 501,502,502
  501 CONTINUE
      FF1=16.*1.33/RE
      GO TO 506
  502 CONTINUE
      FF1=.079*((((G/VH)**2)*D/(DENS*144.))**.25)/(RE**.2)
  506 CONTINUE


      QDOF=FF1*2.*VH**2*G/(32.2*QENSL)
      IF (TWTS-14.) 102,103,103
  102 CONTINUE
      PHG=62.4*(1.-HL)*((QENSL-QENS)*HL/2.
      PZ=PHG-QDOF*ZIL*(62.4/(64.4*QENS))
      DENSW=94.43-(TW-116.)*.0362
      PHH=(DENSW-DENS)*HL/2.
      PZ=PZ-PHH*HL
      GO TO 110
  103 CONTINUE
      IC=0
      ZH=0.
      Z(1)=ZH+HL
      PZ=DENS*(Q-Z(1))-QDOF*(ZIL-Z(1))-G*G/(64.4*DENS)
      NZN=NN-1
      DZ=HL/NZN
      QDOT=QT/RS
      DO 20 IN=2,NN
      IC=IN-1
      ACC=32.174*(QDOT/Q)
      TLE=TLE+QDOT*ACC/(VEL*G)
      Z(IN)=Z(IN-1)-DZ
      TW=TLE+QDOT/RH
      P=PZ+DZ*DENS
      TSAT=14.7*(P/14.7)**(.0362*RH/4.4)
      HFG=970.3-(.695)*(TSAT-212.)-(1.-RH)/2.*(TSAT-116.)
      PZ=P-DZ*DENS
      TWTS=TW-TSAT
      IF (TWTS-14.) 104,104,104
  104 CONTINUE
      IC=IC+1
      IF (IC.EQ.1) 105,105,106
  105 CONTINUE
      ZIL=Z(IN)
      TLE=TLE
      ALP(IC)=0.
      S=1.
```

```
      GO TO 30
  106 CONTINUE
      ZSATD=AM*.2777/(TSAT-TLE(1))/(OPRI*3.1416*DU)
      ZPLUS=(ZMAX-Z(IC))/ZSATD
      TPLUS=TANH(ZPLUS)
      TLTLT=TPLUS*(TSAT-TLE(1))
      OPTI=OT/AS
      TLC=TLTLT+TLE(1)
      X=(OPTI*3.141)*DU*(Z(IC)-Z(IN))/AM-C*TLTLT)/(HEG-C*(TSAT-TLE))
      S=1.
      AK=(X/(1.-X))*(DENSL/DENSV)/S
      ALP(IC)=AK/(1.+AK)
   30 CONTINUE
      DENSL=28.41-((.0*T-.4)*TLE-110.))
      DENSV=.4*((.4*T-.04)*TLE-110.))
      IF (ALP(IC)-.5) 107,107,108
  107 DL=DENSL
      GO TO 109
  108 CONTINUE
      S=.5
      AK=(X/(1.-X))*(DENSL/DENSV)/S
      ALP(IC)=AK/(1.+AK)
      DL=(1.-ALP(IC))*DENSL+ALP(IC)*DENSV
  109 CONTINUE
```

```
      IF (IC-1) 10,1,10
    1 CONTINUE
      PROM=0.
      GO TO 12
   11 CONTINUE
      PROM=(G/(DENSL*(.3048**2.)))*(((1.-X)/(1.-ALP(IC)))**2.)
      PROM=PROM*(ALP(IC)-ALP(IC-1))/DZ
   12 CONTINUE
      RMN=(1.-2./(VIS*(1.-ALP(IC))))
      FF1=.25*(((PROM*11-1.)/(.2/21))**.1)/(RMN**.2)
      DPDF=FF1*.5*(DENSL*(1.-ALP(IC)))**2.)/(DEQ*32.2*DL)
      P=P+144.*DL*(Z(IC)-Z(IC-1))*DPDF*Z
      GO TO 21
  101 CONTINUE
      DENS=28.41-((.0*T-.4)*TLE-110.))
      P=P-144.*(Z(IC)-Z(IC-1))*.2
   20 CONTINUE
      GO TO 201 IC=1,MN
      ALP(IC)=0.
  201 CONTINUE
  110 CONTINUE
      RETURN
      END
```

APPENDIX VII

EXPERIMENTAL DATA AND CALCULATED RESULTS

A PERFORMANCE DATA

a) Power Dissipation and Circulation Rates (W - n Risers; T_i 116 F)

i) Experimental Data

Riser	L_H	Power (W)	Mass Flow	T_e (mv)	P_e (" of Hg)	Limit
W - 5/8	7'	762	1.4"	2.086	35"	Min
		2054	3.0"	2.295	31"	Max
	4'	610				Min
		1605				Max
	3'	734				Min
		1875				Max
W - I	7'	1320	4.1"	2.108	27"	Min
		3790	10"	2.269	23"	Max
	4'	1080				Min
		2730				Max
	3'	1260				Min
		3200				Max

(Cont'd)

Riser	L_H	Power (VA)	Mass Flow	T_e (mv)	P_e (" of Hg)	Limit
W - 1½	7'	1613	8.2"	2.095	24"	Min
		4020	15"	2.250	22"	Max
	4'	1170				Min
		2980				Max
	3'	1380				Min
		3400				Max
W - 1½	7'	1760	10.5"	2.096	24"	Min
		4140	17.3"	2.187	21"	Max
	4'	1345				Min
		3000				Max
	3'	1640				Min
		2770				Max

ii) Calculated Results

Riser A_r/A_{ts}	l_H/H	Power (Btu/hr)	$\dot{q}''$ (Btu/hr ft^2)	Mass Flow lb/hr	T_e (°F)	P_e (psi)	π_1	π_2	Limit
				1.14×10^3	124.4	8.250	.31	.33	Min
W - 5/8	0.5	2650	2580	1.66 "	133.3	7.625	.64	.69	Max
		7000	6800	1.1[illegible] "					Min
	0.29	2600	4300	[illegible] "					Max
		6850	11,410	1.5[illegible] "					Min
0.89	0.21	2500	5880	[illegible] "					Max
		6400	15,020	2.37 "					
				1.95×10^3	125.2	6.75	.34	.41	Min
W - 1	0.5	4250	4150	3.06 "	132.0	5.723	.59	.80	Max
		12,900	12,600	2.23 "					Min
	0.29	4600	7660	2.7[illegible] "					Max
		11,650	19,400	[illegible] "					Min
2.28	0.21	4300	10,100	1.98 "					Max
		10,300	24,200	3.0 "					
				2.77×10^3	124.7	6.32	.32	.40	Min
W - 1½	0.5	5500	5370	3.35 "	131.4	5.37	.57	.81	Max
		13,700	13,400	2.[illegible] "					Min
	0.29	5000	8350	[illegible] "					Max
		12,700	21,200	[illegible] "					Min
3.56	0.21	4700	11,050	[illegible] "					Max
		11,300	26,580	[illegible] "					
				3.13×10^3	124.7	6.32	.32	.40	Min
W - 1½	0.5	6000	5850	4.02 "	130.9	5.13	.55	.81	Max
		14,100	13,750	[illegible] "					Min
	0.29	5750	9600	[illegible] "					Max
		12,850	21,400	[illegible] "					Min
5.1	0.21	5600	13,150	[illegible] "					Max
		9450	22,240	[illegible] "					

Upflow Data (Experimental and Calculated Results)

Riser A_r/A_{ts}	L_H/H	Power (KW)	Power (Btu/hr)	Limit
W - 5/8 0.89	0.5	1.115 5.27	3880 18,000	Min Max
W - Y 2.28	0.5	1.115 5.27	3800 18,000	Min Max
W - 1½ 3.56	0.5	1.115 5.27	3800 18,000	Min Max
W - 1½ 5.1	0.5	1.115 5.27	3500 18,000	Min Max

b) Riser Behaviour

1) Experimental Data

Riser	Power (KW)	Mass Flow (" of 113)	Nucleating Requirement
I - 5/8	0.770	1.45	Inserts
	1.114	1.8	"
	1.585	2.3	"
	1.815	2.45	"
W - 5/8	0.72	1.4	30x1.65 VI
	1.114	1.8	"
	1.64	2.45	"
	2.05	2.95	"
O - 1	1.38	4.7	0.75" Dia Or.
	1.815	5.4	"
	2.39	7.3	"
	2.99	10.0	"
	3.73	10.1	"
D - 1	1.476	5.3	0.25" Dia Discs
	1.611	5.5	"
	2.70	9.0	"
	3.52	12.0	"
	4.09	13.7	"
W - 1	1.476	4.7	58.5x3.3 VI
	2.7	10.0	"
	3.52	13.8	"
	4.09	16.0	"
D - 1½	1.63	8.3	0.5" Dia Discs
	2.355	9.8	"
	3.31	12.1	"
	3.95	14.7	"
W - 1½	1.63	7.7	90x5.1 VI
	2.355	9.9	"
	3.280	12.8	"
	4.065	15.7	"
D - 1½	1.142	2.5	1.25" Dia Discs
	1.395	3.2	"
	2.125	4.7	"
	3.020	6.1	"
W - 1½	1.77	11.2	120x13.1 VI
	2.70	12.7	"
	3.81	15.8	"
	4.17	17.4	"

11) Calculated Results

Riser A_r/A_{ts}	Power (Btu/hr)	Grinar (lb/hr ft^2)	Nucleating Requirement
I - 5/8	2.7×10^3	0.54×10^6	Inserts
	3.8 "	0.61 "	"
0.89	5.4 "	0.69 "	"
	6.2 "	0.71 "	
W - 5/8	2.45×10^3	0.54×10^6	170 Btu/hr
	3.8 "	0.61 "	"
0.89	5.6 "	0.71 "	"
	7.0 "	0.78 "	"
0 - 1	4.7×10^3	0.39×10^6	.75" Dia Or.
	6.2 "	0.41 "	"
2.28	8.2 "	0.48 "	"
	10.2"	0.56 "	"
	12.2"	0.57 "	"
D - 1	4.7×10^3	0.41×10^6	$A_o/A_r = 0.93$
	5.5 "	0.42 "	"
2.28	9.2 "	0.53 "	"
	12.0"	0.62 "	"
	14.0"	0.66 "	"
W - 1	4.7×10^3	0.38×10^6	650 Btu/hr
	9.2 "	0.56 "	"
2.28	12.0"	0.65 "	"
	14.0"	0.71 "	"
D - 1½	5.5×10^3	0.33×10^6	$A_o/A_r = 0.84$
	8.0 "	0.36 "	"
3.56	11.3"	0.40 "	"
	13.5"	0.44 "	"
W - 1½	5.5×10^3	0.32×10^6	1550 Btu/hr
	8.0 "	0.36 "	"
3.56	11.2"	0.41 "	"
	13.9"	0.45 "	"
D - 1½	3.9×10^3	0.13×10^6	$A_o/A_r = 0.3$
	4.8 "	0.14 "	"
5.1	7.3 "	0.17 "	"
	10.3"	0.20 "	"
W - 1½	6.1×10^3	0.26×10^6	2750 Btu/hr
	9.2 "	0.28 "	"
5.1	13.0"	0.31 "	"
	14.2"	0.33 "	"

c) Other Effects

Experimental and Calculated Results

Driver	Transistor	Power (W)	mW/hr	Limit
Q - 1	Typical	1.62 4.08	4.20×10^3 19.9"	Min Max
	2.69	1.76 4.25	6.0×10^3 14.55"	Min Max
	11.1	1.70 4.25	2.8×10^3 42.2"	Min Max
	12.7	1.74 4.35	10.7×10^3 16.5"	Min Max
	7.4 7.2	1.84 4.30	6.2×10^3 14.65"	Min Max
	11.7 11.9	1.69 4.35	2.0×10^3 15.3"	Min Max
Q - 1	Valve oscillating Side open	1.38 4.08	5.7×10^3 19.9"	Min Max
	2 turns	1.38 4.08	1.7×10^3 19.9"	Min Max
	3 turns	1.38 3.34	6.2×10^3 11.4"	Min Max
	22 turns	2.05 2.91	7.0×10^3 19.0"	Min Max

B. HEAT TRANSFER RESULTS

a) Wall and Fluid Temperatures

i) Experimental Data

T_w	I = 5/8, 7' Heater				I = 5/8, 3' Heater			
	q 773	1230	1596	1820	782	1000	1420	1455
z_w	m 1.5	2.0	2.2	2.3	1.0	1.5	2.0	2.0
-0.05	1.915	1.945	2.01	1.99	1.90	1.955	1.955	1.99
0	1.97	2.01	2.08	2.08	1.953	2.0	2.017	2.039
0.04	2.011	2.05	2.126	2.14	1.986	2.145	2.05	2.075
0.73	2.175	2.215	2.296	2.345	2.205	2.26	2.265	2.305
0.8	2.529	2.64	2.724	2.82	2.806	2.85	2.856	2.88
1.5	2.575	2.725	2.8	2.869	2.895	2.94	2.951	2.97
1.8	2.551	2.695	2.848	2.88	2.835	2.887	2.9	2.972
1.83	2.548	2.69	2.84	2.882	2.855	2.887	2.905	2.92
2.47	2.515	2.665	2.81	2.855	2.85	2.92	2.94	2.922
2.72	2.5	2.65	2.775	2.84	2.815	2.89	2.9	2.875
3.08	2.47	2.63	2.745	2.815	2.785	2.846	2.844	2.27
3.4	2.46	2.628	2.695	2.77	2.18	2.235	2.24	1.865
3.6	2.11	2.151	2.178	2.2	1.86	1.96	1.87	1.88
3.65	2.46	2.59	2.71	2.785	1.872	1.88	1.88	1.88
5.8	2.408	2.518	2.61	2.65	1.872	1.89	1.88	1.872
8.8	1.877	1.88	1.875	1.87	1.875	1.875	1.88	1.88

(Cont'd)

0 - 1, 4' Heater
0 - 1, 4' Heater
0 - 1, 7' Heater
2510
6.2
2400
7.2
2460
7.1
1822
5.4
2390
6.6
2300
7.8
1958
7.2
1472
5.2
3550
10.4
3350
10.4
3190
10.4
2700
6.7

ii) Calculated Results

T	I - 5/8, 7' Heater				I - 5/8, 3' Heater			
	q 773	1230	1596	1820	782	1000	1320	1455
x	m 1.5	2.0	2.2	2.3	1.0	1.5	2.0	2.0
-0.05	116.8	118.1	120.9	120.0	116.2	118.5	118.6	120.0
0	119.2	120.9	123.9	123.9	118.5	120.5	121.6	122.1
0.04	120.9	122.6	125.9	126.5	119.9	122.2	122.6	123.7
0.73	128.0	129.7	133.2	135.3	129.5	131.6	131.9	133.6
0.80	143.4	148.0	153.7	155.7	155.1	157.0	157.2	158.3
1.3	145.2	151.6	154.8	158.7	159.0	160.9	161.3	162.1
1.6	144.1	150.3	157.0	158.3	156.3	158.6	159.0	162.2
1.83	144.0	150.1	156.6	158.2	157.2	159.6	159.4	160.4
2.5	142.6	149.0	155.3	157.2	157.0	160.0	160.9	160.1
2.72	142.0	148.4	153.9	156.6	155.5	158.7	159.1	158.1
2.98	140.7	147.5	152.5	155.5	154.2	156.9	156.7	152.1
3.4	140.2	145.2	150.3	153.6	128.2	130.8	130.8	114.7
3.6	135.2	137.0	138.1	129.1	114.5	114.5	114.9	115.3
3.95	140.2	145.8	157.0	154.2	115.0	115.3	115.3	115.3
5.8	138.0	142.7	146.7	146.4	115.0	115.3	115.3	115.0
8.8	115.2	115.5	115.1	114.9	115.2	115.2	115.3	115.3

(Cont'd)

0 - 11.7' Heater				0 - 11.5' Heater			
0.05							
0.2	2700	3190	3360	3500	1472	1958	2300	2390	1620	2560	2503	2420
E	9.7	10.4	10.4	10.4	2.5	6.2	6.8	7.2	5.1	8.1	8.2	8.2

iii) Experimental Data

T_1	I - 5/8, 7' Heater				I - 5/8, 3' Heater			
	q 773	1230	1596	1820	782	1000	1320	1455
z_1	m 1.5	2.0	2.2	2.3	1.0	1.5	2.0	2.0
0.26	2.695	2.77	2.858	2.918	2.685	2.755	2.778	2.828
1.31	2.658	2.728	2.816	2.863	2.61	2.67	2.703	2.728
2.02	2.641	2.7	2.754	2.82	2.523	2.582	2.609	2.61
2.72	2.609	2.658	2.718	2.762	2.441	2.496	2.518	2.54
3.42	2.584	2.624	2.67	2.702	2.38	2.393	2.393	2.385
4.46	2.521	2.569	2.6	2.63	2.382	2.397	2.4	2.386
5.50	2.496	2.5	2.536	2.558	2.382	2.397	2.4	2.383
7.52	2.4	2.4	2.403	2.4	2.385	2.397	2.403	2.392

T_1	0 - 1, 7' Heater				0 - 1, 4' Heater				0 - 1, 3' Heater			
	q 2700	3190	3360	3550	1472	1958	2300	2390	1820	2260	2400	2510
z_1	m 9.7	10.4	10.4	10.4	5.5	7.2	7.8	7.9	5.4	7.1	7.2	9.2
0.26	2.77	2.825	2.85	2.85	2.685	2.728	2.758	2.77	2.731	2.77	2.793	2.786
1.31	2.733	2.776	2.805	2.805	2.685	2.728	2.755	2.773	2.611	2.639	2.658	2.653
2.02	2.7	2.733	2.759	2.759	2.67	2.71	2.736	2.755	2.514	2.54	2.555	2.555
2.72	2.662	2.696	2.724	2.724	2.615	2.66	2.672	2.685	2.579	2.45	2.453	2.44
3.42	2.618	2.659	2.663	2.663	2.552	2.6	2.61	2.619	2.408	2.408	2.41	2.425
4.46	2.57	2.593	2.6	2.6	2.482	2.498	2.579	2.526	2.408	2.408	2.41	2.425
5.50	2.511	2.513	2.528	2.528	2.409	2.409	2.409	2.409	2.406	2.406	2.41	2.425
7.52	2.411	2.411	2.401	2.401	2.393	2.409	2.409	2.409	2.406	2.406	2.41	2.425

iv) Calculated Results

T_1 — I - 5/8, 7' Heater — I - 5/8, 3' Heater

z_1	$\dot{q}$ 773	1230	1596	1820	782	1000	1320	1455
	m 1.5	2.0	2.2	2.3	1.0	1.5	2.0	2.0
0.26	125.9	128.5	131.5	133.5	125.5	127.9	128.7	130.4
1.31	124.6	127.0	130.0	131.6	123.0	125.0	126.2	127.0
2.02	124.0	126.0	127.9	130.2	120.0	122.0	122.9	123.0
2.72	122.9	124.6	126.7	128.2	117.1	119.0	119.8	119.9
3.42	122.1	123.4	125.0	126.1	115.1	115.5	115.5	115.2
4.46	119.9	121.5	122.6	123.6	115.1	115.6	115.7	115.3
5.50	119.1	119.2	120.4	121.2	115.1	115.6	115.7	115.2
7.52	115.7	115.7	115.8	115.7	115.2	115.6	115.8	115.5

T_1 — 0 - 1, 7' Heater — 0 - 2, 4' Heater — 0 - 1, 3' Heater

z_1	$\dot{q}$ 2700	3190	3360	3550	1472	1958	2300	2500	1820	2260	2400	2510
	m 9.7	10.4	10.6	10.4	5.5	7.2	7.8	7.9	5.4	7.1	7.2	9.2
0.26	128.5	130.3	131.2	131.2	125.5	127.0	128.0	128.5	127.1	128.5	129.2	129.0
1.31	127.2	128.7	129.7	129.7	125.5	127.0	127.9	128.6	123.0	124.0	124.6	124.4
2.02	126.0	127.2	128.1	128.1	125.0	126.4	127.3	127.9	120.0	120.5	121.1	121.1
2.72	124.7	125.9	126.9	126.9	123.1	124.7	125.1	125.5	121.9	117.5	117.6	117.1
3.42	123.2	124.6	124.8	124.8	121.0	122.6	123.0	123.3	116.0	116.0	116.1	116.6
4.46	121.6	122.4	122.6	122.6	118.6	119.1	119.8	120.1	116.0	116.0	116.1	116.6
5.50	119.6	119.6	120.1	120.2	116.0	116.0	116.0	116.0	115.9	115.9	116.1	116.6
7.52	116.1	116.1	115.8	115.8	115.5	116.0	116.0	116.0	115.9	115.9	116.1	116.6

b) Forced Convection

Riser & Heater	z	$\dot{q}_1$ h	$\dot{q}_1$ N_{Re}	$\dot{q}_1$ N_{Nu}	$\dot{q}_2$ h	$\dot{q}_2$ N_{Re}	$\dot{q}_2$ N_{Nu}	$\dot{q}_3$ h	$\dot{q}_3$ N_{Re}	$\dot{q}_3$ N_{Nu}	$\dot{q}_4$ h	$\dot{q}_4$ N_{Re}	$\dot{q}_4$ N_{Nu}
I - 5/8 7"	1.3	129.4	8864	68.9	170.3	10,462	91.9*	221.9	11,552	119.4	230.0	11,533	124.2
	1.8	130.7	8840	69.5	172.1	10,383	91.9*	195.2	11,200	104.8	221.1	11,473	119.1
	1.83	131.3	8840	69.8	173.3	10,383	92.5*	197.2	11,200	105.8	219.8	11,473	118.4
	2.47	131.1	8820	71.2	171.9	10,331	91.6*	195.2	10,979	104.5	215.0	11,410	115.4
	2.72	135.8	8880	72.1	173.0	10,293	92.1*	201.8	10,913	107.8	214.6	11,320	115.0
	3.08	141.2	8754	74.8	174.0	10,227	92.5*	204.9	10,883	109.3	215.2	11,247	115.1
	3.64	137.6	8725	72.8	178.5	10,161	94.7*	205.8	10,810	109.5	213.0	11,120	113.6
	5.8	129.5	8560	68.06	169.7	9973	89.3*	198.5	10,510	104.6	211.6	11,803	111.6
I - 5/8 37"	1.3	177.5	7450	94.2	228.3	9450	121.7	302.1	11,058	161.2	338.1	11,245	180.9
	1.8	180.3	7230	95.3	227.4	9080	120.6	299.2	10,660	158.9	311.0	10,880	165.4
	1.83	175.5	7230	92.8	226.6	9080	120.2	296.4	10,660	157.3	325.3	10,880	173.0
	2.47	165.0	7110	86.8	201.8	8710	106.4	262.6	10,110	138.6	298.2	10,119	157.5
	2.72	167.4	6940	87.9	202.5	8605	106.6	265.9	10,000	140.0	303.0	10,900	159.6
	3.08	166.9	6875	87.4	203.6	8527	106.8	270.4	9897	141.9	293.9	9903	146.6

Note: *Data used to obtain forced convection correlation

Riser & Heater	z	$\dot{q}_1$ h	N_{Re}	N_{Nu}	$\dot{q}_2$ h	N_{Re}	N_{Nu}	$\dot{q}_3$ h	N_{Re}	N_{Nu}	$\dot{q}_4$ h	N_{Re}	N_{Nu}
0 - 17'	0.79	311.3	23,010	166.9*	360.0	26,790	193.4	337.3	29,450	208.7	455.3	41,200	245.3
	1.3	304.4	22,950	162.9*	374.4	26,374	200.9	403.5	28,780	216.9	425.5	40,400	228.7
	1.8	307.4	22,880	164.1*	359.8	25,100	192.7	381.7	26,500	204.7	446.5	37,100	239.4
	1.83	302.4	22,880	161.5*	362.7	25,100	194.2	385.3	26,500	206.6	445.4	37,100	238.8
	2.47	329.7	22,780	175.6*	348.0	23,960	185.8	353.7	24,170	189.1	358.4	24,170	191.6
	5.8	311.4	22,050	163.8*	349.8	22,755	184.2*	309.6	22,890	163.0*	328.9	22,890	173.2
0 - 14'	2.47	262.8	16,890	139.6*	339.2	19,820	180.7	363.7	21,510	194.0	400.6	21,990	213.8
	2.72	269.5	16,810	143.0*	340.6	19,770	181.1	370.5	21,000	197.3	391.1	21,400	208.4
	3.08	268.6	16,788	142.3*	340.9	19,572	180.9	356.0	20,471	189.2	376.9	20,729	200.4
	3.4	276.1	16,620	146.0*	351.0	19,340	185.9	392.0	20,140	207.9	385.1	20,340	204.3
	3.6	271.2	16,610	143.2*	342.6	19,320	181.3	370.4	20,120	196.2	380.1	20,320	201.4
	3.65	281.9	16,610	148.7*	340.1	19,320	179.9	369.1	20,120	195.5	378.7	20,320	200.6

Note: *Data used to obtain forced convection correlation

Riser & Heater	z	$\dot{q}_1$ h	N_{Re}	N_{Nu}	$\dot{q}_2$ h	N_{Re}	N_{Nu}	$\dot{q}_3$ h	N_{Re}	N_{Nu}	$\dot{q}_4$ h	N_{Re}	N_{Nu}
0 - 1 3'	0.73	393.0	17,530	209.5	498.0	22,330	265.9	538.3	22,760	287.8	576.3	22,890	308.1
	0.79	387.8	17,530	206.5	492.8	21,860	263.0	532.4	22,100	284.5	569.4	22,300	304.2
	1.28	380.2	16,800	201.6	478.1	20,320	254.0	521.6	20,520	272.1	552.1	21,980	293.6
	1.8	357.0	16,450	188.6	458.3	18,890	242.3	491.3	19,150	260.0	517.6	21,650	274.0
	1.83	363.7	16,450	192.0	458.4	18,890	242.3	491.9	19,150	260.2	519.4	21,650	274.9
	2.47	313.3	16,240	164.6	397.2	18,920	208.8	423.3	18,900	222.6	460.2	21,360	242.2
	2.72	319.1	16,300	167.3	387.3	18,700	203.1	412.2	18,760	216.3	448.4	21.100	235.5

c) Subcooled Nucleate Boiling

Riser & Heater	q"	$T_w - T_s$	$N_{Re,b}$	$N_{Nu,b}$
I - 5/8 7'	5419	15.2	0.273	0.0025
		18.0	0.271	0.0029
		17.7	0.271	0.0029
	6057	19.1	0.304	0.0031
		19.5	0.303	0.0031
		19.6	0.303	0.0032
I - 5/8 3'	6295	18.7	0.318	0.0031
		16.9	0.316	0.0027
		17.8	0.316	0.0029
	8082	20.7	0.408	0.0034
		19.3	0.405	0.0031
		19.3	0.405	0.0031
	10,634	21.4	0.536	0.0035
		20.0	0.533	0.0032
		20.3	0.532	0.0033
	11,740	22.6	0.59	0.0037
		23.5	0.586	0.0038
		21.8	0.586	0.0035
0 - 1 7'	10,700	23.6	0.526	0.0037*
		21.9	0.524	0.0034*
		22.5	0.522	0.0035*
		22.3	0.521	0.0035*
	11,270	23.8	0.554	0.0037*
		22.0	0.552	0.0034*
		23.0	0.55	0.0036*
		22.7	0.55	0.0035*
0 - 1 4'	11,128	21.9	0.545	0.0034
		21.4	0.544	0.0033
		20.8	0.543	0.0032
		19.3	0.541	0.003
		19.8	0.54	0.003
		20.0	0.54	0.0031

Note: *Data used to obtain boiling correlation

(Cont'd)

Riser & Heater	$\dot{q}''$	$T_w - T_b$	$N_{Re,b}$	$N_{Nu,b}$
0 - 14'	13,106	26.0	0.642	0.0041*
		24.9	0.641	0.0039*
		25.7	0.639	0.0040*
		21.7	0.637	0.0033*
		23.3	0.636	0.0036*
		23.3	0.636	0.0036*
	13,611	24.3	0.667	0.0038*
		24.6	0.666	0.0038*
		25.2	0.664	0.0039*
		23.8	0.662	0.0037*
		23.9	0.661	0.0037*
		23.9	0.66	0.0037*
0 - 13'	14,650	23.8	0.732	0.0038*
		24.1	0.732	0.0039*
		23.5	0.729	0.0037*
		24.5	0.725	0.0039
		23.7	0.72	0.0037
	18,206	25.9	0.899	0.0041*
		25.6	0.899	0.0041*
		25.6	0.895	0.004*
		25.5	0.89	0.004
		25.4	0.89	0.004
	19,312	25.7	0.956	0.0041*
		25.8	0.955	0.0041*
		25.5	0.951	0.004
		25.2	0.946	0.0039
		25.1	0.946	0.0039
	20,250	26.4	0.991	0.0041
		26.6	0.991	0.0041
		26.0	0.987	0.004
		26.7	0.982	0.0041
		26.5	0.982	0.0041

Note: *Data used to obtain boiling correlation

C VOID FRACTION

a) Subcooled Nucleate Boiling

i) Experimental Data

I - 5/8, 7' Heater

z	$\dot{q}$ 773 / m 1.5	1230 / 3.0	1596 / 2.2	1820 / 2.3
1.06	93.7	93.4	92.0	88.5
1.23	93.7	93.4	90.0	88.5
1.73	93.8	93.5	92.0	91.2
1.87	93.8	93.5	93.0	92.0
3.21	93.9	93.7	93.7	93.5
3.79	93.9	93.9	93.7	93.5

I - 5/8, 3' Heater

z	782 / 1.0	1000 / 1.5	1320 / 2.0	1455 / 2.0
1.06	90.0	88.0	87.5	85.5
1.23	90.0	88.5	87.5	85.5
1.73	92.5	90.0	90.0	92.5
1.87	92.5	90.0	90.0	92.5
3.21	94.5	94.5	94.5	94.5
3.79	94.5	94.5	94.5	94.5

O - 1, 7' Heater

z	$\dot{q}$ 2700 / m 9.7	3190 / 10.4	3360 / 10.4	3550 / 10.4
1.06	93.4	82.5	76.0	46.8
1.23	93.4	83.5	77.0	50.0
1.73	93.5	88.5	84.0	69.0
1.87	93.5	89.0	85.5	80.2
3.21	93.8	93.7	93.7	93.7
3.79	93.8	93.8	93.8	93.8

O - 1, 4' Heater

z	1472 / 5.5	1958 / 7.2	2300 / 7.8	2390 / 7.9
1.06	93.6	90.0	90.0	89.5
1.23	93.6	90.0	90.0	87.5
1.73	93.7	87.4	85.4	84.0
1.87	93.7	87.4	85.4	84.0
3.21	93.8	93.5	93.5	93.5
3.79	93.8	93.8	93.8	93.8

O - 1, 3' Heater

z	1820 / 5.4	2260 / 7.1	2400 / 7.2	2510 / 9.2
1.06	91.6	85.0	84.0	81.0
1.23	91.6	87.0	86.0	83.0
1.73	94.0	93.0	92.5	92.5
1.87	94.0	93.0	93.0	93.0
3.21	94.4	94.4	94.4	94.4
3.79	94.4	94.4	94.4	94.4

ii) Calculated Results

I - 5/8, 7' Heater

z	q 773 / n 1.5	1230 / 2.0	1596 / 2.2	1820 / 2.3
1.06	-	-	0.038	0.042
1.23	-	-	0.038	0.042
1.73	-	-	0.016	0.020
1.87	-	-	0.006	0.015
3.21	-	-	-	-
3.79	-	-	-	-

I - 5/8, 3' Heater

z	782 / 1.0	1000 / 1.5	1320 / 2.0	1455 / 2.0
1.06	0.046	0.066	0.071	0.092
1.23	0.046	0.066	0.071	0.092
1.73	0.020	0.045	0.044	0.044
1.87	0.020	0.045	0.044	0.044
3.21	-	-	-	-
3.79	-	-	-	-

0 - 1, 7' Heater

z	q 2700 / m 9.7	3190 / 10.4	3360 / 10.4	2550 / 10.4
1.06	-	0.12	0.19	
1.23	-	0.11	0.18	
1.73	-	0.055	0.11	
1.87	-	0.050	0.09	
3.21	-	-	-	
3.79	-	-	-	

0 - 1, 4' Heater

z	1472 / 5.5	1958 / 7.2	2300 / 7.8	2390 / 7.9
1.06	-	0.020	0.039	0.044
1.23	-	0.025	0.039	0.044
1.73	-	0.068	0.037	0.103
1.87	-	0.068	0.037	0.103
3.21	-	0.002	0.002	0.023
3.79	-	-	-	-

0 - 1, 3' Heater

z	1820 / 5.4	2260 / 7.1	2400 / 7.2	2510 / 9.2
1.06	0.025	0.099	0.11	0.12
1.23	0.025	0.08	0.08	0.10
1.73	-	0.014	0.019	0.020
1.87	-	-	-	-
3.21	-	-	-	-
3.79	-	-	-	-

b) Vertical Flashing Flow

1) Experimental Data

Density Measurement

z	T_1 = 128 F	T_1 = 131.3 F	T_1 = 133.5 F	T_1 = 135.2 F
2.8	-	-	-	91.0
4.0	-	-	-	88.1
5.0	-	-	-	79.0
6.3	-	-	87.4	67.0
7.6	-	89.5	70.9	58.7
8.25	-	75.5	55.2	49.6
9.1	-	62.8	46.0	41.2
10.1	88.1	52.5	39.4	34.6
10.8	72.1	47.0	36.6	30.9
11.4	61.0	45.3	33.8	28.1

Temp. Measurement

z	T_1 = 128 F	T_1 = 131.3 F	T_1 = 133.5 F	T_1 = 135.2 F
0.24	2.172	2.248	2.30	2.345
3.30	2.165	2.245	2.297	2.326
5.1	2.155	2.228	2.296	2.275
6.0	2.157	2.226	2.270	2.231
7.8	2.153	2.190	2.150	2.147
9.8	2.148	2.055	2.045	-
12.8	1.920	1.920	1.915	1.917

Pressure Measurement

z	T_1 = 128 F	T_1 = 131.3 F	T_1 = 133.5 F	T_1 = 135.2 F
3.06	1.8	1.0	0.2	0.8
0.54	0.2	0.2	0.2	0.3
0.54	0.2	0.2	0.2	0.3
0.87	0.5	0.3	0.3	1.2
1.79	0.2	0.3	4.0	10.8
2.04	1.1	10.4	14.4	18.2
3.06	17.6	23.8	26.2	29.9

11) Calculated Results

Void Fraction

z	T_1 = 128 F	T_1 = 131.3 F	T_1 = 133.5 F	T_1 = 135.2 F
2.8	–	–	–	0.02
4.0	–	–	–	0.05
5.0	–	–	–	0.15
6.2	–	–	0.06	0.28
7.2	–	0.04	0.24	0.37
8.25	–	0.12	0.41	0.47
9.1	–	0.33	0.51	0.56
10.1	0.66	0.44	0.58	0.63
10.8	0.73	0.50	0.61	0.67
11.4	0.33	0.54	0.64	0.70

Temperature

z	T_1 = 128 F	T_1 = 131.3 F	T_1 = 133.5 F	T_1 = 135.2 F
0.24	128.0	131.3	133.5	135.2
3.30	127.6	131.0	133.3	134.7
5.1	127.3	130.4	133.1	132.3
6.0	127.4	130.2	132.0	130.5
7.8	127.1	128.6	126.9	126.7
9.8	126.8	123.0	122.5	–
12.8	117.1	117.1	116.8	116.9

Pressure Gradient

z	T_1 = 128 F	T_1 = 131.3 F	T_1 = 133.5 F	T_1 = 135.2 F
3.06	0.669	0.671	0.672	0.672
0.54	0.669	0.669	0.669	0.664
0.54	0.669	0.669	0.669	0.641
0.87	0.664	0.670	0.670	0.641
1.79	0.677	0.675	0.617	0.509
2.94	0.664	0.533	0.476	0.450
3.06	0.514	0.455	0.432	0.398

Liquid Superheating and Ship Data

T_i		$T_f - T_{mt}$ Meas. T_f	$T_f - T_{mt}$ Theor. T_f	S Assuming Equilib.	S Meas. Temp.	S Other.
128.0	0.25	5.7	6.4	14.6	5.1	-
	0.35	4.7	6.7	11.0	7.3	-
	0.55	0	5.2	6.9	4.8	-
131.3	0.16	4.9	5.2	18.6	11.6	1.5
	0.39	2.8	6.8	9.3	6.4	-
	0.51	1.2	6.0	6.0	5.8	-
	0.62	0	4.8	5.6	5.5	-
133.5	0.02	4.0	5.0	-	-	1.5
	0.35	3.7	6.7	9.8	6.8	-
	0.55	3.5	6.0	6.6	4.8	-
	0.7	0	3.8	4.8	4.6	-
135.2	0.26	6.3	6.7	13.8	14.9	-
	0.43	4.5	6.7	9.4	5.5	-
	0.6	2.6	5.5	6.2	4.6	-
	0.76	0	0.1	4.0	3.7	-

D PRESSURE DROP

a) Subcooled Nucleate Boiling

i) Experimental Data

p	I - 5/8, 7' Heater				I - 5/8, 3' Heater			
	q 773	1230	1596	1820	782	1000	1320	1455
z	m 1.5	2.0	2.2	2.3	1.0	.5	2.0	2.0
0.52	0.8	1.6	1.9	1.2	0.8	0.9	1.1	1.1
1.28	4.0	4.8	4.1	3.9	3.1	2.9	3.4	3.8
0.71	1.8	2.0	2.2	2.2	1.8	1.8	2.2	2.2
0.71	1.8	2.0	2.2	2.1	1.6	1.7	2.2	1.9
1.04	2.2	3.0	3.2	3.4	2.0	2.3	3.0	3.0
1.04	2.0	2.9	3.2	3.1	2.1	2.3	3.0	2.8
2.02	4.4	6.0	5.8	8.0	4.0	5.0	6.5	6.8
3.04	7.8	10.4	11.6	10.8	6.4	8.5	10.1	10.7

p	0 - 1, 7' Heater				0 - 1, 4' Heater				0 - 1, 3' Heater			
	q 2700	3190	3360	2550	1472	1958	2300	2590	1820	2260	2400	2510
z	m 9.7	10.4	10.4	10.4	5.2	7.2	7.8	7.8	5.4	7.1	7.2	9.2
0.52	2.0	2.8	5.1	10.2	1.6	1.9	1.8	2.0	2.4	3.0	3.4	3.5
1.28	10.0	10.7	11.1	18.5	7.1	8.9	8.6	9.4	9.4	11.9	14.0	14.4
0.71	6.2	6.5	6.4	6.8	4.1	5.4	5.2	5.4	5.4	6.6	5.1	5.5
0.71	6.3	6.6	6.6	6.6	4.1	5.5	5.2	5.4	5.4	6.6	5.1	5.5
1.04	10.0	10.5	10.5	10.5	5.9	7.6	8.0	8.4	8.0	10.4	11.8	12.4
1.04	9.9	10.1	10.5	10.4	5.9	7.6	8.0	8.4	8.0	10.4	11.8	12.4
2.20	17.0	18.1	19.0	20.0	10.1	13.8	15.0	16.2	14.4	20.0	24.0	25.6
3.04	31.4	33.2	33.4	33.6	17.6	22.4	24.4	24.4				

ii) Calculated Results.

P	I - 5/8, 7' Heater				I - 5/8, 3' Heater			
	q 773	1230	1596	1820	782	1000	1320	1455
z	m 1.5	2.0	2.2	2.5	1.0	1.5	2.0	2.0
0.52	0.642	0.598	0.582	0.620	0.642	0.66	0.66	0.65
1.28	0.597	0.58	0.595	0.60	0.617	0.620	0.610	0.602
0.71	0.613	0.605	0.597	0.597	0.613	0.615	0.597	0.597
0.71	0.613	0.605	0.597	0.601	0.613	0.617	0.597	0.607
1.04	0.625	0.604	0.598	0.593	0.631	0.623	0.604	0.604
1.04	0.631	0.607	0.598	0.602	0.629	0.623	0.604	0.609
2.02	0.623	0.601	0.604	0.573	0.629	0.615	0.594	0.59
3.04	0.613	0.590	0.577	0.585	0.626	0.606	0.591	0.586

P	0 - 1, 7' Heater				0 - 1, 4' Heater				0 - 1, 3' Heater			
	q 2220	3190	3360	2550	1472	1958	2300	2390	1820	2240	2400	2510
z	m 9.7	10.4	10.4	10.4	5.5	7.2	7.5	7.9	7.1	7.1	7.2	9.2
0.52	0.577	0.533	0.517	0.144	0.598	0.588	0.582	0.577	0.555	0.544	0.517	0.506
1.28	0.465	0.45	0.441	0.283	0.529	0.490	0.512	0.485	0.538	0.47	0.416	0.397
0.71	0.438	0.434	0.43	0.414	0.522	0.47	0.474	0.454	0.526	0.494	0.482	0.474
0.71	0.434	0.422	0.422	0.422	0.522	0.478	0.478	0.458	0.522	0.498	0.49	0.482
1.04	0.414	0.41	0.41	0.46	0.536	0.485	0.471	0.458	0.520	0.501	0.49	0.439
1.04	0.417	0.412	0.398	0.404	0.550	0.479	0.468	0.458	0.523	0.506	0.50	0.458
2.20	0.447	0.432	0.419	0.405	0.544	0.492	0.475	0.459	0.526	0.488	0.488	0.446
3.04	0.394	0.377	0.375	0.373	0.522	0.477	0.459	0.499	0.50	0.466	0.462	0.438

Friction Factors With and Without Surface Boiling

N_{Re}	f_1
8620	0.0083
10,190	0.0077
11,100	0.0085*
10,670	0.0084
11,460	0.0074*
10,990	0.008
7080	0.013*
6810	0.011
8800	0.0081*
8330	0.0087
10,220	0.0083*
9700	0.01
10,250	0.009*
9680	0.01
22,400	0.008
24,000	0.007*
23,200	0.0081
24,170	0.007*
23,310	0.0083
24,170	0.0088*
23,300	0.008
16,600	0.0076
19,500	0.0086*
19,200	0.0079
19,500	0.0084
20,400	0.0078*
19,600	0.0089
20,640	0.0085*
16,600	0.0073*
16,000	0.0088
19,180	0.0083*
18,330	0.008
19,400	0.0068*
18,480	0.0082
21,900	0.0088*
20,900	0.0077

Note: *with surface boiling

b) Vertical Flashing Flow

T_i = 128 F

z	(P/z) Exp.	(P/z) Homo.	Density Eq(A - 19)	Density Exp.	f Exp.
1.77	0.669	0.664	93.4	93.4	0.008
3.98	0.669	0.665	93.4	93.4	0.008
4.53	0.669	0.665	93.4	93.4	0.008
5.53	0.664	0.665	93.4	93.4	0.008
6.87	0.677	0.665	93.5	93.5	0.008
8.77	0.664	0.665	93.5	93.5	0.008
11.27	0.514	0.485	65.8	69.9	0.038

T_i = 131.3 F

(P/z) Exp.	(P/z) Homo.	Density Eq(A - 19)	Density Exp.	f Exp.
0.671	0.673	93.1	93.1	0.007
0.669	0.673	93.1	93.1	0.007
0.669	0.673	93.2	93.2	0.007
0.670	0.673	93.2	93.2	0.007
0.675	0.673	93.2	93.2	0.009
0.533	0.522	68.4	69.9	0.022
0.455	0.372	44.5	56.4	0.024

T_i = 133.5 F

z	(P/z) Exp.	(P/z) Homo.	Density Eq(A - 19)	Density Exp.	f Exp.
1.77	0.672	0.674	92.9	92.9	0.007
3.98	0.669	0.674	93.0	93.0	0.007
4.53	0.669	0.674	93.0	93.0	0.007
5.53	0.67	0.674	93.0	93.0	0.007
6.87	0.617	0.575	75.6	81.5	0.026
8.77	0.476	0.415	49.8	58.6	0.023
11.27	0.432	0.325	34.2	49.7	0.016

T_i = 135.2 F

(P/z) Exp.	(P/z) Homo.	Density Eq(A - 19)	Density Exp.	f Exp.
0.672	0.666	90.9	90.9	0.011
0.664	0.649	88.3	90.5	0.014
0.641	0.644	83.7	86.6	0.017
0.641	0.574	73.7	83.2	0.027
0.509	0.489	60.9	63.7	0.019
0.45	0.407	45.2	51.5	0.017
0.398	0.343	28.6	36.4	0.009

VITA AUCTORIS

1943 Born in Yugoslavia on August 18.

1963 Completed high school at Essex District High School, Essex, Ontario in June.

1967 Received the degree of Bachelor of Applied Science in Mechanical Engineering from the University of Windsor, Windsor, Ontario.

1968 Received the degree of Master of Applied Science in Mechanical Engineering at the University of Windsor, Windsor, Ontario.

1973 Currently a candidate for the Degree of Doctor of Philosophy in Mechanical Engineering at the University of Windsor, Windsor, Ontario.